Technical University of Liberec

Faculty of Mechatronics and Interdisciplinary Engineering Studies

---

Department of Electrical Engineering

HABILITATION THESIS

Piezoelectrically active systems with ferroelectric materials: Physical aspects and applications in acoustics

Piezoelektricky aktivní systémy s feroelektrickými materiály: Fyzikální aspekty a aplikace v akustice

2005

Ing. Pavel Mokrý, Ph. D.

Technical University of Liberec

Faculty of Mechatronics and Interdisciplinary Engineering Studies

Department of Electrical Engineering

HABILITATION THESIS

Piezoelectrically active systems with ferroelectric materials: Physical aspects and applications in acoustics

Piezoelektricky aktivní systémy s feroelektrickými materiály: Fyzikální aspekty a aplikace v akustice

Author: Ing. Pavel Mokrý, Ph. D.

Number of Pages: 159
Number of Appendices: 2
Number of Figures: 32

In Liberec, February 2005 (revised version, March 2005)

Acknowledgements

I would like to express my thanks to all my colleagues from Ceramics Laboratory at the Swiss Federal Institute of Technology Lausanne (EPFL) and to all my colleagues from Department of Physics at the Technical University of Liberec. Especially to Professor Jan Fousek and Professor Alexander K. Tagantsev, who have been opening so many interesting problems and initiating a lot of fascinating questions, and for giving me their helpful comments and critical remarks during the preparation of our joint papers. I would like to thank to Professor Paul C. McIntyre of Stanford University and to Professor Susan Trolier-McKinstry of the W. M. Keck Smart Materials Integration Laboratory at the Pennsylvania State University for their stimulating discussions on the origin of electrode-adjacent layers and on defect chemistry and interface thermodynamics in ferroelectrics, and for their comments on experimental and application aspects of extrinsic contributions in piezoelectric ceramics. The help of Associated Professor Antonín Kopal is greatly appreciated.

I would like to express my sincere gratitude to all my colleagues from the Kobayasi Institute of Physical Research for their help on the project of noise and vibration suppression devices. Especially to Professor Eiichi Fukada, Dr. Kohei Yamamoto and Dr. Munehiro Date for a very close cooperation and many interesting discussions during work on the theoretical part of the project. Likewise I would like to thank to Dr. Hidekazu Kodama, Dr. Tomonao Okubo and Dr. Kazunori Kimura of Kobayasi Institute of Physical Research and Yuhei Oikawa of Gakushuin University for their providing of many experimental data and for many useful discussions. The help of Professor Takeo Furukawa of Tokyo University of Science is greatly appreciated. Equally important was the help, organization assistance and enormous support of Tetsuya Doi, Kazuo Manno and Jiro Kaku of Kobayasi Institute of Physical Research.

My special thanks goes out to Bryan H. Atwood of Hitachi Central Research Laboratory for his help with a "language polishing" of a couple of papers and for his very stimulating discussions on SRAM, DRAM and FRAM technology. Last but not least, part of this work would not be possible without the help and cooperation of Emeritus Professor Jinzo Kobayashi of Waseda University, who also gave me the opportunity to meet so many interesting people.

This work was supported by the Ministry of Education of the Czech Republic (Projects No. VS 96006, No. MSM 242200002 and No. FRVŠ 1013/2001) and by the Grant Agency of the Czech Republic (Projects No. 202/00/1245 and No. 202/03/0569). Between the years 2001 and 2003 a part of this work was done within the internal research project "Noise and vibration suppression devices" supported by Kobayasi Institute of Physical Research and by the Scholarship of the Japanese Government (Monbusho). From 2003 till 2004 a part of this work was done within a research project "Switching, degradation and microwave features of ferroelectric thin films" of Ceramics Laboratory at the Swiss Federal Institute of Technology Lausanne (EPFL) supported by Swiss National Science Foundation.

Preface

Many decades after the discovery of piezoelectricity in 1880 by Pierre and Jacques Currie the overwhelming number of practical applications of this phenomenon has become an integral part of our lives. The subsequent discovery of ferroelectricity brought forth a new class of materials with piezoelectric properties hundreds of times stronger than that of quartz. Possibility of changing the polarization states in ferroelectric materials by the action of external electric fields has broadened scientists' horizons for inventing further applications. In addition, when two and more polarization states appear in a sample and form a domain pattern, a quite new type of phenomena influences the macroscopic properties of ferroelectric materials. In some applications, the presence of domain patterns is quite appreciable and they enhances the dielectric response in high permittivity capacitors or piezoelectric response in electromechanical actuators. In other applications, the presence of domains has a disastrous impact on their proper function as, for example, in pyroelectric sensors or nonvolatile ferroelectric memories. That is why our understanding and control of ferroelectric domains are essential for all currently pursued applications of ferroelectric thin films and may well be the key for future applications. In parallel, from the academic point of view, this topis is complex and rich in fascinating aspects, which have not yet been explored in depth. These are the reasons, why I become so curious to study domain patterns in ferroelectrics.

In a variety of applications of ferroelectric and piezoelectric materials, physical and application aspects of two devices are discussed in more detail in this work. First, I am concerned with ferroelectric thin films, which are nowadays used in computer memory devices. It appears that the quality of ferroelectric thin films is affected by many physical phenomena, whose understanding is essential for the future development of memory devices. Since their principal function is based on a spontaneous polarization reversal, switching measurement techniques are often used for a characterization of ferroelectric thin films. In this thesis, it is shown that also small signal dielectric response can bring a lot of information on a quality of ferroelectric thin films, which were put into the polydomain state by the electric cycling. My second scope of interest covers the research and development of applications utilizing piezoelectric materials in acoustics.

Due to different character of these two subjects, the thesis has been divided into two parts. The first part is devoted to the physical aspects and the role of domain patterns in ferroelectric devices and ferroelectric thin films, in particular. The second part is dedicated to the applications of ferroelectric polymer films in acoustics. Each of these parts has the same structure. It begins with an introduction to the state of art in the field focusing on application aspects and reviewing the opened problems, which are discussed in this thesis. Following this introductory part, the collection of selected publications is presented. Finally, brief summary recollects the main results, where I also present some points, which were not included in the original papers due to the lack of space, and additional comments on experimental and application aspects of the presented results. Finally, I attach appendices where additional information, which can be helpful for the reader but which goes little beyond the scope of the thesis, can be found. I believe that this structure of the thesis is the best option for the sake of presentation and the maximum asset for the reader.

Liberec
February 2005

Pavel Mokrý

Contents

List of Figures

Additional figures are in papers A to J.

List of Symbols

Part I: Role of domain patterns in ferroelectric devices

a_+, a_-	width of domains where the spontaneous polarization is oriented along and against the vector of spontaneous polarization		m
a	domain spacing (half-period of the domain pattern)	$a = (a_+ + a_-)/2$	m
a_w	thickness of the domain wall		m
$a_{\mathrm{eq}}(t)$	equilibrium domain spacing at given film thickness		m
$a_{\mathrm{eq}}(V)$	equilibrium domain spacing at given applied voltage		m
A	asymmetry coefficient	$A = (a_+ - a_-)/2a$	1
$A_{\mathrm{eq}}(V)$	equilibrium value of asymmetry coefficient at given voltage on electrodes		1
B	slab factor	$B = d/h$	1
$\beta^e_{ij}, \beta^\tau_{ij}$	clamped and free impermittivity tensor		$\mathrm{F}^{-1}\mathrm{m}$
c	parameter of dielectric anisotropy of ferroelectric layer	$c = \sqrt{\varepsilon_a/\varepsilon_c}$	1
$c^P_{\mu\nu}, c^E_{\mu\nu}$	elastic stiffness coefficient at zero polarization and zero electric field		Pa
C	capacitance of the ferroelectric film (per unit are of the sample)		F
d	total thickness of the surface layers		m
$d_{i\mu}, h_{i\mu}$	piezoelectric coefficients matrix		Cm^{-2}
D_i	electric displacement		Cm^{-2}
Δx	displacement of the domain wall		m
$e_{0,6}, S^s_6$	shear component of spontaneous strain		1
e_{ij}	mechanical strain tensor	$e_{ij} = \partial u_i/\partial x_j$	1
E_i	electric field vector	$E_i = -\partial\varphi/\partial x_i$	Vm^{-1}
E_{ext}	external (applied) electric field		Vm^{-1}
ε_0	vacuum permittivity		Fm^{-1}
$\varepsilon^{(1)}_{ij}, \varepsilon_d$	relative lattice permittivity of the surface layers		1
$\varepsilon^{(2)}_{ij}, \varepsilon_a, \varepsilon_c$	relative permittivity of crystal lattice in the ferroelectric layer		1
ε_m	relative domain wall (extrinsic) contribution to permittivity of the ferroelectric layer, which is controlled by lattice pinning of domain walls		1
ε_f	relative permittivity of the ferroelectric layer, which would be measures in the surface-layer-free capacitor	$\varepsilon_f = \varepsilon_c + \varepsilon_m$	1
$\varepsilon_{\mathrm{el}}$	relative extrinsic contribution to permittivity of the ferroelectric layer, which is controlled by the electric field in the surface layer		1
ε_w	relative domain wall (extrinsic) contribution to permittivity of the ferroelectric layer, which is controlled by the electric field in the surface layer	$1/\varepsilon_w = 1/\varepsilon_m + 1/\varepsilon_{\mathrm{el}}$	1
$\varepsilon_{\mathrm{mod}}$	relative apparent (effective) permittivity of the surface layer		1
g	parameter of dielectric anisotropy of ferroelectric layer	$g = \sqrt{\varepsilon_a\,\varepsilon_c}$	1
G	Gibbs electric energy (per unit area of the sample)		Jm^{-2}
G_{el}	Gibbs electric energy controlled by the electric field (per unit area of the sample)		Jm^{-2}

G_m	Gibbs electric energy controlled by the lattice pinning of domain walls (per unit area of the sample)		$\mathrm{Jm^{-2}}$
h	thickness of the ferroelectric layer		m
φ_f	Electrostatic potential in the ferroelectric layer		V
φ_g	Electrostatic potential in the electrode-adjacent layers		V
λ	degree of spontaneous polarization screening	$\sigma_f = -\lambda\sigma_b$	1
$\lambda_{d,f}$, $\mu_{d,f}$	Lamè coefficients (components of elastic stiffness tensor in isotropic material) of the surface and ferroelectric layers		Pa
P_0, P_S	spontaneous polarization along the ferroelectric axis direction		$\mathrm{Cm^{-2}}$
P_N	average (net) spontaneous polarization of the ferroelectric layer	$P_N = P_0(a_+ - a_-)/2a$	$\mathrm{Cm^{-2}}$
R	domain pattern coefficient	$R = \pi h/2a$	1
$R_{\mathrm{eq}}(V)$	equilibrium value of domain pattern coefficient at given voltage on electrodes		1
$s^{(1)}_{ijkl}$	elastic compliance tensor of the surface layers		$\mathrm{Pa^{-1}}$
$s^{(2)}_{ijkl}$	elastic compliance tensor of the ferroelectric layer		$\mathrm{Pa^{-1}}$
S_6^{eff}	average (net) shear strain of ferroelectric film		1
σ_w	energy density of the domain wall (per unit area)		$\mathrm{Jm^{-2}}$
σ_0	density of free charges on the electrodes (per unit area of the sample)		$\mathrm{Cm^{-2}}$
σ_b	density of bound charges due to spontaneous polarization at the interface of ferroelectric and surface layers (per unit area of the sample)		$\mathrm{Cm^{-2}}$
σ_f	density of compensation, or screening, (free) charges at the interface of ferroelectric and surface layers (per unit area of the sample)		$\mathrm{Cm^{-2}}$
t	thickness of the film	$t = h + d$	m
T	temperature		K
T_c	temperature of the phase transition		K
τ_{ij}	mechanical stress		$\mathrm{Nm^{-2}}$
τ_{ext}	external (applied) mechanical stress		$\mathrm{Nm^{-2}}$
u	displacement of the ferroelectric sample in the direction of the external (applied) mechanical force		m
u_i	components of the mechanical displacement vector		m
U_w	Helmholtz free energy of domain walls (per unit area of the sample)		$\mathrm{Jm^{-2}}$
U_{el}	Helmholtz free energy of the electric field (per unit area of the sample)		$\mathrm{Jm^{-2}}$
U_{def}	Helmholtz free energy of the elastic deformation (per unit area of the sample)		$\mathrm{Jm^{-2}}$
V, U	voltage on the electrodes		V

Part II: Piezoelectric materials in noise and vibration suppression devices

α	ratio of the external capacitance over the sample capacitance	$\alpha = C/C_s$	1
α_0	absorption coefficient		1
β^T_{ij}	impermittivity tensor at a constant mechanical stress		1
c, c_0	phase velocity of sound in air		$\mathrm{m\,s^{-1}}$
c_1	effective phase velocity of sound in a porous material	$c_1 = \sqrt{p_0/\varrho_1}$	$\mathrm{m\,s^{-1}}$
C	external capacitor capacitance		F
C_s	capacitance of the piezoelectric cylindrical membrane		F
C_0	capacitance of the feedback circuit capacitor		F
d_{jr}	piezoelectric coefficient tensors		$\mathrm{Cm^{-2}}$
D_3	radial component of the electric displacement		$\mathrm{Cm^{-2}}$
E_3	radial component of the electric field		$\mathrm{Vm^{-1}}$
ε^T_{33}	relative permittivity of mechanically free sample		1
h	thickness of the piezoelectric membrane		m
H	distance between the cylindrical membrane and backing wall		m
k_{31}	electromechanical coupling factor	$k^2_{31} = d^2_{31}/(s^E_{11}\varepsilon^T_{33})$	1
p_0, p_t, p_r	sound pressures of the incident, transmitted and reflected sound waves		Pa

δp	acoustic pressure difference at the opposite sides of the membrane	Pa
ω	angular frequency of the sound in steady state	$\mathrm{rad\,s^{-1}}$
ω_0	critical frequency of the required maximal sound shielding or absorption	$\mathrm{rad\,s^{-1}}$
π_0	porosity of a porous material (defined as ratio of the volume of air in the material over the total volume of the material)	1
P	amplitude of the acoustic pressure difference at the opposite sides of the membrane	Pa
Q_m	mechanical quality factor	1
R	radius of curvature of the piezoelectric cylindrical membrane	m
R_0, TL	transmission loss	dB
R_1, R_2	potentiometer resistances in the feedback circuit	Ω
ϱ	mass density of the piezoelectric cylindrical membrane	$\mathrm{kg\,m^{-3}}$
ϱ_0	mass density of air	$\mathrm{kg\,m^{-3}}$
ϱ_1	effective density of gas particles in the porous material	$\mathrm{kg\,m^{-3}}$
σ_1	specific dynamic frictional resistance of air particles in porous material	
$s^D_{\mu\nu}$, $s^E_{\mu\nu}$	elastic compliance of the electrically clamped and the electrically free sample	$\mathrm{Pa^{-1}}$
$s^\star_{11}$	effective value of the dynamic elastic compliance	$\mathrm{Pa^{-1}}$
S_1	circumferential strain tensor component	1
T_1	circumferential stress tensor component	Pa
V^+_in, V^-_in	voltages on inverting and non-inverting inputs of an operational amplifier	V
V_out	voltage output an operational amplifier output	V
w	displacement of the membrane in the radial direction by	m
W	amplitude of the membrane displacement in the radial direction by	m
Y	effective value of the Young's modulus controlled by the feedback circuit	Pa
Y_0	Young's modulus of the piezoelectric membrane $Y_0 = 1/s^E_{11}$	Pa
Z	specific acoustic impedance of the membrane	

Part I

Role of domain patterns in ferroelectric devices

Introduction

It is hard to imagine other research field, which contributed to such an extent to a technological development, than the material science. Contemporary trends towards miniaturization push the device designers' needs to the limits allowed by the laws of nature. This is the reason why nowadays so much interest is focused on a search and investigation of materials, which can move the results of applied scientists closer to those limits.

In 1921 the discovery of dielectric hysteresis in rochelle salt by Valasek [1] was the first encounter with one of the most fascinating phenomena in solid state physics — the crystal lattice of a material can exist in two or more metastable states, which can be switched by applying the electric field or mechanical stress. Figure 1 shows that in Valasek's dielectric measurements two values of charge on capacitor electrodes at the zero applied field were measured during the electric cycling. It corresponds to two possible values of polarization in the crystal of rochelle salt. Since the value of polarization remained nonzero even when the electrodes of the capacitor were short-circuited, it was understood that the polarization in the crystal had a constant component termed *permanent (i.e. spontaneous) polarization.* In addition, the spontaneous polarization vector of the crystal could be reversed under the action of an external applied field. This feature, the existence of spontaneous polarization vector which may be changed under the action of an external electric field, is a common property of all materials called *ferroelectrics.*

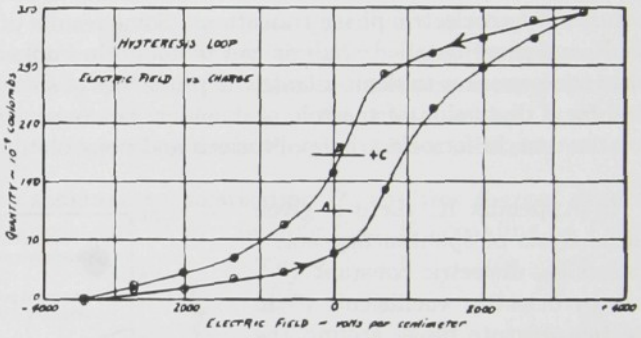

FIGURE 1: Hysteresis loop in the measurement of the charge versus electric field applied to a capacitor of rochelle salt discovered by Valasek. (From Ref. [1])

It is not surprising that any ferroelectric material is not always in a ferroelectric phase. As water can be found in a form of ice, liquid or vapor, depending on pressure and temperature, as the solid ferroelectric material can be found in phases that are not ferroelectric. Transitions between the ferroelectric and non-ferroelectric (paraelectric) phases are called ferroelectric phase transitions. These phenomena usually occur at a narrow temperature region around so called *temperature of a phase transition* T_0. Above temperature T_0, the crystal lattice is stabilized in a certain arrangement of molecules by a thermal motion. With a decrease in temperature, the thermal motion of molecules becomes unable to keep the crystal lattice in the same arrangement. At the temperature T_0, the crystal lattice becomes instable and the structure of molecules in the unit cell is transformed into a different arrangement of the crystal lattice, which becomes stable again. Since this model of a phase transition is characterized by the displacement of atoms at the phase transition temperature, which leads to the change of the crystal symmetry, such phase transitions are called *phase transitions of the displacive type.*

On the other hand, there exists another possibility of changing the crystal symmetry. In some materials, there exist, already in the paraelectric phase, a possibility of finding particles in two

different positions in the unit cell. But due to thermal motion at rather high temperatures, the particles have enough energy for hopping between the both positions, which are occupied uniformly. The crystal symmetry is, on average, the same as if the particles would be in the center of the unit cell. With a decrease in temperature, the hopping particles have not enough energy for keeping the equal occupation of the both positions. In this situation, a long-range interactions between the particles start to play a role and there appears a difference in probabilities of finding a particle in different positions. The phase transition, in which a change of symmetry occurs as a result of redistribution of particles over equiprobable positions, are called *phase transitions of the order-disorder type.*

So far a large number of ferroelectric materials has been discovered. The diversity of these materials in composition, structure, symmetry and micro-mechanism of the phase transition is evidently an indication of the difference in molecular generation of spontaneous polarization. However, there was identified a complex of properties that are common to all crystals capable to undergo the ferroelectric phase transition. In particular, the macroscopic behavior of all substances clearly manifest a similarity in temperature dependence of the spontaneous polarization and dielectric constant in the region of the phase transition. This accounts for the fact that the phenomenological theory of ferroelectric phase transitions has been developed extensively. Applying the phenomenological theory of L. D. Landau to ferroelectric materials, it is possible to obtain a qualitative overview on features of ferroelectric phase transitions. Some results of Landau theory are presented in Appendix K and more detailed analysis can be found in books [2, 3]. Here there are presented only its basic consequences to demonstrate the properties of so called uniaxial ferroelectrics, which will be used for a discussion of the role of domains, i.e. regions which differ in value of the spontaneous polarization, in ferroelectric applications and non-volatile memory devices, in particular.

In Appendix K, there is given the analysis of spontaneous polarization P_0, dielectric constant $\chi^{p,T}$ and pyroelectric coefficient γ^p in the temperature range around the second order phase transition in uniaxial ferroelectrics. The typical temperature dependencies of these physical properties are shown in Fig. 2. There are also indicated specific temperature regions around the phase transition, which are suitable for a utilization in applications. For example, a material with the peak dielectric constant in the paraelectric phase

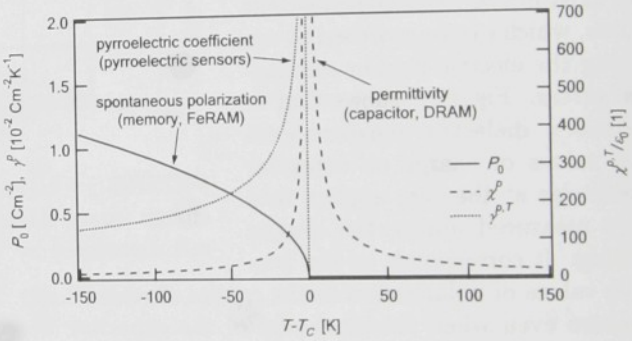

FIGURE 2: Typical temperature dependencies of spontaneous polarization P_0, dielectric constant $\chi^{p,T}$ and pyroelectric coefficient γ^p in uniaxial ferroelectric material near the second-order phase transition. Note the indicated temperature regions for possible applications.

$$\chi^{p,T} = \frac{C}{T - T_C}$$

is suitable for *high permittivity capacitors,* where C is the *Currie-Weiss constant* and T_C is the *Currie temperature.* Large switchable spontaneous polarization in the ferroelectric phase

$$P_0 \propto \pm\sqrt{T_C - T}$$

can be employed in *ferroelectric memory applications.* Abrupt temperature change of the spontaneous polarization in the vicinity of the phase transition

$$\gamma^p = (\partial P/\partial T)_p \propto \pm 1/\sqrt{T_C - T}$$

is sought for *pyroelectric sensors.*

It is seen that large values of dielectric and pyroelectric constants and the presence of spontaneous polarization made the ferroelectric materials immediately attractive candidates for a variety

of applications. If a certain material should be considered for a high permittivity capacitor application, the specific value of the transition temperature T_C should be below room temperatures. On the other hand, the value of T_C should be above room temperatures in ferroelectric memory applications. Construction of pyroelectric sensors requires materials with the transition temperature in the range of room temperatures.

It should be pointed out that the above temperature dependencies were calculated under the assumption that the materials are *mono-domain single crystals.* It means that the spatial distribution of spontaneous polarization is uniform over the volume of the sample. In addition, it is assumed that the application of the electric field does not change their state. Unfortunately, in ordinary ferroelectric materials these assumptions do not strictly hold and actual device materials often exhibit a *domain pattern.* It means that the volume of the crystal is split into regions called *domains,* which differ in values of the spontaneous polarization. It turns out that the presence of domains in ferroelectric materials tremendously affects their macroscopic properties and the role of domains in ferroelectric devices is discussed in more detail in the next section.

Role of domain patterns in ferroelectric single crystals

In an ideal infinite ferroelectric the spontaneous polarization is uniform over the volume of the crystal. On the other hand, in real crystals the spatial distribution of the spontaneous polarization is affected by the presence of crystal surfaces and imperfections of the crystal lattice. In addition, the quality of ferroelectric thin films is deteriorated by the interaction with a substrate.

Appearance of bound charges due to spontaneous polarization $\boldsymbol{P}_0$ and free charges ϱ_f at the surface of the ferroelectric results in an existence of depolarizing field $\boldsymbol{E}$ according to Poisson equation

$$\operatorname{div} \boldsymbol{E} = \frac{1}{\varepsilon_0 \varepsilon} \left(\varrho_f - \operatorname{div} \boldsymbol{P}_0 \right).$$

When the bound charges due to spontaneous polarization are not compensated by the free charges at the surface of the ferroelectric, the nonzero depolarizing field gives rise to a contribution to the energy of the system:

$$U_{\text{dep}} = \frac{1}{2} \int_V \boldsymbol{E} \left(\boldsymbol{D} - \boldsymbol{P}_0 \right) dV, \tag{1}$$

where $\boldsymbol{D}$ is the electric displacement.

When a ferroelectric crystal is cooled down from the paraelectric phase to the ferroelectric phase in the absence of external electric fields, there exist at least two equivalent directions along which the spontaneous polarization may occur. In order to minimize U_{dep}, different regions of the crystal polarize in each of these directions forming the *domains.* The depolarizing field, which appear on cooling, is usually sufficient to prevent any net spontaneous polarization $\boldsymbol{P}_N$ to occur in a virgin crystal ($\boldsymbol{P}_N = 0$) where $\boldsymbol{P}_N$ is equal to

$$\boldsymbol{P}_N = \frac{1}{V} \int_V \boldsymbol{P}_0(\boldsymbol{x})\, dV(\boldsymbol{x}). \tag{2}$$

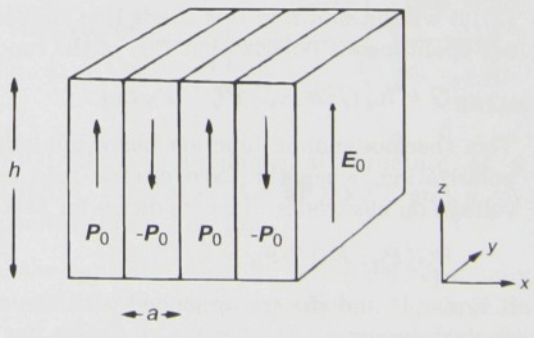

FIGURE 3: Scheme of a sample (thickness h) with periodic domain pattern and the zero net spontaneous polarization $\boldsymbol{P}_N$.

This situation is seen in Fig. 3. Since the sign of pyroelectric coefficient alter from domain to domain in the same way as the sign of $\boldsymbol{P}_0$, it is evident that the net value of pyroelectric coefficient

is also zero in a virgin crystal. This fact has important consequences, which are essential in a construction of ferroelectric devices. It was already mentioned that the great change of polarization with temperature is important for the function of pyroelectric sensors and materials with a phase transition temperature near the room temperature are utilized in such devices. Now it is essential that when the pyroelectric sensor is overheated above the phase transition temperature, a domain pattern can appear during cooling the material down making the device malfunctioning.

An example of qualitatively different effect of domain patterns in ferroelectric, the temperature dependence of dielectric constant in uniaxial ferroelectric potassium dihydrogen phosphate (KDP), is shown in Fig. 4. Detailed derivation of the temperature dependence of permittivity along the ferroelectric axis ε_3 is given in Section K.2 of Appendix K. It is seen that below the phase transition temperature T_0 the temperature dependence of dielectric constant is equal to

$$\varepsilon_3 = \frac{C}{2\,(T_0 - T)}. \tag{3}$$

This prediction of the Landau theory for mono-domain single crystal is shown by dashed line in Fig. 4. If the measured temperature dependence above and below the transition temperature are compared, it is evident that the measured values of dielectric constant below T_0 are much greater than predicted by the phenomenological Landau theory. A possible origin of this disagreement can be attributed to the existence of domains in the ferroelectric single crystal of KDP.

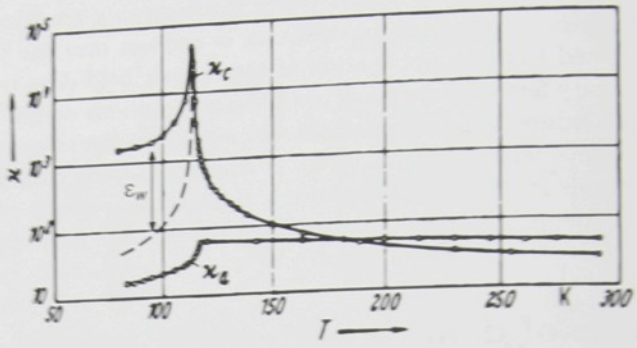

FIGURE 4: Temperature dependence of dielectric constant in potassium dihydrogen phosphate (KDP). Solid line represents the measured values, dashed line represents theoretical predictions of Landau phenomenological theory (mono-domain single crystal). Symbol ε_w stands for the domain wall (extrinsic) contribution to dielectric constant. (From Ref. [6])

When an external electric field $\boldsymbol{E}_0$ is applied to the polydomain ferroelectric sample in Fig. 3, domain boundaries separating domains, which are called *domain walls*, are shifted. This shift of domain walls changes the spatial distribution of spontaneous polarization, so that the net spontaneous polarization P_N is nonzero. The change of P_N contributes to the dielectric response of the ferroelectric polydomain sample. Since this contribution is due to domain wall shifts, it is called *domain wall (extrinsic) contribution to permittivity*. Qualitatively, the mechanism that controls the extrinsic contributions can be easily understood with use of the Gibbs electric energy of ferroelectric polydomain capacitor. From the Landauer formula (see Sec. L.3 in Appendix L) and Eq. (2), it will be shown in this thesis that the leading terms (linear and quadratic with respect to the net spontaneous polarization P_N) of the function G per unit area of a ferroelectric capacitor are

$$G = h\left[1/(2\varepsilon_0\varepsilon_w)\,P_N^2 - P_N E_0\right]. \tag{4}$$

This thermodynamic function has a minimum for the equilibrium value of the net spontaneous polarization, when the fixed electric field is kept in the ferroelectric capacitor by the constant voltage on electrodes. The condition for this minimum is given by equation:

$$\partial G(P_N, E_0)/\partial P_N = 0. \tag{5}$$

If Eqs. (4) and (5) are appended with the expression for capacitance per unit area of the ferroelectric capacitor

$$C/A = \varepsilon_0\varepsilon_{\rm eff}/h = P_N/(hE_0) + \varepsilon_0\varepsilon_c/h, \tag{6}$$

where ε_c is the permittivity of the crystal lattice (i.e. permittivity, which would be measured in mono-domain ferroelectric capacitor according to Landau theory), the effective permittivity of the ferroelectric polydomain sample is obtained immediately:

$$\varepsilon_{\rm eff} = \varepsilon_c + \varepsilon_w. \tag{7}$$

where ε_w is the extrinsic contribution to permittivity, shown in Fig. 4.

Now it is clear that the presence of domain patterns in ferroelectric samples has a strong impact on their macroscopic properties and it plays an essential role in all devices utilizing ferroelectric materials in a temperature range below the phase transition. There exist two principal mechanisms of a formation of domain patterns: first, *spatial fluctuations of the order parameter* (i.e. polarization) during the phase transition, and second, a *nucleation of domains,* which results in a decrease of the depolarizing field energy U_{dep}. In principle it is possible to say that domains can appear in every device after a time long enough to allow the nucleation of new domains at given conditions (external and depolarizing fields, temperature, presence defects, etc.) resulting in the minimum of the energy of the system. It means that the second mechanism is essential in ferroelectric devices whose operational temperatures are below the phase transition temperature.

Recently, ferroelectric thin films have been relatively successfully used in memory devices. Since the principal function of these devices is based on spontaneous polarization reversal, understanding of domain nucleation and deep insight into properties of equilibrium domain patterns with zero net spontaneous polarization are essential for a further development of these devices. Next section gives an overview on some physical aspects of applications of ferroelectric materials in memory devices.

Ferroelectric materials in memory applications

Recently, very large scale integrated semiconductor memories using ferroelectric films have been intensively investigated. The impetus for this research came from two directions. The first direction is represented by the Dynamic Random Access Memory (DRAM), which belongs to so called *volatile memory devices* characterized by the loss of all memory data when the electric power is shut off. Although DRAM memory is widely used because of its high integration capability, its further miniaturization has recently reached the technological limits, since the conventional silicon micromachining technology coupled with silicon oxide or nitride is limited in its ability to produce fine-scale high capacitance capacitors. The second direction is represented by the Ferroelectric Random Access Memory (FRAM), which belongs to a group of *non-volatile memory devices,* in which the stored information is retained even if the power to the chip is interrupted.

In DRAM, the ferroelectric material is used in the thin-film form as a capacitor. The reason can be explained on the description of basic operation of DRAM memory. Figure 5 shows the the fundamental structure of DRAM, which is composed of a transistor and a capacitor. The capacitor is connected to the source of a Metal-Oxide-Semiconductor Field Effect Transistor (MOSFET). Writing into one DRAM element (bit cell) is realized by using the x-y addressing in such a way, that the voltage is applied on the both gate and drain electrodes simultaneously, so that the capacitor is accumulating the charge *(memorizing)*. Since the accumulated charge leaks, the capacitor must be recharged repeatedly *(refreshing)*. It sometimes happens that the natural radiation changes the amount of charge on the capacitor and sometimes destroys the memory *(soft error)*. In order to retain stored data, the capacitance of the memory capacitor must be higher that 30 fF.

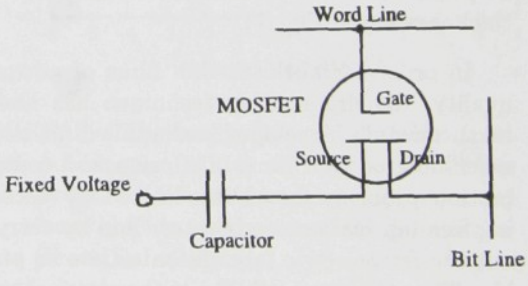

FIGURE 5: Fundamental structure of a DRAM, composed of a MOSFET and a capacitor (From Ref. [5]).

Now a simple estimation can explain what makes the difference, when a ferroelectric material is used in DRAM. Considering that the capacitor is made of dielectrics of permittivity ε_d and some characteristic dimension L, the capacitance of such a capacitor scales as $C \propto \varepsilon_0 \varepsilon_d L$. The typical permittivity of silicon oxide, which is employed in the most of DRAMs, is about 5 and the characteristic dimension is about $L \propto C/\varepsilon_0 \varepsilon_d$. The density of the present day DRAM is limited

primarily by the capacitor area per bit cell and the transistors take up relatively very little area, as it is seen in Fig. 6. Ferroelectrics usually have a large dielectric constant from 100 to 1000 and if it is used, the characteristic dimension L can be 100 times smaller, so that the present limits that are reached by complicated stacking, hollowing and trenching of the dielectric material can be relaxed. It means that much higher integration is possible or less frequent refreshing of the memory is needed, so that the memory can work at higher speed.

Since the high permittivity is essential for DRAM and ferroelectric hysteresis must be avoided, utilization of a material in the paraelectric phase is required. The first material studied for this purpose was strontium titanate ($SrTiO_3$), which does not exhibit hysteresis in its polarization versus field curve and has no permittivity peak in the temperature dependence. It has a dielectric constant around 300 at room temperature and strontium titanate films are superior to the conventional ferroelectrics also from the manufacturing point of view.

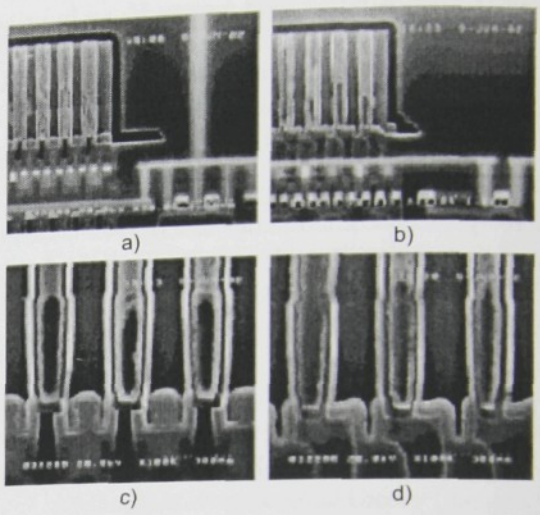

FIGURE 6: Realization of a conventional DRAM structure based on silicon oxide. Needed values of capacitances are achieved using hollowing and trenching of the dielectric material. It is seen that transistors take up only a little space in the memory bit cell; view from a bit line direction (a), (c) and word line direction (b), (d); Insets (c), (d) show details from the insets (a), (b). (From Ref. [7]).

The reason is that most of the conventional ferroelectric thin films exhibit a decrease in permittivity with decreasing film thickness. This is called *size effect on permittivity* and it usually occurs when the thickness of the conventional film is decreased below 200 nm. Although the mechanisms, which lead to the size effect on permittivity, are not absolutely clear, it is believed that it is due to the interaction of the ferroelectric film and the substrate at their interface. The advantage of an application of strontium titanate films in DRAM devices is that $SrTiO_3$ films retain a relative permittivity of about 220 down to thicknesses of about 50 nm and the size effect on permittivity fully manifests itself below these thicknesses (see Fig. 7).

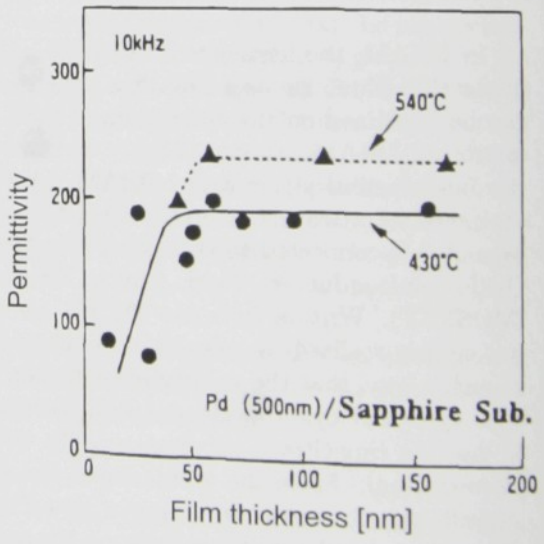

FIGURE 7: Thickness dependence of the dielectric constant in $SrTiO_3$.

In order to fabricate thin films of adequate quality, the dry etching technique has had to be successfully developed and applied for micromachining of such films. Diffusion and contamination problems have been solved by decreasing film fabrication temperature and by carrying out the ferroelectric fabrication as late as possible. Thus the compatibility of the classical semiconductor processing has been established, and prototypes of 256 Mbit DRAM device have been fabricated and their function verified.

Another type of a device is realized, when a ferroelectric thin film with a large polarization-electric field hysteresis is used as a memory capacitor in the structure shown in Fig. 5. When a voltage is applied to the gate and the FET assumes the "on" state, a pulse voltage to the drain generates a drain current, which is dependent on the remanent polarization state of the ferroelectric capacitor.

When a positive voltage pulse is applied just after the negative voltage pulses a large drain current is observed, which includes the contribution due to the spontaneous polarization reversal.

However, a second positive voltage pulse generates only a small current, because the spontaneous polarization in the ferroelectric capacitor is not reversed. Thus the observed current amount for a positive pulse can indicate the initial polarization state. Since the memory information stored in the capacitor of this memory device is always destroyed by its reading process and its state is always switched to "off", a writing process similar to DRAM refreshing is required after every reading event, in order to retain the original memory state.

Since the large voltage is applied on the ferroelectric film every reading process in FRAM, the polarization hysteresis decreases with increasing cycles. This is called *fatigue* and it was one of the most serious problems at the early stages of the FRAM research to overcome. The physical origin of fatigue is not clear so far. A possible mechanism was related to the generation and diffusion of oxygen vacancies in the electrode-adjacent regions but the latest studies show no correlation between the fatigue that the oxygen vacancies redistribution [8]. Using ^{18}O oxygen tracers, Schloss et al. [9] studied the generation and drift of oxygen vacancies during the voltage cycling of PZT thin films using secondary ion mass spectroscopy (SIMS). In order to better understand the oxygen vacancy motion and its possible relationship to changes in ferroelectric switching behaviour, Wang and McIntyre have recently performed a systematic investigation of oxygen tracer diffusion in PZT thin films [10]. Nevertheless, independently on the origin of fatigue, new electrode materials ruthenium oxide (RuO_2) and iridium (Ir) have been found to exhibit improvement in fatigue in comparison with the conventional platinum (Pt) electrodes. Furthermore, new layered structure thin film ferroelectric material based on $BiSr_2Ta_2O_9$, called Y1 and patented by Symmetrix, shows the superior anti-fatigue properties.

Not only fatigue but also the effect called *imprint,* or *preferred polarization state,* is one of the major concerns in the contemporary development of ferroelectric non-volatile memories. Imprint is indicated by the voltage shift of a hysteresis loop. In Figure 8 this shift was induced by a thermal treatment of the sample. A possible explanation for this effect is an existence of internal bias field, which is produced by free charges injected from the electrodes and trapped in the electrode-adjacent regions of the ferroelectric thin film. The asymmetric position of the hysteresis loop causes the difference in switching currents and it is the origin of the read failure of ferroelectric non-volatile memory. It has to pointed out that the imprint characteristics also depends on the testing method and other techniques than hysteresis loop measurements have been used to identify the origin of imprint including the LIMM (Laser Intensity Modulation Method invented by Lang and Das-Gupta [13]) results by Chen and Yao [14], who estimated the distribution of space charge $\varrho_f(z)$ as a function of film depth. It is seen that understanding the processes of charge transport across the electrode-adjacent layers is of great importance for future development of ferroelectric non-volatile memories.

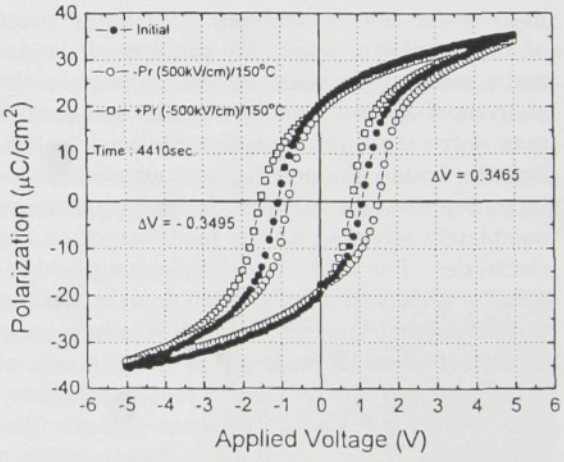

FIGURE 8: Thermally induced imprint (preferred polarization state) in 100 nm PZT film doped by 5%La. Effect of imprint is pronounced as a voltage shift in the hysteresis loop measurement. (From Ref. [12])

To summarize this section, it is seen that the development of ferroelectric non-volatile memories depends on a deep understanding of physical properties of ferroelectric thin films, whose quality is affected by three phenomena: first, by the *size effect on permittivity,* which is essential in a construction of DRAM memory devices; second, by the *fatigue,* which represents one of the major issues limiting the life time of ferroelectric non-volatile memories, since from a practical point of view the time until the polarization degradation is observed of more than 10^{15} cycles is required; and finally, by the *imprint,* which is the source of read failure in FRAM memories. Several experimental investigations [15, 21, 23] indicated that these effects are associated with a deterioration of the quality of ferroelectric thin films in the electrode-adjacent regions. Since principal function

of ferroelectric non-volatile memories is based on a spontaneous polarization reversal, switching measurement techniques are often used for a characterization of ferroelectric thin films [15]. On the other hand, some experimental observations [21, 23] also indicated that the small signal dielectric response of ferroelectric thin films can bring information about phenomena associated with the electrode-adjacent regions. Since the existence of these regions play an important role in a number of domain related phenomena, some of them are introduced in the next section.

Introduction to the collection of publications

During 1990's, research on ferroelectric thin films was booming due to an active stimulation by activities in the applications of ferroelectric materials in memory devices. Up to day, ferroelectric memories represents the most successful commercial application of ferroelectric materials, where the ferroelectric nature, i.e. the switchable spontaneous polarization, is actively utilized. Although a great progress has been made during that period of time mainly in the experimental research, there remained several fundamental questions unanswered and solution of those questions would be a contribution to understanding the ferroelectric state and the control over the domain formation, which is essential in a design and development of future ferroelectric devices.

In Paper A, the equilibrium configuration of 180° domain pattern and its response to external electric field is analyzed. From the point of view of electrostatics, the problem of the domain pattern formation can be reduced to the analysis of effect of depolarizing field on the domain formation. In an ideal ferroelectric capacitor the bound charges due to spontaneous polarization at the surface of the ferroelectric are completely screened by the free charges on the electrodes. The absence of depolarizing field results in a formation of a mono-domain state in the ferroelectric capacitor, which is energetically most favorable. However, it is not the case of many observations of domain patterns in ferroelectric films even in the presence of electrodes. A possible driving force for the domain pattern formation during the phase transition is the imperfect screening of bound charges due to spontaneous polarization by free charges on the electrodes, which gives rise to a depolarizing field and its energy is minimized by the formation of domains. This leads researchers to the concept of so called *surface layer model,* in which it is considered that the quality of a ferroelectric material is deteriorated in electrode-adjacent regions.

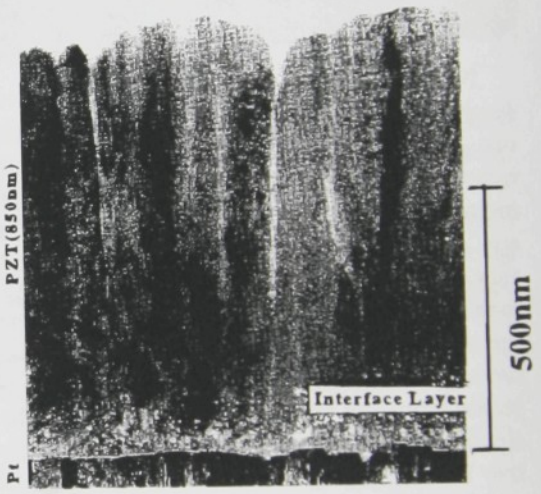

FIGURE 9: Cross-sectional TEM image of an 850 nm thick PZT film with pyrochlore grains that preferentially nucleate at the initial stages on platinum electrodes (From Ref. [17]).

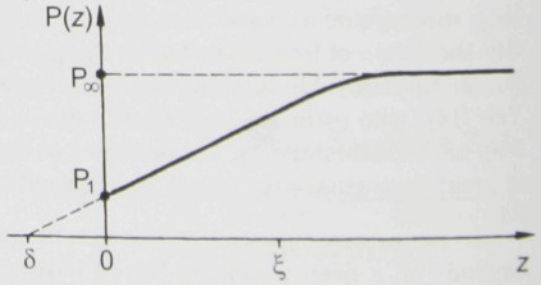

FIGURE 10: Variation of the local polarization $P(z)$ in the vicinity of a free surface situated at $z = 0$ forming the surface layer. Symbols P_∞ and P_1 denote the polarization in the bulk and at the surface. (From Ref. [27]).

Despite of a wide acceptance of the *passive layer model,* the nature of these layers is not clear [16] and the direct observations of well-defined layers are rather scarce. The rare example of direct observation of a passive layer is the work of Hase et al. [17] describing a formation of 100 nm thick layer of pyrochlore grains during multi-target sputtering onto Pt-coated Si substrates (see Fig. 9). In the case of ferroelectric ceramic, grain boundaries represent another origin of passive layers [18, 19]. On the other hand,

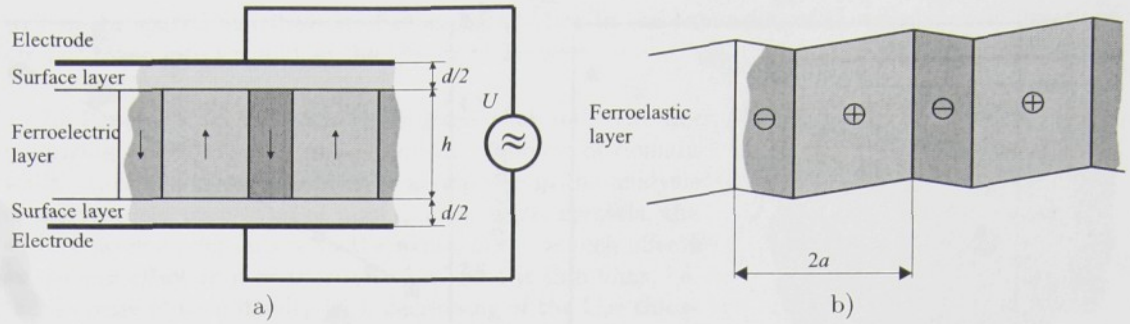

FIGURE 11: Scheme of a ferroelectric capacitor with the surface layers, side view a), ferroelastic domain pattern, top view b)

most of the high-resolution transmission electron microscope studies show no evidence of electrode-adjacent passive layers. Nevertheless, Abe et al. [20] demonstrated that a well-defined dielectric layer may not be necessary for an experimental agreement with the passive layer model and various mechanisms of film-electrode interactions have been proposed: creation of variable depletion layers associated with the Schottky barriers [21, 22], low permittivity layers due to the oxygen vacancy entrapment at ferroelectric-electrode interfaces [23], local suppression of polarization states in the near-electrode regions [24], local diffusion of electrode material into the ferroelectric [25], or chemically distinct surface phase [26]. The last example that can be mentioned here is the classical work of Kretchmer and Binder [27], in which the variation of the local polarization due to the presence of depolarizing field in the vicinity of a *free* surface of ferroelectric film has been analyzed, as it is shown in Fig. 10. It may seem that this case of the ferroelectric film without electrodes is not relevant to the surface layer model of a ferroelectric capacitor, but it has to be pointed out that similar effects on polarization produced by the depolarizing field can be produced by the flexo-electric effect by strain gradients due to the difference in crystal lattice constants of the electrode and the ferroelectric [28].

Independently of the origin, all the above-mentioned phenomena are associated with a deterioration of the spontaneous polarization of the crystal lattice in electrode-adjacent regions. Effect of these regions on depolarizing field can be described within the surface layer model shown in Fig. 11. In this model, it is considered that the ferroelectric layer of thickness h is separated from electrodes by two low-permittivity dielectric layers of the total thickness d. Domain pattern spacing is denoted by a symbol a. In Paper A, it is considered that the domain walls are planes and that their equilibrium position is controlled by the condition for the minimum Gibbs electric energy per unit area of the capacitor. In this particular case the Gibbs electric function is given by Eq. (L.3) in Sec. L.1 of Appendix L, where the Helmholtz free energy is given by Eq. (K.32) in Sec. K.3 of Appendix K. If it is considered that the spatial distribution spontaneous polarization is uniform within each domain and it is inhomogeneous only at domain boundaries, the Gibbs electric energy has two contributions $G = G_w + G_{\rm el}$: first, the *energy due to domain walls*, G_w, and second, the *energy due to electric field*, $G_{\rm el}$. Minimum of this thermodynamic function gives the conditions for several parameters of the equilibrium configuration of the domain pattern. First it is the equilibrium domain spacing $a_{\rm eq}$ and the net spontaneous polarization P_N at given applied voltage U on electrodes, which is proportional to the parameter A, i.e. the volume fraction of domains with the vector of spontaneous polarization oriented along and against the electric field:

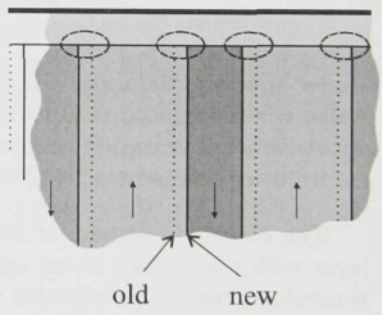

FIGURE 12: Sources of restoring forces due to increase of electric and mechanical energies when the planar domain walls are shifted from equilibrium.

$$A = \frac{1}{V P_0} \int_V P_0(\boldsymbol{x})\, dV(\boldsymbol{x}).$$

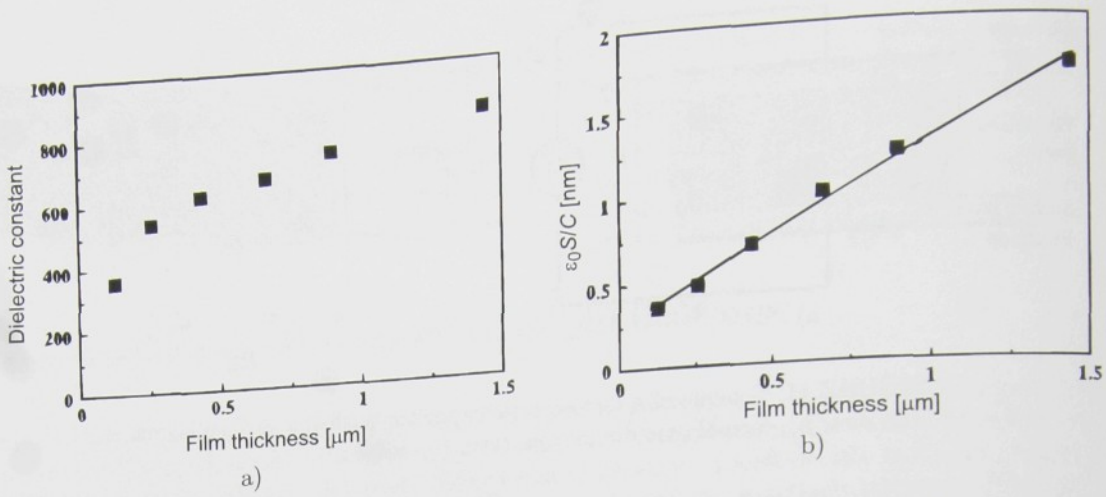

FIGURE 13: Film thickness dependence of dielectric constant a) and inverse capacitance per unit area of the sample b) in PZT films in the thickness range from 60 nm to 1400 nm (From Ref. [17]).

When the domain wall is shifted from its equilibrium position, an increase of energy due to electric field is produced in the regions indicated by ovals in Fig. 12. Knowing the response of the net spontaneous polarization $P_N = P_0 A$ to the external electric field, the effective dielectric constant ε_{eff} of the ferroelectric capacitor with a domain pattern is calculated. Analyzing the formula for ε_{eff}, intrinsic and extrinsic contribution to permittivity can be identified.

Paper B represents a marginal extension of Paper A valid for ferroelectric-ferroelastic materials with noncentrosymmetric paraelectric phase. According to our available information only crystals of KDP family belong to this category. In these materials the vector of spontaneous polarization is proportional to spontaneous shear strain (see Sec. K.2 in Appendix K):

$$P_{0,3} = (h_{36}/c_{66}^{P})\, e_{0,6}.$$

Under this consideration, the average shear strain $e_{\text{eff},6}$ is changed due to the shift of domain walls, which is proportional to the change of the volume fraction of domains with the vector of spontaneous polarization oriented along and against the electric field. This is the source of extrinsic contribution to piezoelectric coefficient $d_{\text{eff},36}$.

The evident weakness of Paper B is the disregard of mechanical interaction of ferroelastic layer with the surface layers and the electrodes. This drawback is eliminated in Paper C where generalized results for effective values of permittivity $\varepsilon_{33}^{\text{eff}}$, piezoelectric coefficient d_{36}^{eff} and elastic compliance s_{66}^{eff} are presented under the consideration of the mechanical interaction of ferroelastic and surface layers. Again it is possible to identify the intrinsic and extrinsic contributions. This generalization greatly extended the applicability of this model to purely ferroelastic materials.

Interrelation of domain wall contributions to dielectric, piezoelectric and mechanical properties of a ferroelectric-ferroelastic layered composite sample is analyzed in Paper C. In 1966, thermodynamic relations between anomalous quantities near a lambda transition in anisotropic dielectrics was analyzed within a Landau theory in the work of Janovec [29], who showed that the material properties with anomalous temperature dependence in the vicinity of a phase transition are linearly related within the temperature region $(T_C - T) < 16°$, where the constants of proportionality give the numerical values of the components of a tensor describing the change of T_C due to mechanical stress. Since these results were obtained within the Landau theory, which is the "local theory", it was not absolutely clear whether these interrelations are valid also in systems with domain patterns and in the temperature regions far from the phase transition. The reason is that the domain pattern formation is controlled by clearly "nonlocal phenomena" associated with a creation of depolarizing field. In addition, the spatial distribution and fluctuations of the order parameter as

well as the spatial distribution of other parameters in the expansion of thermodynamic functions are not taken into account in the theory of Janovec.

In Papers A to D is was considered that only the depolarizing field controls the equilibrium response of domain walls. Although this assumption is acceptable in the analysis of macroscopic properties of high quality single crystals, the surface layer model fails with the explanation of such effects as the *size effect on permittivity* in ferroelectric thin films, i.e. the decrease of permittivity with decreasing of the film thickness, which is shown in Fig. 13. Origin of the size effect can be attributed to the presence electrode-adjacent regions and its analysis using the surface layer model is given in Paper E. In order to successfully explain the size effect, the purely electrostatic approach has been generalized by the consideration of so called *lattice pinning of domain walls*. This kind of pinning of domain walls is e.g. due to lattice defects, which is sketched in Fig. 14. The effect of lattice pinning can be considered in our theory by introducing an extra term G_m into the expansion of Gibbs electric energy $G = G_m + G_{\mathrm{el}}$. In this model we also do not restrict our analysis to domain patterns with the equilibrium value of the domain spacing a, which is usually far from equilibrium in real samples and its value also depends on the prehistory of the sample.

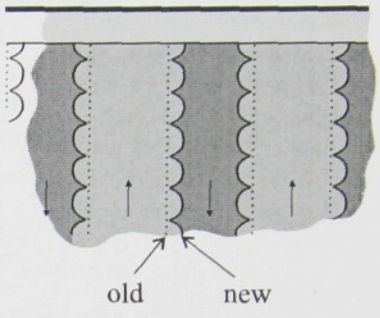

FIGURE 14: Sources of restoring forces due to lattice pinning of domain walls under the effect of external applied field.

Another effect, which can originate due to the existence of surface layers is the *imprint*, i.e. the preferential polarization states in ferroelectric thin films. This phenomenon can be caused by a free charge transport across the surface layer, which results in the spontaneous polarization screening. In Paper F, the possibility of the investigation of the free charge transport mechanism using dielectric measurements performed on ferroelectric polydomain thin films is analyzed.

Finally in Paper G, the possibility of stress-free coexistence of four ferroelectric-ferroelastic domain states along a line is analyzed.

For the sake of presentation, the articles A-D are presented in their revised versions. There are two main reasons for the revision of the papers: first, the unification of symbols used in the thesis, so that the reader of this thesis is not distracted by differences in symbols of the original versions of the articles, and second, the elimination of misprints in the original versions of the articles.

Collection of Publications

Paper A

Displacement of 180° Domain Walls in Electroded Ferroelectric Single Crystals: the Effect of Surface Layers on Restoring Force

(Revised version)

Poster at the European Conference on Applications of Polar Dielectrics, Montreux, 1998.

Published in *Ferroelectrics*, Vol. 223, No. 1-4, Pg. 127-134 (1999)

List of citations

1. P. Mokrý, A. K. Tagantsev, N. Setter, Size effect on permittivity in ferroelectric polydomain thin films, *Physical Review B* **70**(17): Art. No. 172107 (2004)

2. A. Kopal, P. Mokrý, Interrelation of domain wall contributions to dielectric, piezoelectric and mechanical properties of a ferroic layer composite sample, *Ferroelectrics* **290**: Pg. 125-131 (2003)

3. H. Beige et al., *Polar oxides: Properties, characterization and imaging*, (POLECER, 2003), Ch. 8, p. 135

4. S. K. Streiffer, J. A. Eastman, D. D. Fong, C. Thompson, A. Munkholm, M. V. R. Murty, O. Auciello, G. R. Bai, G. B. Stephenson, Observation of nanoscale 180 degrees stripe domains in ferroelectric $PbTiO_3$ thin films, *Physical Review Letters* **89**(6): Art. No. 067601 (2002)

5. P. Mokrý, A. Kopal, J. Fousek, Extrinsic contributions in a nonuniform ferroic sample: Dielectric, piezoelectric and elastic, *Ferroelectrics* **257**(1-4): Pg. 211-220 (2001)

6. A. K. Tagantsev, Comment on "Abrupt appearance of the domain pattern and fatigue of thin ferroelectric films", *Physical Review Letters* **87**(17): Art. No. 179702 (2001)

7. A. M. Bratkovsky, A. P. Levanyuk, Very large dielectric response of thin ferroelectric films with the dead layers, *Physical Review B* **63**(13): Art. No. 132103 (2001)

8. A. M. Bratkovsky, A. P. Levanyuk, Abrupt appearance of the domain pattern and fatigue of thin ferroelectric films, *Physical Review Letters* **84**(14): Pg. 3177-3180 (2000)

DISPLACEMENTS OF 180° DOMAIN WALLS IN ELECTRODED FERROELECTRIC SINGLE CRYSTALS: THE EFFECT OF SURFACE LAYERS ON RESTORING FORCE[1]

A. KOPAL[a2], P. MOKRÝ[a], J. FOUSEK[ab] and T. BAHNÍK[a]

[a]Dept. of Physics, Technical University, CZ-46117 Liberec, Czech Republic
[b]Materials Research Laboratory, Pennsylvania State University, State College, PA 16801

Abstract

Macroscopic properties of ferroelectric samples, including those in form of thin films, are, to large extent, influenced by their domain structure. In this paper the free energy is calculated for a plate-like sample composed of nonferroelectric surface layers and ferroelectric central part with antiparallel domains. The sample is provided with electrodes with a defined potential difference. The effect of applied field and its small changes on the resulting domain structure is discussed. This makes it possible to determine the restoring force acting on domain walls which codetermines dielectric and piezoelectric properties of the sample. Calculations of the potential and free energy take into account interactions of opposite surfaces and are applicable also to thin films.

Keywords: Ferroelectric domains; extrinsic contributions to permittivity

A.1. INTRODUCTION

It is known that samples of ferroelectric single crystals often posses a surface layer whose properties differ from those of the bulk. It may be a layer produced during the growth of a crystalline plate or produced during the preparation of a plate-like sample. Many observations gave evidence to the fact that such a layer is either nonferroelectric or does not take part in the switching process of the internal part; in any case its permittivity is believed to differ from that of a homogeneous sample in the ferroelectric phase. Its existence is expected to greatly influence macroscopic properties of bulk samples[A1,2,3,4] as well as of thin films.[A5] In this paper two such consequences are investigated. First we reconsider the problem of equilibrium domain structure in a ferroelectric sample possessing a surface layer, previously discussed by Bjorkstam and Oettel.[A6] Second, we evaluate the restoring force acting on 180° domain walls due to the layer; this will make it possible to estimate the extrinsic contributions to permittivity, piezoelectric coefficients and elastic compliances of a ferroelectric sample. Investigations of crystals of the KDP family revealed the existence of huge wall contributions to these properties.[A7,8]

In previous papers on a related subject[A2], depolarizing field was considered as the source of energy which slows down the motion of a single domain wall in a dc electric field, as the wall departs from its original position by substantial distances. In contrast to such models we investigate very small deviations of walls forming a regular domain pattern.

A.2. GEOMETRY, VARIABLES AND ENERGY OF THE SYSTEM

We consider a plate-like electroded sample of infinite area with major surfaces perpendicular to the ferroelectric axis z. Central ferroelectric part with antiparallel domains (2.) is separated from

[1]Supports of the Ministry of Education (Project VS 96006) and of the Grant Agency of the Czech Republic (Grant 2022/96/0722) are gratefully acknowledged.
[2]e-mail: antonin.kopal@vslib.cz

the electrodes (0.), (4.) by nonferroelectric layers (1.), (3.) (see Fig. A.1). The spatial distribution of the electric field $\boldsymbol{E}$ is determined by the applied potential difference $V = \varphi^{(4)} - \varphi^{(0)}$ and by the bound charge $\mathrm{div}\boldsymbol{P}_0$ on the boundary of ferroelectric material, where $\boldsymbol{P}_0$ stands for spontaneous polarization. Geometrical, electrical and material parameters of the system are shown in Fig. A.1.

We further introduce the symbols

$$\begin{aligned} c &= \sqrt{\varepsilon_a/\varepsilon_c}, \\ g &= \sqrt{\varepsilon_a\,\varepsilon_c}, \\ S_0 &= \sum_{n=1,3,5}^{\infty} \frac{1}{n^3} \doteq 1.052 \end{aligned}$$

and several geometrical parameters:

$$B = \frac{d}{h}$$

the domain pattern factor

$$R = \frac{\pi h}{2a}, \quad 2a = a_+ + a_-$$

and the asymmetry factor

$$A = \frac{a_+ - a_-}{a_+ + a_-}\,.$$

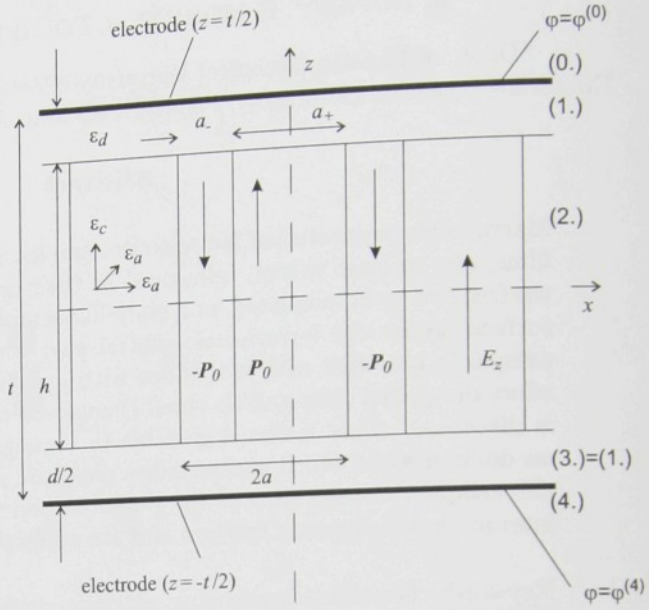

FIGURE A.1: Geometry of the model

The ferroelectric material itself is approximated by the equation of state

$$\begin{aligned} D_x &= \varepsilon_0\varepsilon_a E_x, \\ D_z &= \varepsilon_0\varepsilon_c E_z + P_0, \end{aligned}$$

where P_0 is the spontaneous polarization along the ferroelectric axis. This linear approximation limits the validity of our calculations to the temperature region not very close below the transition temperature T_c. Domain walls are assumed to have surface energy density σ_w and zero thickness.

The total free energy of the system includes the domain wall energy and the electrostatic energy whose density is $(1/2)\boldsymbol{E}\cdot(\boldsymbol{D}-\boldsymbol{P}_0)$. First, Laplace equations have to be solved for electric potentials in the bulk and in the surface layers, fulfilling the requirement of potential continuity as well as conditions of continuity of normal components of $\boldsymbol{D}$ and tangential components of $\boldsymbol{E}$. A rather cumbersome calculation leads to the following formula for Gibbs electric energy per unit area of the system (in $\mathrm{J\,m^{-2}}$):

$$G = \frac{2}{\pi}\sigma_w R + P_0 A\,\frac{P_0 A\,Bt - 2\varepsilon_0\varepsilon_d V\,(1+B)}{2\varepsilon_0\,(1+B)\,(\varepsilon_d + B\,\varepsilon_c)} + \frac{4P_0^2 t}{\varepsilon_0\pi^2 R(1+B)}\sum_{n=1}^{\infty}\frac{\sin^2\left(n\pi(1+A)/2\right)}{n^3(\coth nBR + g\coth nRc)}\,. \tag{A.1}$$

The first term represents domain wall contribution while the last one is the depolarization energy. In the second term we recognize the effect of layers (1.) and (3.) and of the applied voltage.

Let us compare expression with formulae deduced and used in previous papers. For $V = 0$ and $s \to \infty$, $\varepsilon_d = 1$ and $A = 0$ the system goes over into an isolated ferroelectric plate with "neutral" domain structure, placed in vacuum. In this case the equation (A.1) reduces to the expression given by Kopal et al.[A9] for ferroelectric plates of finite thickness in which the interaction of the two surfaces is accounted for. If the plate is thick this interaction can be neglected and Eq. (A.1) simplifies to the classical formula of Mitsui and Furuichi[A10] (cf. Eq. (9) in Ref. [A9]) which is

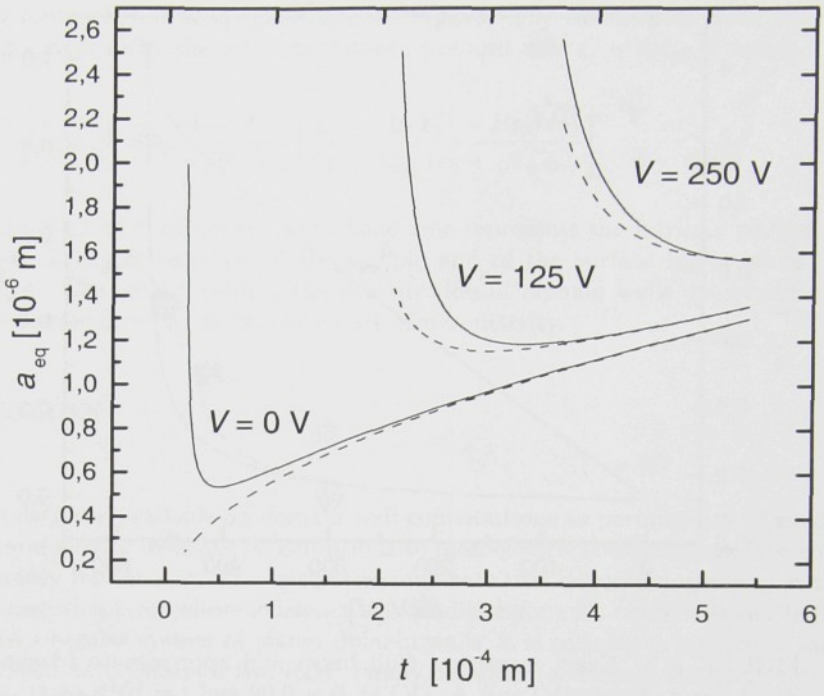

FIGURE A.2: Exact numerical (full lines) and approximate (dashed lines) results for $a_{\rm eq}(t)$ at different values of potential difference V and $B = 0.02$.

often used to determine the value σ_w from the observed width of domain patterns. Finally, in the limit of $V = 0$ our formula (A.1) should converge to the expression deduced by Bjorkstam and Oettel.[A6] In fact this is not the case and it appears that the electric displacement as expressed in Ref. [A6] does not satisfy all boundary conditions.

A.3. EQUILIBRIUM DOMAIN STRUCTURE FOR $V = 0$

If the system is short-circuited, the equilibrium domain pattern is symmetric, i.e. $A_{\rm eq} = 0$. The shape factor $R^0_{\rm eq}$ and from it also the value of $a^0_{\rm eq}$ can be found by numerical methods. As an example, the full lines in Fig. A.2 shows the $a_{\rm eq}(\mathcal{D})$ dependence at constant h/d and different values of potential difference V. As it was shown in the previous paper[A9], the critical thickness $h_{\rm crit}$ can be defined by the formula

$$h_{\rm crit} \cong 4\,\varepsilon_0 \sigma_w \sqrt{\varepsilon_a \varepsilon_c}/P_0^2$$

so that for $h \gg h_{\rm crit}$ the interaction energy of sample surfaces can be neglected. Then the minimum energy occurs for

$$a^0_{\rm eq} = \frac{1}{P_0}\left[\frac{\pi^3 \varepsilon_0 \left(\varepsilon_d + \sqrt{\varepsilon_a\,\varepsilon_c}\right)\,\sigma_w}{8 S_0 (1+B)}\right]^{1/2} \sqrt{t}\,. \tag{A.2}$$

and the dependence $a^0_{\rm eq}(t)$ in this approximation is shown by a dashed line with $V = 0\,$V in the Fig. A.2. The approximate results in the Fig. A.2 with $V = 250\,$V and $V = 500\,$V are based on Eqs. (A.3) and (A.4). In these numerical calculations we have used the following values which roughly apply to crystals of RbH_2PO_4 below the transition temperature: $P_0 = 5.7 \times 10^{-2}\,{\rm C\,m^{-2}}$, $\varepsilon_a = 10, \varepsilon_c = 100, \varepsilon_d = 10$, $h_{\rm crit} = 5.4 \times 10^{-8}\,$m. The value $\sigma_w = 5 \times 10^{-3}\,{\rm J\,m^{-2}}$ is often considered typical for ferroelectrics.

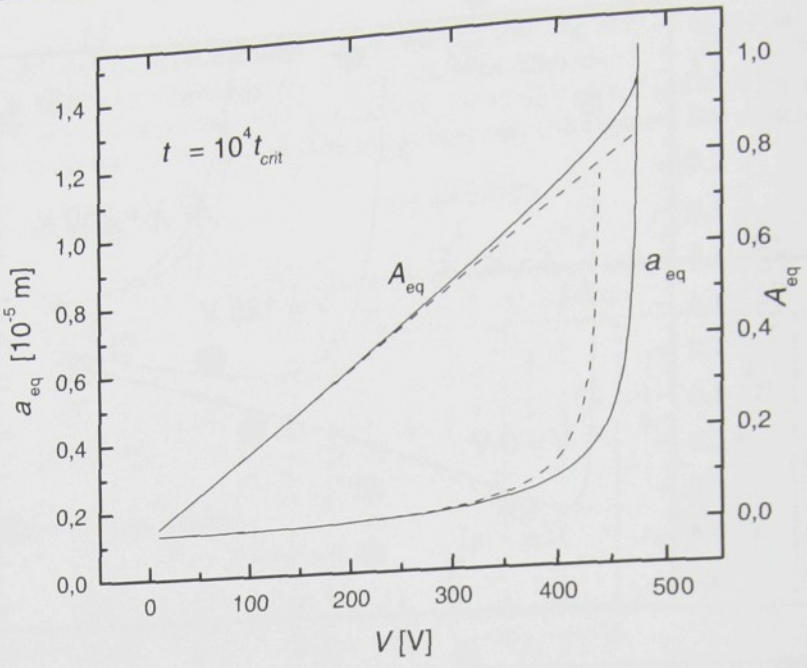

FIGURE A.3: Exact numerical (full lines) and approximate (dashed lines) results for $a_{\rm eq}(V)$ and $A_{\rm eq}(V)$ at $B = 0.02$ and $t = 10^4 t_{\rm crit}$.

A.4. RESPONSE OF DOMAIN STRUCTUTE TO EXTERNAL ELECTRIC FIELD

When an external potential difference V is applied, the asymmetry parameter becomes nonzero and at the same time the period $a = (a_+ + a_-)/2$ changes. Both these quantities can be found again by determining the minimum of G given by Eq. (A.1) numerically. Full lines in Fig. A.3 demonstrate both these dependencies for the following numerical values: $B = 0.02$, $t = 10^4\, t_{\rm crit} = 10^4\,(1 + B)\, h_{\rm crit}$. Starting from a certain applied voltage the domain spacing a grows very fast with increasing V. To discuss the macroscopic properties of the sample such as permittivity, the dependence $A_{\rm eq}(V)$ is more important. We recognize that in a considerable region of the applied voltage this dependence is almost linear.

The $A_{\rm eq}(V)$, $a_{\rm eq}(V)$ resp. $R_{\rm eq}(V)$ dependence can be approximated by an explicit formula if the following inequalities are satisfied: $A \ll 1$, $BR \gg 1$ and $Rc \gg 1$. Then it holds

$$A_{\rm eq}(V) \cong \varepsilon_0 \varepsilon_d\,(1 + B)\,\frac{V/t}{P_0}\left[B - \frac{2\log 2\,(\varepsilon_d + B\,\varepsilon_c)}{R^0_{\rm eq}\,(\varepsilon_d + \sqrt{\varepsilon_a \varepsilon_c})}\right]^{-1} \tag{A.3}$$

$$R_{\rm eq}(V) \cong R^0_{\rm eq}\sqrt{1 - \frac{\pi^2 \ln 2}{4\,S_0}\,A^2_{\rm eq}(V)}\ . \tag{A.4}$$

These approximations, shown in Fig. A.3 by dashed lines, are based on the limit of the sum in Eq. (A.1).

A.5. EXTRINSIC PERMITTIVITY

The nonzero value of the asymmetry parameter means that an extra bound charge is deposited on the electrodes due to the domain wall shifts and this in turn represents an increase of effective permittivity of the whole system crystal plus both surface layers. The increase of the electrostatic energy when domain walls leave their original equilibrium positions for $E \neq 0$ serves as the source

of a restoring force when field is again reduced to zero. The calculations show that the effective permittivity ε_{eff} defined by the total capacitance per unit area $C = \varepsilon_0 \varepsilon_{\text{eff}}/t$ equals

$$\varepsilon_{\text{eff}} = \frac{\varepsilon_c (1+B)}{1 + B\varepsilon_c/\varepsilon_d} + \frac{1+B}{1+B\varepsilon_c/\varepsilon_d} \left[\frac{B}{\varepsilon_d} - \frac{2 \ln 2 \, (1 + B\varepsilon_c/\varepsilon_d)}{R^0_{\text{eq}} \left(\varepsilon_d + \sqrt{\varepsilon_a \, \varepsilon_c} \right)} \right]^{-1} \tag{A.5}$$

In this formula the first term on the right-hand side represents the intrinsic part of permittivity, given by linear dielectric response of the sample and of the surface layers when domain walls are kept at rest. The second term is the contribution of domain walls displacement to effective permittivity, often referred to as extrinsic part of permittivity.

A.6. DISCUSSION

Numerous data are available on domain wall contributions to permittivity in single crystals of ferroelectrics and also on extrinsic contributions to piezoelectric coefficients in ferroelectrics which are simultaneously ferroelastic. Our calculations indicate that depolarizing energy can be an effective source of restoring force whose existence is a condition for such contributions. In fact since the model assumes a regular system of planar domain walls, it is suitable in particular for ferroelastic ferroelectrics such as crystals of the KDP family in which a dense pattern of 180° domains is known to exist.[A11,12] It was found that in a wide temperature range below the Curie point of crystals of RbH_2PO_4 and deuterated KDP, the piezoelectric coefficient d_{36} is greatly enhanced compared to its expected value for single domain samples.[A13] Recently, this was confirmed by simultaneous measurements of permittivity ε_3, elastic compliance s_{66} and piezoelectric coefficient d_{36} of RbH_2PO_4. A thorough discussion of d_{36} in this case will be the subject of a forthcoming paper Kopal *et al.*. Here we comment on the extrinsic part of ε_3. For simplicity, let us assume that $\varepsilon_d = \varepsilon_c$. This is not an unreasonable assumption since the assumed surface layer for KDP-type samples can be supposed to have a similar chemical composition as the bulk. Then the extrinsic part of Eq. (A.5) reduces to

$$\left(\frac{B}{\varepsilon_c} - \frac{2 \ln 2 \, (1+B)}{R^0_{\text{eq}} \left(\varepsilon_c + \sqrt{\varepsilon_a \, \varepsilon_c} \right)} \right)^{-1} .$$

Numerically, the second term in the brackets represents a small correction to the first term when approximations (A.3) and (A.4) are valid. If it is neglected, we obtain as an approximation

$$\varepsilon_{z,\text{extrinsic}} \cong \frac{\varepsilon_c}{B} = \varepsilon_c \frac{h}{d} . \tag{A.6}$$

This shows that a very thin surface layer can lead to a considerable extrinsic enhancement of permittivity. Nevertheless, the simple implication: $d \to 0 \Rightarrow \varepsilon_{z,\text{extrinsic}} \to \infty$ is not correct, because the assumptions needed for validity of (A.3), (A.4), (A.5) and (A.6) are violated if d is small enough.

A more general formulation of the restoring force can be used to calculate the extrinsic part of d_{36} for the same geometry of domains. In a recent paper[A14] Sidorkin deduced the dispersion law of wall contributions to permittivity, however, in his treatment the existence of a surface layer is not explicitly considered.

It was shown beyond any doubt that small motions of 90° domain walls are responsible for a considerable enhancement of permittivity ε_3 and piezoelectric coefficients d_{31}, d_{33} in poled ferroelectric ceramics.[A15,16] One of the sources of the restoring force responsible for these wall contributions is the elastic energy at grain boundaries.[A17] Since these boundaries may differ in chemical composition from the bulk of grains[A18], surface layers can be expected to form so that the mechanism proposed in the present paper may also play a role in ceramic samples.

References

[A1] R. C. Miller and A. Savage, *J. Appl. Phys.* **32** (1961) 714.
[A2] M. E. Drougard and R. Landauer, *J. Appl.Phys.* **30** (1959) 1663.
[A3] H. E. Müser, W. Kuhn and J. Albers, *phys. stat. sol. (a)* **49** (1978) 51.
[A4] D. R. Callaby, *J. Appl. Phys.* **36** (1965) 2751.
[A5] A. K. Tagantsev, C. Pawlaczyk, K. Brooks and N. Setter, *Integrated ferroelectrics* **4** (1994) 1.
[A6] J. L. Bjorkstam and R. E. Oettel, *Phys. Rev.*, **159** (1967) 427.
[A7] E. Nakamura, *Ferroelectrics*, **135** (1992) 237.
[A8] M. Štula, J. Fousek, H. Kabelka, M. Fally and H. Warhanek, *J. Korean Phys. Soc. (Proc. Suppl.)*, **32** (1998) 758.
[A9] A. Kopal, T. Bahník and J. Fousek, *Ferroelectrics* **202** (1997) 267.
[A10] T. Mitsui and J. Furuichi, *Phys. Rev.*, **90**(2) (1953) 193.
[A11] A. Fousková, P. Guyon and J. Lajzerowicz, *Compt. Rend.* **262**(13) (1966) 907.
[A12] J. Bornarel, *Ferroelectrics* **71** (1987) 255.
[A13] L. A. Shuvalov, I. S. Zheludev, A. V. Mnatskanyan and T. Z. Ludupov, *Bulletin Acad. Sci. USSR Phys. Ser.* **31** (1967) 1963.
[A14] A. S. Sidorkin, *J. Appl. Phys.* **83** (1998) 3762.
[A15] G. Arlt and H. Dederichs, *Ferroelectrics* **29** (1980) 47.
[A16] Q. M. Zhang, H. Wang, N. Kim and L. E. Cross, *J. Appl. Phys.* **75**(1) (1994) 454.
[A17] G. Arlt and N.A. Pertsev, *J. Appl. Phys.* **70** (1991) 2283.
[A18] H. Heydrich and U. Knauer, *Ferroelectrics* **31** (1981) 151.

Paper B

On the Extrinsic Piezoelectricity

(Revised version)

Poster on European Meeting on Ferroelectricity, Prague 1999.

Published in *Ferroelectrics*, Vol. 238, No. 1-4, Pg. 203-209 (2000)

List of citations

1. A. Kopal, P. Mokrý, J. Fousek and T. Bahník, Extrinsic contributions in a nonuniform ferroic sample: Dielectric, piezoelectric and elastic, *Ferroelectrics* **257**(1-4): Pg. 211-220 (2000)

2. T. Sluka and A. Kopal, Extrinsic contributions to macroscopic properties of ferroic layer composites, *Ferroelectrics* (accepted for publication, 2005) Ms. No. O-14

ON THE EXTRINSIC PIEZOELECTRICITY

A. KOPAL[a3], P. MOKRÝ[a], J. FOUSEK[ab] and T. BAHNÍK[a]

[a]Dept. of Physics, Technical University, CZ-46117 Liberec, Czech Republic
[b]Materials Research Laboratory, Pennsylvania State University, State College, PA 16801

Abstract

This work presents a continuation of our last paper, concerning the theory of the response of an antiparallel domain structure in a plate-like electroded sample to external electric field. The theory is based on the exact formula for free energy of the system, formed of a central ferroelectric part, isolated from electrodes (with a defined potential difference) by a surface layers. Our calculations are applicable also to thin films. It is usual to use the term 'extrinsic' for the contribution of domain walls displacement to macroscopic properties of a sample. In our last paper we discussed the extrinsic contribution to permittivity. In this work we concentrate on extrinsic contribution to piezoelectric coefficients in ferroelectrics which are simultaneously ferroelastics. As an example, we calculate the extrinsic contribution to d_{36} piezoelectric coefficient of RbH_2PO_4, that was recently measured in a wide range of temperature below Curie point.

Keywords: Ferroelectric domains; extrinsic contributions to piezoelectricity

B.1. INTRODUCTION

Samples of ferroelectric single crystals often posses a surface layers. Its existence greatly influences properties of bulk samples[B1,2,3,4] as well as of thin films.[B5] Equilibrium domain structure in the system, mentioned above in the abstract, and the role of the surface layers was first discussed by Bjorkstam and Oettel[B6] in a special case of shorted electrodes. In our recent paper[B7] we reconsidered this problem in a general case of nonzero voltage between electrodes, discussing the response of the domain structure to external electric field. Our calculations are valid also for thin films and present, in fact, continuation of our discussion of domain structures of thin films[B8].

In[B7] we used our theoretical results for prediction of extrinsic contribution to permittivity of the sample. In the next two sections we give a short review of notation, description of the model and basic results from[B7]. In last two sections we discuss as an example the extrinsic contribution to d_{36} piezoelectric coefficient of RbH_2PO_4. We compare our predictions with the recent measurements of record values $\sim 4000\,\mathrm{pC/N}$ in temperature range 35 K under critical temperature 146 K[B9] (see also[B10]).

B.2. DESCRIPTION OF THE MODEL

We consider a plate-like electroded sample of infinite area with major surfaces perpendicular to the ferroelectric axis z. Central ferroelectric part with antiparallel domains (2.) is separated from the electrodes (0.), (4.) by nonferroelectric layers (1.),(3.) (see Fig. B.1). The spatial distribution of the electric field $\boldsymbol{E}$ is determined by the applied potential difference $V = \varphi^{(4)} - \varphi^{(0)}$ and by the bound charge $\mathrm{div}\boldsymbol{P}_0$ on the boundary of ferroelectric material, where $\boldsymbol{P}_0$ stands for spontaneous polarization. Geometrical, electrical and material parameters of the system are shown in Fig. B.1.

[3]e-mail: antonin.kopal@vslib.cz

We further introduce the symbols

$$c = \sqrt{\varepsilon_a/\varepsilon_c},$$
$$g = \sqrt{\varepsilon_a\,\varepsilon_c},$$

and several geometrical parameters: the slab factor

$$B = \frac{d}{h},$$

the domain pattern factor

$$R = \frac{\pi h}{2a}, \quad 2a = a_+ + a_-,$$

and the asymmetry factor

$$A = \frac{a_+ - a_-}{a_+ + a_-}\,.$$

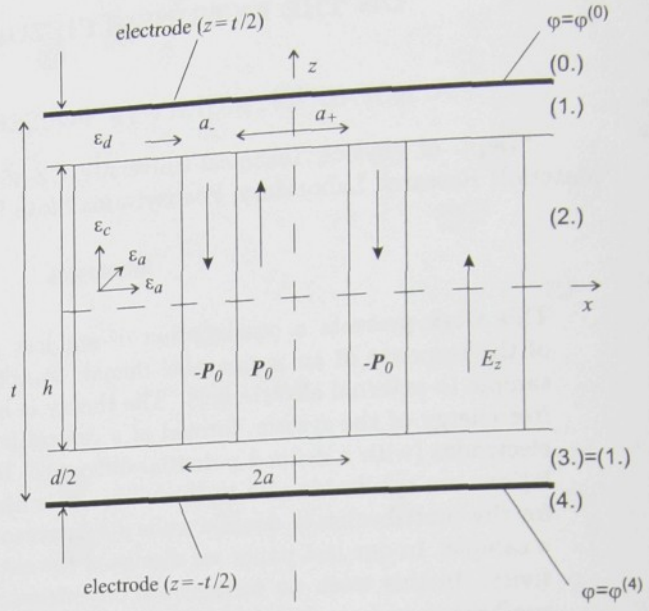

FIGURE B.1: Geometry of the model

The ferroelectric material itself is approximated by the equation of state

$$D_x = \varepsilon_0\varepsilon_a E_x,$$
$$D_z = \varepsilon_0\varepsilon_c E_z + P_0,$$

where P_0 is the spontaneous polarization along the ferroelectric axis. This linear approximation limits the validity of our calculations to the temperature region not very close below the transition temperature T_c. Domain walls are assumed to have surface energy density σ_w and zero thickness.

B.3. GIBBS ELECTRIC ENERGY OF THE SYSTEM, EQUILIBRIUM DOMAIN STRUCTURE

Rather cumbersome calculations[B7] lead to the following formula for Gibbs electric energy per unit area of the system (in $\mathrm{J\,m^{-2}}$)

$$G = \frac{2}{\pi}\sigma_w R + P_0 A\,\frac{P_0 A\,Bt - 2\varepsilon_0\varepsilon_d V\,(1+B)}{2\varepsilon_0\,(1+B)\,(\varepsilon_d + B\,\varepsilon_c)} + \frac{4P_0^2 t}{\varepsilon_0\pi^2 R(1+B)}\sum_{n=1}^{\infty}\frac{\sin^2\left(n\pi(1+A)/2\right)}{n^3(\coth nBR + g\coth nRc)}\,. \tag{B.1}$$

The first term represents domain wall contribution while the last one is the depolarization energy. In the second term we recognize the effect of layers (1.) and (3.) and of the applied voltage.

In this model we neglect the mechanical interactions between components of the system. For given slab factor B and voltage V, the equilibrium domain structure, characterized by $R_{\mathrm{eq}}(V)$ and $A_{\mathrm{eq}}(V)$, corresponds to local minimum of G. In general a minimum can be found by numerical methods, but for $BR \gg 1$ and $Rc \gg 1$, the $R_{\mathrm{eq}}(V)$ and $A_{\mathrm{eq}}(V)$ can be approximated by explicit formulae. For purpose of this paper we use the following formula for $A_{\mathrm{eq}}(V)$

$$A_{\mathrm{eq}}(V) \cong \frac{\varepsilon_0 V}{tP_0}\left[\frac{B}{\varepsilon_d(1+B)} - X\right]^{-1} \tag{B.2}$$

where

$$X = \frac{2\ln 2\,(1 + B\varepsilon_c/\varepsilon_d)}{R^0_{\mathrm{eq}}\,(1+B)(\varepsilon_d + \sqrt{\varepsilon_a\,\varepsilon_c})}$$

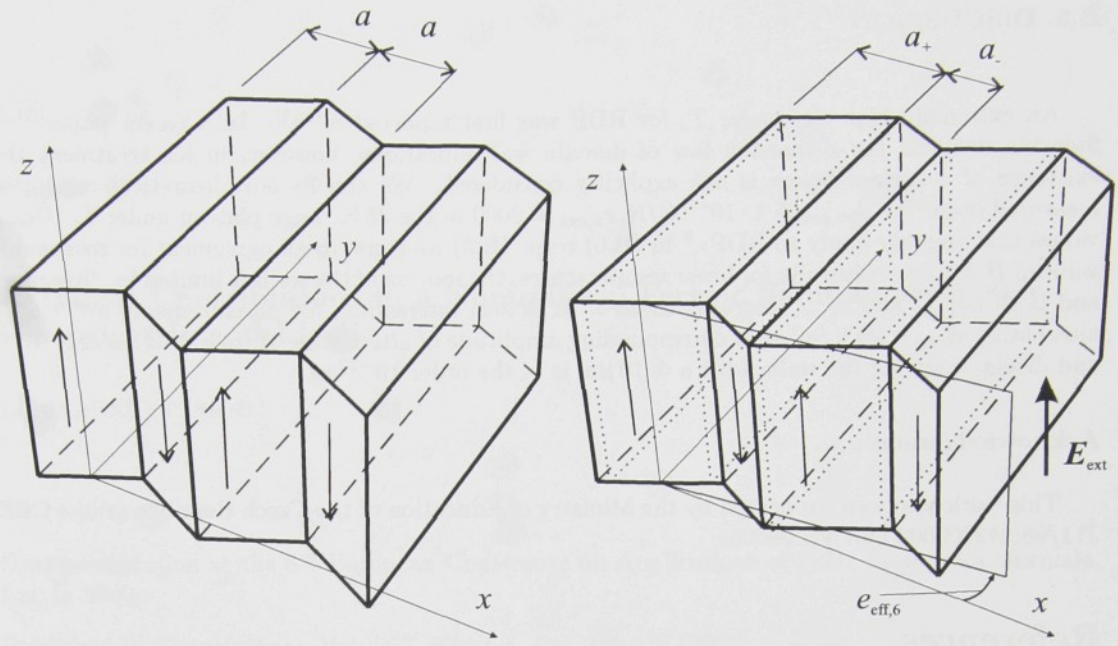

FIGURE B.2: Symmetric domain structure with spontaneous strain $e_{0,6}$, (a) $E_{\text{ext}} = 0, A = 0$, (b) $E_{\text{ext}} \neq 0, A \neq 0$

is considered as a small correction and R^0_{eq} is equilibrium value of R for zero voltage V. For the extrinsic contribution to permittivity of the sample we get from (B.2) (see also[B7])

$$\varepsilon_{\text{ext}} = \left\{ \left(1 + B \frac{\varepsilon_c}{\varepsilon_d} \right) \left[\frac{B}{(1+B)\,\varepsilon_d} - X \right] \right\}^{-1} \tag{B.3}$$

B.4. EXTRINSIC PIEZOELECTRICITY

As an example, in this section we work out the approximate prediction of extrinsic contribution to d_{36} of RbH_2PO_4 (RDP), based on our simple model. RDP is a ferroelastic with spontaneous strain $e_{0,6}$, opposite in opposite polarized domains. In the Fig.B.2a there is $x - y$ cut through symmetric domain structure ($A = 0$, $E_{\text{ext}} = V/t = 0$). The situation after application of E_{ext} is shown in Fig.B.2b ($A \neq 0$). A simple geometric consideration leads to the formula for average strain $e_{\text{eff},6}$ of the sample (we neglect the mechanical coupling of the central part with the rest of the sample)

$$e_{\text{eff},6} = e_{0,6} A \tag{B.4}$$

For the extrinsic coefficient d_{36} we get from (B.2) and (B.4)

$$d_{36} \equiv \frac{e_{\text{eff},6}}{E_3} = \frac{\varepsilon_0 e_{0,6}}{P_0} \left[\frac{B}{(1+B)\,\varepsilon_d} - X \right]^{-1} \tag{B.5}$$

neglecting the small X and for $B \ll 1$ we get more simple formula[4]

$$d_{36} = \frac{\varepsilon_0 \varepsilon_d e_{0,6}}{P_0 B} \,. \tag{B.6}$$

[4]The limit $B \to 0$ in (B.6) is not correct, because the assumptions needed for validity of (B.2) are violated if B is very small.

B.5. DISCUSSION

An extremely high d_{36} under T_c for RDP was first reported in[B11]. In a recent paper[B12], Sidorkin deduced the dispersion law of domain wall vibrations, however, in his treatment the existence of a surface layers is not explicitly considered. We can fit our theoretical results to measured ones[B9] - $d_{36,ext} \doteq 4 \cdot 10^{-9}\,\mathrm{C/N}, \varepsilon_{z,ext} = 2000$ in the 35 K range plateau under T_c. Using values that roughly apply to RDP: [5] in (B.6) resp. (B.3) we come to an agreement for reasonable value of $B \doteq 0.04$. Naturally for lower temperatures, the motion of the walls is limited by "freezing" and both $d_{36,ext}$ and $\varepsilon_{z,ext}$ decrease to zero. It is also interesting, for measurements in[B9] with alternating $E_{ext} \doteq 20\,\mathrm{V/m}$, that corresponding amplitude of alternating A from (B.2) is only 10^{-5} and displacement of the walls with $a \doteq 10\,\mu\mathrm{m}$ is of the order $10^{-10}\,\mathrm{m}$.

Acknowledgements

This work has been supported by the Ministry of Education of the Czech Republic grants CEZ: J11/98:242200002 and VS 96006.

References

[B1] R. C. Miller and A. Savage, *J. Appl. Phys.* **32** (1961).
[B2] M. E. Drougard and R. Landauer, *J. Appl..Phys* **30** (1959).
[B3] H. E. Müser, W. Kuhn and J. Albers, *Phys. Stat. Sol.(a)* **49** (1978).
[B4] D. R. Callaby, *J. Appl. Phys.* **36** (1965).
[B5] A. K. Tagantsev, C. Pawlaczyk, K. Brooks and N. Setter, *Integrated ferroelectrics* **4** (1994).
[B6] J. L. Bjorkstam and R. E. Oettel, *Phys. Rev.* **159** (1967).
[B7] A. Kopal, P. Mokrý, J. Fousek, T. Bahnik, to appear in Ferroelectrics.
[B8] A. Kopal, T. Bahník and J. Fousek, *Ferroelectrics* **202** (1997).
[B9] M. Štula, J. Fousek, H. Kabelka, M. Fally and H. Warhanek, *J. Kor. Phys. Soc. (Proc. Suppl.)* **32** (1998).
[B10] E. Nakamura, *Ferroelectrics* **135** (1992).
[B11] L. A. Shuvalov, I. S. Zheludev, A. V. Mnatskanyan and Ts.-Zh. Ludupov, I. Fiala, *Bull. Acad. Sci. USSR, Phys. Ser.* **31** (1967).
[B12] A. S. Sidorkin, *J. Appl. Phys.* **83** (1998).

[5] $P_0 = 4 \cdot 10^{-2}\mathrm{C/m^2}, \varepsilon_d \doteq \varepsilon_c \doteq 100, e_{0,6} \doteq 0.015$, see[B9].

Paper C

Extrinsic Contributions in a Nonuniform Ferroic Sample: Dielectric, Piezoelectric and Elastic

(Revised version)

Oral presentation at the 5th European Conference on Applications of Polar Dielectrics, Jurmala, Latvia 2000.

Published in *Ferroelectrics*, Vol. 257, No. 1-4, Pg. 211-220 (2001)

List of citations

1. A. Kopal, P. Mokrý, Interrelation of domain wall contributions to dielectric, piezoelectric and mechanical properties of a ferroic layer composite sample, *Ferroelectrics* **290**: Pg. 125-131 (2003)
2. L. Burianová, A. Kopal, J. Nosek, Characterization of advanced piezoelectric materials in the wide temperature range, *Materials Science And Engineering B-Solid State Materials For Advanced Technology* **99**(1-3): Pg. 187-191 (2003)
3. T. Sluka and A. Kopal, Extrinsic contributions to macroscopic properties of ferroic layer composites, *Ferroelectrics* (accepted for publication, 2005) Ms. No. O-14

EXTRINSIC CONTRIBUTIONS IN A NONUNIFORM FERROIC SAMPLE: DIELECTRIC, PIEZOELECTRIC AND ELASTIC

P. MOKRÝ[a6], A. KOPAL[a] and J. FOUSEK[ab]

[a]Dept. of Physics, Technical University, CZ-46117 Liberec, Czech Republic
[b]Materials Research Laboratory, The Pennsylvania State University, State College, PA 16801

Abstract

The contribution $\Delta\varepsilon$ of extremely small motions of domain walls to small-signal permittivity of a multidomain ferroelectric sample has been a research issue for many years. In ferroelastic ferroelectrics such motions contribute also to their piezoelectric (by Δd) and elastic (by Δs) properties. Data about their simultaneous existence are scarce but those available point to mutual proportionality of $\Delta\varepsilon$, Δd and Δs, as expected. To understand the magnitude of extrinsic contributions, the origin of the restoring force acting on domain walls must be understood. In the present contribution the theory has been developed based on the model of a plate-like sample in which the ferroelectric- ferroelastic bulk is provided with a nonferroic surface layer. Motion of domain walls in the bulk results in a change of electric and elastic energy both in the bulk and in the layer, which provides the source of restoring force. This makes it possible to determine all mentioned extrinsic contributions. We discuss the applicability of the model to available data for single crystals and also for ceramic grains.

Keywords: Extrinsic permittivity, extrinsic piezoelectricity, extrinsic elastic moduli, surface layer

C.1. INTRODUCTION

The problem of extrinsic (domain wall) contributions has been addressed by many authors, both experimentally and theoretically. In the prevailing number of cases, only extrinsic permittivity has been studied. For piezoelectric ceramics, Arlt et al.[C1] were the first to address the problem of wall contributions to all involved properties: permittivity ε, elastic compliances s and piezoelectric coefficients d. In this and related papers, the existence of the restoring force is assumed and its origin was not specified. Later, Arlt and Pertsev[C2] offered a more involved approach: when domain wall in a ceramic grain is shifted, uncompensated bound charge appears on the grain boundary, producing electric field. Simultaneously, if the involved domains are ferroelastic, a wall shift results in mechanical stress in surrounding grains. Thus the shift is accompanied by the increase of both electric and elastic energies, leading to restoring forces. Results of these theories have been successfully related to experimental data on all three mentioned contributions: $\Delta\varepsilon$, Δs and Δd.[C1,2]

While there exist a number of such data for ceramic materials[C1,3,4], information for single crystals is rather scarce. Understandably, for nonferroelastic ferroelectrics such as TGS only data on $\Delta\varepsilon$ are available;[C5] on the other hand for crystals which are both ferroelectric and ferroelastic with more than two domain states, dense domain systems are rather chaotical, difficult to approach theoretically. In the present paper, we have in mind ferroelectric and ferroelastic crystals with only two domain states. In particular, crystals belonging to the KH_2PO_4 family belong to this category and have been intensively studied. Nakamura et al.[C6,7] determined $\Delta\varepsilon_{33}$ for KH_2PO_4, CsH_2PO_4 and CsH_2AsO_4. For KH_2PO_4, Nakamura and Kuramoto[C8] proved the existence of both $\Delta\varepsilon_{33}$ and Δs_{66} while Δd_{36} was measured for RbH_2PO_4[C9]. For the same material, all quantities $\Delta\varepsilon_{33}$, Δd_{36} and Δs_{66} have been measured by Štula et al.[C10] It was found that all these contributions are

[6]e-mail: pavel.mokry@vslib.cz

mutually proportional when measured as a function of temperature, in the temperature interval between T_C and T_C-35 K. Several other ferroics for which our approach may be applicable will be mentioned at the end of this paper.

In single crystals, the origin of the restoring force is usually connected to domain wall pinning on crystal lattice defects. In our recent papers[C11,12] we introduced the model of a passive surface layer to calculate the restoring force for domain walls and the resulting extrinsic permittivity and piezoelectric coefficient. In fact, the influence of a surface layer on the properties of a ferroelectric sample was discussed repeatedly several decades ago. In particular, in connection with the sidewise motion of domain walls in $BaTiO_3$, thickness dependence of the coercive field, asymmetry of a hysteresis loop or the problem of energies of critical nuclei, theoretically impossibly high.

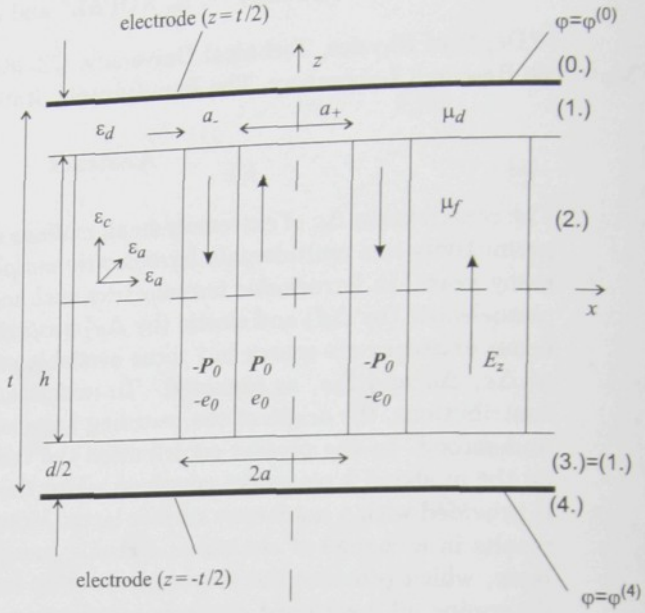

FIGURE C.1: Geometry of the model in x-z plane

In the present paper, we return to this approach. However, in contrast to previous calculations, we offer a more involved model. The shift of a domain wall induced by the application of electric field or elastic stress results in the increase of *both* electric and elastic energies. In the following, these are explicitly calculated which makes it possible to determine all extrinsic coefficients $\Delta\varepsilon_{33}$, Δs_{66} and Δd_{36}. Their dependence on the sample properties will be discussed.

C.2. DESCRIPTION OF THE MODEL

We consider a plate-like sample elecroded sample of infinite area with major surfaces perpendicular to the ferroelectric axis z. The material is both ferroelectric and feroelastic; domains with antiparallel polarisation differ in the sign of spontaneous shear. However, we shall approximate the material in the ferroelectric phase by the equation of state

$$\begin{aligned} D_x &= \varepsilon_0 \varepsilon_a E_x, \\ D_z &= \varepsilon_0 \varepsilon_c E_z + P_0, \end{aligned}$$

neglecting the intrinsic piezoelectricity. As we shall see, this does not supress the existence the extrinsic piezoelectricity, which is one of the aims of our calculations. In the preceding equation, we also neglect nonlinear terms; for 2nd order phase transitions this limits the validity of our calculations to the temperature region not

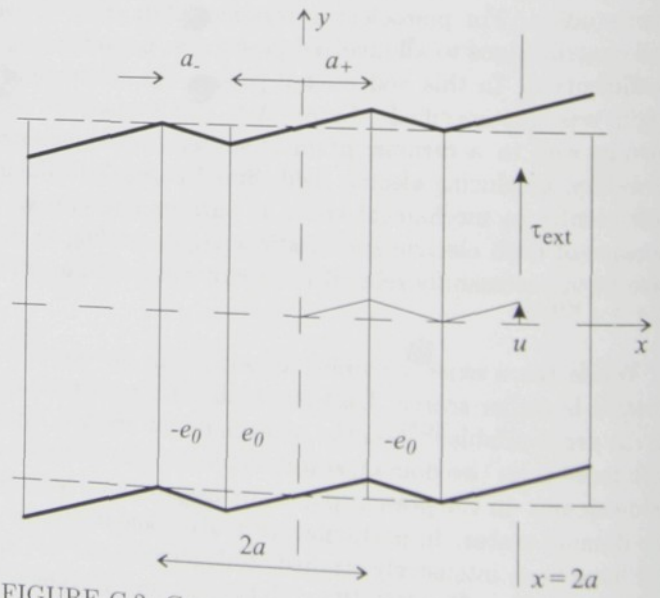

FIGURE C.2: Geometry of the model in x-y plane

very close bellow the temperature T_C. Domain walls are assumed to have surface energy density σ_w and zero thickness.

For simplicity, we approximate elastically anisotropic material of the sample by the elastically isotropic one. Neglecting again the intrinsic piezoelectricity, its mechanical properties are described by equations for stress tensor components

$$\begin{aligned} \tau_{ij}^{(1)} &= 2\mu_d e_{ij}^{(1)}, \\ \tau_{ij}^{(2)} &= 2\mu_f \left(e_{ij}^{(2)} - e_{0,ij} \right), \end{aligned}$$

where μ_d and μ_f are Lame coefficients of the passive layers and the bulk respectively; e_{ij} is the strain tensor, $e_{0,ij}$ is the spontaneous strain tensor of the central ferroelastic part. We suppose that the only nonzero components of the spontaneous strain tensor are $e_{0,12} = e_{0,21} = \pm e_0$ in the a_+ resp. a_- domain, see Fig. C.2. We introduce the asymmetry factor

$$A = \frac{a_+ - a_-}{a_+ + a_-}.$$

We neglect thermal interactions and suppose that the sample is thermally isolated. To keep the constant voltage V on the sample, the electrodes should be connected to external electrical source. In the same way, to keep constant external stress $\tau_{\mathrm{ext},12} = \tau_{\mathrm{ext}}$, the sample should be deformed by external mechanical force. The infinitesimal work of these external sources should be taken into consideration when discussing the variations of the energy of the isolated system sample + sources.

C.3. HELMHOLTZ FREE ENERGY

In what follows we consider three contributions to Helmholtz free energy, calculated per unit area of the plate-like sample (in the x-y plane):

The energy of domain walls per unit area of the sample

$$U_w = \sigma_w \, h/a \qquad \left[\mathrm{J \cdot m^{-2}}\right],$$

the electric field energy per unit area of the sample

$$U_{\mathrm{el}}(V,\, A) = \frac{1}{2} \int_V E_i \, (D_i - P_{0,i}) \, \mathrm{d}V,$$

where the integration is taken over parallelepiped $x \in \langle 0,\, 2a \rangle$, $z \in \langle -t/2,\, t/2 \rangle$, $y \in \langle 0,\, 1\,\mathrm{m}^2/2a \rangle$, and energy of elastic deformations per unit area of the sample:

$$\begin{aligned} U_{\mathrm{def}}(\tau_{\mathrm{ext}},\, A) &= \frac{1}{2} \int_V \tau_{ij} \, (e_{ij} - e_{0,ij}) \, \mathrm{d}V, \qquad \text{resp.} \\ U_{\mathrm{def}}(u,\, A) &= \frac{1}{2} \int_V \tau_{ij} \, (e_{ij} - e_{0,ij}) \, \mathrm{d}V, \end{aligned}$$

where the integration is taken over the same region, in the first case for constant external stress τ_{ext} in the plane $x = 2a$, in the second one for constant displacement u in the plane $x = 2a$. In both cases, the displacement for $x = 0$ is chosen to be zero and the boundaries of the sample in x-y plane are free of stress.

To find the U_{el} and U_{def}, we have calculated electric potential and mechanical displacement inside the sample by Fourier method. We present here only the relative simple results for a "dense

pattern approximation", that is for $d,\, h \gg a$:

$$\begin{aligned} U_{\mathrm{el}}(V,\, A) &= \frac{dh\, A^2 P_0^2 + V^2\, \varepsilon_0^2 \varepsilon_d \varepsilon_c}{2\varepsilon_0\, (\varepsilon_d\, h + \varepsilon_c\, d)}, \\ U_{\mathrm{def}}(\tau_{\mathrm{ext}},\, A) &= \frac{ht^2 \mu_f \tau_{\mathrm{ext}}^2}{2\,(\mu_d\, d + \mu_f\, h)^2} + \frac{d\mu_d}{2}\left(2Ae_0 + \frac{t\tau_{\mathrm{ext}}}{\mu_d\, d + \mu_f\, h}\right)^2, \\ U_{\mathrm{def}}(u,\, A) &= \frac{\mu_d d u^2 + \mu_f h\,(2u - 8Ae_0 a)^2}{8a^2}. \end{aligned}$$

Infinitesimal work of the electric source at constant voltage V per unit area of the sample plate is

$$\delta W_{\mathrm{el}} = V\, \delta\sigma_0 \qquad \left[\mathrm{J \cdot m^{-2}}\right],$$

where σ_0 is constant Fourier component of the free charge density on the positive electrode, calculated as

$$\sigma_0(V,\, A) = \frac{P_0 A + \varepsilon_0 \varepsilon_c\, V/h}{1 + \varepsilon_c d/\,(\varepsilon_d h)}. \tag{C.1}$$

Infinitesimal work of the mechanical source, deforming the parallelepiped is

$$\delta W_{\mathrm{def}} = \tau_{\mathrm{ext}}\, t/(2a)\, \delta u \qquad \left[\mathrm{J \cdot m^{-2}}\right],$$

It is easy to prove that the equilibrium domain structure for $V = 0$, $\tau_{\mathrm{ext}} = 0$ resp. $u(x = 2a) = 0$ is symmetric (i.e. A=0), with domain width

$$a_{\mathrm{eq}} = \sqrt{3.68\, h\sigma_w}\left[4e_0^2\, \frac{\mu_d \mu_f}{\mu_d + \mu_f} + \frac{P_0^2}{\varepsilon_0\,\left(\varepsilon_d + \sqrt{\varepsilon_a\, \varepsilon_c}\right)}\right]^{-\frac{1}{2}}. \tag{C.2}$$

It can be shown (see e.g.[C11]) that within a large interval of the applied voltage the average width

$$a = (a_+ + a_-)\,/2$$

remains constant. This is why U_w can be also considered as constant.

C.4. EXTRINSIC CONTRIBUTIONS $\Delta\varepsilon_{33}$, Δs_{66} and Δd_{36}

We calculate the equilibrium effective $\varepsilon_{33}^{\mathrm{eff}}$ of the sample from the relations

$$D_3^{\mathrm{eff}} = \sigma_0(V,\, A) = \varepsilon_{33}^{\mathrm{eff}}\, E_3^{\mathrm{ext}} = \varepsilon_{33}^{\mathrm{eff}}\, \frac{V}{t}. \tag{C.3}$$

We keep $\tau_{\mathrm{ext}} = 0$, V=constant and we take into account that variation of "Helmholtz free energy of the sample + the work of electric source" is zero in equilibrium:

$$\frac{\partial U_{\mathrm{el}}(V,\, A)}{\partial A}\, \delta A + \frac{\partial U_{\mathrm{def}}(\tau_{\mathrm{ext}} = 0,\, A)}{\partial A}\, \delta A - \delta W_{\mathrm{el}} = 0.$$

Solving this standard problem, we get $A = A(V)$ and from the Eqs. (C.1), (C.3) the effective $\varepsilon_{33}^{\mathrm{eff}}$. For $\mu_d = \mu_f = \mu$, $\varepsilon_d = \varepsilon_c = \varepsilon_z$ we obtain the relatively simple result:

$$\varepsilon_z^{\mathrm{eff}} = \varepsilon_z + \varepsilon_z\, \frac{h}{d} \cdot \left[\frac{P_0^2\, h}{P_0^2\, h + 4\, e_0^2\, \varepsilon_0\, \varepsilon_z\, \mu t}\right]. \tag{C.4}$$

TABLE C.1: Numerical estimate of $\Delta\varepsilon_{33}$, Δs_{66} and Δd_{36} for different values of surface layer thickness. The following numerical constants have been used: $P_0 = 4\cdot10^{-2}\,\mathrm{C\,m^{-2}}$, $\varepsilon_z = 100$, $e_0 = 0.015$, $\mu = 6\cdot10^{9}\,\mathrm{Pa}$, $\sigma_w = 5\cdot10^{-3}\,\mathrm{J\,m^{-2}}$, $h = 5\cdot10^{-4}\,\mathrm{m}$.

	$d = 0.5\cdot10^{-6}\,\mathrm{m}$	$d = 2.5\cdot10^{-6}\,\mathrm{m}$	$d = 5\cdot10^{-6}\,\mathrm{m}$
$\Delta\varepsilon_{33}$ [1]	12 000	2 500	1 200
Δd_{36} $[\mathrm{C\,m^{-2}}]$	$4.1\cdot10^{-8}$	$8.3\cdot10^{-9}$	$4.1\cdot10^{-9}$
Δs_{66} $[\mathrm{Pa^{-1}}]$	$1.6\cdot10^{-8}$	$3.2\cdot10^{-9}$	$1.6\cdot10^{-9}$

The effective elastic compliance of the sample is

$$s_{66}^{\mathrm{eff}} = 4s_{1212}^{\mathrm{eff}} = \frac{2e_{12}^{\mathrm{eff}}}{\tau_{\mathrm{ext}}} = \frac{u}{2\,a\,\tau_{\mathrm{ext}}}.$$

We put $V = 0$ (shorted sample), apply constant external shear stress τ_{ext} and postulate, that variation of "Helmholtz free energy of the sample + the work of mechanical source" is zero in equilibrium

$$\frac{\partial U_{\mathrm{el}}(0,\,A)}{\partial A}\,\delta A + \frac{\partial U_{\mathrm{def}}(u,\,A)}{\partial A}\,\delta A - \delta W_{\mathrm{def}} = 0.$$

Solving this problem, we get $u = u(\tau_{\mathrm{ext}})$ and we get for $\mu_d = \mu_f = \mu$, $\varepsilon_d = \varepsilon_c = \varepsilon_z$:

$$s_{66}^{\mathrm{eff}} = \frac{1}{\mu} + \frac{1}{\mu}\cdot\frac{h}{d}\left[\frac{4\,e_0^2\,\varepsilon_0\,\varepsilon_z}{(P_0^2/\mu) + 4\,e_0^2\,\varepsilon_0\,\varepsilon_z}\right]. \tag{C.5}$$

To find the effective piezoelectric coefficient of the sample

$$d_{36}^{\mathrm{eff}} = \frac{D_3^{\mathrm{eff}}}{\tau_{\mathrm{ext},6}} = \frac{\sigma_0}{\tau_{\mathrm{ext},6}},$$

we put $V = 0$, apply τ_{ext} and solve the problem

$$\frac{\partial U_{\mathrm{el}}(0,\,A)}{\partial A}\,\delta A + \frac{\partial U_{\mathrm{def}}(u,\,A)}{\partial A}\,\delta A + \frac{\partial U_{\mathrm{def}}(u,\,A)}{\partial u}\,\delta u - \delta W_{\mathrm{def}} = 0.$$

From here we obtain $A = A(\tau_{\mathrm{ext}})$. Inserting this result into Eq. (C.1) we obtain $\sigma_0 = \sigma_0(\tau_{\mathrm{ext}})$. For $\mu_d = \mu_f = \mu$, $\varepsilon_d = \varepsilon_c = \varepsilon_z$ we get finally for the effective piezoelectric coefficient

$$d_{36}^{\mathrm{eff}} = \frac{h}{d}\cdot\left[\frac{2e_0\,P_0\,\varepsilon_0\,\varepsilon_z}{P_0^2 + 4\,e_0^2\,\varepsilon_0\,\varepsilon_z\,\mu}\right]. \tag{C.6}$$

The same result we get for the inverse piezoelectric effect.

C.5. DISCUSSION

The above calculation leads to explicite formulae (C.4) to (C.6) for extrinsic permittivity, extrinsic elastic compliance and extrinsic piezoelectric coefficient, resp. Numerical values for all involved material coefficients are available for single crystals of RbH_2PO_4: $P_0 = 4\cdot10^{-2}\,\mathrm{C\,m^{-2}}$, $\varepsilon_z = 100$, $e_0 = 0.015$ and $\mu = 6\cdot10^{9}\,\mathrm{Pa}$. To obtain numerical estimates for particular samples we put $\sigma_w = 5\cdot10^{-3}\,\mathrm{J\,m^{-2}}$ and $h = 5\cdot10^{-4}\,\mathrm{m}$ and choose three values of surface layer thickness, namely $d = 0.5\cdot10^{-6}\,\mathrm{m}$, $d = 2.5\cdot10^{-6}\,\mathrm{m}$ and $d = 5\cdot10^{-6}\,\mathrm{m}$. Table C.1 shows resulting values of all three extrinsic variables. These numbers appear very realistic and confirm the applicability of the model presented in this paper.

It is appropriate to pay some attention to the fact that also the formula (C.2) gives a reasonable numerical estimation for the width of equilibrium domain pattern. With numerical values specified at Tab. C.1 we obtain $a_{\mathrm{eq}} \cong 1\,\mu\mathrm{m}$.

In the approach analyzed above, the source of the restoring force acting on domain walls is the interaction of ferroic sample with a passive surface layer. Very often, the origin of restoring forces is connected with domain wall pinning to defects. Understandably, the latter mechanism cannot be excluded for ferroics of any chemical composition. On the other hand, passive surface layers can be formed during sample preparations and in particular for water-soluble crystals their appearance is a very likely: samples are polished in water-containing media, the procedure obviously leading to the presence of a passive surface layer. The example analyzed numerically above, crystals of RbH_2PO_4, falls into this category. However, extrinsic properties of a number of other crystals have been studied. Thus, e.g., for $LiTlC_4H_4O_6 \cdot H_2O$ (species 222-$P\varepsilon ds$-2_y) [C13] very strong and nonhysteretic dependence of s_{44}^E as a function of applied field E was measured. This is possible to explain by a strong contribution of domain walls with a pronounced restoring force. The above model would lead to such behavior. Similarly, large extrinsic contributions to s_{11} have been measured[C14] for $(NH_4)_4LiH_3(SO_4)_4$, species 4-εds-2.

Acknowledgements

This work has been supported by the Ministry of Education of the Czech Republic (Projects No. VS 96006 and No. MSM 242200002) and by the Grant Agency of the Czech Republic (Project No. 202/00/1245).

References

[C1] G. Arlt and H. Dederichs, *Ferroelectrics* **29** (1980) 47.
[C2] G. Arlt and N. A. Pertsev, *J. Appl. Phys.* **70** (1991) 2283.
[C3] Q. M. Zhang, W. Y. Pan, S. J. Jang and L. E. Cross, *J. Appl. Phys.* **64** (1988) 6445.
[C4] Q. M. Zhang, H. Wang, N. Kim and L. E. Cross, *J. Appl. Phys.* **75** (1994) 454.
[C5] J. Fousek, Z. Málek, A. J. Salim and N. S. Al Ali: *Proc. Phys. Soc.* **80** (1962) 1199.
[C6] E. Nakamura *Ferroelectrics* **135** (1992) 237.
[C7] E. Nakamura, K. Deguchi, K. Kuramoto, I. Hirata, T. Ozaki and J. Ogami, *Ferroelectrics* **143** (1993) 157.
[C8] E. Nakamura and K. Kuramoto, *J. Phys. Soc. Jpn.* **57** (1988) 2182.
[C9] L. A. Shuvalov, I. S. Zheludev, A. V. Mnatskanyan and Ts. Zh. Ludupov, *Bull. Acad. Sci. USSR, Phys. Series* **31** (1967) 1963.
[C10] M. Štula, J. Fousek, H. Kabelka, M. Fally and H. Warhanek, *J. Korean Phys. Soc.* **32** (1998) S758.
[C11] A. Kopal, P. Mokrý, J. Fousek and T. Bahník, *Ferroelectrics* **223** (1999) 127.
[C12] A. Kopal, P. Mokrý, J. Fousek and T. Bahník, *Ferroelectrics* **238** (2000) 203.
[C13] E. Sawaguchi and L. E. Cross, *Appl. Phys. Letters* **18** (1971) 1.
[C14] M. D. Zimmermann and W. Schranz, *Ferroelectrics* **190** (1997) 99.

Paper D

Interrelation of domain wall contributions to dielectric, piezoelectric and mechanical properties of a ferroic layer composite sample

(Revised version)

Invited talk at the 7th International Symposium on Ferroic Domains and Mesoscopic Structures, Giens, France, Sept. 2002,

Published in *Ferroelectrics*, Vol. 290, No. 1-4, Pg. 125-131 (2001)

INTERRELATION OF DOMAIN WALL CONTRIBUTIONS TO DIELECTRIC, PIEZOELECTRIC AND MECHANICAL PROPERTIES OF A FERROIC LAYER COMPOSITE SAMPLE

A. KOPAL[7] and P. MOKRÝ

Dept. of Physics, International Center for Piezoelectric Research, Technical University, CZ-46117 Liberec, Czech Republic

Abstract

Interrelations of domain wall (extrinsic) contributions to dielectric, piezoelectric and mechanical properties of ferroic samples are a hot subject of both theoretical and experimental research. Recently,we have derived theoretical formulas for such contributions, using model of composite layer sample: central single-crystal ferroelectric-ferroelastic layer, isolated from electrodes by passive layers. Here we present more general results, discussing the dependence of the contributions on geometric and material parameters of the composite and including in a special case intrinsic piezoelectricity. We also discuss the above-mentioned interrelation and compare our results with measurements of all the contributions on the same RDP sample in a wide temperature interval under the phase transition. It seems that both calculated and observed results remind of the so called Pippard-Janovec thermodynamic relations.

Keywords: Ferroic layer composite, extrinsic contributions, piezoelectricity

D.1. INTRODUCTION

The problem of extrinsic contributions to dielectric, piezoelectric and mechanical properties has been addressed by many authors. In prevailing number, only extrinsic permittivity has been studied. Arlt et al. [D1,2] and Herbiet *et al.* [D3] were the first, who addressed the domain wall contributions to all involved properties: permittivity ε, elastic compliance s and piezoelectric coefficient d in piezoelectric ceramics (see also a later work of Zhang *et al.* [D4]). In this paper, we have in mind ferroelectric and ferroelastic crystals with only two domain states, in particular, the KH_2PO_4 family. In our recent papers, we studied the equilibrium domain structure in thin films [D5] and equilibrium contributions to permittivity [D6], piezoelectric coefficient [D7] and to all these properties including elastic compliance [D8]. In these papers [D6,7,8] we have used the model of passive layers (ferroic layer composite), theoretically discussed first by Fedosov and Sidorkin [D9], then developed by Tagantsev *et al.* [D10] and Bratkovsky and Levanyuk [D11,12].

In this paper we shall concentrate on following questions: how the geometric and material parameters of the composite effect the extrinsic contributions, and what is the mutual relation of contributions to ε, s and d on the same sample.

In the following sections, we first introduce the model and basic symbols for geometric and material properties of the sample. Then we recapitulate briefly our method of theoretical derivation of equilibrium extrinsic contributions, described in detail in [D8]. Afterwards, we shall summarize and discuss the new results, mentioned above and try to compare them with experiment. Also, in a special case of equal material properties of both passive and central layers, we include the effect of intrinsic piezoelectricity. These three topics were not discussed in [D8].

[7]e-mail: antonin.kopal@vslib.cz

D.2. MODEL DESCRIPTION

We consider a plate-like electroded sample of infinite area with major surfaces perpendicular to the ferroelectric axis z. Domains with antiparallel spontaneous polarization $P_{0,3} = \pm P_0$ differ in the sign of spontaneous shear $e_{0,12} = \pm e_0$. We suppose that usual linear state equations are valid, including intrinsic piezoelectricity. For simplicity we consider the sample to be elastically isotropic. The geometric parameters, characterizing the sample and domain structure, are shown in Figs. D.1 and D.2.

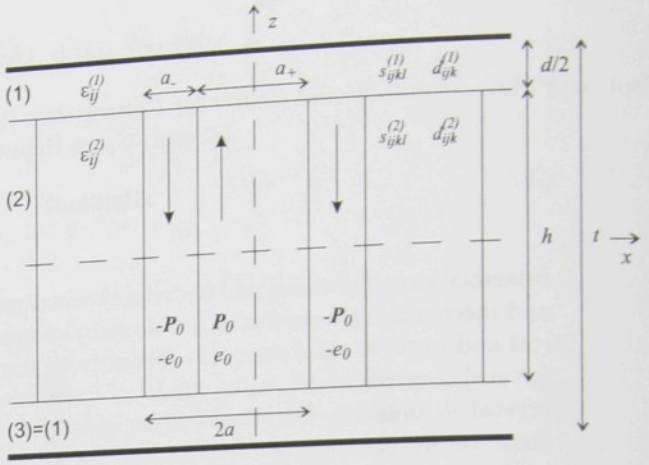

FIGURE D.1: Geometry of the model in $x - z$ plane.

We introduce the following symbols $\varepsilon_{33}^{(1)}$, the component of relative permittivity of the passive layer; $\varepsilon_{33}^{(2)}$, the same component for the central ferroic layer; $s_{1212}^{(1)}$ and $s_{1212}^{(2)}$, the shear component of the compliance tensor of the passive and central ferroic layers, respectively; $d_{312}^{(1)}$ and $d_{312}^{(2)}$, the piezoelectric coefficient of the passive and central ferroic layers, respectively; a_+ resp. a_-, the width of the corresponding domain; $2a$, the period of the domain structure; d, the total width of the passive layers; h, the width of the central layer; u, the shear displacement at $x = 2a$; $\tau = \tau_{12ext}$, the external shear stress acting on the sample; V, the external voltage on the electrodes; $A = (a_+ - a_-)/(a_+ + a_-)$, the asymmetry factor of the domain structure, expressing the displacement of the domain walls from the symmetric position.

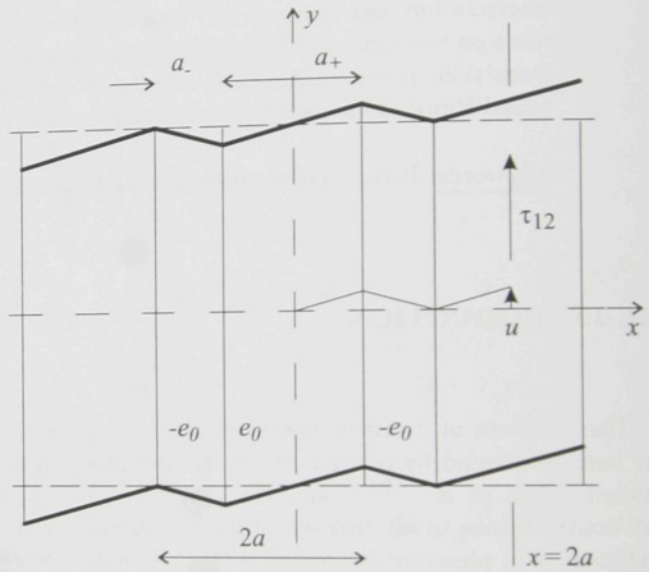

FIGURE D.2: Geometry of the model in $x - y$ plane.

D.3. EFFECTIVE PARAMETERS OF THE SAMPLE

In this short article, it is not possible to reproduce the whole process of derivation of effective equilibrium permittivity $\varepsilon_{33}^{\text{eff}}$ at zero external stress, compliance s_{1212}^{eff} at zero voltage V, and piezocoefficient d_{312}^{eff} of the sample. The process is based on the calculation of the total energy density U of the sample, i.e., electrostatic energy, deformation energy and domain walls energy per unite surface area of the sample in the $x - y$ plane, as a function of free parameters A, V and u resp. τ. In equilibrium, the variation of the total energy of the isolated system: *sample* + *electric source* + *mechanical source* is zero. Solving this standard problem, we can find the equilibrium reaction of the sample on external voltage or stress. The process is described in [D8] and we shall prepare more detailed publications in this direction.

Because of great complexity of the problem, we shall use the "thick sample" approximation, valid when

$$h,\, d \gg a. \tag{D.1}$$

In this case, we can neglect all higher Fourier components of the tensor of deformation and electric field, except the constant one. Nevertheless, the formulas for effective parameters are still very complex because of the intrinsic piezoelectricity. If this is neglected, we get reasonably simple and symmetric results:

$$\varepsilon_{33}^{\mathrm{eff}} = \varepsilon_{33}^{(1)} \frac{t}{d} \frac{P_0^2 \left(s_{1212}^{(2)} d + s_{1212}^{(1)} h\right) + e_0^2 \varepsilon_0 \varepsilon_{33}^{(2)} d}{e_0^2 \varepsilon_0 \left(\varepsilon_{33}^{(2)} d + \varepsilon_{33}^{(1)} h\right) + P_0^2 \left(s_{1212}^{(2)} d + s_{1212}^{(1)} h\right)}, \tag{D.2}$$

$$s_{1212}^{\mathrm{eff}} = s_{1212}^{(1)} \frac{t}{d} \frac{e_0^2 \varepsilon_0 \left(\varepsilon_{33}^{(2)} d + \varepsilon_{33}^{(1)} h\right) + P_0^2 s_{1212}^{(2)} d}{e_0^2 \varepsilon_0 \left(\varepsilon_{33}^{(2)} d + \varepsilon_{33}^{(1)} h\right) + P_0^2 \left(s_{1212}^{(2)} d + s_{1212}^{(1)} h\right)}, \tag{D.3}$$

$$d_{312}^{\mathrm{eff}} = s_{1212}^{(1)} \varepsilon_{33}^{(1)} \frac{h}{d} \frac{e_0 P_0 \varepsilon_0 t}{e_0^2 \varepsilon_0 \left(\varepsilon_{33}^{(2)} d + \varepsilon_{33}^{(1)} h\right) + P_0^2 \left(s_{1212}^{(2)} d + s_{1212}^{(1)} h\right)}. \tag{D.4}$$

For thin films, when condition (D.1) does not hold, numerical methods should be applied.

In the homogeneous composite case $\varepsilon_{33}^{(1)} = \varepsilon_{33}^{(2)} = \varepsilon_{33}$, $s_{1212}^{(1)} = s_{1212}^{(2)} = s_{1212}$, $d_{312}^{(1)} = d_{312}^{(2)} = d_{312}$, we need not to neglect intrinsic piezoelectricity and results are still very simple and symmetric:

$$\varepsilon_0 \varepsilon_{33}^{\mathrm{eff}} = \varepsilon_0 \varepsilon_{33} + \frac{h}{d} \frac{P_0^2}{P_0^2/(\varepsilon_0 \varepsilon_{33}) + e_0^2/s_{1212} + P_0 e_0/d_{312}}, \tag{D.5}$$

$$s_{1212}^{\mathrm{eff}} = s_{1212} + \frac{h}{d} \frac{e_0^2}{P_0^2/(\varepsilon_0 \varepsilon_{33}) + e_0^2/s_{1212} + P_0 e_0/d_{312}}, \tag{D.6}$$

$$d_{312}^{\mathrm{eff}} = d_{312} + \frac{h}{d} \frac{e_0 P_0}{P_0^2/(\varepsilon_0 \varepsilon_{33}) + e_0^2/s_{1212} + P_0 e_0/d_{312}}. \tag{D.7}$$

D.4. DISCUSSION

Equations (D.2)-(D.4) express the dependence of sample effective parameters on both material and geometric parameters of the layer composite. At first, we can mention that for homogeneous composite, these relations transform to (D.5)-(D.7), without the terms containing d_{312}. Intrinsic piezoelectricity is neglected in equations (D.2)-(D.4). Second, we can find the effective parameters of the ferroic sample with thick metal electrodes and without dielectric passive layers, taking the limit of infinite $\varepsilon_{33}^{(1)}$ in (D.2)-(D.4). Third, the denominator on the right in discussed relations is the same and we can easily express the ratio of effective parameters.

Now, we can explore the limits $e_0 \to 0$ (pure ferroelectric) or $P_0 \to 0$ (pure ferroelastic). In the first case we get

$$\varepsilon_{33}^{\mathrm{eff}} = \varepsilon_{33}^{(1)} t/d, \tag{D.8}$$

$$s_{1212}^{\mathrm{eff}} = \frac{s_{1212}^{(1)} s_{1212}^{(2)} t}{s_{1212}^{(2)} d + s_{1212}^{(1)} h}. \tag{D.9}$$

In equation (D.8), we find the simple result that domainwalls motion is nownot damped by mechanical interaction with passive layers, as reported in [D6]. In Eq. (D.9) we can easily recognize the pure intrinsic compliance of the composite, without any extrinsic contribution. In the second case we get

$$\varepsilon_{33}^{\text{eff}} = \frac{\varepsilon_{33}^{(1)}\varepsilon_{33}^{(2)}t}{\varepsilon_{33}^{(2)}d + \varepsilon_{33}^{(1)}h}. \tag{D.10}$$

$$s_{1212}^{\text{eff}} = s_{1212}^{(1)}t/d. \tag{D.11}$$

Now we have got an inverse situation: in equation (D.10), there is pure intrinsic permittivity, without any extrinsic contribution, while equation (D.11) is a simple formula that can be implicitly found in [D8]. Naturally, $d_{312}^{\text{eff}} = 0$ in both limits. We should mention, that simple limit $d \to 0$ in equations (D.8) and (D.11) does not work, because condition (D.1) for the thick sample approximation is violated. In the general case, $P_0 \neq 0$, $e_0 \neq 0$, the effective permittivity and compliance take the value in the corresponding intervals (D.10) to (D.8), or (D.9) to (D.11).

Let us now turn to the homogeneous case of equations (D.5)-(D.7), where intrinsic piezoelectricity is included. First, we can see that intrinsic and extrinsic contributions are now explicitly separated.We denote the extrinsic contributions $\Delta\varepsilon_0\varepsilon$, Δs, Δd. The interrelation of the contributions is now rather simple:

$$\Delta\varepsilon_0\varepsilon : \Delta s : \Delta d = P_0^2 : e_0^2 : e_0 P_0. \tag{D.12}$$

From equation (12), we get the simple condition

$$\frac{\Delta\varepsilon_0\varepsilon\Delta s}{(\Delta d)^2} = 1. \tag{D.13}$$

The authors of Ref. [D13] have measured all three effective parameters on the same RbH_2PO_4 sample in the temperature interval of 90 to 140 K under the critical point, resulting in an experimental value of 1,05 for the ratio in equation (D.13). They have come to the similar result on the base of much more elementary considerations. In [D8], we presented discussion of other facts concerning the agreement of theory and that experiment.

Under the critical temperature of the ferroelectric phase transition, P_0 and e_0 often undergo substantial changes with changing temperature. Nevertheless, their ratio is almost constant in a wide temperature interval. This can be explained by simple physical considerations. The crystals of KDP family undergo the first order phase transition, which is close to the second order one, because discontinuous change of P_0 and e_0 is relatively small. From the Landau-Ginzburg theory that is in a good agreement with experiment in this case, we get that both P_0 and e_0 are proportional to $(T_c - T)^{1/2}$ in the region of temperature T under the critical one T_c. As a result, the ratios in equation (D.12) should remain also constant in this temperature interval. This is fully confirmed by the above-mentioned measurements in Ref. [D13]. The situation here is very similar to that discussed in connection with the so-called Pippard-Janovec relations (see the excellent theoretical work of Janovec (1966) [D14]). It is obvious that the results, expressed by equations (D.12), (D.13), are general and independent on the model. On the other side, results (D.2)-(D.7) are partially characteristic for our model because of the presence of geometric factors a and b and the material factors, characteristic of the passive layers.

Acknowledgements

The authors are indebted to Prof. J. Fousek for valuable information and cooperation and to Prof. V. Janovec for illuminating discussions. This work was supported by the Grant Agency of the Czech Republic, project GAČR 202/00/1245 and by the Ministry of Education of Czech Republic, project MSM 242 200 002.

References

[D1] G. Arlt and N. A. Pertsev, *J. Appl. Phys.* **70**, 2283 (1991).
[D2] G. Arlt and H. Dederichs, *Ferroelectrics* **29**, 47 (1980).
[D3] R. Herbiet, U. Robels, H. Dederichs, and G. Arlt, *Ferroelectrics* **98**, 107 (1989).
[D4] Q. M. Zhang, H. Wang, N. Kim, and L. E. Cross, *J. Appl. Phys.* **75**, 459 (1994).
[D5] A. Kopal, T. Bahník, and J. Fousek, *Ferroelectrics* **202**, 267 (1997).
[D6] A. Kopal, P. Mokrý, J. Fousek, and T. Bahník, *Ferroelectrics* **223**, 127 (1999).
[D7] A. Kopal, P. Mokrý, J. Fousek, and T. Bahník, *Ferroelectrics* **238**, 203 (2000).
[D8] P. Mokrý, A. Kopal, and J. Fousek, *Ferroelectrics* **257**, 211 (2001).
[D9] V. N. Fedosov and A. S. Sidorkin, *Sov. Phys. Solid State* **18**, 964 (1976).
[D10] A. K. Tagantsev, C. Pawlaczyk, K. Brooks, and N. Setter, *Integrated Ferroelectrics* **4**, (1994).
[D11] A. M. Bratkovsky and A. P. Levanyuk, *Phys. Rev. Lett.* **84**, 3177 (2000).
[D12] A. M. Bratkovsky and A. P. Levanyuk, *Phys. Rev. Lett.* **85**, 4614 (2000).
[D13] M. Štula, J. Fousek, H. Kabelka, M. Fally, and H. Warhanek, *J. Kor. Phys. Soc.* **32**, 758 (1998).
[D14] V. Janovec, *J. Chem. Phys.* **45**, 1874 (1966).

Paper E

Size effect on permittivity in ferroelectric polydomain thin films

Published in *Physical Review B*, Vol. 70, No. 17, Pg. 172107

List of citations

1. T. Sluka and A. Kopal, Extrinsic contributions to macroscopic properties of ferroic layer composites, *Ferroelectrics* (accepted for publication, 2005) Ms. No. O-14

SIZE EFFECT ON PERMITTIVITY IN FERROELECTRIC POLYDOMAIN THIN FILMS

P. MOKRÝ[8], and A. K. TAGANTSEV, and N. SETTER

Ceramics Laboratory, Materials Department, EPFL Swiss Federal Institute of Technology, CH-1015 Lausanne, Switzerland

Abstract

The impact of electrode-adjacent passive layers on the small signal dielectric response of a ferroelectric film containing a 180° domain pattern has been analyzed. It is shown that, for a realistic physical situation, the so called *in-series capacitors formula* is still applicable for the description of the dielectric response of this system however with some apparent values of the passive layer permittivity $\varepsilon_{\mathrm{mod}}$, which is a function of parameters of the ferroelectric and the layers. It is also shown that the suppressive effect of the passive layer on the permittivity of the ferroelectric film can be significantly reduced when the permittivity of the ferroelectric is mainly controlled by the extrinsic (domain) contribution.

PACS: 77.55.+f, 77.80.-e, 84.32.Tt, 77.80.Dj

Keywords: Dielectric thin films, capacitors, domain structure

Large dielectric response of ferroelectrics is known to be easily affected by many factors like the electric field, mechanical stress or lattice imperfections. One comes across these phenomena in ferroelectric thin films and ceramics where the dielectric response in the regions close to the film surface or grain boundaries may be essentially reduced due to aforementioned factors. As a result the whole system feels these regions as low dielectric constant (passive) layers inserted in or attached to the high permittivity material. When oriented perpendicular to the applied field, these layers behave as capacitances connected in series to the remaining high permittivity parts of the material and may tremendously decrease the effective permittivity of the material. It is this effect that is presently pleaded guilty for the difference of dielectric constants in thin films [E1].

For the interpretation of suppression effect of the passive layer, one routinely uses the *in-series capacitor formula*. For the description of the out-of-plane capacitance C of a sandwich ferroelectric/dielectric structure of an area A, this formula reads

$$\varepsilon_0 A/C = (h/\varepsilon_f) + (d/\varepsilon_d). \tag{E.1}$$

where h and ε_f are the thickness and permittivity of the ferroelectric layer and d and ε_d are those of the dielectric layer, respectively; $\varepsilon_0 = 8.854 \times 10^{-12}\, F/m$. The real experimental situation always corresponds to the passive layer, which is much thinner than the ferroelectric layer, $h \gg d$. Equation (E.1) describes the capacitance of a parallel plate capacitor containing the sandwich structure, in which electric field is homogeneous in the capacitor plane. Strictly speaking Eq. (E.1) may not work if the dielectric permittivity of the ferroelectric is controlled by the domain contribution. The reason for this is that, in the presence of the passive layer, the domain structure of the ferroelectric will lead to the appearance of inhomogeneous (stray) fields in the vicinity of the layer [E2]. Thus, an important question arises: Can the in-series capacitor formula be applied for the description of the permittivity of ferroelectric/dielectric structures in the case where the permittivity of the ferroelectric is essentially controlled by the domain contribution?

Some theoretical studies that could answer this question were performed in terms of a model of ferroelectric capacitor with a domain pattern and two dielectric layers [E3,4], as shown in Fig. E.1. However, a very important aspect of the problem was neglected in these papers. Namely, the lattice

[8]e-mail: pavel.mokry@vslib.cz

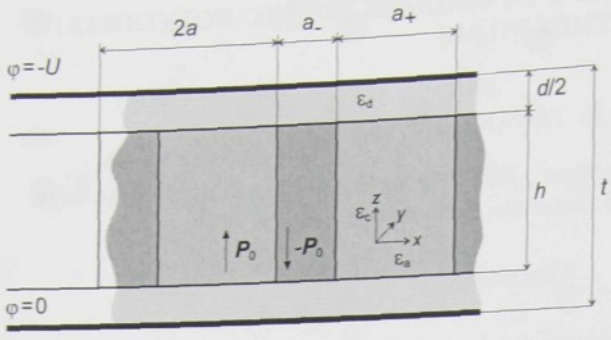

FIGURE E.1: Schema of the electroded ferroelectric film with passive layers. It is always considered that $h \gg d$.

pinning of domain walls in the ferroelectric (due to their coupling with crystalline potentials and defects), which essentially controls the permittivity even in high quality crystals [E5], was ignored. For this reason, the prediction of these papers, an infinite dielectric permittivity in the limit of a vanishing passive layer, is inconsistent with a finite permittivity of any real ferroelectric material. Another simplification made in Refs. [E3,4] is that only the case of the equilibrium 180° domain pattern was considered. This kind of pattern was never experimentally observed in the layered ferrolectric/dielectric structures. In real systems, the domain pattern is expected to be controlled by the prehistory of the sample so that the domain spacing may be essentially different from its equilibrium value. In view of the aforementioned simplifications, the discussion of the problem [E6,4,2] based on results obtained in Refs. [E3,4] cannot be considered as conclusive. Thus, the problem of applicability of in-series capacitor formula to the polydomain situation remained open.

In this letter, we address this problem in terms of the same model as in the previous works (see Fig. E.1), however our analysis is free of the principle simplification adopted in the earlier works - we do not neglect the lattice pinning of the domain walls. We consider the permittivity of the ferroelectric itself as being controlled by the sum of intrinsic and finite domain (extrinsic) contributions. We mean that if the ferroelectric with the given domain pattern were placed in a passive-layer-free capacitor, the permittivity $\varepsilon_f = \varepsilon_c + \varepsilon_m$ would be measured, where ε_c and ε_m are the crystal lattice and extrinsic contributions. In addition, we do not restrict our analysis to the case of the equilibrium domain pattern.

The principle result of the letter is that in the case where the domain pattern in the ferroelectric is dense (i.e. domain spacing is smaller than the thickness of the ferroelectric), Eq. (E.1) can be generalized to the form:

$$\varepsilon_0 A/C = (h/\varepsilon_f) + (d/\varepsilon_{\mathrm{mod}}), \tag{E.2}$$

with $\varepsilon_{\mathrm{mod}}$ being the apparent permittivity of the passive layer

$$\varepsilon_{\mathrm{mod}} = \frac{\varepsilon_d}{1 - (\varepsilon_m/\varepsilon_f)^2\, \xi(d/a)}, \tag{E.3}$$

where d and a stand for the thickness of the passive layer and the the domain spacing, respectively; the function $\xi(d/a)$ reaches values of 1 to 0 in the limits of $d/a \to 0$ and $d/a \to \infty$, respectively. For the periodic and symmetric domain pattern ($a_+ = a_-$ in Fig. E.1), the function $\xi(d/a)$ is given by Eq. (E.13) and shown in Fig. E.2. Thus, the derived relation justifies the use of the in-series capacitors approach for the analysis of the dielectric response of polydomain ferroelectric films. At the same time, this analysis shows a way of getting additional information on the parameters of the studied system.

To obtain the above result, we follow the approach of the previous works [E3,2]. Using the "hard ferroelectric" approximation, we express the electric displacement of the ferroelectric layer as a sum of the constant spontaneous polarization P_0 (whose orientation alters from domain to domain) and the linear dielectric response of the crystal lattice:

$$D_x = \varepsilon_0 \varepsilon_a E_x, \tag{E.4a}$$

$$D_z = \varepsilon_0 \varepsilon_c E_z \pm P_0. \tag{E.4b}$$

We adopt the thermodynamic potential (per unit area of the sample) of the system with a given voltage U on the electrodes $G = G_{\rm el} + G_m$, which includes: first, the energy of the electric field with the subtracted work produced by the external voltage sources, $G_{\rm el}$ and, second, the lattice pinning energy of the domain wall in the ferroelectric itself, G_m. In order to calculate the small signal dielectric response, we use the lowest (linear and quadratic) terms of the expansion of G with respect to the average (net) spontaneous polarization of the ferroelectric layer $P_N = P_0\,(a_+ - a_-)/(2a)$. Symbols a_+ and a_- stand for the width of domains where the vector of the spontaneous polarization is oriented along and against the direction of the applied electric field, respectively. We address in detail the case of the symmetric ($a_+ = a_-$) domain pattern, i.e. we set $P_N = 0$ in the absence of the applied voltage U.

For the considered situation, the leading terms of $G_{\rm el}$ are readily available in the literature [E3,?] in the form:

$$G_{\rm el} = h\left[\frac{P_N^2}{2\varepsilon_0\varepsilon_{\rm el}} - \frac{P_N\,U/h}{1+\varepsilon_c d/(\varepsilon_d h)}\right], \tag{E.5}$$

where

$$\begin{aligned} \frac{1}{\varepsilon_{\rm el}} &= \frac{d}{\varepsilon_d h + \varepsilon_c d} + \frac{4a}{\pi h}\sum_{n=1}^{\infty}\frac{(-1)^n}{n\,D_n}, \\ D_n &= \varepsilon_d\coth\frac{n\pi d}{2a} + \sqrt{\varepsilon_a\varepsilon_c}\coth\left(\sqrt{\frac{\varepsilon_a}{\varepsilon_c}}\frac{n\pi h}{2a}\right). \end{aligned} \tag{E.6}$$

Here the parameter $1/\varepsilon_{\rm el}$ has the meaning of the contribution to the inverse dielectric susceptibility of the system, which is controlled by the electrostatic energy of the domain pattern.

Function G_m can be expressed in terms of the extrinsic contribution ε_m to permittivity (in the sense as it was introduced above [9]):

$$G_m = \frac{hP_N^2}{2\varepsilon_0\varepsilon_m}. \tag{E.7}$$

Then, the function G has a compact form

$$G = h\left[\frac{P_N^2}{2\varepsilon_0\varepsilon_w} - \frac{P_N\,U/h}{1+\varepsilon_c d/(\varepsilon_d h)}\right], \tag{E.8}$$

where $1/\varepsilon_w = 1/\varepsilon_m + 1/\varepsilon_{\rm el}$.

The response of the net spontaneous polarization P_N to the voltage U applied to the capacitor can be found from the condition for the minimum of the thermodynamic potential G:

$$\partial G(P_N, U)/\partial P_N = 0. \tag{E.9}$$

To calculate the effective capacitance per unit area of the system C/A, Eqs. (E.5-E.9) should be appended with the relation

$$C/A = \frac{P_N/U + \varepsilon_0\varepsilon_c/h}{1+\varepsilon_c d/(\varepsilon_d h)} \tag{E.10}$$

obtained in Refs. [E3,2]. Finally, Eqs. (E.5-E.10) yield

$$\frac{\varepsilon_0 A}{C} = \frac{h}{\varepsilon_c+\varepsilon_w} + \frac{d}{\varepsilon_d}\left[1 - \left(\frac{\varepsilon_w}{\varepsilon_c+\varepsilon_w}\right)^2\frac{h}{h+h_c}\right], \tag{E.11}$$

where

$$h_c = \frac{d}{\varepsilon_w}\,\frac{\varepsilon_c^2}{\varepsilon_c+\varepsilon_w}.$$

[9] The validity of Eq. (E.7) can be readily verified. Setting in Eqs. (E.6) and (E.8) $d \to 0$, from Eqs. (E.8) and (E.9) we get: $P_N = \varepsilon_0\varepsilon_m U/h$ in accordance with the definition of ε_m.

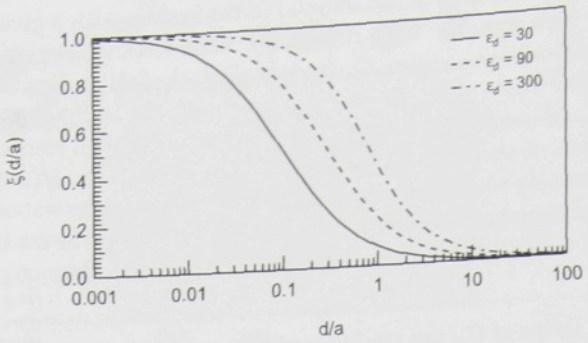

FIGURE E.2: Function $\xi(d/a)$ versus the fraction d/a for three values of the passive layer permittivity ε_d; ε_a, $\varepsilon_c = 300$.

Though formula (E.11) is similar to the in-series capacitors formula given by Eq. (E.1), the contribution of domain walls movements to the dielectric response of the system ε_w contains the function $\varepsilon_{\rm el}$, which depends, in general, on the film thickness h. Thus in general, Eq. (E.11) is not consistent with Eq. (E.1). However, in the addressed case of the dense domain pattern (i.e. for $h > a$), Eq. (E.11) can be simplified down to the form consistent with Eq. (E.1), which will be referred below as *dense pattern approximation*:

$$\frac{\varepsilon_0 A}{C} = \frac{h}{\varepsilon_c + \varepsilon_m} + \frac{d}{\varepsilon_d}\left[1 - \left(\frac{\varepsilon_m}{\varepsilon_c + \varepsilon_m}\right)^2 \xi(d/a)\right], \tag{E.12}$$

where

$$\xi(\tau) = \frac{4\varepsilon_d}{\pi\tau}\sum_{n=1}^{\infty}\frac{(-1)^{n+1}}{nD_n^{\infty}(\tau)}, \tag{E.13}$$

$$D_n^{\infty}(\tau) = \varepsilon_d \coth(n\pi\tau/2) + \sqrt{\varepsilon_a \varepsilon_c}. \tag{E.14}$$

Here $\xi(\tau)$ is a function decreasing from 1 to 0 with increasing τ. The plots of this function for three sets of the parameters of the studied system are shown [10]. in Fig. E.2 Taking into account that $\varepsilon_f = \varepsilon_c + \varepsilon_m$, we thus arrive at the result announced above, Eqs. (E.2) and (E.3). The physical reason for the simplification of the h dependence of the inverse capacitance of the system down to a linear one is as follows. In the case of the dense domain pattern the stray fields created by the periodic charge distribution at one electrode essentially decay within the distance of about a from this electrode. Thus, the effective capacitance of the passive layer becomes independent of the film thickness.

Comparing the obtained result to the simple "in-series" formula, Eq. (E.1), we see that though the slope of the h dependence is the same (permittivity of the ferroelectric itself), in the polydomain case, the offset of this dependence brings information not only on the d/ε_d parameter of the passive layer but also on the period of the domain pattern and the distribution of the dielectric response of the ferroelectric material itself between the intrinsic (ε_c) and extrinsic (ε_m) contributions.

The effect of the domain spacing on the offset of the h dependence of the inverse capacitance predicted by Eq. (E.12) is illustrated in Fig. E.3. It is seen that, in the polydomain case, this offset can be essentially smaller than that predicted by the simple "in-series" formula shown with dashed line. In this figure, the predictions of the dense pattern approximations, Eq. (E.12), are compared to those of the exact formula Eq. (E.11). It is seen that, for dense domain patterns, i.e. for $h > a$, the former provides a very good approximation. The sensitivity of the extrapolated offset of the h dependence of the inverse capacitance to the distribution of the dielectric response of the ferroelectric material between the extrinsic and intrinsic contributions is seen from Eq.(E.12). The greater the fraction $\varepsilon_m/\varepsilon_f$, the greater the difference between the apparent permittivity $\varepsilon_{\rm mod}$ and the passive layer permittivity ε_d.

[10] The curves were calculated numerically, the limiting values (for $d/a \to 0$ and $d/a \to \infty$) being also checked analytically.

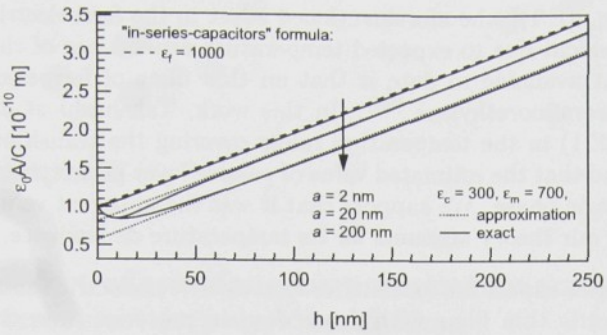

FIGURE E.3: Inverse capacitance per unit area of the ferroelectric capacitor $\varepsilon_0 A/C$ versus the thickness of the ferroelectric layer h for different values of the domain spacing a; $d = 2\,\mathrm{nm}$ and $\varepsilon_d = 20$. The results of the exact theory are compared with their dense pattern approximations and "in-series" formula. Note that the offset of the approximation $d/\varepsilon_{\mathrm{mod}}$ decreases with an increase of the domain spacing a. For $a = 2\,\mathrm{nm}$, all three curves coincides.

Two qualitative predictions following from the results presented in this letter are worth mentioning. First, in the limit of thick passive layer $d \gg a$, the dense pattern approximation, Eq. (E.12), reduces down to Eq. (E.1) disregarding the other parameters of the system, since $\xi(d/a) \to 0$ at $d/a \to \infty$. The physical reason behind this effect is that, in this case, the stray fields occupy only a small ($\sim a/d$) fraction of the passive layer so that their contribution to the total energy and inverse permittivity [the sum in Eq.(E.6)] can be neglected. This readily leads to $\xi(d/a) \to 0$.

The second prediction relates to the situation where the permittivity of the ferroelectric itself is dominated by the extrinsic contribution, i.e. $\varepsilon_m \gg \varepsilon_c$, and the domain spacing significantly exceeds the thickness of the passive layer, i.e. $a \gg d$. In this case $\varepsilon_m/(\varepsilon_c + \varepsilon_m) \to 1$ and $\xi(d/a) \approx 1 - \pi d/(4a)$, so that the two terms in the bracket in Eq. (E.12) start to cancel each other. Physical interpretation of this phenomenon is that, in this case, the energy densities of the depolarizing fields in opposite domains are equal to within $d/a \to 0$, disregarding the value of the ratio a_+/a_- of the domain pattern. This implies an *essential reduction* of the suppressive effect of the passive layers, which is driven by the difference in these energy densities. In terms of the effective capacitance density of the passive layer, this corresponds to its increase from $\varepsilon_0\varepsilon_d/d$ to $(\varepsilon_0\varepsilon_d/d)\cdot(4a/\pi d)$.

For the special case of infinite domain wall mobility, i.e. in the limit $\varepsilon_m \to \infty$ (so that $\varepsilon_f \to \infty$), our both aforementioned conclusions are consistent with the results by Kopal *et al.* [E3] and Bratkovsky and Levanyuk [E2].

The above analysis addresses the case of the dense, periodic and symmetric domain pattern. However, some of the results obtained above can be readily extended to the more general case of a dense pattern, which can be characterized by a typical domain spacing a. Namely, the qualitative conclusions of the two preceding paragraphs hold for the more general case, since the physical argumentations summoned for these conclusions are equally applicable to this case. Formal estimates [E7] performed for this case showed that, in the limits $d/a \to 0$ and $d/a \to \infty$, the main result of the letter, Eqs. (E.2) and (E.3), holds (with $\xi = 1$ and $\xi = 0$), respectively.

The key element of our model, *taking into account the finite domain wall mobility in the ferroelectric itself*, makes the model quite realistic. However, we should recognize three factors limiting its applicability. First, we consider films with 180° domains crossing the film thickness from one electrode to another. Second, following the analysis in Refs. [E2,3] we consider that domain walls are straight. Due to inhomogeneous fields, effects of domain wall bending can contribute to the dielectric response of a ferroelectric material. Straightforward electrostatic calculations show that the domain wall bending contribution to the free energy is $G \propto aP_N^2/\varepsilon_0$ with a proportionality factor of about one [E7]. When this term is much smaller than G_m [given by Eq. (E.7)] the effects of domain wall bending are negligible. The above condition leads to an estimate for the upper limit of the film thickness h below which our theory is applicable: $h \ll \varepsilon_m a$. Finally, the applicability of our macroscopic theory fails for ultra thin films (e.g. films of thicknesses about few unit cells).

We believe that the obtained results provide an efficient and simple tool for the interpretation of the dielectric data on ferroelectric thin films. As a prediction of the theory ready to be checked experimentally, we can indicate the temperature dependence of the extrapolated offset of the A/C vs. h dependence. Namely, in the films where the dielectric data in the paraelectric phase suggests

the presence of a passive layer [based on Eq. (E.1)], the aforementioned offset in the ferroelectric phase may be essentially temperature dependent due to expected temperature dependence of the ratio $\varepsilon_m/\varepsilon_c$. The only relevant experiment available to date is that on thin films of ferroelectric copolymer of vinidilene fluoride and tetrafluorethylene [E8]. In this work, Takahashi *et al.* performed the analysis according to Eq. (E.1) in the temperature range covering the transition temperature of the ferroelectric. It was found that the estimated value of passive layer permittivity was temperature dependent in the ferroelectric phase. We suppose that it was the apparent value of this permittivity that was evaluated and our theory accounts for its temperature dependence.

To summarize, it is shown that the in-series capacitors formula for ferroelectric-dielectric sandwich structures can be applied to ferroelectric thin films with dense domain patterns, however with an apparent value of the passive layer permittivity $\varepsilon_{\mathrm{mod}}$, which is a function of the whole set of parameters of the system except the film thickness h. The use of Eq. (E.2) to the analysis of the experimental data can provide additional information on the ferroelectric, namely, on the distribution of the dielectric response of ferroelectric material between intrinsic (ε_c) and extrinsic (ε_m) contributions.

This project was supported by the Swiss National Foundation and by the Ministry of Education of the Czech Republic, project MSM 242200002.

References

[E1] O. G. Vendik, S. P. Zubko, and L. T. Ter-Martirosayn, Appl. Phys. Lett. **73**, 37 (1998)
[E2] A. M. Bratkovsky, and A. P. Levanyuk, Phys. Rev. B, **63**, 132103 (2001)
[E3] A. Kopal, P. Mokrý, J. Fousek, and T. Bahník, Ferroelectrics **223**, 127 (1999)
[E4] A. M. Bratkovsky, and A. P. Levanyuk, Phys. Rev. Let. **87**, 179703 (2001)
[E5] M. E. Lines and A. M. Glass, *Principles and applications of ferroelectrics and related materials*, Oxford University Press, 1979
[E6] A. K. Tagantsev, Phys. Rev. Lett. **87**, 179702 (2001)
[E7] P. Mokrý and A. K. Tagantsev (unpublished)
[E8] Y. Takahashi, A. Kitahama, and T. Furukawa, IEEE Trans. Dielectr. Electr. Insul. **11**, 227 (2004)

Paper F

Effect of spontaneous polarization screening on dielectric response of ferroelectric polydomain films

Oral presentation at the 7th European Conference on Applications of Polar Dielectrics, Liberec, Czech Republic 2004.

Accepted for publication in *Ferroelectrics*, 2004

EFFECT OF SPONTANEOUS POLARIZATION SCREENING ON DIELECTRIC RESPONSE OF FERROELECTRIC POLYDOMAIN FILMS

P. MOKRÝ[11], and A. K. TAGANTSEV, and N. SETTER

Ceramics Laboratory, Materials Department, EPFL Swiss Federal Institute of Technology, CH-1015 Lausanne, Switzerland

Abstract

A theoretical study on the effect of spontaneous polarization screening on the dielectric response of ferroelectric films with 180° domains going through the film thickness (through-domains) is presented. It has been shown by several researchers that the dielectric response of ferroelectrics is always deteriorated (e.g. due to electric field, mechanical stress, or lattice imperfections) in the thin electrode-adjacent passive regions. As a result, these regions behave as a low permittivity material reducing the total dielectric response of the ferroelectric capacitor. This "depolarizing" effect can be modeled by a low permittivity layer between the ferroelectric and the electrode. The strong electric field in the dielectric layer can induce free charge injection from the electrode to the ferroelectric-dielectric layer interface. We study how these free charges affect the dielectric response of the ferroelectric capacitor with through-domains. We found that their presence strongly influences the domain wall contribution to permittivity of the ferroelectric. This effect is controlled to a great extent by the domain wall thickness.

PACS: 77.55.+f, 77.80.-e, 84.32.Tt, 77.80.Dj

Keywords: Dielectric thin films, capacitors, domain structure

F.1. INTRODUCTION

A commonly reported trend in the most extensively studied films of perovskites like lead zirconate titanate and barium strontium titanate compounds is a reduction of their permittivity with decreasing film thickness. Numerous indirect experimental observations [F1,2,3,4,5,6,7] lead the researchers to the conclusion that the observed size effect is due to the existence of electrode-adjacent passive layers in the investigated capacitors. Despite of a wide acceptance of the *passive layer concept*, the nature of these layers is not clear [F1] and the direct observations of well-defined layers are rather scarce. A rare example of direct observation of passive layer is the work of Hase *et al.* [F2] describing a formation of 100 nm thick layer of pyrochlore grains during multi-target sputtering onto Pt-coated Si substrates. In the case of ferroelectric ceramic, grain boundaries represent another origin of passive layers [F8,3]. On the other hand, most of the high-resolution transmission electron microscope studies show no evidence of electrode-adjacent passive layers. Nevertheless, Abe *et al.* [F9] demonstrated that a well-defined dielectric layer may not be necessary for an experimental agreement with the passive layer concept and various mechanisms of film-electrode interactions have been proposed: creation of variable depletion layers associated with the Schottky barriers [F4,5], low permittivity layers due to the oxygen vacancy entrapment at ferroelectric-electrode interfaces [F6], local suppression of polarization states in the near-electrode regions [F7], local diffusion of electrode material into the ferroelectric [F10], or chemically distinct surface phase [F11].

Independently of the origin, all the above-mentioned phenomena are associated with a deterioration of the spontaneous polarization of the crystal lattice in electrode-adjacent regions. The

[11] e-mail: pavel.mokry@vslib.cz

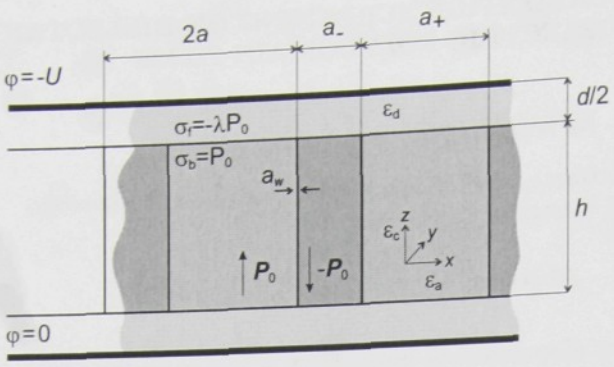

FIGURE F.1: Scheme of the electroded ferroelectric film with passive layers.

bound charges due to the nonzero divergence of the spontaneous polarization produce a strong electric field in these regions, which triggers a free charge injection from the electrodes to compensate the bound charges. It is known that the phenomena of the free charge injection play an essential role in switching characteristics of thin ferroelectric films. In the next sections, we show that the charge injection has also an impact on the dielectric response of ferroelectric polydomain thin films.

F.2. DESCRIPTION OF THE MODEL

In this article, we analyze the dielectric response of the system shown in Fig. F.1. We consider the structure of a ferroelectric non-ferroelastic layer with lamellar antiparallel domain pattern crossing the layer thickness h and two dielectric surface layers of the total thickness d and permittivity ε_d, which separate the bulk from the electrodes. Using the "hard ferroelectric" approximation, we express the electric displacement of the ferroelectric as a sum of the linear dielectric response of the crystal lattice and the constant spontaneous polarization P_0 (whose orientation differs from domain to domain):

$$D_x = \varepsilon_0 \varepsilon_a E_x, \tag{F.1a}$$

$$D_z = \varepsilon_0 \varepsilon_c E_z \pm P_0. \tag{F.1b}$$

We consider that the spontaneous polarization P_0 is constant within each domain and its abrupt change to zero at the interface of the ferroelectric and dielectric layers leads to the appearance of a bound charge of the surface density $\sigma_b = P_0$. Due to finite conductivity of the passive layer, we consider an injection of free (screening) charges of the surface density σ_f from the electrodes to compensate the bound charges. To characterize the degree of this compensation, a factor λ called *degree of screening* is introduced in a way that $\sigma_f = -\lambda\sigma_b$. For given widths a_+ and a_- of domains, where the vector of the spontaneous polarization is oriented along and against the direction of the applied field, respectively, we define the average (net) spontaneous polarization of the ferroelectric layer $P_N = P_0\,(a_+ - a_-)/(2a)$, where $a = (a_+ + a_-)/2$ is the domain spacing.

Change of domains widths a_+ and a_- is a source of the domain (extrinsic) contribution to the permittivity of the ferroelectric layer. We consider that the extrinsic contribution is controlled, first, by the electric field produced by the bound and screening charges σ_b and σ_f, respectively, and, second, by the lattice pinning of domain walls in the ferroelectric material itself. We mean that if the ferroelectric with the given domain pattern were placed in a passive-layer-free capacitor, the permittivity $\varepsilon_c + \varepsilon_m$ would be measured, where ε_c and ε_m are the crystal lattice and extrinsic contributions.

In this study, we address the case of non-poled domain pattern. It means that we set $a_+ = a_-$ in the absence of the applied voltage U on the electrodes. We also do not restrict our analysis to the case of the equilibrium domain period. In real systems the domain spacing a is typically controlled by the prehistory of the sample and may be essentially different from its equilibrium value.

Analysis of the effect of spontaneous polarization screening on the dielectric response in our model requires a consideration of the finite domain wall thickness a_w. The reason for this is as follows. Let us consider, for the moment, the limiting case of complete screening (we set $\lambda = 1$) and the abrupt change of the spontaneous polarization at domain boundaries, i.e. $a_w = 0$. If the domain walls are in their original positions, the bound charges are completely compensated by free charges and hence no depolarizing field is produced in the system. When the domain walls are shifted by $\Delta x = (a_+ - a_-)/2$, there appears a periodic distribution of uncompensated bound charges in a form of stripes of the surface charge density $\sigma = 2P_0$ and the width Δx at the interfaces of the ferroelectric and dielectric layers. Straightforward calculations show that the electrostatic energy change produced by these domain wall shifts corresponds to a non-physical singularity in the dielectric response. Our further analysis shows that this singularity can be regularized if a finite domain wall thickness is considered.

In this article, we focus our analysis only on the linear dielectric response of the system and, therefore, it is sufficient to consider that at the domain boundary the spontaneous polarization changes, for example from P_0 to $-P_0$, linearly within a distance a_w representing the domain wall thickness. In the considered situation of the non-poled domain pattern and partial screening of the bound charges ($0 < \lambda < 1$), the domain wall shift Δx is proportional to the net spontaneous polarization of the ferroelectric layer, $P_N = (P_0/a)\,\Delta x$. Using this parameter, we can express the spatial periodic distribution of the total charge density at the interface of the ferroelectric and dielectric layers $\sigma(x) = \sigma_b(x) + \sigma_f(x)$ in a form of Fourier series

$$\sigma(x) = P_N + \sum_{n=1}^{\infty} \frac{8aP_0}{a_w \pi^2 n^2} \left\{ \sin\left[\frac{n\pi}{2}\left(1 + \frac{P_N}{P_0}\right)\right] - \lambda \sin\left(\frac{n\pi}{2}\right)\right\} \sin\left(\frac{n\pi a_w}{2a}\right) \cos\left(\frac{n\pi x}{a}\right). \quad \text{(F.2)}$$

F.3. DIELECTRIC RESPONSE

To obtain the effective dielectric response of the ferroelectric polydomain thin film, we follow the approach of the previous works [F12,13]. We adopt the thermodynamic potential G (per unit area of the sample) of a system with a given voltage U on the electrodes and free charges σ_f inside the system. Function $G = G_{el} + G_m$ includes, first, the energy of the electric field with the subtracted work produced by the external voltage sources, G_{el}; and second, the pinning energy of the domain wall in the ferroelectric itself, G_m. In order to calculate the small signal dielectric response, we use the lowest (linear and quadratic) terms of the expansion of G with respect to the net spontaneous polarization of the ferroelectric layer P_N.

Leading terms of the function $G_{\rm el}$ for a similar model are already available in the literature[F12,13], however with a different distribution of charges at the interface of the ferroelectric and passive layers than that given by Eq.(F.2). In our model we have

$$G_{\rm el} = h\left[\frac{P_N^2}{2\varepsilon_0 \varepsilon_{\rm el}} - \frac{P_N U/h}{1 + \varepsilon_c d/(\varepsilon_d h)}\right], \quad \text{(F.3)}$$

where

$$\frac{1}{\varepsilon_{\rm el}} = \frac{d}{\varepsilon_d h + \varepsilon_c d} + \frac{8a^3}{a_w^2 \pi^3 h} \sum_{n=1}^{\infty} \frac{\lambda - (-1)^n(\lambda - 2)}{n^3 D_n} \sin^2\left(\frac{n\pi a_w}{2a}\right), \quad \text{(F.4)}$$

$$D_n = \varepsilon_d \coth\frac{n\pi d}{2a} + \sqrt{\varepsilon_a \varepsilon_c}\coth\left(\sqrt{\frac{\varepsilon_a}{\varepsilon_c}}\frac{n\pi h}{2a}\right).$$

It is seen that the function $1/\varepsilon_{el}$ is sensitive to the thickness of the domain wall a_w.

Function G_m can be expressed in terms of the extrinsic contribution ε_m to permittivity (in the

sense as it was introduced above [12]):

$$G_m = \frac{hP_N^2}{2\varepsilon_0\varepsilon_m}. \tag{F.5}$$

Then, the function G has a compact form

$$G = h\left[\frac{P_N^2}{2\varepsilon_0\varepsilon_w} - \frac{P_N U/h}{1+\varepsilon_c d/(\varepsilon_d h)}\right], \tag{F.6}$$

where

$$1/\varepsilon_w = 1/\varepsilon_{\rm el} + 1/\varepsilon_m \tag{F.7}$$

has a meaning of the contribution to the inverse dielectric susceptibility of the system, which is controlled, first, by electrostatic energy of the domain pattern and, second, by the pinning energy of the crystal lattice, respectively.

To calculate the effective capacitance per unit area of the system C/A, Eqs. (F.3-F.6) should be appended with the relation

$$C/A = \frac{P_N/U + \varepsilon_0\varepsilon_c}{1+\varepsilon_c d/(\varepsilon_d h)} \tag{F.8}$$

obtained in Refs. [F12,13], where the response of the net spontaneous polarization P_N to the voltage U applied to the capacitor [F14] can be found from the condition for the minimum of the thermodynamic potential G:

$$\partial G(P_N, U)/\partial P_N = 0. \tag{F.9}$$

Finally, Eqs. (F.3-F.9) yield

$$\frac{\varepsilon_0 A}{C} = \frac{h}{\varepsilon_c+\varepsilon_w} + \frac{d}{\varepsilon_d}\left[1 - \left(\frac{\varepsilon_w}{\varepsilon_c+\varepsilon_w}\right)^2 \frac{h}{h+h_c}\right], \tag{F.10}$$

where

$$h_c = \frac{d}{\varepsilon_w}\,\frac{\varepsilon_c^2}{\varepsilon_c+\varepsilon_w}.$$

If the domain pattern in the ferroelectric is dense (i.e. domain spacing is smaller than the thickness of the ferroelectric, $a < h$), the inhomogeneous (stray) fields produced by the periodic charge distribution $\sigma(x)$ at one electrode essentially decay with the distance of about a from this electrode to the other. Thus, the effective capacitance of the passive layer becomes independent of the film thickness h and Eq. (F.10) can be simplified to a form, which will be referred below as the *dense pattern approximation*:

$$\varepsilon_0 A/C = (h/\varepsilon_f) + (d/\varepsilon_{\rm mod}), \tag{F.11}$$

with $\varepsilon_f = \varepsilon_c + \varepsilon_m$ and $\varepsilon_{\rm mod}$ being the permittivity of the ferroelectric and apparent permittivity of the passive layer, respectively,

$$\varepsilon_{\rm mod} = \frac{\varepsilon_d}{1-(\varepsilon_m/\varepsilon_f)^2\,\xi(d/a,\lambda)}. \tag{F.12}$$

Here the function $\xi(\tau,\lambda)$ is given by formula

$$\xi(\tau,\lambda) = \frac{8\varepsilon_d a^2}{a_w^2\pi^3\tau}\sum_{n=1}^{\infty}\frac{(-1)^n(\lambda-2)-\lambda}{n^3 D_n^{\infty}(\tau)}\sin^2\left(\frac{n\pi a_w}{2a}\right), \tag{F.13}$$

$$D_n^{\infty}(\tau) = \varepsilon_d\coth(n\pi\tau/2) + \sqrt{\varepsilon_a\varepsilon_c}. \tag{F.14}$$

[12] The validity of Eq. (F.8) can be readily verified. Setting in Eqs. (F.6) and (F.9) $d \to 0$, from Eqs. (F.9) and (F.10) we get: $P_N = \varepsilon_0\varepsilon_m U/h$ in accordance with the definition of ε_m.

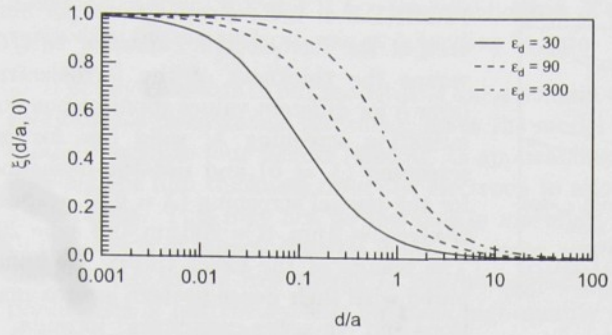

FIGURE F.2: Function $\xi(d/a, \lambda)$ versus the fraction d/a for three values of the passive layer permittivity ε_d; the absence of free charges in the system is considered for all three curves $\lambda = 0$; ε_a, $\varepsilon_c = 300$.

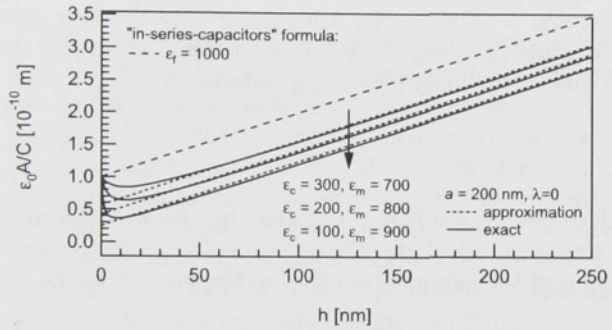

FIGURE F.3: Effect of the distribution of the ferroelectric layer permittivity ε_f between the intrinsic ε_c and extrinsic ε_m parts on the thickness dependence of the inverse capacitance per unit area of the ferroelectric capacitor $\varepsilon_0 A/C$ in the absence of screening charges $\lambda = 0$; $d = 2\,\mathrm{nm}$, $a = 200\,\mathrm{nm}$ and $\varepsilon_d = 20$. Solid lines represent the exact numerical results [see Eq. (F.10)], dotted lines represent dense pattern approximations [see Eq. (F.11)]. Dashed line shows the predictions of the "in-series-capacitors" formula [see Eq. (F.15)]. Note that the offset of the approximations $d/\varepsilon_{\mathrm{mod}}$ decreases with increasing the fraction $\varepsilon_m/\varepsilon_f$.

In the absence of screening charges (i.e. $\lambda = 0$), the function $\xi(d/a, 0)$ reaches values of 1 to 0 in the limits $d/a \to 0$ and $d/a \to \infty$, respectively. The plots of this function for three sets of the parameters of the studied system are shown in Fig. F.2. The curves were calculated numerically, the limiting values (for $d/a \to 0$ and $d/a \to \infty$) being also checked analytically.

F.4. DISCUSSION

Figures F.3 and F.4 show the h dependence of the of inverse capacitance per unit area of the ferroelectric capacitor $\varepsilon_0 A/C$ for two sets of parameters of the system. It is seen that the slope of dense pattern approximation is equal to the permittivity of the ferroelectric itself ε_f and the offset of this dependence brings information not only on the d/ε_d parameter of the passive layer but also on the period of the domain pattern a, on the distribution of the dielectric response of the ferroelectric material itself between the intrinsic (ε_c) and extrinsic (ε_m) contributions, and on the degree of screening λ.

Several qualitative predictions following from the results presented in this article are worth mentioning:

First, if the thickness of the passive layer is greater than the domain spacing (i.e. $d \gg a$), the fast decaying stray fields in the passive layer have a negligible contribution to the electrostatic energy of the domain pattern and the dense pattern approximation, Eq. (F.11), reduces down to so called "in-series-capacitors" formula

$$\varepsilon_0 A/C = (h/\varepsilon_f) + (d/\varepsilon_d) \tag{F.15}$$

disregarding the other parameters of the system, since $\xi(d/a, \lambda) \to 0$ at $d/a \to \infty$.

Second, when the domain spacing significantly exceeds the thickness of the passive layer, i.e.

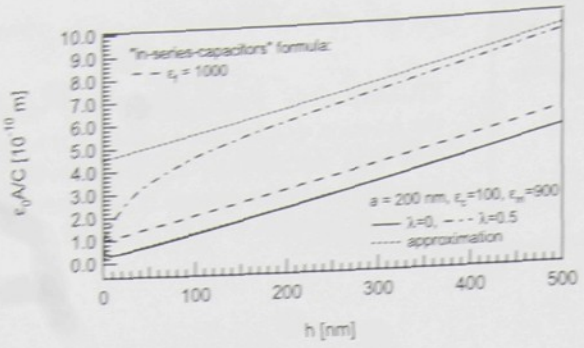

FIGURE F.4: Inverse capacitance per unit area of the ferroelectric capacitor $\varepsilon_0 A/C$ versus the thickness of the ferroelectric layer h for different values spontaneous polarization screening λ; solid line for no screening ($\lambda = 0$) and dot-and-dash line for the partial screening ($\lambda = 0.5$), respectively; $d = 2\,\mathrm{nm}$, $a = 200\,\mathrm{nm}$ and $\varepsilon_d = 20$. The results of the exact theory are compared with their dense pattern approximations and "in-series-capacitors" formula.

$a \gg d$, the energy densities of the stray fields becomes very sensitive to the presence of the screening charges. In the absence of screening charges, the energy densities of the depolarizing field in opposite domains are equal to within $d/a \to 0$, since the fields differ only by their sign, except small regions close to the domain walls, disregarding the value of the ratio a_+/a_- of the domain pattern. Then the apparent permittivity of the dead layer $\varepsilon_{\mathrm{mod}}$ reduces to

$$\frac{\varepsilon_d}{1-(\varepsilon_m/\varepsilon_f)^2}.$$

In addition, when the permittivity of the ferroelectric itself is dominated by the extrinsic contribution, i.e. $\varepsilon_m \gg \varepsilon_c$, the two terms in denominator of the above expression start to cancel each other. This implies the *essential reduction* of the suppressive effect of the passive layers, i.e. $\varepsilon_0 A/C \approx (d/\varepsilon_d) \cdot (\pi d/4a)$.

The sensitivity of the extrapolated offset of the h dependence of the inverse capacitance predicted by Eq. (F.11) on the distribution of the dielectric response of the ferroelectric between the extrinsic and intrinsic contributions is illustrated in Fig. F.3. The appreciable effect of an increase of the effective capacitance of the passive layer is seen with an increase of the ratio $\varepsilon_m/\varepsilon_f$. In this figure, the predictions of the dense pattern approximations, Eq. (F.11), are compared to those of the exact formula Eq. (F.10). It is seen that, for dense domain patterns, i.e. for $h > a$, the former provides a very good approximation.

The effect of degree of the spontaneous polarization screening λ on the offset of the h dependence of the inverse capacitance predicted by Eq. (F.11) is illustrated in Fig. F.4. It is seen that, in the absence of screening charges, i.e. for $\lambda = 0$, this offset can be essentially smaller than that predicted by the simple "in-series-capacitors" formula shown with dashed line. On the other hand, the presence of screening charges represents a real pinning the domain walls by the electric field resulting in an essential suppressive effect on the effective capacitance of the passive layer, which can be greater than predicted by "in-series-capacitors" formula as shown by dot-and-dash line.

Third, if the domain walls are strongly pinned by the crystal lattice, i.e. $\varepsilon_m \ll \varepsilon_c$, the domain wall displacements are negligible even in high applied electric field. In this case, the inverse effective extrinsic contribution to permittivity of the ferroelectric layer $1/\varepsilon_w$ is dominated by the lattice pinning contribution $1/\varepsilon_m$ [see Eq. (F.7)]. Then the dielectric response of the ferroelectric capacitor in the polydomain state is the same as it would be measured in single domain state and Eq. (F.10) reduces down to the "in-series-capacitances" formula:

$$\varepsilon_0 A/C = (h/\varepsilon_c) + (d/\varepsilon_d). \tag{F.16}$$

Fourth, in ultrathin films it is possible that the thickness of the passive layer greatly exceeds the thickness of the ferroelectric, i.e. $h \ll d$. Then the contribution to the extrinsic permittivity of the ferroelectric, which is controlled by the electrostatic energy of the domain pattern, can be approximated by $\varepsilon_{\mathrm{el}} \approx \varepsilon_c + \varepsilon_d(h/d)$ and again Eq. (F.10) reduces down to the "in-series-capacitors" formula (F.15). Physical interpretation of this phenomenon is that, in this case, the stray fields occupy only a small ($\sim h/d$) fraction of the volume of the system so that their contribution to the total energy and the inverse permittivity [the sum in Eq. (F.4)] can be neglected. This is actually

indicated in Figs. F.3 and F.4, where predictions of the exact formula Eq. (F.10) converge to the value d/ε_d on the vertical axis at h tending to zero.

The key elements of our model: the finite domain wall mobility in the ferroelectric itself and the spontaneous polarization screening, make the model quite realistic. However, as its limitation we should recognize four factors limiting its applicability. First, we consider films with 180° domains crossing the film thickness from one electrode to another. Second, we consider that domain walls are straight. This may not be the case in materials with non-ferroelastic 180° domain walls due to the effects of inhomogeneous fields. However, our analysis shows that the domain wall bending contribution to the free energy G can be neglected in systems where $h \ll \varepsilon_m a$. It means that predictions of our theory fails for thick high-quality samples with dense domain patterns. Third, our estimations on the effects of electrostatic domain wall pinning by screening charges requires an assumption that the injected free charges from the electrode are immobile compared to the mobility of domain walls. Finally, the applicability of the macroscopic theory fails for ultrathin films.

We believe that the obtained results provide a useful tool for the interpretation of the dielectric data on ferroelectric thin films. As a prediction of the theory ready to be checked experimentally, we can indicate the temperature dependence of the extrapolated offset of the A/C vs. h dependence. Namely, in the films where the dielectric data in the paraelectric phase suggests the presence of a passive layer [based on Eq. (F.1)], the aforementioned offset in the ferroelectric phase may be essentially temperature dependent due to expected temperature dependence of the ratio $\varepsilon_m/\varepsilon_c$. In addition, it is expected that the offset should be increasing with time as the free charge injection progresses. Thus this works indicates that the slow deterioration of the capacitance of ferroelectric capacitors due to spontaneous polarization screening can be considered as a possible origin of fatigue in ferroelectric polydomain thin films.

Acknowledgements

This project was supported by the Swiss National Science Foundation, by the Ministry of Education of the Czech Republic (MSM 242200002), and by the Grant Agency of the Czech Republic (GACR 202/03/0569).

References

[F1] L. J. Sinnamon, R. M. Bowman, and J. M. Gregg, *Appl. Phys. Lett.* **78**, 1724 (2001)
[F2] T. Hase, T. Sakuma, Y. Miyasaka, K. Hirata, and N. Hosokawa, *Jpn. J. Appl. Phys.* **32**, 4061 (1993)
[F3] L. J. Sinnamon, M. M. Saad, R. M. Bowman, and J. M. Gregg, *Appl. Phys. Lett.* **81**, 703 (2002)
[F4] S. K. Dey, J. J. Lee, and P. Alluri, *Jpn. J. Appl. Phys.* **34**, 3142 (1995)
[F5] C. Basceri, S. K. Streiffer, A. I. Kingon, and R. Waser, *J. Appl. Phys.* **82**, 2497 (1997)
[F6] J. J. Lee, C. L. Thio, and S. B. Desu, *J. Appl. Phys.* **78**, 5073 (1995)
[F7] O. G. Vendik, and S. P. Zubko, *J. Appl. Phys.* **88**, 5343 (2000)
[F8] S. Stemmer, S. K. Streiffer, N. D. Browning, C. Basceri, and A. I. Kingon, *Interface Science* **8**, 209 (2000)
[F9] K. Abe and Sh. Komatsu, *Jpn. J. Appl. Phys.* **32**, L1157 (1993)
[F10] I. Stolichnov, A. K. Tagantsev, N. Setter, J. S. Cross, and M. Tsukada, *Appl. Phys. Lett.* **75**, 1790 (1999)
[F11] V. Craciun and R. K. Singh, *Appl. Phys. Lett.* **76**, 1932 (2000)
[F12] A. Kopal, P. Mokrý, J. Fousek, and T. Bahník, *Ferroelectrics* **223**, 127 (1999)
[F13] A. M. Bratkovsky, and A. P. Levanyuk, *Phys. Rev. B*, **63**, 132103 (2001)
[F14] The validity of Eq. (F.8) can be readily verified. Setting in Eqs. (F.6) and (F.9) $d \to 0$, from Eqs. (F.9) and (F.10) we get: $P_N = \varepsilon_0 \varepsilon_m U/h$ in accordance with the definition of ε_m.

Paper G

Elastic aspects of domain quadruplets in ferroics

Invited talk at the 4th Asian Meeting on Ferroelectrics, Bangalore, India 2003.

Submitted to *Journal of Applied Physics*, Ref: Ms. #JR04-2472 Date Received 08/03/04

ELASTIC ASPECTS OF DOMAIN QUADRUPLETS IN FERROICS

P. MOKRÝ[a13], and J. FOUSEK[b]

[a]Ceramics Laboratory, Materials Department, EPFL Swiss Federal Institute of Technology, CH-1015 Lausanne, Switzerland

[b]Dept. of Electrical Engng., Faculty of Mechatronics and Interdisciplinary Engineering Studies, Technical University of Liberec, CZ-46117 Liberec, Czech Republic

Abstract

Coexistence of ferroelectric ferroelastic domains in some materials plays an important role in practical area of domain engineering. Here the problem is discussed theoretically from the point of view of elastic aspects. Domain quadruplets are considered, i.e. systems of four ferroelastic domains coinciding along one intersection line. Conditions at which the elastic energy of quadruplets is zero are specified; they would allow for the existence of permissible quadruplets. The problem has been solved for the species $m\bar{3}m$-$m_x m_y 2_z$, $m\bar{3}m$-$2_{xy} m_{\bar{x}y} m_z$, $m\bar{3}m$-$3m$, and $m\bar{3}m$-$4mm$. It is shown that, in general, no mechanically compatible (stress-free) permissible quadruplets exist. The results make it possible to specify those conditions for spontaneous strain components which must be complied to allow for energetically acceptable quadruplets. These conditions are fulfilled in the orthorhombic phase of $KNbO_3$. The theoretical approach offered in this paper can be used for specific discussions of the existence of multidomain states in thin films where some components of spontaneous strain need not play an essential role.

PACS: 77.80.Dj

Keywords: ferroelastics, ferroelectrics, domain quadruplets, $KNbO_3$, domain engineering

G.1. DESIGNATION OF THE PROBLEM AND ITS PRACTICAL ASPECTS

The problem of domain coexistence in a ferroic sample is of high importance from the point of view of macroscopic material properties and application possibilities. There exist 212 ferroic species defined by point symmetries of parent and ferroic phases whose symmetry aspects were analyzed by Aizu [G1,2]. The number n of domain states is defined by the symmetry of the given species and is limited by the relation $2 \leq n \leq 48$.

In a normally produced ferroic (ferroelastic and/or ferroelectric) sample all domain states may be existing. Under usual conditions, domain patterns in ferroic samples are formed during cooling, at the phase transition temperature T_{TR}. Domains representing different domain states are usually formed at various edges of the sample or, in materials with the second order phase transition, at paraelectric-ferroic phase boundaries. The formed domains represent a number of domain states and the question is whether the former are electrically and elastically compatible. If not, their coexistence would be associated with additional electric and/or elastic energy. The electrical compatibility plays a role in ferroelectric materials and is specified by the requirement $\mathrm{div}\, \boldsymbol{P}_S = 0$. There is a number of observations showing that this condition may not play a significant role in static systems, because of charge compensation possibility. The coexistence of domains ("head-to-head" coupling) separated by domain walls with $\mathrm{div}\, \boldsymbol{P}_S \neq 0$ has been frequently observed (see e.g. ref. [G3]). A crucial role may play the condition of elastic compatibility, related to ferroelastic materials. In the available discussions [G4,5], the conditions of stress-free coexistence

[13]e-mail: pavel.mokry@vslib.cz

of two ferroelastic domains in all ferroic species were specified. However, in the case of materials representing species with $n > 2$ the following question can be asked: can more than two ferroelastic domain states coexist without requiring a strain additional to the spontaneous strain $\boldsymbol{u}_S$ in any of them? In other words: can such domains coexist separated by domain walls without any elastic energy?

This question plays a substantial role in the currently very essential research area connected with ferroic materials. Multiple systems of domains can be arranged in fundamentally different ways, defining several kinds of "domain engineering" (DE) [G6,7]. Domain-geometry engineering (DGE) specifies particular geometries of domains; it was this approach by which the concept of DE was originally introduced [G8]. Domain-average engineering (DAE) specifies samples in which a defined number of domain states is represented by domains of irregular geometry.

By now the DGE was considered for just two domain states with antiparallel $\boldsymbol{P}_S$, even for very interesting domain geometries [G9]. For such states, the elastic conjunction of domains is not a problem. This is no longer true when the domains in a sample represent more than two domain states. The elastic aspect of their coexistence is a very essential problem from the points of view of physical properties and of possible applications. An infinite number of types of domain systems can be proposed. Many interesting domain patterns including $n > 2$ states have been observed; let us just mention the Forsbergh pattern [G10] and Arlt patterns [G11] in $BaTiO_3$. Their symmetries have not been specified yet and their macroscopic properties are unknown. Such domain configurations could offer attractive application aspects. Recently DAE has become a very essential research area because of possible functions of polydomain systems in PZN-PT and PMN-PT crystals [G12,13,14,15]. Piezoelectrically promising properties of DAE systems in $KNbO_3$ crystals were also demonstrated [G16]. Attention has been also drawn to the study of piezoelectric response of ferroelectric ferroelastic domain structures in potassium niobate and potassium niobate-tantalate nano-rods [G17].

In most ferroelastic species, two mechanically compatible domains can be separated by one of two walls of the W_f (of a fixed orientation) and/or of the S class (of a general orientation matched to spontaneous strains) [G4]. These *permissible domain walls* (PDW's) are mutually perpendicular when the spontaneous strain $\boldsymbol{u}_S$ is approaching zero; i.e. at T_C for a second order transition. We can easily imagine a system of four domains separated by such two walls. The symmetries of multidomain systems have been specified by Erhart and Cao [G18] for the case when the domain coexistence aspects due spontaneous strains are neglected. This is an effective approach for materials with the second order phase transition, close to T_C. At lower temperatures and for materials with a first order transition, due to the final value of $\boldsymbol{u}_S$ the two walls angle is no longer 90° and they may not cross each other without additional elastic strain. Thus in general, four ferroelastic domains do not seem to be mechanically compatible. However, several observations of specific domain patterns addressing the possibility of coexistence of four ferroelastic domain states have been published and in the following sections we discuss this problem in more detail.

G.2. OBSERVATIONS

Mutually perpendicular ferroelastic walls were observed in a number of ferroelastic samples and explained by additional elastic strains [G19]. Often these strains are visible due to the elastooptic effect. However, several examples of systematic domain patterns with coinciding ferroelastic walls have been recognized [G10,11]. The most tempting data of well defined domain patterns of four domain states have been offered for $KNbO_3$ crystals, in its orthorhombic phase [G20,21]. Fig. G.1 shows the observed domains in this material; wall orientations are specified in the cubic coordinates. We suggest to designate this domain geometry as *domain quadruplets*. These are reliable observations and in what follows we shall discuss this case in particular, as well as the possibility of domain quadruplets in the additional species of $KNbO_3$ and several other perovskites. Are the observed systems of domain walls elastically compatible for this species or are the observed domain systems energetically acceptable because of very small values of certain components of spontaneous strain?

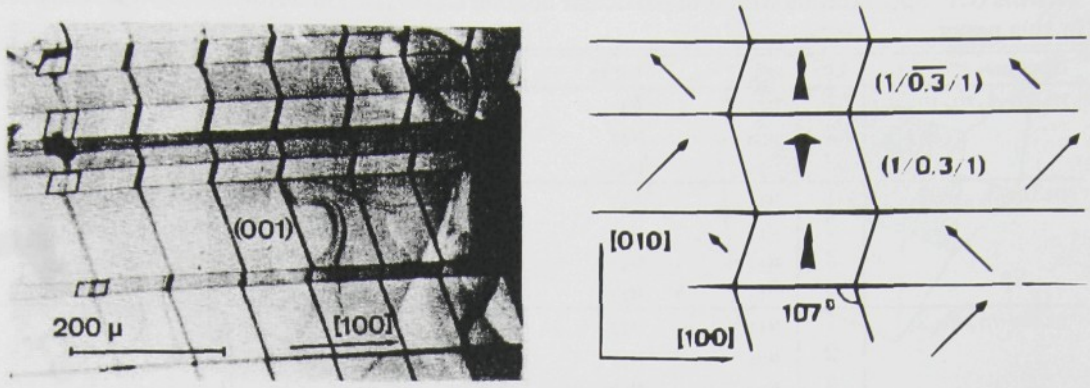

a) b)

FIGURE G.1: (a) Optical observation of domains in the orthorhombic phase of $KNbO_3$. (b) Domain quadruplets are represented. Arrows show the $\boldsymbol{P}_S$ directions. From Ref. [G13].

G.3. THEORETICAL APPROACH

Let us address the elastic aspects of domain coexistence focusing on four particular species: $m\bar{3}m$-$P\varepsilon ds$-$3_{xyz}m_{\bar{x}y}$ (representing $BaTiO_3$, $KNbO_3$, $PbZrO_3$ crystals), $m\bar{3}m$-$P\varepsilon ds$-$4_z m_x m_{xy}$ ($BaTiO_3$, $KNbO_3$, $PbTiO_3$), $m\bar{3}m$-$P\varepsilon ds$-$2_{xy}m_{\bar{x}y}m_z$, and $m\bar{3}m$-$P\varepsilon ds$-$m_x m_y 2_z$ ($BaTiO_3$, $KNbO_3$, $PbHfO_3$, $Cd_2Nb_2O_7$, HCl). Each of these species is characterized by the number $n_{\text{elast}} = n/2$ of ferroelastic domain states. List of tensor components of spontaneous strains in considered species is shown in Tab. G.1. On the basis of Refs. [G4,5], it is easy to designate PDW's for all ferroelastic domain pairs.

In the following, the problem of domain quadruplets will be addressed, with a particular geometrical arrangement shown in Fig. G.2. We assume the realistic situation: first, the volume of the crystal is split by three domain walls into four domains denoted by symbols A, B, C, and D; second, the domain pairs A, B and C, D are separated by one and the same PDW, which is denoted as wall N with normal vector $\boldsymbol{n}$; and finally, the B,C domains are separated by wall M_{BC} with normal vector $\boldsymbol{m}_{BC}$ while A, D are separated by wall M_{AD} with normal vector $\boldsymbol{m}_{AD}$.

Now we specify the *first requirement*: the four domains should coexist for $\boldsymbol{u}_S \to 0$. The condition is that the intersection line of walls M_{AB} and N equals the intersection line of walls M_{CD} and N. If this is so, we can speak about *quasipermissible quadruplets*. If we define

$$\boldsymbol{t}_{BC} = \boldsymbol{n} \times \boldsymbol{m}_{BC}, \qquad \boldsymbol{t}_{AD} = \boldsymbol{n} \times \boldsymbol{m}_{AD}, \tag{G.1a}$$

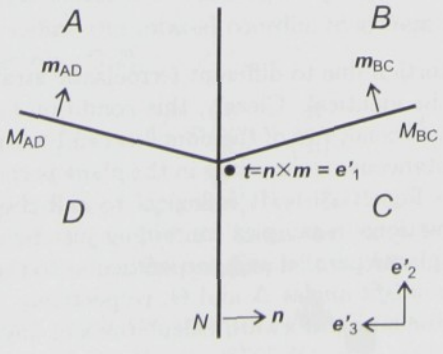

FIGURE G.2: Geometrical arrangement of four domain states A, B, C, and D in the considered domain quadruplet; N, M_{BC}, and M_{AD} are permissible domain walls (with normal vectors $\boldsymbol{n}$, $\boldsymbol{m}_{BC}$ and $\boldsymbol{m}_{AD}$, respectively), which have a common intersection line of the direction $\boldsymbol{t}$. Vectors $\mathbf{e}'_1$, $\mathbf{e}'_2$ and $\mathbf{e}'_3$ form the basis of the coordinate system S', which is attached to the domain quadruplet.

TABLE G.1: Spontaneous strains of particular domain states (DS) in ferroelastic species considered in this paper.

Species	DS	$w_{S,11}$	$w_{S,22}$	$w_{S,33}$	$w_{S,23}$	$w_{S,13}$	$w_{S,12}$
$m\bar{3}m$-$4_z m_x m_{xy}$	1	w_{11}	w_{22}	w_{33}	0	0	0
	2	w_{33}	w_{11}	w_{22}	0	0	0
	3	w_{22}	w_{33}	w_{11}	0	0	0
$m\bar{3}m$-$\bar{3}_{xyz} m_{\bar{2}xy}$	1	w_{11}	w_{11}	w_{11}	w_{12}	w_{12}	w_{12}
	2	w_{11}	w_{11}	w_{11}	w_{12}	$-w_{12}$	$-w_{12}$
	3	w_{11}	w_{11}	w_{11}	$-w_{12}$	$-w_{12}$	w_{12}
	4	w_{11}	w_{11}	w_{11}	$-w_{12}$	w_{12}	$-w_{12}$
$m\bar{3}m$-$m_x m_y 2_z$	1	w_{11}	w_{22}	w_{33}	0	0	0
	2	w_{33}	w_{11}	w_{22}	0	0	0
	3	w_{22}	w_{33}	w_{11}	0	0	0
	4	w_{22}	w_{11}	w_{33}	0	0	0
	5	w_{33}	w_{22}	w_{11}	0	0	0
	6	w_{11}	w_{33}	w_{22}	0	0	0
$m\bar{3}m$-$2_{xy} m_{\bar{2}xy} m_z$	1	w_{11}	w_{11}	w_{33}	0	0	w_{12}
	2	w_{33}	w_{11}	w_{11}	w_{12}	0	0
	3	w_{11}	w_{33}	w_{11}	0	w_{12}	0
	4	w_{11}	w_{11}	w_{33}	0	0	$-w_{12}$
	5	w_{33}	w_{11}	w_{11}	$-w_{12}$	0	0
	6	w_{11}	w_{33}	w_{11}	0	$-w_{12}$	0

TABLE G.2: Permissible domain quadruplets for species $m\bar{3}m$-$Pnda$-$4_z m_x m_{xy}$.

$ABCD$	n	m_{AD}	m_{BC}	Ω	Δ	Θ	$ABCD$	n	m_{AD}	m_{BC}	Ω	Δ	Θ
1 2 1 2	$(10\bar{1})$	(101)	(101)	Ω_1	0	0	1 2 1 2	(101)	$(10\bar{1})$	$(10\bar{1})$	Ω_1	0	0
1 3 1 3	(011)	$(01\bar{1})$	$(01\bar{1})$	Ω_1	0	0	1 3 1 3	$(01\bar{1})$	(011)	(011)	Ω_1	0	0
2 3 2 3	(110)	$(1\bar{1}0)$	$(1\bar{1}0)$	$-\Omega_1$	0	0	2 3 2 3	$(1\bar{1}0)$	(110)	(110)	$-\Omega_1$	0	0

$$\Omega_1 = \frac{-4\,(w_{11}-w_{33})}{2+w_{11}+w_{33}}$$

($\boldsymbol{t}_{BC}$ and $\boldsymbol{t}_{AD}$ are the directions of intersection lines of PDW's), the mentioned condition reads

$$\boldsymbol{t}_{BC} \times \boldsymbol{t}_{AD} = 0. \tag{G.1b}$$

Using Eq. (1), possible domain quadruplets which might lead to domain geometries specified in Fig. G.1 can be selected. Understandably, we also allow for the possibility that the domains A and C (or B and D) represent the same domain state. In Tables G.2-G.5 we show all quasipermissible quadruplets in discussed species.

Now we stipulate the *second requirement*, which specifies the conditions that four domains representing a quasipermissible quadruplet should coexist without any additional strain, *when* $\boldsymbol{w}_S \neq 0$ *is taken into account*. Such a domain system would portray a *permissible quadruplet*. The analysis is based on specifying the geometrical requirements for mechanical compatibility, which result in formulation of three conditions for components of spontaneous strain tensor $\boldsymbol{w}_{S,kl}$. Their graphical representation is shown in Fig. G.3.

First, in all four coinciding domains lattice distortion due to different ferroelastic strains along the three domain walls N, M_{BC}, and M_{AD} must be identical. Clearly, this condition is satisfied when domain walls N, M_{BC}, and M_{AD} are PDW's. Second, two of the domains can be expected to be separated by an angle Ω because of different spontaneous strain values in the plane perpendicular to the common intersection line $\boldsymbol{t}=\boldsymbol{t}_{BC}=\boldsymbol{t}_{AD}$ (see Fig. G.3b). It is logical to call the angle Ω *clapping angle* [G4,5], as such it was defined for situations in samples containing just two. Similar incompatibility of shear spontaneous strains in the planes parallel and perpendicular to the domain wall N can lead to the presence of other two *shear misfit angles* Δ and Θ, respectively (see Figs. G.3c and G.3d). In the following text we indicate the straightforward calculations of angles Ω, Δ, and Θ.

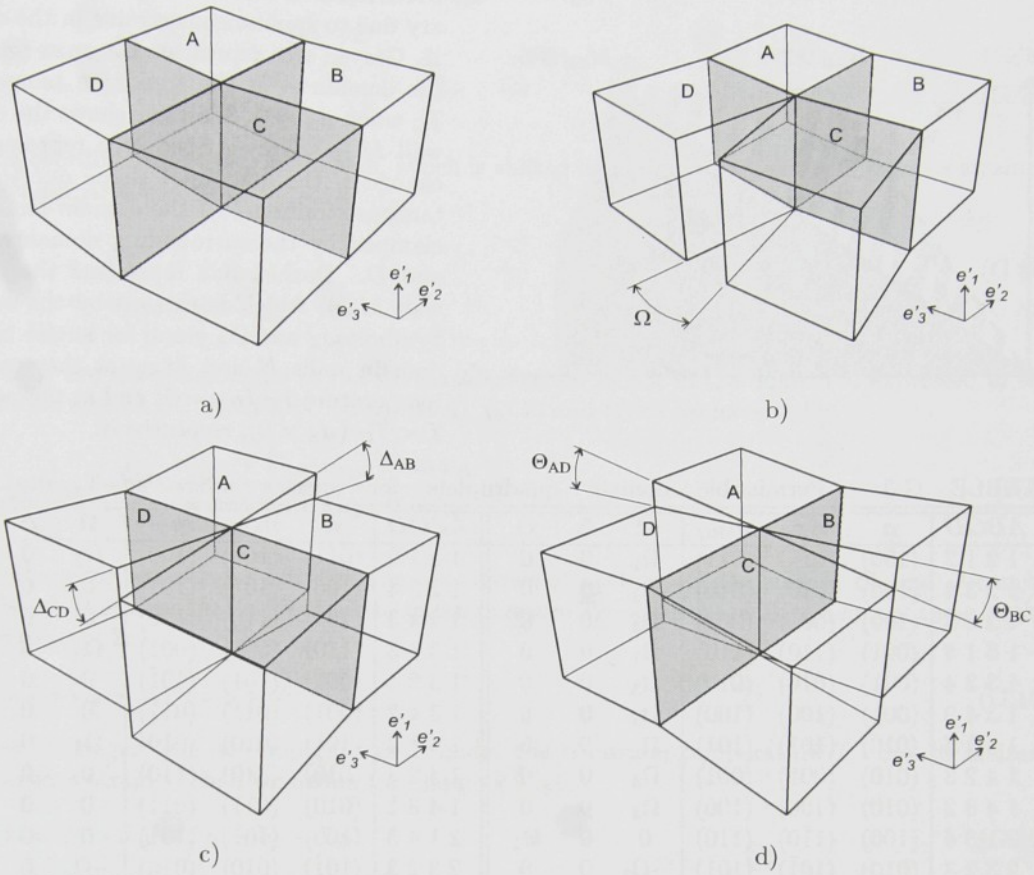

FIGURE G.3: Graphical representations of mechanical compatibility of domain quadruplets, i.e. four ferroelastic domains coexisting along a line; Grayed planes represent common domain walls of the adjacent domains where no additional stresses are required to "stick" the domain quadruplet together; (a) permissible domain quadruplet, i.e. stress-free coexistence of four domains, (b) mechanical incompatibility of shear ($u'_{S,23}$) and normal ($u'_{S,22}$ and $u'_{S,33}$) components spontaneous strains yields the presence of clapping angle Ω; (c) and (d) difference of shear ($u'_{S,12}$ and $u'_{S,13}$) components of spontaneous strains lead to the presence of shear angles Δ and Θ.

It is convenient to transform the spontaneous strain tensors of domain states A, B, C, and D into a rotated coordinate system, which is attached to the quadruplet. Let us consider the basis the coordinate system S of the paraelectric phase:

$$\mathbf{e}_1 = (100), \qquad \mathbf{e}_2 = (010), \qquad \mathbf{e}_3 = (001). \tag{G.2}$$

Now we define the rotated coordinate system S', which is attached to the intersection of domain walls (see Fig. G.2):

$$\mathbf{e}'_1 = \frac{\boldsymbol{t}}{||\boldsymbol{t}||}, \qquad \mathbf{e}'_2 = \frac{\boldsymbol{t}}{||\boldsymbol{t}||} \times \frac{\boldsymbol{n}}{||\boldsymbol{n}||}, \qquad \mathbf{e}'_3 = -\frac{\boldsymbol{n}}{||\boldsymbol{n}||}. \tag{G.3}$$

Knowing the bases $\mathbf{e}_i$ and $\mathbf{e}'_i$, we can define a transformation matrix a_{ij} by the equations $a_{ij} = \mathbf{e}'_i \cdot \mathbf{e}_j$, where i, j = 1, 2, 3. Then, the components of spontaneous strain tensors in the coordinate system attached to the quadruplet are obtained from $u'_{S,ij} = a_{ik}\, a_{ik}\, u_{S,kl}$.

Now we reach the principal goal of this paper, the analysis of the mechanical compatibility of the domain quadruplet when $\boldsymbol{u}_S \neq 0$. Let us start with the calculation of the *clapping angle*

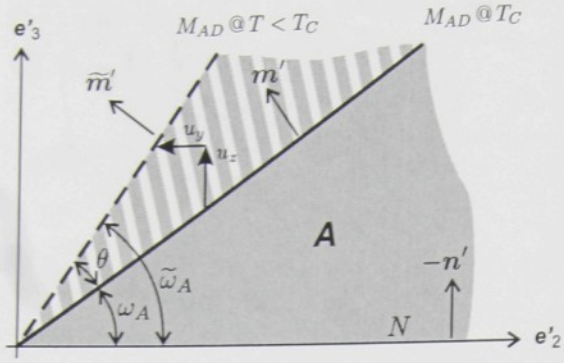

FIGURE G.4: Rotation of the domain boundary due to spontaneous strains in the domain A. Grayed area represents the cross-section of the domain A at the transition temperature T_C when $\boldsymbol{u}_S = 0$. Solid line shows the domain wall M_{AD}. Gray-striped area represents the change of the domain A shape due to spontaneous strains $\boldsymbol{u}_S$, if the domain remain unclamped by the surrounding domains B, C, and D. Dashed line represents the domain wall M_{AD}, which is rotated by the angle θ. Symbols ω_A and $\widetilde{\omega}_A$ stand for angles between domain walls N and M_{AD} at the transition temperature T_C ($\boldsymbol{u}_S = 0$) and at temperature $T < T_C$ ($\boldsymbol{u}_S \neq 0$), respectively.

TABLE G.3: Permissible domain quadruplets for species $m\bar{3}m$-$P\bar{4}ds$-$3_{xyz}m_{\bar{x}y}$.

$ABCD$	$\boldsymbol{n}$	$\boldsymbol{m}_{\mathrm{AD}}$	$\boldsymbol{m}_{\mathrm{BC}}$	Ω	Δ	Θ	$ABCD$	$\boldsymbol{n}$	$\boldsymbol{m}_{\mathrm{AD}}$	$\boldsymbol{m}_{\mathrm{BC}}$	Ω	Δ	Θ
1 2 1 2	(100)	(011)	(011)	Ω_1	0	0	1 2 1 2	(011)	(100)	(100)	Ω_2	0	0
1 2 3 4	(100)	(010)	(010)	Ω_3	0	0	1 2 3 4	(100)	(101)	$(10\bar{1})$	0	0	$-\Theta_1$
1 2 4 3	(100)	(001)	(001)	Ω_3	0	0	1 2 4 3	(100)	(110)	$(1\bar{1}0)$	0	0	Θ_1
1 3 1 3	(001)	(110)	(110)	Ω_1	0	0	1 3 1 3	(110)	(001)	(001)	Ω_2	0	0
1 3 2 4	(001)	(010)	(010)	Ω_3	0	0	1 3 2 4	(001)	(101)	$(10\bar{1})$	0	0	Θ_1
1 3 4 2	(001)	(100)	(100)	Ω_3	0	0	1 3 4 2	(001)	(011)	$(01\bar{1})$	0	0	$-\Theta_1$
1 4 1 4	(010)	(101)	(101)	Ω_1	0	0	1 4 1 4	(101)	(010)	(010)	Ω_2	0	0
1 4 2 3	(010)	(001)	(001)	Ω_3	0	0	1 4 2 3	(010)	(110)	$(1\bar{1}0)$	0	0	$-\Theta_1$
1 4 3 2	(010)	(100)	(100)	Ω_3	0	0	1 4 3 2	(010)	(011)	$(01\bar{1})$	0	0	Θ_1
2 1 3 4	(100)	$(1\bar{1}0)$	(110)	0	0	Θ_1	2 1 4 3	(100)	$(10\bar{1})$	(101)	0	0	$-\Theta_1$
2 3 2 3	(010)	$(10\bar{1})$	$(10\bar{1})$	$-\Omega_1$	0	0	2 3 2 3	$(10\bar{1})$	(010)	(010)	$-\Omega_2$	0	0
2 3 4 1	(010)	(011)	$(01\bar{1})$	0	0	$-\Theta_1$	2 4 2 4	(001)	$(1\bar{1}0)$	$(1\bar{1}0)$	$-\Omega_1$	0	0
2 4 2 4	$(1\bar{1}0)$	(001)	(001)	$-\Omega_2$	0	0	2 4 3 1	(001)	(011)	$(01\bar{1})$	0	0	Θ_1
3 1 4 2	(001)	$(10\bar{1})$	(101)	0	0	$-\Theta_1$	3 2 4 1	(010)	(110)	$(1\bar{1}0)$	0	0	Θ_1
3 4 3 4	(100)	$(01\bar{1})$	$(01\bar{1})$	Ω_1	0	0	3 4 3 4	$(01\bar{1})$	(100)	(100)	Ω_2	0	0

$$\Omega_1 = \frac{-4\sqrt{2}\,u_{12}}{1+u_{11}+u_{12}}, \qquad \Omega_2 = \frac{-4\sqrt{2}\,u_{12}}{1+u_{11}}, \qquad \Omega_3 = \frac{-4\,u_{12}}{1+u_{11}}, \qquad \Theta_1 = -2\,u_{12}.$$

Ω. First consider two plane boundaries of the domain A, i.e. domain walls N and M_{AD}, at the transition temperature T_C when $\boldsymbol{u}_S = 0$. Let us denote the angle between these two domain walls by a symbol ω_A (see Fig. G.4). Then the normal directions of the domain walls N and M_{AD} can be easily expressed in the coordinate system S' as functions of the angle ω_A: $\boldsymbol{n}' = (0, 0, -1)$, $\boldsymbol{m}' = (0, -\sin\omega_A, \cos\omega_A)$. The position of the domain walls (specified by coordinates x', y' and z') is given by equations:

$$z' = 0, \text{ for the wall } N, \tag{G.4a}$$

$$y' \sin\omega_A - z' \cos\omega_A = 0, \text{ for the wall } M_{AD}. \tag{G.4b}$$

At temperatures T below the transition temperature T_C, the material in the domain A is subjected to the spontaneous strain $\boldsymbol{u}_S$. If the domain A is not clamped by the surrounding domains B, C and D, the spontaneous strain results in a rotation of the domain wall M_{AD} by an angle θ. This results in a change of the angle between the domain walls, which is then equal to

$$\widetilde{\omega}_A = \omega_A + \theta, \tag{G.5}$$

as it is shown in Fig. G.4. Position of the rotated domain wall M_{AD} is given by the equation

$$\widetilde{y}' \sin\widetilde{\omega}_A - \widetilde{z}' \cos\widetilde{\omega}_A = 0, \tag{G.6}$$

where

$$\widetilde{y}' = y' + u_y, \tag{G.7a}$$
$$\widetilde{z}' = z' + u_z \tag{G.7b}$$

are the coordinates of the domain wall, which is shifted by u_y and u_z due to spontaneous strain in the domain A:

$$u_y = u'_{S,22}\, y' + u'_{S,23}\, z', \tag{G.8a}$$
$$u_z = u'_{S,23}\, y' + u'_{S,33}\, z'. \tag{G.8b}$$

Here $u'_{S,ij}$ are the components of the spontaneous strain tensor in the domain A expressed in the coordinate system S'. From Eqs. (G.4), (G.6), (G.7) and (G.8) we have:

$$\tan\widetilde{\omega}_A = \frac{\widetilde{z}}{\widetilde{y}} = \frac{u'_{S,23} + \left(1 + u'_{S,33}\right)\tan\omega_A}{1 + u'_{S,22} + u'_{S,23}\tan\omega_A}. \tag{G.9}$$

In the same way, angles between the boundaries of unclamped domains B, C, and D can be calculated. It is clear that at the transition temperature T_C, when $\boldsymbol{u}_S \to 0$, the sum of these angles equals exactly 2π:

$$\omega_A + \omega_B + \omega_C + \omega_D = 2\pi. \tag{G.10}$$

This is no longer true at temperatures T under the transition temperature T_C due to nonzero spontaneous strains. Then we define the clapping angle

$$\Omega = 2\pi - \widetilde{\omega}_A - \widetilde{\omega}_B - \widetilde{\omega}_C - \widetilde{\omega}_D. \tag{G.11}$$

Similarly, the shear misfit angles Δ and Θ can be calculated, however the resulting expressions are much simpler. In this case we need only to compare the shear spontaneous strains in the planes perpendicular to and parallel with the domain wall N, since the lattice distortions along PDW's forming the domain quadruplet are the same.

$$\Delta_{AB} \approx u'_{S,12}(A) - u'_{S,12}(B), \tag{G.12}$$
$$\Delta_{CD} \approx u'_{S,12}(C) - u'_{S,12}(D), \tag{G.13}$$
$$\Theta_{BC} \approx u'_{S,13}(B) - u'_{S,13}(C), \tag{G.14}$$
$$\Theta_{AD} \approx u'_{S,13}(A) - u'_{S,13}(D). \tag{G.15}$$

In all considered species, it is $\Delta_{AB} = \Delta_{CD} = \Delta$ and $\Theta_{BC} = \Theta_{AD} = \Theta$. If even one of the angles Ω, Δ, and Θ is nonzero, unperturbed coexistence of four domains in the discussed species and geometry is not possible; no permissible quadruplet can exist except for specific cases of particular values of the $\boldsymbol{u}_S$ components. In quasipermissible quadruplets Ω, Δ, and Θ are *equal zero*, since real lattice distortions are not yet taken into account. In permissible quadruplets, they play an essential role. For the discussed species clapping angles and shear misfit angles have been calculated and are included in the data of Tabs. G.2-G.5.

Should any of the quadruplets included in this table be permissible, it is required that all values of Ω, Δ, and Θ equal zero. This is not the case, in general, for any of quadruplets of our geometry in all discussed species shown in Tabs. G.2-G.5.

Nevertheless, our results do not exclude any possibility of a stress-free or mechanically acceptable existence of domain quadruplets in a limited temperature range or in samples of particular composition. Data in Tabs. G.2-G.5 show formulae for angles Ω, Δ, and Θ. These values are functions of spontaneous strain components $u_{S,ij}$, which can be controlled by the composition of samples made of solid solutions of two or more components. So, there is a possibility that for a

material of the engineered composition all the angles Ω, Δ, and Θ for a particular domain system can be negligibly small. In this case, our results provide an efficient and useful tool, which can be used in the practical area of domain engineering to specify conditions for spontaneous strains components which must be complied to allow the mechanically compatible (stress-free) or energetically acceptable coexistence of four ferroelastic domain states.

G.4. COMPARISON WITH EXPERIMENTAL DATA AND ADDITIONAL CONCLUSIONS

The results of our analysis can be compared with the above mentioned experimental observations of domain quadruplets in $KNbO_3$ crystals. Two such systems were observed in this material. The one published by Wiesendanger [G20] and shown in Fig. G.1 contains both W_f and S-walls. It corresponds to the domain system $ABCD = 1452$. The second quadruplet in this material was observed by Li Lian et al. [G21] and corresponds to the domain system $ABCD = 1254$. The observed quadruplets were fully reproducible in different parts of several $KNbO_3$ samples. Both these systems are highlighted in Tab. G.5. We see that both of them have zero clapping angle Ω. Thus the only mismatch of spontaneous shear strains leads to the nonzero value $\Theta_2 = -\sqrt{2}\,u_{12}$. Then, it is the strain component u_{12}, which must be very small if the domain quadruplet should realize. And this is indeed the case: at room temperature the $\boldsymbol{u}_S$ components in the orthorhombic phase of $KNbO_3$ are [G22]: $u_{11} = 0.004$, $u_{12} = -0.002$, and $u_{33} = -0.013$. Let us note that using these values, the parameter a specifying the orientation of the S-wall equals $a = 0.26$. This value is in a good agreement with the experimentally observed [G20] orientations of the S-wall (1/0.3/1) and (1/-0.3/1).

Using formulae in Tab. G.5 we can obtain numerical values for clapping angles Ω and shear misfit angles Θ, which correspond to the spontaneous strains in the orthorhombic phase of $KNbO_3$ at room temperature: $\Omega_1 = 1°55'53''$, $\Omega_2 = 1°55'59''$, $\Omega_3 = 1°54'1''$, $\Omega_4 = 21'8''$, $\Omega_5 = 29'53''$, $\Omega_6 = 21'18''$, $\Theta_1 = 56'46''$, and $\Theta_2 = 10'36''$. It follows from these results that although the coexistence of the four specified domain states is not stress-free in the two observed cases, it is these domain systems, which represent configurations with minimum elastic energy, because the value of Θ_2 represents the smallest value in Tab. G.5. Other quadruplets would lead to higher elastic incompatibility and thus to higher energy in $KNbO_3$ samples at room temperature.

G.5. SUMMARY

In crystals of $KNbO_3$ representing species $m\bar{3}m$-$P\varepsilon ds$-$2_{xy}m_{\bar{x}y}m_z$ the coexistence of four domain states was repeatedly observed. Here we discuss theoretically the essential aspect of the problem of domain quadruplets, their realization from the point of view of spontaneous strains of coinciding domains. A general theory is specified and employed for four ferroelectric species represented by a number of materials, in particular by often studied perovskites: $m\bar{3}m$-$m_xm_y2_z$, $m\bar{3}m$-$2_{xy}m_{\bar{x}y}m_z$, $m\bar{3}m$-$3m$, and $m\bar{3}m$-$4mm$. It is shown that, in general, no mechanically compatible (stress-free) quadruplets exist. Nevertheless, the results make it possible to specify those conditions for spontaneous strain components which must be complied to allow for energetically acceptable quadruplets. These conditions are fulfilled in the orthorhombic phase of $KNbO_3$.

It is appropriate to mention that the theoretical approach offered in this paper can be used for specific discussions of the coincidence of multidomain states in thin films where some components of spontaneous strain need not play an essential role.

Acknowledgements

Part of this work (P.M.) was done within the framework of the Swiss National Research Program on Nano-Science (NCCR) and also supported by the Grant Agency of the Czech Republic GACR

202/03/0569. The work of the second author (J.F.) was supported by the Ministry of Education of Czech Republic under Research Program MSM 242200002.

References

[G1] K. Aizu, Phys. Rev. **146**, 423 (1966).
[G2] K. Aizu, J. Phys. Soc. Jpn. **27**, 387 (1969).
[G3] S.P. Yudin, T.V. Panchenko and A.Y. Kudzin, Ferroelectrics **18**, 45 (1978).
[G4] J. Fousek and V. Janovec, J. Appl. Phys. **40**, 135 (1969).
[G5] J.Sapriel, Phys. Rev. B **12**, 5128 (1975).
[G6] J. Fousek, D.B. Litvin and L.E. Cross, J. Phys. Condens. Matter **13**, L33 (2001).
[G7] J. Fousek and L. E. Cross, Ferroelectrics **293**, 430 (2003).
[G8] Duan Feng, Nai-ben Ming, Jing-Fen Hong, Yong-Shun Yang, Jin-Song Zhu, Zhen Yang and Ye-Ning Wang, Appl. Phys. Lett. **37**, 607 (1980).
[G9] S.-N. Zhu, Y.-Y. Zhu, E.-Q. Qin, H.-F. Wang, C.-Z. Ge and N.-B. Ming, Phys. Rev. Letters **78**, 2752 (1997).
[G10] P.W. Forsbergh, Jr., Phys. Rev. **76**, 1187 (1949).
[G11] G. Arlt and P. Sasko, J. Appl. Phys. **51**, 4956 (1980).
[G12] S-E. Park, S. Wada, L. E. Cross and T. R. Shrout, J. Appl. Phys. **86**, 2746 (1999).
[G13] S. Wada, S-E. Park, L. E. Cross and T. R. Shrout, Ferroelectrics **221**, 147 (1999).
[G14] Bei Jiang, Jianhua Yin and W. Cao, IEEE Transactions on Ultrasonics, Ferroelectrics and Frequency Control, **47**, 285 (2000).
[G15] Jianhua Yin and W. Cao, J. Appl. Phys. **92**, 444 (2002).
[G16] S. Wada, A. Seike and T. Tsurumi, Jpn. J. Appl. Phys. **40**, 5690 (2001).
[G17] G. Suyal, E. Colla, R. Gysel, M. Cantoni, and N. Setter, Nano Letters **4**, 1339 (2004).
[G18] J. Erhart and W. Cao, J. Appl. Phys. **94**, 3436 (2003).
[G19] E. K. H. Salje, *Phase Transitions in Ferroelastic and Co-elastic Crystals* (Cambridge University Press, 1990).
[G20] E. Wiesendanger, Czech. J. Phys. **23**, 91 (1973).
[G21] Li Lian, T. C. Chong, H. Kumagai, M. Hirano, Lu Taijing and S. C. Ng, J. Appl. Phys. **80**, 376 (1996).
[G22] Landolt-Bornstein, *Numerical data and functional relationships in science and technology*, New Series Vol. III/28b (Springer, New York, 1981).

TABLE G.4: Permissible domain quadruplets for species $m\bar{3}m$-$Pads$-$m_x m_y 2_z$.

$ABCD$	n	m_{AD}	m_{BC}	Ω	Δ	Θ	$ABCD$	n	m_{AD}	m_{BC}	Ω	Δ	Θ
1 4 1 4	(1$\bar{1}$0)	(1$\bar{1}$0)	(1$\bar{1}$0)	$-\Omega_1$	0	0	1 4 1 4	(1$\bar{1}$0)	(1$\bar{1}$0)	(1$\bar{1}$0)	$-\Omega_1$	0	0
1 4 2 6	(1$\bar{1}$0)	(01$\bar{1}$)	(10$\bar{1}$)	$-\Omega_2$	0	$-\Theta_1$	1 4 2 6	(1$\bar{1}$0)	(011)	(101)	$-\Omega_2$	0	Θ_1
1 4 2 6	(1$\bar{1}$0)	(01$\bar{1}$)	(101)	Ω_2	0	Θ_1	1 4 2 6	(110)	(011)	(10$\bar{1}$)	Ω_2	0	$-\Theta_1$
1 4 3 5	(1$\bar{1}$0)	(10$\bar{1}$)	(01$\bar{1}$)	Ω_3	0	Θ_2	1 4 3 5	(1$\bar{1}$0)	(101)	(011)	Ω_3	0	$-\Theta_2$
1 4 3 5	(110)	(10$\bar{1}$)	(011)	Ω_3	0	$-\Theta_2$	1 4 3 5	(110)	(101)	(01$\bar{1}$)	Ω_3	0	Θ_2
1 5 1 5	(10$\bar{1}$)	(101)	(101)	Ω_4	0	0	1 5 1 5	(101)	(10$\bar{1}$)	(10$\bar{1}$)	Ω_4	0	0
1 5 2 4	(10$\bar{1}$)	(1$\bar{1}$0)	(01$\bar{1}$)	$-\Omega_5$	0	Θ_3	1 5 2 4	(10$\bar{1}$)	(110)	(011)	$-\Omega_5$	0	$-\Theta_3$
1 5 2 4	(101)	(1$\bar{1}$0)	(011)	$-\Omega_5$	0	$-\Theta_3$	1 5 2 4	(101)	(110)	(01$\bar{1}$)	$-\Omega_5$	0	Θ_3
1 5 3 6	(10$\bar{1}$)	(01$\bar{1}$)	(1$\bar{1}$0)	$-\Omega_2$	0	Θ_1	1 5 3 6	(10$\bar{1}$)	(011)	(110)	Ω_2	0	Θ_1
1 5 3 6	(101)	(01$\bar{1}$)	(110)	Ω_2	0	$-\Theta_1$	1 5 3 6	(101)	(011)	(1$\bar{1}$0)	$-\Omega_2$	0	$-\Theta_1$
1 6 1 6	(01$\bar{1}$)	(011)	(011)	Ω_6	0	0	1 6 1 6	(011)	(01$\bar{1}$)	(01$\bar{1}$)	Ω_6	0	0
1 6 2 5	(01$\bar{1}$)	(10$\bar{1}$)	(1$\bar{1}$0)	$-\Omega_3$	0	$-\Theta_2$	1 6 2 5	(01$\bar{1}$)	(101)	(110)	Ω_3	0	$-\Theta_2$
1 6 2 5	(011)	(10$\bar{1}$)	(110)	Ω_3	0	Θ_2	1 6 2 5	(011)	(101)	(1$\bar{1}$0)	$-\Omega_3$	0	Θ_2
1 6 3 4	(01$\bar{1}$)	(1$\bar{1}$0)	(10$\bar{1}$)	$-\Omega_5$	0	$-\Theta_3$	1 6 3 4	(01$\bar{1}$)	(110)	(101)	Ω_5	0	$-\Theta_3$
1 6 3 4	(011)	(1$\bar{1}$0)	(101)	$-\Omega_5$	0	Θ_3	1 6 3 4	(011)	(110)	(10$\bar{1}$)	Ω_5	0	Θ_3
2 4 2 4	(10$\bar{1}$)	(101)	(101)	$-\Omega_6$	0	0	2 4 2 4	(101)	(10$\bar{1}$)	(10$\bar{1}$)	$-\Omega_6$	0	0
2 4 3 6	(10$\bar{1}$)	(1$\bar{1}$0)	(01$\bar{1}$)	$-\Omega_3$	0	Θ_2	2 4 3 6	(10$\bar{1}$)	(110)	(011)	$-\Omega_3$	0	$-\Theta_2$
2 4 3 6	(101)	(1$\bar{1}$0)	(011)	$-\Omega_3$	0	$-\Theta_2$	2 4 3 6	(101)	(110)	(01$\bar{1}$)	$-\Omega_3$	0	Θ_2
2 5 2 5	(01$\bar{1}$)	(011)	(011)	$-\Omega_1$	0	0	2 5 2 5	(011)	(01$\bar{1}$)	(01$\bar{1}$)	$-\Omega_1$	0	0
2 5 3 4	(01$\bar{1}$)	(10$\bar{1}$)	(1$\bar{1}$0)	Ω_2	0	Θ_1	2 5 3 4	(01$\bar{1}$)	(101)	(110)	$-\Omega_2$	0	Θ_1
2 5 3 4	(011)	(10$\bar{1}$)	(110)	$-\Omega_2$	0	$-\Theta_1$	2 5 3 4	(011)	(101)	(1$\bar{1}$0)	Ω_2	0	$-\Theta_1$
2 6 2 6	(1$\bar{1}$0)	(110)	(110)	$-\Omega_4$	0	0	2 6 2 6	(110)	(1$\bar{1}$0)	(1$\bar{1}$0)	$-\Omega_4$	0	0
2 6 3 5	(1$\bar{1}$0)	(01$\bar{1}$)	(10$\bar{1}$)	Ω_5	0	Θ_3	2 6 3 5	(1$\bar{1}$0)	(011)	(101)	Ω_5	0	$-\Theta_3$
2 6 3 5	(110)	(01$\bar{1}$)	(101)	$-\Omega_5$	0	$-\Theta_3$	2 6 3 5	(110)	(011)	(10$\bar{1}$)	$-\Omega_5$	0	Θ_3
3 4 3 4	(01$\bar{1}$)	(011)	(011)	$-\Omega_4$	0	0	3 4 3 4	(011)	(01$\bar{1}$)	(01$\bar{1}$)	$-\Omega_4$	0	0
3 5 3 5	(1$\bar{1}$0)	(110)	(110)	Ω_6	0	0	3 5 3 5	(110)	(1$\bar{1}$0)	(1$\bar{1}$0)	Ω_6	0	0
3 6 3 6	(10$\bar{1}$)	(101)	(101)	Ω_1	0	0	3 6 3 6	(101)	(10$\bar{1}$)	(10$\bar{1}$)	Ω_1	0	0
4 1 5 3	(1$\bar{1}$0)	(01$\bar{1}$)	(10$\bar{1}$)	$-\Omega_3$	0	$-\Theta_2$	4 1 5 3	(1$\bar{1}$0)	(011)	(101)	$-\Omega_3$	0	Θ_2
4 1 5 3	(110)	(01$\bar{1}$)	(101)	Ω_3	0	Θ_2	4 1 5 3	(110)	(011)	(10$\bar{1}$)	Ω_3	0	$-\Theta_2$
4 1 6 2	(1$\bar{1}$0)	(10$\bar{1}$)	(01$\bar{1}$)	Ω_2	0	Θ_1	4 1 6 2	(1$\bar{1}$0)	(101)	(011)	Ω_2	0	$-\Theta_1$
4 1 6 2	(110)	(10$\bar{1}$)	(011)	Ω_2	0	$-\Theta_1$	4 1 6 2	(110)	(101)	(01$\bar{1}$)	Ω_2	0	Θ_1
4 2 5 1	(10$\bar{1}$)	(1$\bar{1}$0)	(01$\bar{1}$)	Ω_5	0	$-\Theta_3$	4 2 5 1	(10$\bar{1}$)	(110)	(011)	Ω_5	0	Θ_3
4 2 5 1	(101)	(1$\bar{1}$0)	(011)	Ω_5	0	Θ_3	4 2 5 1	(101)	(110)	(01$\bar{1}$)	Ω_5	0	$-\Theta_3$
4 2 6 3	(10$\bar{1}$)	(01$\bar{1}$)	(1$\bar{1}$0)	$-\Omega_3$	0	Θ_2	4 2 6 3	(10$\bar{1}$)	(011)	(110)	Ω_3	0	Θ_2
4 2 6 3	(101)	(01$\bar{1}$)	(110)	Ω_3	0	$-\Theta_2$	4 2 6 3	(101)	(011)	(1$\bar{1}$0)	$-\Omega_3$	0	$-\Theta_2$
4 3 5 2	(01$\bar{1}$)	(10$\bar{1}$)	(1$\bar{1}$0)	$-\Omega_2$	0	$-\Theta_1$	4 3 5 2	(01$\bar{1}$)	(101)	(110)	Ω_2	0	$-\Theta_1$
4 3 5 2	(011)	(10$\bar{1}$)	(110)	Ω_2	0	Θ_1	4 3 5 2	(011)	(101)	(1$\bar{1}$0)	$-\Omega_2$	0	Θ_1
4 3 6 1	(01$\bar{1}$)	(1$\bar{1}$0)	(10$\bar{1}$)	Ω_5	0	Θ_3	4 3 6 1	(01$\bar{1}$)	(110)	(101)	$-\Omega_5$	0	Θ_3
4 3 6 1	(011)	(1$\bar{1}$0)	(101)	Ω_5	0	$-\Theta_3$	4 3 6 1	(011)	(110)	(10$\bar{1}$)	$-\Omega_5$	0	$-\Theta_3$
5 1 6 3	(10$\bar{1}$)	(1$\bar{1}$0)	(01$\bar{1}$)	$-\Omega_2$	0	Θ_1	5 1 6 3	(10$\bar{1}$)	(110)	(011)	$-\Omega_2$	0	$-\Theta_1$
5 1 6 3	(101)	(1$\bar{1}$0)	(011)	$-\Omega_2$	0	$-\Theta_1$	5 1 6 3	(101)	(110)	(01$\bar{1}$)	$-\Omega_2$	0	Θ_1
5 2 6 1	(01$\bar{1}$)	(10$\bar{1}$)	(1$\bar{1}$0)	Ω_3	0	Θ_2	5 2 6 1	(01$\bar{1}$)	(101)	(110)	$-\Omega_3$	0	Θ_2
5 2 6 1	(011)	(10$\bar{1}$)	(110)	$-\Omega_3$	0	$-\Theta_2$	5 2 6 1	(011)	(101)	(1$\bar{1}$0)	Ω_3	0	$-\Theta_2$
5 3 6 2	(1$\bar{1}$0)	(01$\bar{1}$)	(10$\bar{1}$)	$-\Omega_5$	0	$-\Theta_3$	5 3 6 2	(1$\bar{1}$0)	(011)	(101)	$-\Omega_5$	0	Θ_3
5 3 6 2	(110)	(01$\bar{1}$)	(101)	Ω_5	0	Θ_3	5 3 6 2	(110)	(011)	(10$\bar{1}$)	Ω_5	0	$-\Theta_3$

$$\Omega_1 = \frac{-4\sqrt{3}\,(u_{22}-u_{33})\,(3-u_{11}+2u_{22}+2u_{33})}{(6+u_{11}+4u_{22}+u_{33})\,(6+u_{11}+u_{22}+4u_{33})}, \qquad \Omega_4 = \frac{4\,(u_{11}-u_{22})}{2+u_{11}+u_{22}},$$

$$\Omega_2 = \frac{-4\sqrt{3}\,(u_{11}-u_{33})\,(3+2u_{11}-u_{22}+2u_{33})}{(6+4u_{11}+u_{22}+u_{33})\,(6+u_{11}+u_{22}+4u_{33})}, \qquad \Omega_5 = \frac{-4\,(u_{11}-u_{33})}{2+u_{11}+u_{33}},$$

$$\Omega_3 = \frac{4\sqrt{3}\,(u_{11}-u_{22})\,(3+2u_{11}+2u_{22}-u_{33})}{(6+4u_{11}+u_{22}+u_{33})\,(6+u_{11}+4u_{22}+u_{33})}, \qquad \Omega_6 = \frac{-4\,(u_{22}-u_{33})}{2+u_{22}+u_{33}},$$

$$\Theta_1 = -\frac{u_{22}-u_{33}}{\sqrt{6}}, \qquad \Theta_2 = \frac{-u_{11}+u_{33}}{\sqrt{6}}, \qquad \Theta_3 = \frac{u_{11}-u_{22}}{\sqrt{6}}.$$

TABLE G.5: Permissible domain quadruplets for species $m\bar{3}m$-$P\varepsilon ds$-$2_{xy}m_{\bar{x}y}m_z$. Parameter of the S-wall: $a = 2u_{12}/(u_{33} - u_{11}) \approx 2Q_{44}/(Q_{33} - Q_{11})$ is temperature independent.

$ABCD$	$\boldsymbol{n}$	$\boldsymbol{m}_{AD}$	$\boldsymbol{m}_{BC}$	Ω	Δ	Θ	$ABCD$	$\boldsymbol{n}$	$\boldsymbol{m}_{AD}$	$\boldsymbol{m}_{BC}$	Ω	Δ	Θ
1 2 1 2	$(10\bar{1})$	$(1\bar{a}1)$	$(1\bar{a}1)$	$-\Omega_1$	0	0	1 2 1 2	$(1\bar{a}1)$	$(10\bar{1})$	$(10\bar{1})$	$-\Omega_2$	0	0
1 2 4 5	$(10\bar{1})$	(101)	(101)	$-\Omega_3$	0	0	1 2 4 5	$(10\bar{1})$	$(1\bar{a}\bar{1})$	$(1a\bar{1})$	0	0	Θ_1
1 2 5 4†	$(10\bar{1})$	(100)	(001)	0	0	$-\Theta_2$	1 2 5 4	$(10\bar{1})$	(010)	(010)	Ω_4	0	0
1 3 1 3	$(01\bar{1})$	$(\bar{a}11)$	$(\bar{a}11)$	$-\Omega_1$	0	0	1 3 1 3	$(\bar{a}11)$	$(01\bar{1})$	$(01\bar{1})$	$-\Omega_2$	0	0
1 3 4 6	$(01\bar{1})$	(011)	(011)	$-\Omega_3$	0	0	1 3 4 6	$(01\bar{1})$	$(\bar{a}1\bar{1})$	$(a1\bar{1})$	0	0	$-\Theta_1$
1 3 6 4	$(01\bar{1})$	(100)	(100)	Ω_4	0	0	1 3 6 4	$(01\bar{1})$	(010)	(001)	0	0	Θ_2
1 4 1 4	(100)	(010)	(010)	Ω_5	0	0	1 4 1 4	(010)	(100)	(100)	Ω_5	0	0
1 4 2 5	(010)	(101)	(101)	Ω_6	0	0	1 4 2 5	(010)	$(1\bar{a}\bar{1})$	$(1a\bar{1})$	0	0	$-\Theta_2$
1 4 3 6	(100)	(011)	(011)	Ω_6	0	0	1 4 3 6	(100)	$(\bar{a}1\bar{1})$	$(a1\bar{1})$	0	0	Θ_2
1 4 5 2	(010)	$(10\bar{1})$	$(10\bar{1})$	Ω_6	0	0	**1 4 5 2**‡	(010)	$(1\bar{a}1)$	$(1a1)$	0	0	Θ_2
1 4 6 3	(100)	$(01\bar{1})$	$(01\bar{1})$	Ω_6	0	0	1 4 6 3	(100)	$(\bar{a}11)$	$(a11)$	0	0	$-\Theta_2$
1 5 1 5	(101)	$(1\bar{a}\bar{1})$	$(1\bar{a}\bar{1})$	$-\Omega_1$	0	0	1 5 1 5	$(1\bar{a}\bar{1})$	(101)	(101)	$-\Omega_2$	0	0
1 5 2 4	(101)	(100)	(001)	0	0	Θ_2	1 5 2 4	(101)	(010)	(010)	Ω_4	0	0
1 5 4 2	(101)	$(10\bar{1})$	$(10\bar{1})$	$-\Omega_3$	0	0	1 5 4 2	(101)	$(1\bar{a}1)$	$(1a1)$	0	0	$-\Theta_1$
1 6 1 6	(011)	$(\bar{a}1\bar{1})$	$(\bar{a}1\bar{1})$	$-\Omega_1$	0	0	1 6 1 6	$(\bar{a}1\bar{1})$	(011)	(011)	$-\Omega_2$	0	0
1 6 3 4	(011)	(100)	(100)	Ω_4	0	0	1 6 3 4	(011)	(010)	(001)	0	0	$-\Theta_2$
1 6 4 3	(011)	$(01\bar{1})$	$(01\bar{1})$	$-\Omega_3$	0	0	1 6 4 3	(011)	$(\bar{a}11)$	$(a11)$	0	0	Θ_1
2 1 4 5	$(10\bar{1})$	(010)	(010)	$-\Omega_4$	0	0	2 1 5 4	$(10\bar{1})$	$(1a\bar{1})$	$(1\bar{a}\bar{1})$	0	0	Θ_1
2 3 2 3	$(1\bar{1}0)$	$(11\bar{a})$	$(11\bar{a})$	Ω_1	0	0	2 3 2 3	$(11\bar{a})$	$(1\bar{1}0)$	$(1\bar{1}0)$	Ω_2	0	0
2 3 5 6	$(1\bar{1}0)$	(110)	(110)	Ω_3	0	0	2 3 5 6	$(1\bar{1}0)$	$(1\bar{1}a)$	$(1\bar{1}\bar{a})$	0	0	$-\Theta_1$
2 3 6 5	$(1\bar{1}0)$	(010)	(100)	0	0	$-\Theta_2$	2 3 6 5	$(1\bar{1}0)$	(001)	(001)	$-\Omega_4$	0	0
2 4 2 4	(101)	$(1a\bar{1})$	$(1a\bar{1})$	Ω_1	0	0	2 4 2 4	$(1a\bar{1})$	(101)	(101)	Ω_2	0	0
2 4 5 1	(101)	$(1\bar{a}1)$	$(1a1)$	0	0	Θ_1	2 5 2 5	(010)	(001)	(001)	Ω_5	0	0
2 5 2 5	(001)	(010)	(010)	Ω_5	0	0	2 5 3 6	(001)	(110)	(110)	Ω_6	0	0
2 5 3 6	(001)	$(1\bar{1}a)$	$(1\bar{1}\bar{a})$	0	0	Θ_2	2 5 4 1	(010)	$(1\bar{a}1)$	$(1a1)$	0	0	$-\Theta_2$
2 5 6 3	(001)	$(1\bar{1}0)$	$(1\bar{1}0)$	$-\Omega_6$	0	0	2 5 6 3	(001)	$(11\bar{a})$	$(11a)$	0	0	Θ_2
2 6 2 6	(110)	$(1\bar{1}a)$	$(1\bar{1}a)$	Ω_1	0	0	2 6 2 6	$(1\bar{1}a)$	(110)	(110)	Ω_2	0	0
2 6 3 5	(110)	(010)	(100)	0	0	Θ_2	2 6 3 5	(110)	(001)	(001)	Ω_4	0	0
2 6 5 3	(110)	$(1\bar{1}0)$	$(1\bar{1}0)$	Ω_3	0	0	2 6 5 3	(110)	$(11\bar{a})$	$(11a)$	0	0	$-\Theta_1$
3 1 4 6	$(01\bar{1})$	(001)	(010)	0	0	$-\Theta_2$	3 1 6 4	$(01\bar{1})$	$(a1\bar{1})$	$(\bar{a}1\bar{1})$	0	0	$-\Theta_1$
3 2 5 6	$(1\bar{1}0)$	(100)	(010)	0	0	Θ_2	3 2 6 5	$(1\bar{1}0)$	$(1\bar{1}\bar{a})$	$(1\bar{1}a)$	0	0	$-\Theta_1$
3 4 3 4	(011)	$(a1\bar{1})$	$(a1\bar{1})$	Ω_1	0	0	3 4 3 4	$(a1\bar{1})$	(011)	(011)	Ω_2	0	0
3 4 6 1	(011)	$(\bar{a}11)$	$(a11)$	0	0	$-\Theta_1$	3 5 3 5	(110)	$(1\bar{1}\bar{a})$	$(1\bar{1}\bar{a})$	$-\Omega_1$	0	0
3 5 3 5	$(1\bar{1}\bar{a})$	(110)	(110)	$-\Omega_2$	0	0	3 5 6 2	(110)	$(11\bar{a})$	$(11a)$	0	0	Θ_1
3 6 3 6	(100)	(001)	(001)	Ω_5	0	0	3 6 3 6	(001)	(100)	(100)	Ω_5	0	0
3 6 4 1	(100)	$(\bar{a}11)$	$(a11)$	0	0	Θ_2	3 6 5 2	(001)	$(11\bar{a})$	$(11a)$	0	0	$-\Theta_2$
4 1 5 2	(010)	$(1a\bar{1})$	$(1\bar{a}\bar{1})$	0	0	Θ_2	4 1 6 3	(100)	$(a1\bar{1})$	$(\bar{a}1\bar{1})$	0	0	$-\Theta_2$
4 2 5 1	(101)	(010)	(010)	$-\Omega_4$	0	0	4 3 6 1	(011)	(010)	(001)	0	0	Θ_2
4 5 4 5	$(10\bar{1})$	$(1a1)$	$(1a1)$	$-\Omega_1$	0	0	4 5 4 5	$(1a1)$	$(10\bar{1})$	$(10\bar{1})$	$-\Omega_2$	0	0
4 6 4 6	$(01\bar{1})$	$(a11)$	$(a11)$	$-\Omega_1$	0	0	4 6 4 6	$(a11)$	$(01\bar{1})$	$(01\bar{1})$	$-\Omega_2$	0	0
5 2 6 3	(001)	$(1\bar{1}\bar{a})$	$(1\bar{1}a)$	0	0	$-\Theta_2$	5 3 6 2	(110)	(010)	(100)	0	0	$-\Theta_2$
5 6 5 6	$(1\bar{1}0)$	$(11a)$	$(11a)$	Ω_1	0	0	5 6 5 6	$(11a)$	$(1\bar{1}0)$	$(1\bar{1}0)$	Ω_2	0	0

$$\Omega_1 = \frac{-2\sqrt{2}\sqrt{2+a^2}\,(-u_{11} + a\,u_{12} + u_{33})}{2 + u_{11} + a\,(a + a\,u_{11} - 2\,u_{12}) + u_{33}}, \quad \Omega_3 = \frac{4\,(u_{11} - u_{33})}{2 + u_{11} + u_{33}}, \quad \Omega_5 = \frac{-4\,u_{12}}{1 + u_{11}},$$

$$\Omega_2 = \frac{-4\sqrt{2}\,(-u_{11} + a\,u_{12} + u_{33})}{\sqrt{2+a^2}\,(2 + u_{11} + u_{33})}, \quad \Omega_4 = \frac{-2\sqrt{2}\,u_{12}}{1 + u_{11}}, \quad \Omega_6 = \frac{-4\sqrt{2}\,u_{12}}{2 + u_{11} + u_{33}},$$

$$\Theta_1 = u_{11} - u_{33}, \qquad \Theta_2 = -\sqrt{2}\,u_{12}.$$

†Domain quadruplet observed in $KNbO_3$ (see Ref. [G14]).
‡Domain quadruplet observed in $KNbO_3$ (see Ref. [G13]).

Summary

Resume

In the previous part, there have been presented main results of our investigation of macroscopic and other domain related problems, which cover a quite large scope of phenomena in ferroelectric-ferroelastic films. Brief comments on the selected papers are given in following Sections focusing on available experimental results, which can confirm the validity of the presented theories.

Comment on Papers A and B

Main results of Papers A and B are the formulae for the equilibrium domain spacing a_{eq}^{0} and the response of the domain pattern to the applied voltage on electrodes given by parameters $A_{\mathrm{eq}}(V)$ and $R_{\mathrm{eq}}(V)$. Knowing this response, the effective permittivity $\varepsilon_{\mathrm{eff}}$ and piezoelectric coefficient d_{36} are calculated.

As the most relevant experimental results available so far, which can confirm the validity of theory presented in Papers A and B, should be recognized the observation of nanoscale 180° stripe domains in ferroelectric lead titanate ($PbTiO_3$) thin films by Streiffer et al. [30]. In this work, lead titanate epitaxial thin films of thicknesses from 6 to 42 nm on strontium titanate isolating substrates using X-ray scattering were studied. The existence of 180° stripe domain patterns of period 3.7 to 24 nm was observer in these films and it was showed that the dependence of domain period on film thickness agrees well with the theory presented in Paper A.

It has to be also pointed out that Papers A and B are presented in their revised forms. On the contrary to their original versions, the dielectric anisotropy of the surface layer is not considered in this revised version, since it is virtually impossible to obtain any experimental data on dielectric anisotropy of electrode-adjacent regions. In addition, the gain due to less complexity of formulae is appreciable. In the original version of the Papers there were also missing some terms in the formula for the Gibbs electric energy of the ferroelectric capacitor. It was corrected in the revised versions and numerical results were modified accordingly.

Comment on Paper E

In Paper E the earlier concept of surface layer model was adopted and generalized by considering the lattice pinning of domain walls. Within this generalized model, the size effect on permittivity was investigated theoretically. From the experimental point of view, there are many observed data on the size effect on permittivity available in literature [16, 17, 19, 21, 22, 23]. As an example, the size effect observed by Basceri at al. [22] is presented in Fig. 15. In this work, permittivity of fiber-textured barium strontium titanate ($Ba_{0.7}Sr_{0.3}TiO_3$) thin films grown by liquid-source metalorganic chemical vapor deposition is studied as a function of film thickness. The type of thickness dependence observed in this work is attributed to the presence of a constant-valued capacitance of the surface layer, represented by the nonzero intercept of the thickness dependence of inverse capacitance on the vertical axis, in series with the thickness-dependent capacitance of the bulk of the film (see Fig. 15).

Analysis in Paper E indicate that the intercept of the thickness dependence of the inverse capacitance ferroelectric film and the vertical axis (offset) should be temperature dependent. However,

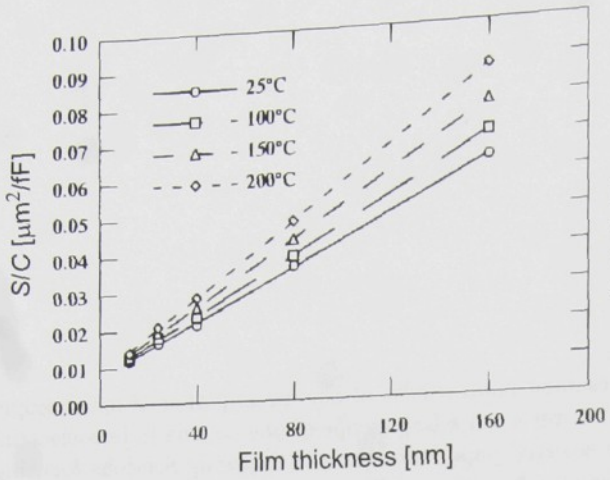

FIGURE 15: Inverse of the zero-bias capacitance density as a function of BST film thickness at temperatures of 25, 100, 150, and 200°C (From Ref. [22])

it is difficult to observe such a temperature dependence of the offset in Fig. 15 due to the limited accuracy of dielectric measurements performed on a set of thin films made of high-permittivity material.

Recently, Takahashi et al. [31] has obtained results on polyvinidilene fluoride (PVDF) polymer films. They performed an analysis of temperature dependencies of dielectric constant of a set of PVDF films of thicknesses down to 10 nm and extracted the temperature dependence of the both permittivity of the ferroelectric layer and surface layers. In addition, they were able to extract the thickness of the surface layer, as it is shown in Fig. 17. As a matter of fact, they provided all necessary data required to check the presented theory. In Fig. 17c there are shown the obtained temperature dependencies of the ferroelectric and the surface layers permittivity. It is very likely that actually it was the temperature dependence of the apparent permittivity of the surface layer $\varepsilon_{\mathrm{mod}}$ measured in their experiment and our theory accounts for its temperature dependence. It is due to the fact that the apparent permittivity $\varepsilon_{\mathrm{mod}}$ is a function of the fraction of the distribution of the dielectric response of the ferroelectric material between the extrinsic and intrinsic contributions. It is known that the extrinsic contributions of considerable values are observed only in a limited temperature range below the phase transition and it is actually in accord with the experimental observation of Takahashi et al., as it is indicated in Fig. 17.

It has to be also pointed out that it is not possible to apply the presented model without any restrictions to complex polymer systems, but published data of hysteresis loops measured in this material (see e.g. the review of Furukawa [32]; also reports of Cho et al. [33] or Chen et al. [34]) show the existence of 180° domain switching. Thus the presence of structures that effectively behave as 180° domains cannot be excluded from the list of phenomena that affect the dielectric response of ferroelectric polymer ultra-thin films.

As a conclusion remark on Paper E, it is necessary to distinguish two different roles of the surface layers on dielectric response in ferroelectric thin films. First, it is clear that the presence of surface layers always deteriorate the intrinsic dielectric response according to the in-series capacitances formula. It means that the dielectric response of mono-domain samples or the samples

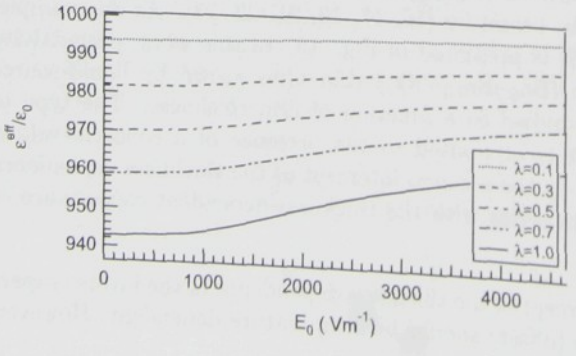

FIGURE 16: Field dependence of the measured permittivity of the ferroelectric film. Parameters of the curves are the values of degree of screening λ Here $d/a = 0.001$.

in the paraelectric phase is always deteriorated due to surface layers. Second, results of Paper E indicate that when the domain spacing is greater than the thickness of the surface layers and when the dielectric response of the ferroelectric layer is dominated by the extrinsic contribution, the deteriorating effect of surface layers is greatly suppressed and the effective dielectric constant of the ferroelectric thin film is dominated by the dielectric response of the ferroelectric layer.

Comment on Paper F

Main result of Paper F is the analysis of the effect of the free charge transport from electrodes across the surface layer on the dielectric response of the ferroelectric polydomain films. The free charges compensate (screen) the bound charges due to spontaneous polarization and it is shown that this polarization screening has a strong pinning impact on the domain walls. As a result it suppresses the extrinsic contribution to the linear dielectric response of the ferroelectric capacitor. Since this suppressive effect can be caused by other phenomena than the charge transport across the surface layer, additional analysis of the dielectric response is required to make decision whether it can be attributed to the spontaneous polarization screening or not. It appears that a hint for the answer can be given by analyzing the dielectric nonlinearity of the ferroelectric polydomain thin film. Figure 16 shows the applied field dependence of the effective permittivity of the ferroelectric capacitor with domain pattern, which indicates an increase of the nonlinearity in the dependence of dielectric constant with increasing the degree of screening λ.

As a conclusion, it can be suggested that using a comprehensive analysis of the dielectric response of ferroelectric polydomain thin films it is possible to study the processes of charge transport in the electrode-adjacent regions. This can provide an additional information on the phenomenon of imprint in ferroelectric thin films for non-volatile ferroelectric memory devices.

Conclusions

Since the ferroelectricity has been discovered it has been obvious to many scientists and engineers that the two stable polarization states $+P$ and $-P$ could be used to encode the 1 and 0 of the Boolean algebra that forms the basis of memory and logic circuitry in all modern computers. Since the spontaneous polarization reversal in the ferroelectric material is used in FRAM, it offers fast and low energy consuming memory devices. This make FRAM more attractive from the application point of view than FLASH or EPROM memory devices. Nevertheless even today, the reliability of FRAM represents one of the major concerns of all leading producers of ferroelectric non-volatile memories. The origin of the reliability problems is the fact that the processing of ferroelectric materials is not absolutely compatible with the "classical" semiconductor processing technology based on silicon. The interaction of the ferroelectric material with the substrate leads to the deterioration of the quality of ferroelectric thin films and it represents a possible source of device failures.

Since the spontaneous polarization reversal plays the principal role in FRAM, switching measurement techniques are used for the characterization of ferroelectric thin films. It is also known that the spontaneous polarization reversal is controlled by the nucleation of domains, which is affected by the quality of the ferroelectric material itself, and the presence of crystal lattice defects plays an essential role in these processes. Since the domain walls are sensitive to the presence of defects in the crystal lattice, there appears a new possibility to use a comprehensive analysis of the small signal dielectric response of ferroelectric polydomain films for studying the processes that affects the quality of the ferroelectric materials. Therefore, it is evident that the presented results provide a simple and useful tool, which can be used for obtaining a lot of additional information on the quality of ferroelectric materials and ferroelectric thin films, in particular.

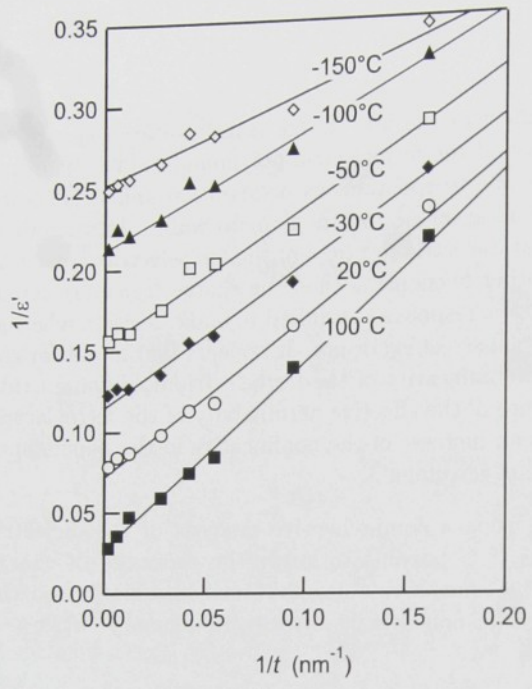

a)

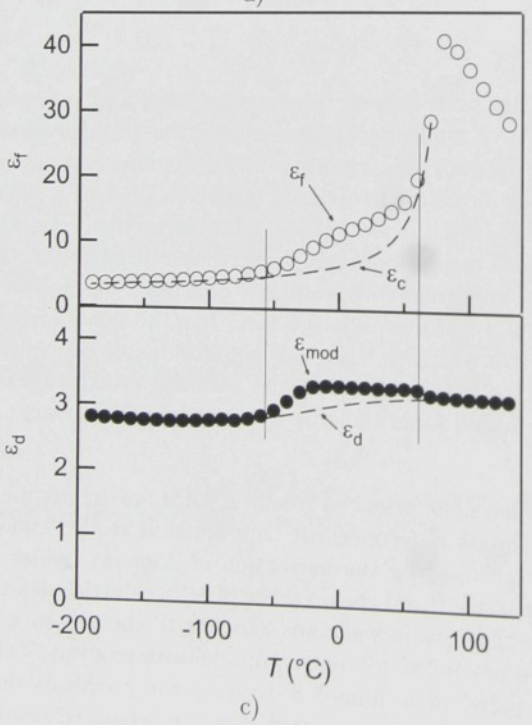

c)

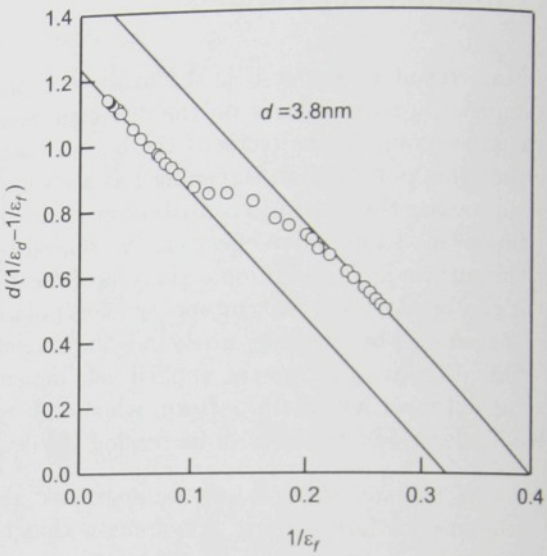

b)

FIGURE 17: Size effect on permittivity in PVDF polymer films analyzed by Takahashi et al. [31]. The thickness dependence of the permittivity at 1 kHz at various temperature. The inverse of effective permittivity is plotted against the inverse of thickness a). The slope of the line in Inset a) is plotted against its intercept on the vertical axis. The two solid lines are the least squares straight line fits in the two linear regions. The common slope of these lines gives the surface layer thickness $d = 3.8\,\mathrm{nm}$ b). The temperature dependence of dielectric permittivity of the ferroelectric layer ε_f (upper) and of the surface ε_d (lower) c).

There were added lines, which indicate the possible temperature dependencies of the intrinsic contributions to permittivity (dashed lines) and the temperature range where the extrinsic contributions are pronounced.

Part II

Piezoelectric materials in noise and vibration suppression devices

Introduction

Thanks to a fast industrial development, our lives have become much more comfortable in many ways. As a side effect of the dynamic urbanization process, space that we live in and its surroundings are becoming increasingly noisy. A human desire for a life in a quiet environment results in a demand for sophisticated devices reducing noise and vibrations. Construction of such devices has become a big contemporary challenge for scientists, researchers and technicians in the field of acoustics.

Principle function of recent systems for noise suppression is based on a superposition of sound waves – the sound coming from noise sources should be completely cancelled or at least suppressed by a sound generated from the noise suppression system. Realization of this technique has been recently well-established in the field of acoustics and the devices are called *active noise control systems* (ANC). The contemporary "classical" ANC system is composed of an ensemble of microphones and speakers connected to a control circuitry, which should make the sound detected by microphones cancelled by the sound generated from speakers. As a result, realization of these systems requires complicated electronics, which makes them of very disadvantageous use and prevents their mass production. For that reason a search for other types of *noise and vibration control systems* (NVC), which could be an alternative to ANC systems, became a very important issue.

Since electroacoustic transduction plays an essential part in the technological realization of every NVC system, piezoelectric materials can be used with a great benefit.

Piezoelectric materials in noise and vibration control systems

Contemporary noise and vibration suppression devices consists of two functional elements: electroacoustic transduction and electric control circuitry. There exist several types of electroacoustic transducers, but the simplest appears to be the *piezoelectric* one. It does not need a permanent magnet as it is required in the *dynamic* type or a bias source as it is required in the *electrostatic* type. Small weight and easy fabrication of piezoelectric electroacoustic transducers are their best advantages. For this reason, they have been also used as parts of systems for noise and vibration control. During last two decades two different ways in a utilization of piezoelectric transducers in these systems have been developed.

In the early applications of piezoelectric materials in NVC systems, piezoelectric elements have been employed (only) as electroacoustic transducers. Schema illustrating such arrangement is shown in Fig. 18. Vibration of a mechanical system is converted using a piezoelectric sensor to electric output signal, which is introduced into a feed-forward controller and fed through a passive electric circuit on the electrodes of a piezoelectric actuator. According to this approach, Ray, Oh and Bar [35] realized the damping of thin cylindrical shells using a system composed of an accelerometer, a piezoelectric actuator and a simple derivative feedback controller. Lin, Liu and Wang [36] simulated the active control of acoustic pressure in a cylindrical cavity with a flexible cylindrical panel using a pair of a piezoelectric actuator and a sensor connected to a linear quadratic optimal controller. Finally, Henry and Clark [37] presented the active control of the sound transmission through a curved panel into a cylindrical enclosure. Nevertheless, realization of these systems, however they can very effectively reduce structural vibration and structural-borne

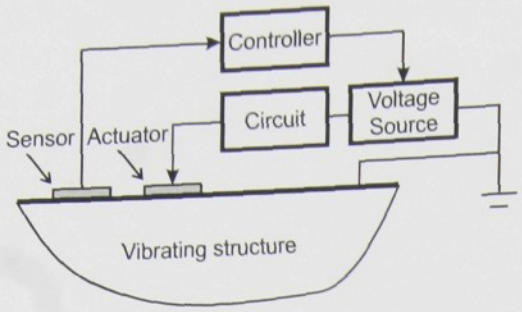

FIGURE 18: Schema of a noise or vibration control system composed of a pair of piezoelectric sensor and actuator connected to complementary control electronics.

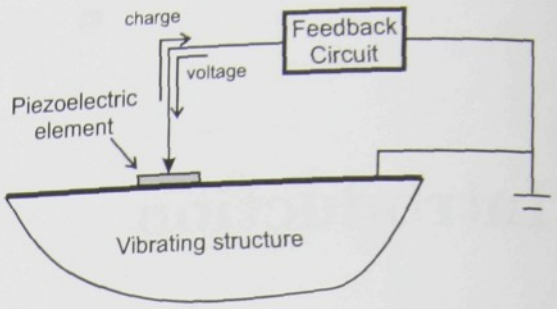

FIGURE 19: Schema of a noise or vibration control system composed of a single piezoelectric element and a feedback circuit.

noise, requires complicated control techniques and advanced electronics. Similar studies by Tsai and Wang [38] or Morgan and Wang [39] indicated that piezoelectric elements can be used for making comparably efficient vibration absorbers, but with less control efforts than it is needed in the purely "classical" ANC systems. This enhancement can be achieved, when the piezoelectric nature of electroacoustic transducers is used properly.

Therefore, an alternative approach has emerged focusing on a utilization of just one piezoelectric element, surprisingly. In this much simpler configuration, which is shown in Fig. 19, the piezoelectric element works as a sensor and an actuator at the same time. It means that the both direct and inverse piezoelectric effects are utilized simultaneously. This is implemented by connecting the piezoelectric element to an external feedback circuit. Feedback action is then realized by changing the voltage on the piezoelectric element according to the change of charge, which is generated on the electrodes. It will be shown later that the simultaneous action of the both piezoelectric effects make it possible to control the effective dynamic elastic properties of the piezoelectric element offering a new approach for vibration damping using piezoelectric materials.

This method was first presented by Forward and Swigert [40, 41] and Edwards and Miyakawa [42] for applications on resonant structures. Later Hagood and von Flotow [43] investigated general possibilities of dissipating the mechanical energy with piezoelectric materials with passive electrical circuits. In the work of Davis and Lesieutre [44], a vibration absorber was actively tuned using the capacitive shunting of piezoelectric element stiffness. Using this technique, the effective dynamic stiffness of piezoelectric ceramics can be increased by an approximately 50% of the ordinary value. Although this amount was enough for required change of the resonant frequency modes, it seemed to be impossible to achieve enough damping efficiency for a complete suppression of vibrations at given frequency range. Finally, Ahmadian and Jeric [45] have applied this technique for the first time in a noise control system. They used lead zirconate titanate (PZT) piezoelectric ceramics to increase transmission loss of a plate with constrained-layer damping materials and reported an increase in the transmission loss of the sound transmitted through the plate by 6 dB at the single frequency 162 Hz and 7 dB in the broad band frequency range of $10 - 10\,000$ Hz.

Piezoelectric curved membrane as a sound suppression element

In the review presented in previous section, piezoelectric PZT ceramics has been used in the noise and vibration suppression devices. Advantage of this material is a large value of electromechanical coupling factor, which makes the feedback control using the piezoelectric effects easily realizable. This makes it possible to suppress vibrations of relatively rigid mechanical structures and to decrease generation of structure-born noise. On the other hand, difference in values of specific acoustic

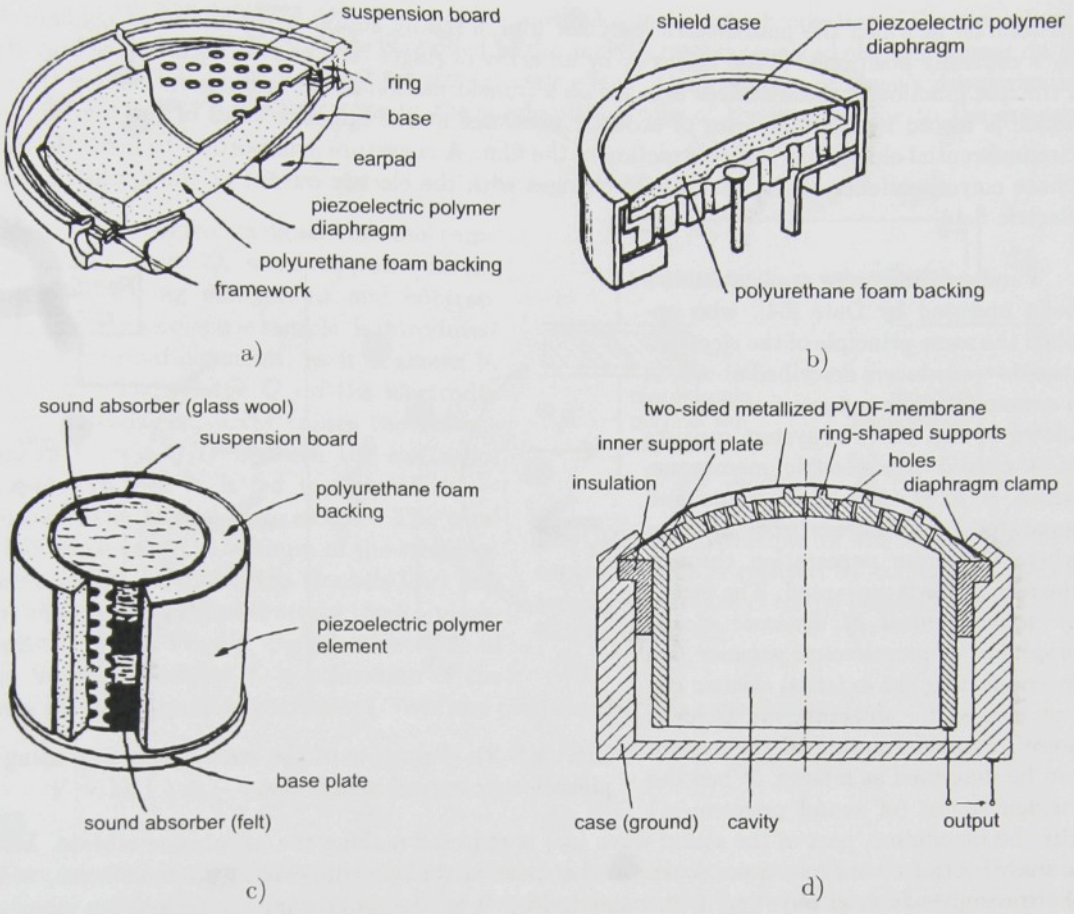

FIGURE 20: Early applications of PVDF polymer in electroacoustic devices: cross-sectional view of a headphone a), a microphone b) and a tweeter c) of Tamura et al. (From Ref. [51]); and cross-sectional view of piezoelectric polymer microphone with a ring supported membrane d) of Lerch and Sessler (From Ref. [53]).

impedances of air and PZT ceramics makes it very difficult to achieve a good overall performance of a noise control system based on a utilization of PZT ceramics. Only an application of light enough and highly piezoelectric material is reasonable in order to achieve the acceptable efficiency of noise control systems.

In the 1950's Fukada et al. investigated piezoelectricity of highly oriented and highly crystalline biological substances, such as collagen, bone, and silk. In the 1960's piezoelectricity of synthetic high polymers, the polypeptides, was found by Fukada et al. [46]. In 1968 the synthetic piezoelectric high polymer, poly(γ-methyl L-glutamate) films were used as transducing elements in experimental microphones and headphones [47], however these transducers have not been commercialized, because the piezoelectric coefficients of those films were not large.

In 1969 piezoelectricity of polyvinidilene fluoride (PVDF) was found by Kawai [48]. This discovery really made a breakthrough in applications of synthetic piezoelectric polymers, since the piezoelectric coefficient of PVDF is almost ten times larger than that of quartz. Two years later, Bergman et al. [49] observed pyroelectricity and second harmonic generation in PVDF. Finally, PVDF was the first polymer for which ferroelectricity was demonstrated by Furukawa et al. [50]. Since that time, electroacoustic transducers that use cylindrically or spherically curved thin films made of piezoelectric high polymer films have been constructed. The first application of ferroelectric PVDF film as a microphone, headphone and tweeter was made by Tamura et al. [51] (see Figs. 20 a, b and c). Lerch and Sessler [52, 53] have developed curved single sheet

structures, in which the piezoelectric polymer film is rigidly supported in a curved configuration by a centrally positioned metal stylus or by an array of ridges on a convex surface (see Fig. 20 d). Principle function of these devices is based on a transformation of the radial movement of the film, which is forced by the difference of acoustic pressures at the opposite sides of the film, into the circumferential elongation and contraction of the film. A curvature is important to make the direct phase correspondence of the sound field changes with the electric output or the applied external electric field.

Fundamentally new application has been invented by Date [54], who applied the same principle of the electroacoustic transducers described above, in a system for noise suppression, which is shown in Fig. 21. The system consists of a curved piezoelectric membrane, which is fixed in a rigid frame and separates noise sources from an area where the noise penetration through the membrane is unwanted. The *method of active control of dynamic elastic properties of piezoelectric polymer film* by connecting the external electric circuit is used for shielding the incident noise. Principal action of the system can be described as follows. When the incident noise (of sound pressure p_i) hits the membrane, part of the sound wave (p_r) is reflected making the membrane vibrate. Membrane vibrations work as a noise source in the space at the opposite side of the membrane, where the transmitted sound wave (p_t) is unwanted. Now it is considered that the membrane vibration is controlled by the effective elastic properties of the membrane, mainly in the low frequency range. When the effective value of the Young's modulus of the membrane becomes very large or almost infinite, the membrane vibrations are completely suppressed as well as the transmitted sound wave ($p_t = 0$). Realization of this idea and a design of such sound shielding systems were made by Okubo et al. [55] and Kodama et al. [56]. Although this preliminary device showed very large peak values of the transmission loss, these promising results were obtained only in a very narrow frequency range. The detailed theoretical analysis of the described mechanism and further experimental investigation were needed to improve this technology for practical applications.

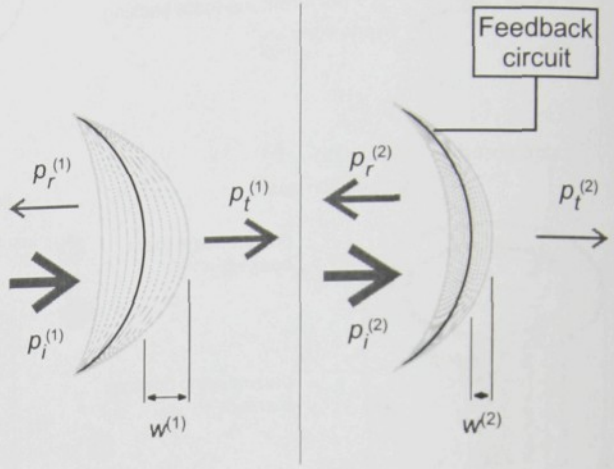

FIGURE 21: Principle of the sound shielding using a piezoelectric curved membrane.

The detail knowledge of vibration modes is essential for the design of final practical applications. Up to date several theoretical works on curved piezoelectric structures are available in literature. Tamura et al. [51] and Edelman [57] dealt with the static analysis. Fiorillo [58] and Naono [59] analyzed the resonance modes assuming uniform vibration displacement and neglecting effects of clamps. In the case of PVDF ultrasound transducers, the effects of clamps were mentioned in the work of Lerch [52], analyzed numerically in the work of Wang and Toda [60] and theoretically in the work of Toda and Tosima [61].

Principle of the active elasticity control

Since the beginnings of a research in the field of piezoelectric materials, the difference between values of elastic compliances of electrically clamped ($s^D_{\mu\nu}$) and electrically free sample ($s^E_{\mu\nu}$) at constant temperature is well-known [62]:

$$s^D_{\mu\nu} = s^E_{\mu\nu} - \beta^T_{ij} d_{i\mu} d_{j\nu},$$

where β^T_{ij} is the impermittivity tensor at a constant mechanical stress and $d_{i\mu}$, $d_{j\nu}$ are piezoelectric coefficient tensors. The above equation can be explained considering the simultaneous action of

the both direct and converse piezoelectric effects, which affect elastic properties of the piezoelectric sample. When a mechanical stress is applied to the sample, uncompensated charges appear on the surface of the sample due to the direct piezoelectric effect. These charges produce a depolarization field, which causes a slight change in the mechanical strain of the sample due to the converse piezoelectric effect.

Elasticity control is based on the same principle. Charge Q, which appears on the electrodes during elongations and contractions of the piezoelectric sample, is introduced into an external capacitor, as it is shown in Fig. 22. The charge Q on the electrodes of the external capacitor causes the voltage change $V = -Q/C$ between the electrodes and the voltage V is fed back to the electrodes of the piezoelectric sample. The total strain of the sample is a sum of the stress induced strain (according to Hooke's law) and the electric field induced strain (direct piezoelectric effect). Finally, the effective value of the Young's modulus Y is a function of the ratio of the external capacitance C over the piezoelectric film capacitance C_s

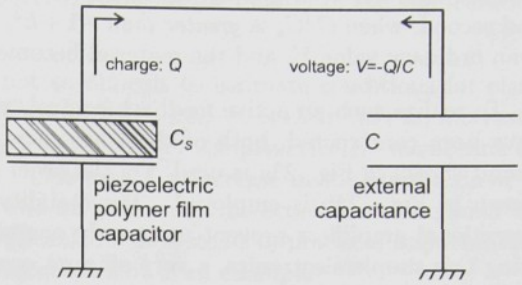

FIGURE 22: Principle of the active elasticity control, which is realized by connecting the external capacitance C to the piezoelectric polymer film capacitor C_s.

$$Y = Y_0 \left(1 + \frac{k^2}{1 - k^2 + C/C_s}\right),$$

where k is the electromechanical coupling factor of the piezoelectric sample ($0 < k < 1$) and Y_0 is the ordinary value of Young's modulus of the piezoelectric sample. As it has been already mentioned in the previous section, if the ordinary capacitor ($C > 0$) is used as the external capacitor, the effective dynamic stiffness of piezoelectric ceramics can be increased by an approximately 50% of the ordinary value. Unfortunately, this is achievable only in the case of strongly piezoelectric materials, such as PZT ceramics. That is why, this technique is often called "PZT shunting". For less piezoelectric materials or for the control of the effective elastic properties to a large extent (theoretically from minus infinity to plus infinity), a more sophisticated method must be used.

In order to achieve a complete control of elastic properties of piezoelectric material, Date [54] has introduced the negative capacitor as *active feedback circuit*. From the above equation it is seen that depending on the value of C/C_s it is possible to identify three regimes of the active elasticity control:

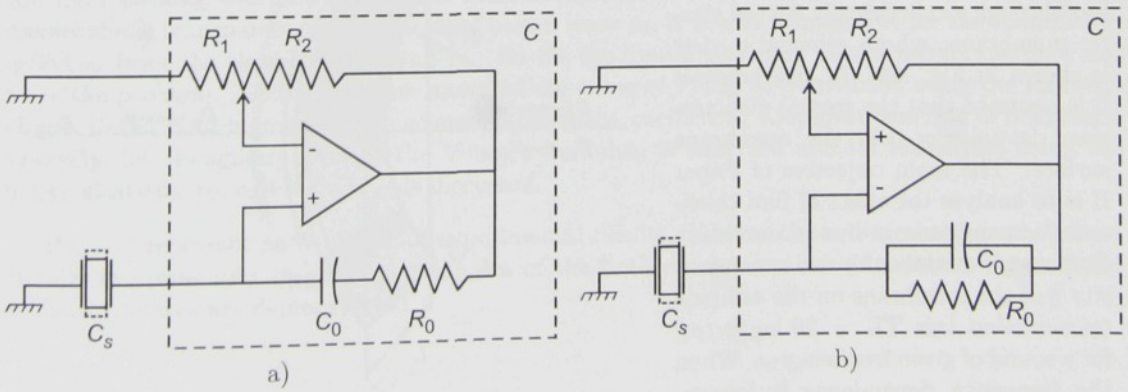

FIGURE 23: Negative Capacitance Circuit for *decreasing* (S-circuit) a), and *increasing* (H-circuit) b) of the effective value of the dynamic Young's modulus.

$$
\begin{array}{lll}
Y < Y_0 & \text{for} & -\infty < C/C_s < -1, \\
Y < 0 & \text{for} & -1 < C/C_s < -1+k^2, \\
Y > Y_0 & \text{for} & -1+k^2 < C/C_s < \infty.
\end{array}
$$

Two regimes are of practical importance: first, when C/C_s is *less than* -1, the effective value of Young's modulus Y is *smaller* than ordinary value Y_0 and the material becomes effectively *softer;* and second, when C/C_s is *greater than* $-1+k^2$, the effective value of Young's modulus Y is *larger* than ordinary value Y_0 and the material becomes effectively *harder.*

To realize such an active feedback control, two types of circuits with an operational amplifier have been constructed, both of them are show in Fig. 23. For effective softening the material, circuit shown in Fig. 23a is used. On the other hand, for effective hardening the material, circuit shown in Fig. 23b is employed. The stability conditions imposed upon the circuits involving operational amplifiers prevent using only one circuit in the both regimes. It will be shown that using this simple electronics, a very efficient control of the vibration of the piezoelectric elements can be produced.

Introduction to the collection of publications

In 2001 three prototypes of the noise and vibration suppression systems have been already successfully realized utilizing piezoelectric materials and the method of active elasticity control: first, it was a system for the *enhancement of noise absorption,* second, a system for the *suppression of noise transmission,* and third, a system for *enhancement of vibration insulation.* In that time, quite advanced experience in the realization of negative capacitance circuits was already available due to analysis of Date [54]. With use of this circuitry, the above mentioned preliminary devices [55, 56] showed very large peak values of noise and vibration suppression properties. Unfortunately, these promising results were obtained only in a very narrow frequency range and the detailed theoretical analysis of the described mechanism and further experimental investigation were needed to improve this technology for practical applications.

A key disincentive to further development of these devices was a lack of knowledge on how the given effective values of elastic properties actually affects the measured acoustic properties of the noise suppression system. It was also not known what are the requirements on the quality of the control circuitry to obtain the desired values of acoustic properties of the system in a wide frequency range. These unanswered questions were approached theoretically in Papers H and I and demonstrated experimentally in Papers H, I and J.

In Paper H there is given a detailed analysis of the acoustic transmission loss through a cylindrically curved elastic membrane, whose schematic view is shown in Fig. 24. In this analysis it is assumed that the spatial displacement is uniform over the membrane surface. The main objective of Paper H is to analyze the effect of film thickness h, membrane radius of curvature R, Young's modulus Y_0 and mass density ϱ of the membrane on the acoustic transmission loss $\mathrm{TL} = 20 \log |p_i/p_t|$ for a sound of given frequency ω. When the frequency dependence is known, qualitative predictions for the effects of Young's modulus and radius of curvature on the frequency profile of the

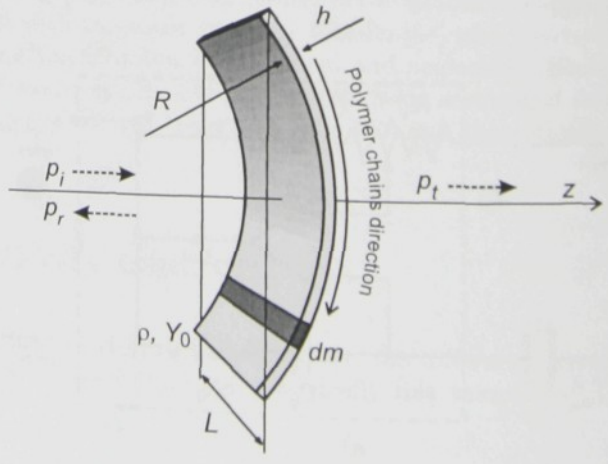

FIGURE 24: Geometrical arrangement of the system for a control of transmission loss using the curved piezoelectric polymer membrane.

acoustic transmission loss are obtained.
Then several types of negative capacitances circuits are considered and it is demonstrated how the active frequency control affects the frequency profile of the acoustic transmission loss. In order to check the validity of this model, experiments were carried out and measured data were fitted in this model. Comparison of theoretical predictions and experimental results is analyzed. Since a good agreement of theory and experiments were obtained, a brief analysis of the feedback circuitry requirements, which have the most important effect on the quality of the suppression of the acoustic transmission loss, is given.

In the case of sound shielding system, it is not so difficult to estimate conditions for elastic properties, which lead to the maximum values of transmission loss. It is clear that an increase of the effective value of Young's modulus results in a hardening of the piezoelectric membrane and a great suppression of the membrane vibrations. This causes a decrease in the amplitude of the acoustic pressure of the transmitted sound wave and an increase in the acoustic transmission loss. Nevertheless, this straightforward logic is not applicable in all systems of practical importance. A system for enhancement of the acoustic absorption coefficient is an example.

In Paper I a more detailed analysis of the relationship between elastic properties of the cylindrically curved membrane and the effective "acoustic response" of a system for an enhancement of sound absorption is given. The main objective of this work is to demonstrate a general method for designing the noise and vibration suppression systems using piezoelectric materials and the technique of active elasticity control. The considered system, which is shown in Fig. 25, consists of a curved cylindrical membrane of thickness h, mass density ϱ, radius of curvature R, and Young's modulus Y_0. This membrane separates noise sources from a rigid backing wall, which is in distance H from the membrane. The problem analyzed in Paper I is to maximize the acoustic absorption coefficient $\alpha_0 = 1 - |p_r/p_i|^2$ of such a system using the active elasticity control technique. It would appear that the maximum softening of the curved membrane might lead to the desired increase of the acoustic absorption coefficient. When the Young's modulus of the membrane is very small, the membrane becomes transparent for the incident sound wave, so that the reflected sound wave might be also decreased. Unfortunately, it is not the case, since it is considered that the transmitted sound wave is perfectly reflected from the rigid backing wall and strikes the membrane from the opposite side. It is clear that if the membrane is transparent for the incident sound wave p_i, it is also transparent for the sound wave reflected from the rigid backing wall p_b. So the maximum softening of the membrane does not solve the problem. Therefore, some intermediate value of Y has to be realized using the feedback circuit to reach an increase in the acoustic absorption coefficient. Moreover, the role of membrane viscosity, i.e. imaginary part of the Young's modulus, is analyzed and its realization using the active elasticity control technique is discussed.

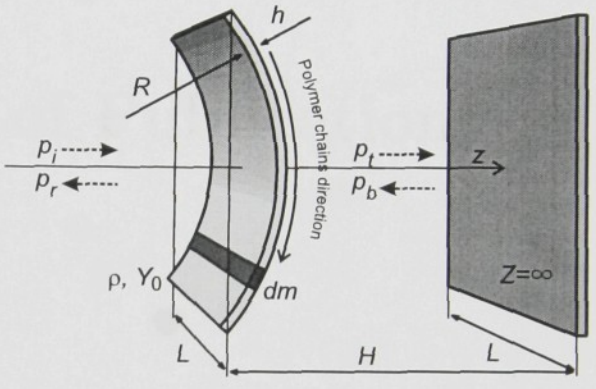

FIGURE 25: Geometrical arrangement of the system for an enhancement of sound absorption using the curved piezoelectric polymer membrane.

Paper J represent an overview of experimental results. Various types of negative capacitances circuits are presented and several examples of the both narrow and wide frequency range sound shielding devices are demonstrated.

Collection of Publications

Paper H

Noise shielding system utilizing thin piezoelectric membrane and elasticity control

Oral presentation at the 11th International Symposium on Elecrets, Melbourne, Australia 2002.

Published in *Journal of Applied Physics*, Vol. 94, No. 1, Pg. 789-796, 1 July 2003

List of citations

1. H. Kodama, T. Okubo, K. Kimura, K. Yamamoto, M. Date, and E. Fukada, Sound Shielding of Piezoelectric PVDF Panel, *Proc. the 33rd International Congress and Exposition on Noise Control Engineering (Internoise-2004)*, Prague, Czech Republic (2004): Art. No. 243

2. K. Kimura, H. Kodama, T. Okubo, K. Yamamoto, M. Date, and E. Fukada, Sound Barrier Panel using Piezoelectric Polymer Films, *Proc. 18th International Congress on Acoustics*, 4-9 April, Kyoto, Japan, 2004

3. E. Fukada, M. Date, K. Kimura, T. Okubo, H. Kodama, P. Mokrý, K. Yamamoto, Sound isolation by piezoelectric polymer films connected to negative capacitance circuits Source, *IEEE Transactions on Dielectrics And Electrical Insulation* **11**(2): Pg. 328-333 (2004)

4. E. Fukada, M. Date, and H. Kodama, Recent Trends on Application of Piezoactive Polymers to Acoustics - Low Frequency Sound Barrier (Invited Review Paper at *Int. Conf. Intelligent Materials*, Pennsylvania State University, 2003)
Published in *Materials Technology* **19**(2): Pg. 83-90 (2004)

5. P. Mokrý, E. Fukada, K. Yamamoto, Sound absorbing system as an application of the active elasticity control technique Source: *Journal of Applied Physics* **94**(11): Pg. 7356-7362 (2003)

6. E. Fukada, M. Date, H. Kodama, Y. Oikawa, Elasticity control of curved piezoelectric polymer films, *Ferroelectrics* (accepted for publication, 2005) Ms. No. O-04

NOISE SHIELDING SYSTEM UTILIZING THIN PIEZOELECTRIC MEMBRANE AND ELASTICITY CONTROL

P. MOKRÝ[14], E. FUKADA, and K. YAMAMOTO

Kobayasi Institute of Physical Research, Kokubunji, Tokyo 185-0022 Japan

Abstract

The description and theoretical analysis of a noise shielding system are presented. In this system, the noise and/or sound are transmitted through the piezoelectric curved membrane, which is connected to an external feedback circuit. Using the principle of elasticity control, i.e. utilization of both direct and inverse piezoelectric effects simultaneously, the movement of the membrane as well as the sound pressure of the transmitted wave can be controlled to a large extent. Transmission loss of an audible sound through the membrane in such system is expressed as a function of a sound frequency, geometrical properties of the membrane and parameters of the feedback circuit. It is used for the comparison of theoretical predictions and experimental data. Using this technique, the increase of the transmission loss of about 60dB in a narrow frequency range or about 7dB in the broad frequency range has been achieved. The performance of this system is discussed.

PACS: 43.50.-x, 77.65.-j, 43.50.Ki

Keywords: Piezoelectric polymers, elasticity control, negative capacitance circuit, transmission loss

H.1. INTRODUCTION

The main objective of this paper is to propound a description and an overall theoretical analysis of the noise shielding system (NS). Recently active noise control systems (ANC) have been well-established in the field of acoustics. The contemporary ANC systems are composed of an ensemble of microphones and speakers with complementary electronics in order to cancel or at least suppress the sound field of an incident noise in some area by the sound generated from the speakers. In the presented system, materials piezoelectric properties are utilized with minimal circuitry requirements. This system should offer an advantageous alternative to ANC systems where complicated electronics are required.

The system consists of the curved piezoelectric membrane, which is fixed in a rigid enough frame. This membrane separates noise sources from an area where the noise penetration through this membrane is unwanted. The incident noise makes the membrane vibrate and this vibration is the effective noise source for the separated area. Using a technique called *elasticity control*, the vibration of the piezoelectric membrane can be totally canceled and, consequently, the sound cannot be transmitted through the membrane.

This system belongs to the group of devices that use cylindrically or spherically curved films made of polyvinidilene fluoride (PVDF) or copolymer of vinidilene fluoride and tetrafluorethylen (P(VDF/TrFE)). These very popular structures have been used in acoustics for many years. PVDF material is very attractive for its small weight, flexibility and low cost. The earliest application as a microphone, in which the piezoelectric film is tensioned over a pad of polyurethane foam, was made by Pioneer Electronic Corporation [H1]. Lerch and Sessler [H2,3] have developed curved single sheet structures, in which the film is rigidly supported in a curved configuration by a centrally positioned

[14]e-mail: pavel.mokry@vslib.cz, On leave from Department of Electrical Engineering and Electromechanical Systems, Technical University of Liberec, Czech Republic

metal stylus or by an array of ridges on a convex surface. The principle of the function of these devices inheres in the transformation of the radial movement of the film, which is forced by the difference of the acoustic pressures at opposite sides of the film into the circumferential elongation and contraction of the film. The curvature is important to make the direct phase correspondence of the sound field changes with the electric output (microphones) or the applied external electric field (speakers).

The discovery of the elasticity control by Date [H4] opened fundamentally new applications based on this principle. The realization of Date's proposal and the design of the noise control measurement system, whose analysis is presented in this paper, was made by Okubo et al. [H5]. Although this preliminary device showed very large peak values of the transmission loss, these promising results were obtained only in a very narrow frequency range. The detailed theoretical analysis of the described mechanism and further experimental investigation were needed to improve this technology for practical applications.

The theoretical investigation presented in this paper is based on the calculation of the *transmission loss* of the sound transmitted through the viscoelastic curved membrane. For a membrane disconnected from a feedback circuit, the calculation of the transmission loss can be separated into two parts. The first one is related with the dynamics of the membrane vibration, the second one is the interaction of the membrane movement and the sound field surrounding the membrane neighbourhood. In the case of the noise control, the membrane vibrations are influenced to a large extent by the action of a feedback circuit.

The vibration problems of curved membranes and shells were addressed by several researchers. The early models assumed uniform displacement and the effects of clamps were neglected. The further developed models by Lerch [H2] and Toda [H7] took the existence of clamps and excitation of the flexural vibration modes into account. Since the forces to flex the very thin polymer film are much smaller than the forces to elongate one, our detailed numerical calculation showed that there is almost no difference between values of the transmission loss expressed using models from the former or the latter group. But this is beyond the scope of this paper.

H.2. DESCRIPTION OF THE NOISE CONTROL MEASUREMENT SYSTEM

A measurement system was constructed [H5] in order to rigorously evaluate the transmission loss of the NS system. Its arrangement is characterized in this section.

H.2.1. Experimental measurement system

There is a schema of the measurement system in Fig. H.1. Using this equipment, the normal incidence transmission loss was measured. The NS system is installed in the middle of an acoustic tube of a rectangular cross-section 40 mm × 40 mm. Transfer functions among four microphone locations were measured to extract the acoustic energies of the incident sound (described by acoustic pressure p_i), reflected sound (p_r) and the transmitted sound (p_t) [H8].

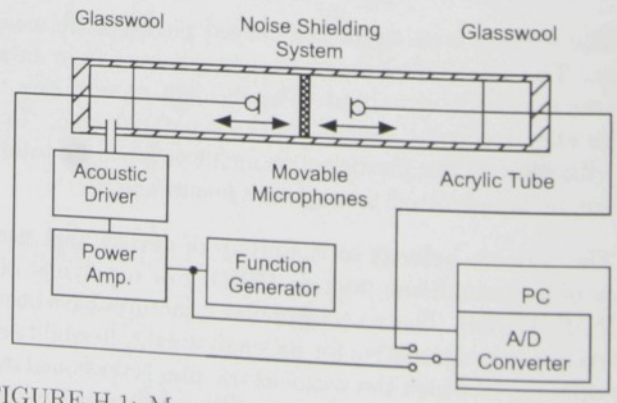

FIGURE H.1: Measurement of normal incidence transmission loss using transfer function technique.

The detail structure of the NS system is shown in Fig. H.2. The cylindrically curved piezoelectric film made of PVDF or P(VDF/TrFE) polymer is rigidly clamped between two thick copper electrodes. The film of thickness 50 μm is provided by electrodes, which are fabricated by evaporation. The urethane foam is inserted between the film and the steel wire mesh fixed in the inner surface of the tube so that the fine film keeps a constant curvature. The feedback circuit, which realizes the elasticity control, is connected to the copper electrodes.

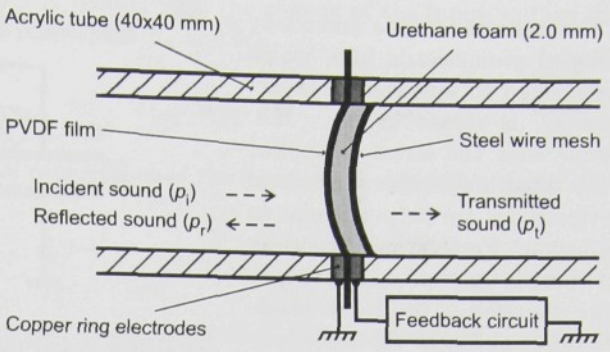

FIGURE H.2: Cross-section of the sound shielding structure with curved piezoelectric film.

H.2.2. Theoretical model

The detailed geometry and the orientation of the piezoelectric film inside the system is shown in Fig. H.3. Symbol h stands for the thickness of the film, R for the radius of curvature of the cylindrical surface, L for the membrane length and ϱ for the mass density of the film. Considering the stronger piezoelectric response, the drawn PVDF or P(VDF/TrFE) film is used in the system. The direction of the drawing of the film and, consequently, the direction of the polymer chains is oriented along the circumference of the cylindrical surface. The 1-axis of the attached coordinate system are oriented to the direction of film drawing, the 2-axis is parallel with the symmetry axis of the cylindrical surface and, finally, the 3-axis is perpendicular to the tangential plane of the cylindrical surface. Since the system is of cylindrical symmetry, the direction of the coordinate axes differs on the membrane surface.

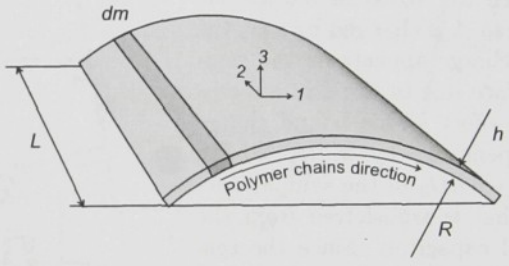

FIGURE H.3: Geometry and the orientation of the piezoelectric film inside the system.

H.2.3. Principles of the elasticity control

Since the beginnings of the study of piezoelectric materials, the difference between the value of the elastic compliance of the electrically clamped ($s^D_{\mu\nu}$) and the electrically free sample ($s^E_{\mu\nu}$) at the constant temperature is well-known [H9]:

$$s^D_{\mu\nu} = s^E_{\mu\nu} - \beta^T_{ij} d_{i\mu} d_{j\nu},$$

where β^T_{ij} is the impermittivity tensor at a constant mechanical stress and $d_{i\mu}$, $d_{j\nu}$ are piezoelectric coefficient tensors. The prior equation can be explained by the simultaneous action of both direct and converse piezoelectric effects. When a mechanical stress is applied to the sample, the uncompensated charges appear on the surface of the sample. These charges produce a depolarization field, which causes a slight change in the mechanical strain of the sample due to the converse piezoelectric effect.

The schema of the uniaxially tensioned piezoelectric film, which is connected to an external capacitance C, is shown in Fig. H.4. Assume that the stress is applied in the direction of the 1 axis and the electrodes are perpendicular to the 3 axis. Furthermore, consider that there is only uniaxial stress T_1 in the direction of the 1-axis inside the sample and that E_3 is the only nonzero component of the electric field applied to the sample. Then, the constitutive equations lead to simplified relationships:

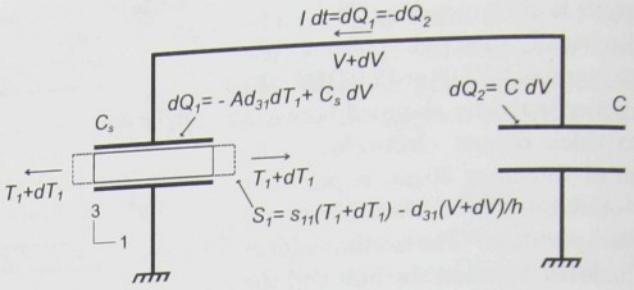

FIGURE H.4: Principle of the elasticity control.

$$S_1 = s_{11}^E T_1 + d_{31} E_3, \tag{H.1a}$$

$$D_3 = d_{31} T_1 + \varepsilon_{33}^T E_3, \tag{H.1b}$$

where D_3 is the component of the electric displacement in the radial direction and S_1 is the strain measuring the relative elongation of the sample in the direction of the 1-axis . Symbol ε_{33}^T stands for the components of the permittivity tensor.

When the stress in the sample of an area A is changed by dT_1, the bound charge appears on the sample surface due to the direct piezoelectric effect. This bound charge is compensated by a free charge $dQ_1 = -A\,dD_3$ of the sample electrode that is transferred from the external capacitor. Since the system of these two capacitors is electrically isolated, the charge change on the external capacitor electrode dQ_2 is equal to the minus charge change on the sample electrode $dQ_2 = -dQ_1$. The charge current causes the voltage change $dV = dQ_2/C$, which is fed back to the sample. The resulting change of the sample strain is given by the sum of the stress induced strain change $s_{11}^E\,dT_1$ and the electric field induced strain change $-d_{31}\,dV/h$. The straightforward calculations [H4] lead to the formula for the effective value of the dynamic elastic compliance:

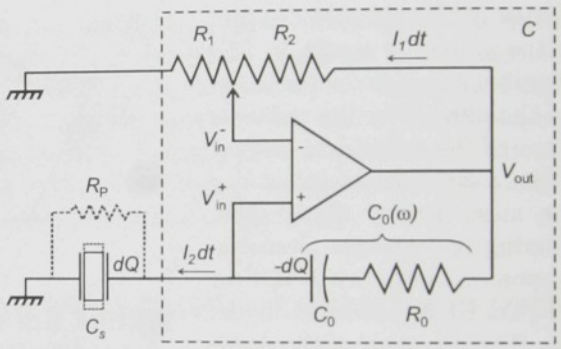

FIGURE H.5: Example of a negative capacitance circuit.

$$s_{11}^\star = s_{11}^E \left(1 - \frac{k_{31}^2}{1+\alpha}\right), \tag{H.2}$$

where $k_{31}^2 = d_{31}^2/(s_{11}^E \varepsilon_{33}^T)$ is the electromechanical coupling factor and $\alpha = C/C_s$ is the ratio of the external capacitance over the sample capacitance. However there is not any significant difference between values of $s_{11}^\star$ and s_{11}^E for positive values of α. Thus, the value of $s_{11}^\star$ can be controlled to a large extent when the negative capacitance ($C < 0$) is connected to the sample.

The example of a circuit that has a negative effective capacitance is shown in Fig. H.5. In this circuit, the input voltages V_{in}^+, V_{in}^- and the output voltage V_{out} are given by relationship $V_{\text{out}} = G(V_{\text{in}}^+ - V_{\text{in}}^-)$, where G is the amplification factor ($G \gg 10^5$). Under normal conditions, when the V_{out} is not saturated, the difference between V_{in}^+ and V_{in}^- is extremely small compared to V_{out} and we can write $V_{\text{in}}^+ = V_{\text{in}}^- = V_{\text{in}}$ with a high accuracy.

When some charge dQ is injected with the electric current density I_2 from the sample to the circuit capacitor C_0, it causes the change of the output voltage according to

$$\frac{R_2}{R_1 + R_2}\,dV_{\text{out}} = -\frac{dQ}{C_0}. \tag{H.3}$$

The change of the output voltage is linearly related with the change of the input voltage due to the feedback through the potentiometer resistances R_1 and R_2

$$dV_{\text{in}} = \frac{R_1}{R_1 + R_2}\, dV_{\text{out}}. \tag{H.4}$$

Using Eqs. (H.3) and (H.4), the effective capacitance of the circuit is then equal to (see [H4])

$$C = \frac{dQ}{dV_{\text{in}}} = -C_0 \frac{R_2}{R_1}. \tag{H.5}$$

The key information in the sound transmission analysis is the knowledge of the membrane vibration response to the sound pressure difference at the opposite sides of the membrane. The detailed function of the whole noise shielding system including the negative capacitance circuit will be studied in the next section.

H.3. SOLUTION OF THE MEMBRANE MOVEMENT

If we assume that the deflection of the film is much smaller than the wavelength of the incident sound, the membrane is under an uniform action of the acoustic pressure difference δp. Let us denote the displacement of the membrane in the radial direction by w and assume that it is uniform over the whole membrane surface. Now consider a small element of the cylindrical membrane, which is shaded in Fig. H.3. Forces acting on this thin stripe of the film are shown in Fig. H.6. When the membrane element shifts from its original position indicated by the dashed line, the circumferential stress T_1 appears due to the membrane expansion. Due to this stress and the membrane curvature, force $d\boldsymbol{F}_3$ acts in the radial direction on the membrane element of the mass dm. The equation of motion of the element in the radial direction is

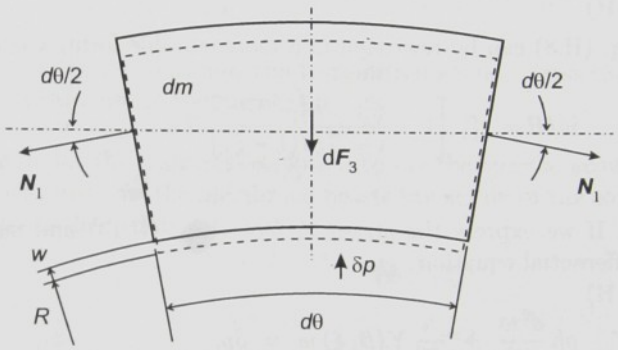

FIGURE H.6: Forces acting on the moving membrane element.

$$dm \frac{d^2 4}{dt^2} = \delta p\, LR\, d\theta \; - \; dF_3, \tag{H.6}$$

where $dm = \varrho h L R\, d\theta$. Using the parameters in Fig. H.6, the radial force can be expressed as $dF_3 = N_1\, d\theta$, where the circumferential force N_1 is obtained by integrating the usual stress T_1 over the membrane cross-section area. Since this stress is assumed to be homogeneous inside the film, we can easily write $N_1 = hL\, T_1$. Then the equation of motion can be rewritten in form:

$$\varrho h R \frac{d^2 w}{dt^2} = \delta p\, R \; - \; hT_1. \tag{H.7}$$

According to elasticity equations expressed in cylindrical coordinates, the circumferential strain S_1 is equal to w/R (see [H10]). Due to the converse piezoelectric effect, the strain S_1 is a function of the stress T_1 and the input voltage of the operational amplifier V_{in}:

$$w/R = s_{11}^E\, T_1 \; - \; d_{31}\, V_{\text{in}}/h. \tag{H.8}$$

The input voltage V_{in} is determined by the electric currents inside the feedback circuit. The total charge $Q = \int I_2\, dt$ that compensates the bound charges on the sample surface of an area A can

be expressed from Eq. (H.1b) using relation $Q = -AD_3$. On the other hand, the voltage of the electrodes of the C_0 capacitor is equal to $V_{\text{in}} - V_{\text{out}} = -Q/C_0$. Thus, we can write the following equation:

$$Ad_{31}\,T_1 - C_s\,V_{\text{in}} = -C_0\,(V_{\text{out}} - V_{\text{in}}). \tag{H.9}$$

The voltages on the resistors R_1 and R_2 are related by relationship:

$$V_{\text{in}}/R_1 = (V_{\text{out}} - V_{\text{in}})/R_2. \tag{H.10}$$

Combining Eqs. (H.9) and (H.10), the input voltage V_{in} can be expressed as function of the stress inside the sample:

$$V_{\text{in}} = \left(1 - \frac{C_0}{C_s}\,\frac{R_2}{R_1}\right)^{-1} \frac{Ad_{31}}{C_s}\,T_1. \tag{H.11}$$

If we denote

$$\beta = C_0/C_s, \quad \xi = R_2/(R_1 + R_2), \tag{H.12}$$

Eq. (H.8) can be rewritten in a more suitable form, according to formula (H.2)

$$w/R = s_{11}^E \left[1 - \frac{k_{31}^2}{1 - \beta\xi/(1-\xi)}\right] T_1. \tag{H.13}$$

If we express the stress T_1 from Eq. (H.13) and substitute into Eq. (H.7), we obtain the differential equation

$$\varrho h\,\frac{d^2w}{dt^2} + \frac{h}{R^2}\,Y(\beta,\xi)\,w = \delta p, \tag{H.14}$$

where

$$Y(\beta,\xi) = Y_0 \left[1 - \frac{k_{31}^2}{1 - \beta\xi/(1-\xi)}\right]^{-1} \tag{H.15}$$

is the effective value of the Young's modulus controlled by the feedback circuit and $Y_0 = 1/s_{11}^E$ is the ordinary value of the Young's modulus of the membrane. Since the mechanical system is harmonically excited, we can assume that

$$w(t) = W\,\mathrm{e}^{i\omega t}, \quad \delta p(t) = P\,\mathrm{e}^{i\omega t}. \tag{H.16}$$

The mechanical damping effects due to material viscosity can be introduced by means of complex elastic compliance s_{11}^E or the Young's modulus Y_0. After substitution of expressions (H.16) into Eq. (H.14), we obtain the linear algebraic equation for the unknown amplitude of the membrane displacement W:

$$-\omega^2 \varrho h\,W + \frac{h}{R^2}\,Y(\beta,\xi)\,W = P. \tag{H.17}$$

Solving the preceding equation, the value of W can be finally expressed as:

$$W = \frac{R^2}{h}\,\left[Y(\beta,\xi) - \omega^2 \varrho R^2\right]^{-1} P. \tag{H.18}$$

This formula represents the dynamic response of the membrane movement to the acoustic pressure difference and it will be used for investigation of the sound shielding properties of the system.

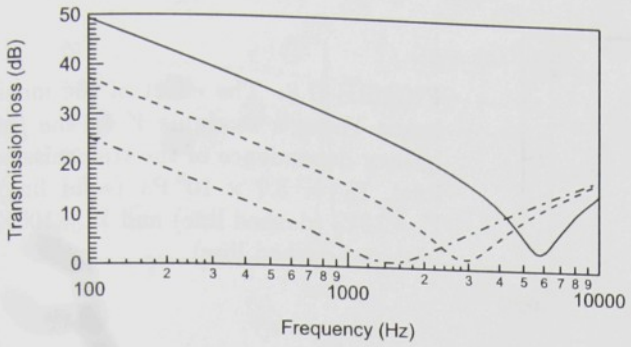

FIGURE H.7: The effect of the radius of the curvature R to the frequency dependence of the transmission loss: $R = 4\,\mathrm{cm}$ (solid line), $R = 8\,\mathrm{cm}$ (dashed line) and $R = 16\,\mathrm{cm}$ (dot-and-dashed line).

H.4. TRANSMISSION LOSS

The sound transmission properties of this system can be evaluated using the *transmission loss* R_0, which is defined as

$$R_0 = 10 \log_{10} |p_i/p_t|^2 , \tag{H.19}$$

where p_i and p_t are the sound pressures of the incident and the transmitted sound, respectively. The value of R_0 depends on the vibration response of the membrane.

The simplest way to obtain the formula for the transmission loss is to use the *specific acoustic impedance* of the membrane Z, which measures how the membrane resists the action of the sound pressure. The specific acoustic impedance is defined by formula:

$$Z = \delta p/v, \tag{H.20}$$

where v is the radial velocity of the membrane. According to the harmonic dependences of the functions w and δp expressed in Eq. (H.16), the specific acoustic impedance of cylindrically curved membrane is

$$Z = \frac{P}{i\omega W} = i\omega\varrho h \left(1 - \frac{Y(\beta, \xi)}{\omega^2 \varrho R^2}\right). \tag{H.21}$$

Knowing the value of the specific acoustic impedance, we can express the transmission loss R_0 as follows (see [H11])

$$R_0 = 10 \log_{10} |1 + Z/(2\varrho_0 c)|^2 , \tag{H.22}$$

where ϱ_0 is the mass density of air and c is the phase velocity of sound in air.

Hence, straightforward algebraic manipulations lead to the final formula

$$R_0 = 10 \log_{10} \left[1 + \frac{Y''}{\omega\zeta} + \frac{(Y'')^2 + \left(Y' - \varrho\omega^2 R^2\right)^2}{(2\omega\zeta)^2}\right], \tag{H.23}$$

where $\zeta = c\varrho_0 R^2/h$ and Y', Y'' are the real and imaginary part of the effective value of the dynamic Young's modulus given by a complex function $Y(\beta, \xi)$.

When the radius of the part of the cylindrical shell goes to infinity, there are no internal stresses inside the membrane, the specific acoustic impedance of the membrane is equal to $i\omega\varrho h$ and the preceding relation reaches the form of the classical mass law for sound insulation of a single wall (see [H11]).

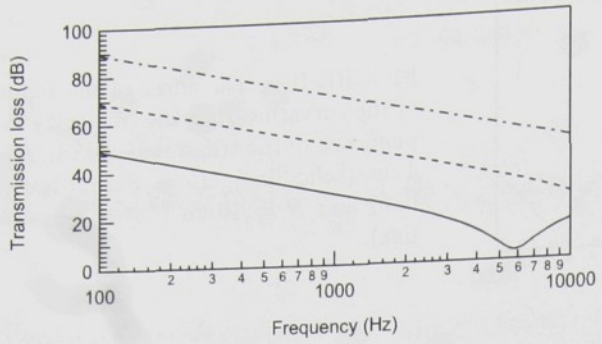

FIGURE H.8: The effect of the membrane Young's modulus Y to the frequency dependence of the transmission loss: $Y_0 = 3.7 \times 10^9$ Pa (solid line), $Y = 10Y_0$ (dashed line) and $Y = 100Y_0$ (dot-and-dashed line).

H.5. EFFECT OF THE FEEDBACK CIRCUIT

The frequency dependences of the transmission loss of the viscoelastic curved membrane are shown in Figs. H.7 and H.8. The numerical results have been obtained using formula (H.23). The following values have been considered: thickness $h = 50\,\mu$m, radius of the membrane curvature $R = 4$ cm, mass density $\varrho = 1770\,\mathrm{kg\,m^{-3}}$, Young's modulus $Y_0 = 3.7$ GPa and mechanical quality factor $Q_\mathrm{m} = Y_0'/Y_0'' = 10$. Physical properties of air have been taken at the normal conditions.

Figures H.7 and H.8 evince the general V-shape of the frequency dependence of the transmission loss. Below the resonant frequency, which corresponds to the minimum of the curve, the membrane movement is suppressed mostly by the forces arisen due to the elastic extensions and contractions of the membrane. On the other hand, the forces due to the membrane inertia suppress the membrane movement in the frequency range above the resonant frequency. That is why we can see the increase of the values of the transmission loss towards lower frequencies. Since the elastic interaction doesn't play an important role in the ordinary sound absorbing materials, such as glass-wool, the increase of the transmission loss in the low frequency range is not clearly observed. This is a notable benefit to use a curved membrane as a passive sound reflector in the low frequency range.

It is evident that smaller values of the radius of the membrane curvature shifts the resonant frequency towards higher frequencies and increase the values of the transmission loss in the low frequency range. Since the radius of the membrane curvature is set up during the design of the system, the another way to control the transmission loss is changing the effective elastic properties of the membrane. If we increase the value of the Young's modulus by a factor 100, the transmission loss is increased by an additional 20dB in the low frequency range. Hence, the elasticity control is realized using the feedback circuit. The behaviour of the feedback action is described by Eq. (H.2). The ratio $\alpha = C/C_s$ and its frequency dependence play an important role in this process.

The frequency dependence of the complex capacitance $C_s^\star$ of the sample made of PVDF or P(VDF/TrFE) film can be approximated by

$$C_s^\star(\omega) = C_s(\infty) + \frac{\Delta C_s}{1 + (i\omega\tau)^\kappa}, \tag{H.24}$$

where ΔC_s is the relaxation strength, τ is the relaxation time and κ describes the distribution of relaxation times. $C_s(\infty)$ is the sample capacitance at very high frequencies [H12]. The capacitance of the feedback circuit $C^\star(\omega)$ is determined by the capacitance of the *reference capacitor* $C_0^\star(\omega)$ inside the circuit. Here, we can distinguish two cases.

H.5.1. Sound shielding in a narrow frequency range

In this case the reference capacitor is made of a capacitor C_0 and a resistor R_0 connected in series. Then, the equivalent complex capacitance of this element is equal to

$$C_0^\star(\omega) = \frac{C_0}{1 + i\omega R_0 C_0}. \tag{H.25}$$

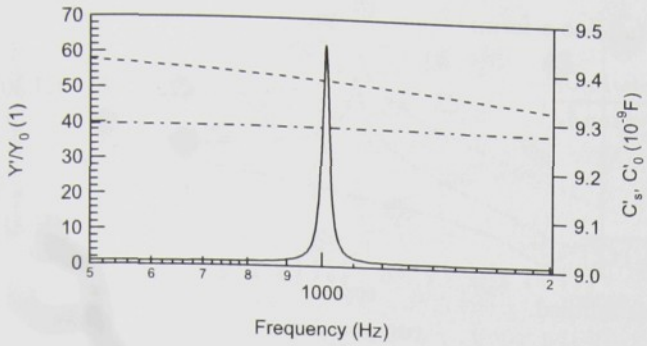

FIGURE H.9: The effect of matching the real parts of capacitances C_s (dashed line) and C_0 (dot-and-dashed line) to the frequency dependence of the ratio Y'/Y_0 (solid line).

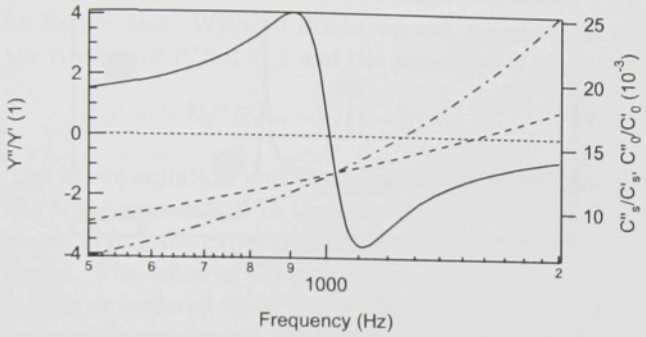

FIGURE H.10: The effect of matching the dielectric loss tangents of capacitances C_s (dashed line) and C_0 (dot-and-dashed line) to the frequency dependence of the effective mechanical damping Y''/Y' (solid line).

In the frequency range of audible sound, the real part of this capacitance is considered to be constant. That is why we can assume that

$$C_0^\star(\omega) \approx C_0'(1 - i\omega R_0 C_0). \tag{H.26}$$

Examples of frequency dependences of $C_s^\star(\omega)$ and $C_0^\star(\omega)$ according to Eqs. (H.24) and (H.25) are shown in Figs. H.9 and H.10.

Choosing the appropriate value of C_0 and adjusting the resistors R_0, R_1 and R_2, the following conditions can be set at some fixed *critical frequency* ω_0:

$$\frac{\xi}{1-\xi}\,\frac{\mathrm{Re}\,C_0^\star(\omega_0)}{\mathrm{Re}\,C_s^\star(\omega_0)} = 1 - k_{31}^2, \tag{H.27a}$$

$$\mathrm{Im}\,C_0^\star(\omega_0) = \mathrm{Im}\,C_s^\star(\omega_0). \tag{H.27b}$$

Then the feedback action is optimal and the effective value of the Young's modulus reaches the peak, as it is shown in the Fig. H.9. In this condition, the sound of the frequency ω_0 is completely reflected by the NS system. The frequency dependence of the effective mechanical damping expressed by the term Y''/Y' is shown in Fig. H.10. As we can see the frequency dependences of capacitances $C_s^\star(\omega)$ and $C_0^\star(\omega)$ influence the effective Young's modulus $Y(\beta, \xi)$ to a large extent.

Since the sound shielding of the NS system is governed by the membrane elasticity in the low frequency range, the profile of the function $\beta^\star(\omega)$ defined by Eq. (H.12) must be investigated in order to evaluate the transmission loss of sound of other frequencies. Since the relaxation time of the PVDF sample is about 10^{-7} s and the NS system works in the frequency range less that 10 kHz, we can approximate the preceding formula using a Taylor expansion

$$C_s^\star(\omega) \approx C_s'(1 - i\tan\delta_s)\,[1 - \gamma^\star\,(\omega/\omega_0 - 1)], \tag{H.28}$$

where $C_s'(1 - i\tan\delta_s)$ is the capacitance of the sample at the critical frequency ω_0 and $\gamma^\star$ represents the frequency change rate of the sample capacitance:

$$\gamma^\star = -\frac{\omega_0}{C_s^\star(\omega_0)}\,\frac{dC_s^\star}{d\omega}\bigg|_{\omega=\omega_0}. \tag{H.29}$$

Then in general the complex function $\beta^\star(\omega)$ has a form:

$$\beta^\star(\omega) = \frac{C_0}{C_s'\left[1-\gamma^\star\left(\omega/\omega_0-1\right)\right]}\,\frac{1-i\omega R_0 C_0}{1-i\tan\delta_s}. \tag{H.30}$$

If it is set such that

$$R_0 = \frac{\tan\delta_s}{\omega_0 C_0}, \quad \xi = \frac{1}{1+C_0/\left[\left(1-k_{31}^2\right)C_s'\right]}, \tag{H.31}$$

then the condition given by Egs. (H.27) is fulfilled.

Figure H.11 shows the experimental data fitted to the theoretical model. We have considered the same geometrical and mechanical parameters as we have used in Figs. H.7 and H.8. The value of the electromechanical coupling factor has been assumed $k_{31} = 0.1$. The dashed line in Fig. H.11 shows the frequency profile of the transmission loss without the the external feedback action. The solid line represents the fitted theoretical curve, which can be realized with the values of dielectric loss tangent $\tan\delta_s = 0.15$ and the frequency change rate of the sample capacitance $\gamma = 0.076$. This dependency has a peak at the critical frequency $f_0 = 0.985\,\mathrm{kHz}$. The decrease of the values of the transmission loss for the frequencies higher than the critical frequency is caused due to the over excitation of the membrane movement by the feedback circuit, which results in an additional unwanted sound generation from the membrane.

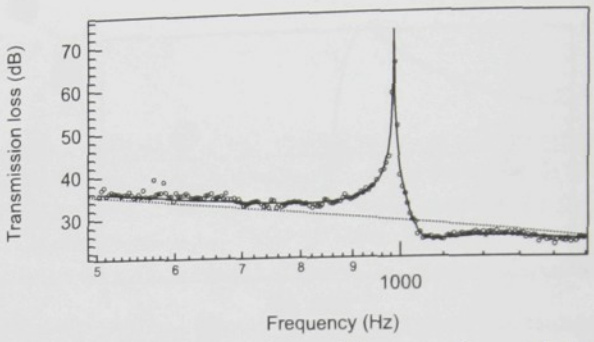

FIGURE H.11: Comparison of the experimental data and the theoretical prediction for the single frequency sound shielding. An increase of 60 dB in the transmission was obtained at the single frequency 1 kHz.

H.5.2. Sound shielding in the broad frequency range

The above example of the elasticity control shows the importance of matching the sample and circuit capacitances. For sound shielding in a broad frequency range, the circuit elements with the distribution of relaxation times should be designed in order to keep accurate enough agreement of capacitances [H6]. One simple solution is to use the same PVDF film as a reference capacitor C_0 in the circuit. Therefore, the ordinary capacitor C_0 is substituted by the capacitor made of PVDF film. Let's denote the frequency dependence of its capacitance by a symbol $C_{s,0}^\star(\omega)$, which is the function of form (H.24) but its parameters may slightly differ from $C_s^\star(\omega)$. Then, the frequency change rates and the dielectric losses of the capacitances $C_{s,0}^\star(\omega)$ and $C_s^\star(\omega)$ are almost equal for

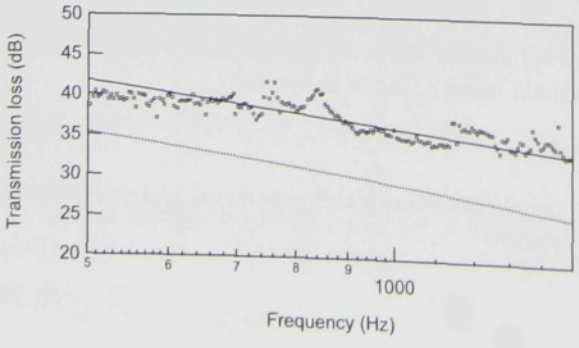

FIGURE H.12: Comparison of the experimental data and the theoretical prediction for the broad band sound shielding. An increase of 7 dB in the transmission was obtained in the broad frequency range between 500 Hz and 1.5 kHz.

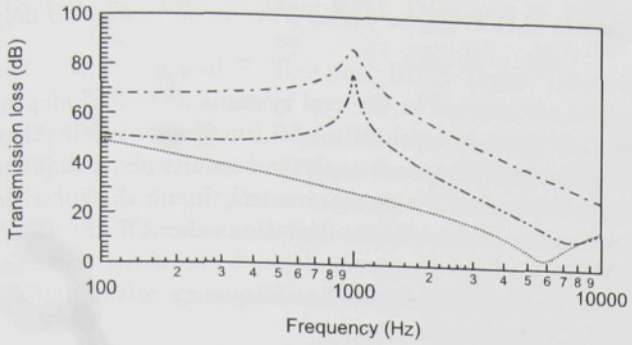

FIGURE H.13: The effect of the circuit for the broad band elasticity control to the frequency dependence of the transmission loss: circuit is off (dotted line); $R_P = 50\,\mathrm{M\Omega}$ (dot-and-dashed line) and $R_P = 5\,\mathrm{M\Omega}$ (double-dot-and-dashed line); $f_0 = 1\,\mathrm{kHz}$.

all frequencies. Without doubt we can assume that $C^\star_{s,0}(\omega) \approx C^\star_s(\omega)$ and put $R_0 = 0$. Thereafter the coefficient $\beta^\star(\omega) \approx 1$ and the ratio $\alpha = C/C_s$ is determined only by the resistances R_1 and R_2:

$$\alpha(\omega) \approx -R_2/R_1 = -\xi/(1-\xi). \tag{H.32}$$

The above equation and Eq. (H.15) suggest the possibility to realize the homogeneous increase of the transmission loss in the very broad frequency range, as it is shown in Fig. H.8. Figure H.12 shows fitting the experimental data of the broad frequency range sound shielding to the theoretical model. The value of the parameter ξ resulting from the fitting is $\xi = 0.4951$ and the parameter α is then considered to be constant for all frequencies.

For some applications, the noise shielding at a specific frequency is required in addition to the uniform noise shielding over the broad frequency range. Our theory may suggest a simple solution for the feedback circuit for such purpose. Let's introduce a large capacitor R_P that is connected to the capacitor C_s in parallel. Then the function $\beta^\star(\omega)$ is of form

$$\beta^\star(\omega) = \frac{C^\star_{s,0}(\omega)/\left[1 + i\omega R_0\, C^\star_{s,0}(\omega)\right]}{C^\star_s(\omega) + 1/(i\omega R_P)}. \tag{H.33}$$

The critical frequency ω_0 of the required maximal sound shielding can be adjusted using resistances R_P and R_0:

$$\begin{aligned} R_0 &= \frac{1}{\omega_0^2 R_P C'_{s,0} C'_s}, \\ \xi &= \left\{1 + \frac{C'_s C'_{s,0}\,(\omega_0 R_P)^2}{(1-k_{31}^2)\left[1 + (\omega_0 R_P C'_s)^2\right]}\right\}^{-1}, \end{aligned} \tag{H.34}$$

where the value of the resistance R_P determines the frequency characteristics of the sound shielding and can be chosen arbitrarily. Using the above equations, example of frequency dependences of transmission loss has been calculated. Result is shown in Fig. H.13. The theory may be useful to design the circuits for other kinds of application.

H.6. DISCUSSION

The transmission loss of sound has been calculated using the vibration analysis of the cylindrically curved viscoelastic membrane. The uniform displacement of the membrane in the radial direction has been taken into account. The maximal amplitude of the membrane displacement $W_{\max}$ can be calculated. From Eq. (H.21) it can be estimated that $|W_{\max}| < |P_{\max}|/|\omega_{\min} Z_{\min}|$, where $P_{\max}$ is the maximum amplitude of the acoustic pressure difference and $\omega_{\min}$ and $Z_{\min}$ are the angular frequency and the specific acoustic impedance of the membrane corresponding to the minimal transmission loss. If we assume that the system is loaded the noise of an 80 dB sound pressure level, the corresponding maximum amplitude of the acoustic pressure difference is smaller

than 0.4 Pa. Using Eq. (H.18), we can estimate that $W_{\max} \approx 4\,\mathrm{nm}$. This value represents only about 0.01% of the membrane thickness.

Nevertheless, the flexural vibrational modes are exerted in the real systems as well. Independently on this approach, we have also developed a more involved model, in which the effects of the clamps of the membrane are taken into account. The exact analytical results show that the resonant frequencies of these vibrational modes depend on the membrane length and thickness. In this case, the frequency dependence of the transmission loss exhibits deviations about 5dB to 10dB around these resonant frequencies, but the V-shape of the frequency dependence of the transmission loss is not significantly distorted and the position of the resonant frequency of the uniform mode is not changed considering the effects of the membrane clamps.

Profiles of the frequency dependences of the transmission loss show the effect of the elasticity of the membrane in the low frequency range. When the complex value $\beta^{\star}(\omega)\xi/(1-\xi)$ tends to $1-k_{31}^2$ on the real axis, the effective value of the Young's modulus goes to infinity. Then the radial movement of the membrane disappears for any arbitrarily high amplitude of the acoustic pressure difference (see Eq. (H.18)). The specific acoustic impedance of the membrane shown in Eq. (H.21) goes to infinity and the transmitted wave vanishes. Hence, the transmission loss at a given frequency goes to infinity according to formula (H.22), as well.

Nevertheless, at the working conditions of the NS system the effective value of the Young's modulus is very sensitive to the value of the external negative capacitance $C < 0$. If we denote $\Delta C = C_s(1-k_{31}^2) + C$, we can for small ΔC approximate $Y/Y_0 \approx k_{31}^2 C_s/\Delta C$. The increase of the transmission loss of about 20 dB requires an increase of the effective value of the Young's modulus by a factor of 10 (see Fig. H.8). Then the relative change of the feedback circuit capacitance $\delta C = \Delta C/C_s$ from the required value must be smaller than 0.1%. This very narrow region of capacitances of the external circuit, in which the markedly raised values of the Young's modulus could be observed, imposes high requirements to the external circuit. Fortunately, this problem can be successfully solved using circuits with distributed relaxations times.

It has been shown that a transmission loss larger than 35 dB in the frequency range from 100 Hz to 2 kHz can be achieved using the NS system composed of a curved piezoelectric membrane and a feedback circuit to enable the dynamic elasticity control. The advantages of this method stem from the small weight, simplicity, low cost, and superb sound shielding performance of the whole system, offering a noise suppression device that can be profitably used in many places such as planes, high speed trains, and similarly noisy environments.

Acknowledgements

Authors would like to express their sincere gratitude to Dr. Hidekazu Kodama of Kobayasi Institute of Physical Research and Yuhei Oikawa of Gakushuin University for their providing of many experimental data and for many useful discussions. One of the authors (P.M.) acknowledges the Scholarship of the Japanese Government. The help of Professor Takeo Furukawa of Tokyo University of Science is greatly appreciated.

This work would not be possible without the help and cooperation of Emeritus Professor Jinzo Kobayashi of Waseda University in Japan and Professor Jan Fousek of Technical University in Liberec, the Czech Republic.

References

[H1] M. Tamura, T. Yamaguchi, T. Oyaba and T. Yoshimi, J. Audio. Eng. Soc. **23**, 21 (1975)
[H2] R. Lerch, J. Acoust. Soc. Am. **66**(4), 952-954 (1979)
[H3] R. Lerch and G. M. Sessler, J. Acoust. Soc. Am. **67**(4), 1379-1381 (1980)
[H4] M. Date, M. Kutani and S. Sakai, J. Appl. Phys. **87**(2), 863-868 (2000)
[H5] T. Okubo, H. Kodama, K. Kimura, K. Yamamoto, E. Fukada and M. Date, in Proceedings of the 17th International Congress on Acoustics, Rome 2001

[H6] H. Kodama, T. Okubo, M. Date and E. Fukada, Mat. Res. Soc. Symp. Proc. **698**, 43-52 (2002)
[H7] M. Toda and S. Toshima, IEEE Trans. Ultrason., Ferroelect., Freq. Contr. **39**(6), 688-692 (1992)
[H8] J. Y. Chung and D. A. Blaser, J. Acoust. Soc. Am. **63**(3), 907-913 (1980)
[H9] J. F. Nye, *Physical Properties of Crystals*, Ch. X, §4.1, p. 185 (Oxford University Press, 1957)
[H10] K. F. Graff, *Wave Motion in Elastic Solids*, §A.9.1, p. 600 (Oxford University Press, 1975)
[H11] Z. Maekawa and P. Lord, *Environmental and Architectural Acoustics*, §5.3, p. 166 (E&FN SPON, 1994)
[H12] T. Furukawa, Phase Transitions **18**, 143-211 (1989)

Paper I

Sound absorbing system as an application of the active elasticity control technique

Published in *Journal of Applied Physics*, Vol. 94, No. 11, Pg. 7356-7362, 1 December 2003

List of citations

1. E. Fukada, M. Date, and H. Kodama, Recent Trends on Application of Piezoactive Polymers to Acoustics - Low Frequency Sound Barrier (Invited Review Paper at *Int. Conf. Intelligent Materials*, Pennsylvania State University, 2003)
   Published in *Materials Technology* **19**(2): Pg. 83-90 (2004)

2. E. Fukada, M. Date, H. Kodama, Y. Oikawa, Elasticity control of curved piezoelectric polymer films, *Ferroelectrics* (accepted for publication, 2005) Ms. No. O-04

SOUND ABSORBING SYSTEM AS AN APPLICATION OF THE ACTIVE ELASTICITY CONTROL TECHNIQUE

P. MOKRÝ[15], E. FUKADA, and K. YAMAMOTO

Kobayasi Institute of Physical Research, Kokubunji, Tokyo 185-0022 Japan

Abstract

Active elasticity control has recently become a promising method used in acoustics to suppress the vibration of mechanical systems or to increase the noise transmission loss. The principle of this technique is based on the simultaneous utilization of both the direct and inverse piezoelectric effects, which is realized by connecting the piezoelectric sample to an external feedback circuit. The action of the feedback circuit results in an essential change of the vibrational response of the system, and a significant change of the resonant frequency in the mechanical system. This leads to the modification of the acoustic properties of the system. For that reason, this technique offers a very general approach to solve vibration and noise problems. To demonstrate this method, the design and theoretical analysis of an experimental realization of a sound absorbing system are presented. The system consists of a curved piezoelectric membrane and a passive sound absorber, which are attached to a rigid backing wall. The theoretical analysis of the system starts from the calculation of the absorption coefficient of an audible sound. This result is used for the determination of the optimal adjustment in the feedback control electronics. The efficiency and the frequency range of the active sound absorption, as well as aspects of the generalization of this method to solve other kinds of noise and vibration problem are discussed.

PACS: 43.50.-x, 77.65.-j, 43.50.Ki

Keywords: Piezoelectric polymers, elasticity control, negative capacitance circuit, absorption coefficient

I.1. INTRODUCTION

The main objective of this article is to demonstrate the application of the *active elasticity control* technique on the design of a sound absorbing (SA) system. The SA system consists of a curved piezoelectric membrane fixed in a rigid frame and connected to an external feedback circuit. The membrane is placed between noise sources and a rigid wall, which supports the whole system. The incident sound makes the membrane vibrate; a part of the sound is reflected, another part is absorbed and transmitted. It is then assumed that the transmitted sound wave is completely reflected from the rigid wall and strikes the membrane from the opposite side. In the usual situation, when the frequency of the incident sound differs from the resonant frequency of the system, most of the incident sound is completely reflected from the SA system. Using the active elasticity control technique, the vibrational response of the system can be changed and the amplitude of the sound wave reflected from the SA system can be completely suppressed.

Recently, piezoelectric materials have been considered as parts of vibration and noise control systems. Ray, Oh and Bar [I1] predicted damping of thin cylindrical shells using a system composed of an accelerometer, a piezoelectric actuator and a simple derivative feedback controller. Lin, Liu and Wang [I2] simulated the active control of the acoustic pressure in a cylindrical cavity with a flexible cylindrical panel using a pair of a piezoelectric actuator and a sensor in conjunction with

[15]e-mail: pavel.mokry@vslib.cz, On leave from Department of Electrical Engineering and Electromechanical Systems, Technical University of Liberec, Czech Republic

a linear quadratic optimal controller. Unfortunately, the realization of these systems, which can very effectively reduce the structural vibration and the structural-borne noise, requires complicated circuitry.

Another method of active vibration absorption has been presented by Davis and Lesieutre [I3]. In this work, the vibration absorber is actively tuned using the capacitive shunting of the piezoelectric element stiffness. Using this technique, the effective dynamic stiffness of piezoelectric ceramics can be increased by approximately 50% of the ordinary value. Independently, Date [54] has used a more sophisticated approach and has developed an evolved technique called *elasticity control*. In this method, the elastic properties of a piezoelectric material are controlled to a large extent using a simple feedback circuit that involves an operational amplifier and works as a negative capacitor or inductor. This technique makes the total control of the effective value of the dynamic Young's modulus possible including the mode, in which the negative values of the effective elastic properties are observed. This method can be beneficially used in noise and vibration control systems. The realization of this proposal and the design of the noise shielding system, was made by Okubo *et al.* [55] and Kodama *et al.* [56].

The theoretical investigation presented in this article is based on a calculation of the acoustic absorption coefficient of the SA system. We start with the analysis of the sound field, which interacts with the membrane vibration. Here we use our previous results [I7] on curved membrane vibration dynamics. Then, we calculate the absorption coefficient, which is governed by elastic properties of the piezoelectric membrane. The analysis of their relationship is used for the determination of the values of the Young's modulus, which lead to the required value of the absorption coefficient. Finally, we finish with the design of the circuit electronics, whose optimal feedback action realizes the needed elastic properties of the piezoelectric membrane.

According to this procedure, the article is organized in five sections. In section I.1, a brief introduction is given. In section I.2, the description of the sound absorbing system is presented. The analysis of the sound field and the calculation of the absorption coefficient are developed in section I.3. In section I.4, the effects of the elasticity control and the feedback circuit are analysed. Section I.5 gives a brief summary of the conclusions.

I.2. DESCRIPTION OF THE SOUND ABSORBING SYSTEM

The frequency dependence of the absorption coefficient is measured using the two-microphone impedance tube system [I8]. According to the standard arrangement, the SA system is installed at the right-hand end of the tube, which is of the rectangular cross section 40 mm × 40 mm. The time dependencies of the acoustic pressure fluctuations are measured at two different positions inside the tube. The transfer function technique is applied in order to extract the amplitudes of the incident (p_i) sound wave and the sound wave (p_r) reflected from the SA system.

Schema of the structure of the SA system are shown in Fig. I.1. The fundamental element of this system is a cylindrically curved thin piezoelectric film, which is made of polyvinidilene fluoride (PVDF) or copolymer of vinidilene fluoride and tetrafluorethylen [P(VDF/TrFE)]. The thickness of the polymer film, which is electroded by aluminium electrodes, is denoted by the symbol h and varies from 40 μm to 200 μm in our experiments. To make the connection between the film electrodes and the external feedback

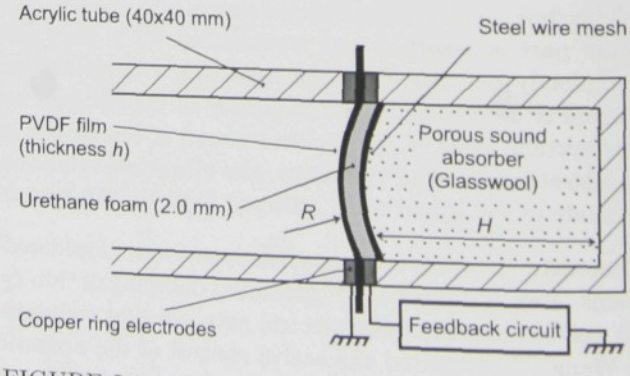

FIGURE I.1: Cross section of the sound absorbing structure with a curved piezoelectric film.

circuit, which actively controls the mechanical damping properties of the membrane, the film is rigidly clamped at its edges inside the tube by thick copper electrodes. The constant radius R of the membrane curvature is essential to make the direct phase correspondence of the sound field changes and the internal stresses inside the membrane. For that reason, the thin film is supported by a steel wire mesh, which is fixed in the inner surface of the tube, and urethane foam, which is inserted between the mesh and the film. In order to obtain the best sound absorbing performance of the system, drawn PVDF or P(VDF/TrFE) film is used due to its stronger piezoelectric response, which is obtained along the direction of the drawing. It is convenient to orient this direction along the circumference of the cylindrical surface. Let us consider that the material properties of the membrane are described by tensor components in a coordinate system, which is attached to any point on the curved membrane surface. Its first axis is oriented with the direction of the film drawing, its second axis is parallel with the symmetry axis of the cylindrical surface, and its third axis is perpendicular to the tangential plane of the cylindrical surface at the certain point.

In order to improve the sound absorbing performance of the system, a passive sound absorber (glasswool) is placed in the space between the SA system and the rigid wall. The distance of the membrane from the rigid end of the tube is denoted by the symbol H. If we neglect the effects of the sound field inhomogeneities caused by the interaction of the curved membrane and the inner surface of the tube, we can consider that only plane waves propagate in the direction of the axis of the tube. In order to simply describe the acoustic wave motion of air particles, let us assume that the cartesian coordinate system is attached to the tube. Its z-axis coincides with the symmetry axis of the tube x- and y-axes are perpendicular to the tube surfaces. The membrane, which is at $z = 0$, splits the tube into two parts. In the left-hand side part of the tube ($z < 0$), the incident and reflected sound waves propagate in air. In the right hand side part of the tube ($z > 0$), the transmitted (p_t) wave and the wave reflected from the rigid wall backing (p_b) propagate in the sound absorbing porous material. For simplicity, we will assume that the thickness of the film supporting structure made of urethane foam and the steel wire mesh is much smaller than the distance H.

Elasticity control plays the key role in the total control of the value of the absorption coefficient of the SA system. The feedback circuit, which has the effective complex capacitance denoted by the symbol C, realizes the simultaneous utilization of the direct and inverse piezoelectric effects leading to an arbitrary change of the effective value of the dynamic Young's modulus. Date [I4] has derived the general formula:

$$Y = Y_0 \left(1 + \frac{k_{31}^2}{1 - k_{31}^2 + \alpha} \right), \tag{I.1}$$

where Y_0 is the ordinary value of the Young's modulus, k_{31} is the electromechanical coupling factor and the parameter α represents the ratio of the feedback circuit capacitance C over the sample capacitance C_s. For positive values of the capacitance ($C > 0$), the effective value of the Young's modulus remains almost unchanged. On the other hand, when the effective capacitance of the feedback circuit is negative ($C < 0$), the effective value of the Young's modulus can reach any arbitrary value from minus infinity to plus infinity.

The circuit that works as a negative capacitor is shown in Fig. I.2. The detail function of this circuit connected to the curved piezoelectric membrane, which is excited by the incident harmonic sound pressure, is analyzed in [I7]. It is shown in [I4,7] that the effective capacitance of the feedback circuit is

$$C = -C_0^* \frac{R_2}{R_1}, \tag{I.2}$$

where C_0^* is the complex capacitance of the *reference capacitor*,

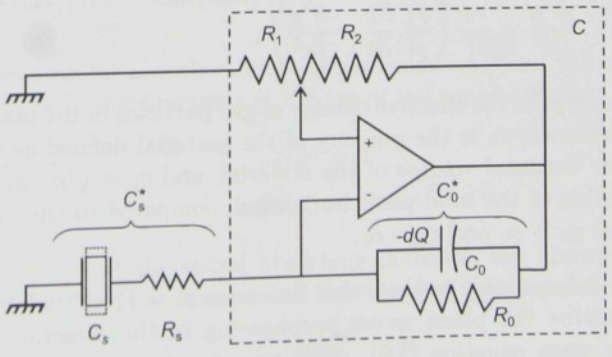

FIGURE I.2: Example of a negative capacitance circuit.

which is made of a vacuum-like capacitor C_0 and a resistor R_0, inside the circuit, with R_1, R_2 as the potentiometer resistances. If we denote

$$\beta = C_0^\star / C_s^\star, \quad \xi = R_2/(R_1 + R_2), \tag{I.3}$$

where $C_s^\star$ is the effective complex capacitance of the sample capacitor C_s combined with a resistor R_s, the effective value of the Young's modulus can be expressed as a function of parameters β and ξ:

$$Y(\beta, \xi) = Y_0 \left(1 + \frac{k_{31}^2}{1 - k_{31}^2 - \beta\xi/(1-\xi)}\right). \tag{I.4}$$

Since it is assumed that the system is harmonically excited by the sound of an angular frequency ω, the mechanical damping effects due to the material viscosity can be introduced by means of the complex value of the Young's modulus Y_0 of the PVDF material. Similarly, the effect of the dielectric relaxation of the piezoelectric membrane can be described by means of the complex value of the capacity C_s.

I.3. ABSORPTION COEFFICIENT

The sound absorption properties of this system can be evaluated using the *absorption coefficient* α_0, which is defined as [I10]

$$\alpha_0 = 1 - |p_r/p_i|^2 . \tag{I.5}$$

Since the sound propagation is quite different in the media on the left-hand side ($z < 0$) and the right-hand side ($z > 0$) from the membrane, it is convenient to write two different wave equations describing the movement of air particles in the tube.

Let us start with the left-hand side of the tube filled with air that, in the absence of sound, has a uniform density ϱ_0, static pressure p_0 and is everywhere of constant temperature. Moreover, let us assume that it is nonviscous and has zero heat conductivity, so that the only energy involved in the acoustic motion is mechanical. According to [I11] we can write the wave equation

$$\frac{\partial^2 p}{\partial z^2} = \frac{1}{c_0^2}\frac{\partial^2 p}{\partial t^2}, \tag{I.6}$$

where c_0 is the phase velocity of sound in air at the given conditions.

In the right-hand side of the tube, the situation is more complicated, since the porous sound absorber is present. According to the classical theory of Beranek [I12], we can write the modified wave equation for air particles in porous medium

$$\frac{\partial^2 p}{\partial z^2} = \frac{\pi_0}{c_1^2}\left(\frac{\sigma_1}{\varrho_1}\frac{\partial p}{\partial t} + \frac{\partial^2 p}{\partial t^2}\right), \tag{I.7}$$

where ϱ_1 is the effective density of gas particles in the material, σ_1 is the specific dynamic frictional resistance, π_0 is the porosity of the material defined as ratio of the volume of air in the material over the total volume of the material, and $c_1 = \sqrt{p_0/\varrho_1}$. If we accept an approximation that the motion of the solid particles is small compared to the motion of the air particles, we can assume that $\varrho_1 = \varrho_0$ and $c_1 = c_0$.

It is possible to show that functions $p_i = P_i\, \mathrm{e}^{\mathrm{i}\omega(t-\gamma_0 z)}$ and $p_r = P_r\, \mathrm{e}^{\mathrm{i}\omega(t+\gamma_0 z)}$, where $\gamma_0 = 1/c_0$, describe the plane waves propagating in the direction of the z-axis in air ($z < 0$) and fulfill the wave equation (I.6). Similarly, functions $p_t = P_t\, \mathrm{e}^{\mathrm{i}\omega(t-\gamma_1 z)}$ and $p_b = P_b\, \mathrm{e}^{\mathrm{i}\omega(t+\gamma_1 z)}$, where $\gamma_1 = \sqrt{(\pi_0/p_0)\,(\varrho_0 - \mathrm{i}\,\sigma_1/\omega)}$, describe plane waves that propagate in the z-direction in the porous sound absorber ($z > 0$) and fulfill the wave equation (I.7). In order to obtain the unknown

amplitudes of the acoustic pressures P_r, P_t, and P_b, complementary conditions must be specified. Assuming steady-state conditions, the gas particle velocity can be expressed as

$$u = -\frac{1}{i\omega\varrho_0}\frac{\partial p}{\partial z}, \qquad \text{for } z < 0, \tag{I.8a}$$

$$u = -\frac{1}{\sigma_1 + i\omega\varrho_0}\frac{\partial p}{\partial z}, \qquad \text{for } z > 0. \tag{I.8b}$$

This function is continuous at the membrane ($z = 0$) and zero at the rigid end of the tube ($z = H$). Moreover, the gas particle velocity is equal to the velocity of the membrane movement $v = i\omega W\,\mathrm{e}^{i\omega t}$.

The detailed analysis [17] of the uniform vibration dynamics of the curved membrane connected to the feedback circuit shows that the amplitude W of the membrane displacement at the steady-state condition is proportional to the amplitude of the difference $P = P_i + P_r - P_t - P_b$ of the acoustic pressures at the opposite sides of the membrane

$$W = \frac{R^2}{h}\left[Y(\beta,\xi) - \omega^2\varrho R^2\right]^{-1} P, \tag{I.9}$$

where $Y(\beta, \xi)$ is the effective complex value of the Young's modulus of the piezoelectric membrane connected to the external feedback circuit.

Proceeding the straightforward calculations we can express the amplitude of the reflected sound wave

$$\frac{P_r}{P_i} = 1 - \frac{2i\omega\zeta}{Y(\beta,\xi) - \varrho\omega^2R^2 + i\omega\zeta\left[1 - i\gamma_1/(\gamma_0\pi_0)\cot(\omega\gamma_1 H)\right]}, \tag{I.10}$$

where $\zeta = \varrho_0 R^2/(h\gamma_0)$. Using the above formula, we can finally obtain the formula for the absorption coefficient:

$$\alpha_0 = \frac{a_1(\omega)\,Y'' + a_2(\omega)}{\left[Y' - a_3(\omega)\right]^2 + \left[Y'' - a_4(\omega)\right]^2}, \tag{I.11}$$

where Y' and Y'' are the real and imaginary part of a complex value of the complex function $Y(\beta, \xi)$, and

$$a_1(\omega) = 4\zeta\omega, \tag{I.12a}$$

$$a_2(\omega) = \left(\frac{4\omega^2\zeta^2}{\gamma_0\pi_0}\right)\frac{\gamma_1'\sinh(2\omega\gamma_1''H) - \gamma_1''\sin(2\omega\gamma_1'H)}{\cos(2\omega\gamma_1'H) - \cosh(2\omega\gamma_1''H)}, \tag{I.12b}$$

$$a_3(\omega) = \varrho\omega^2R^2 + \left(\frac{\omega\zeta}{\gamma_0\pi_0}\right)\frac{\gamma_1'\sin(2\omega\gamma_1'H) + \gamma_1''\sinh(2\omega\gamma_1''H)}{\cos(2\omega\gamma_1'H) - \cosh(2\omega\gamma_1''H)}, \tag{I.12c}$$

$$a_4(\omega) = -\omega\zeta - \left(\frac{\omega\zeta}{\gamma_0\pi_0}\right)\frac{\gamma_1'\sinh(2\omega\gamma_1''H) - \gamma_1''\sin(2\omega\gamma_1'H)}{\cos(2\omega\gamma_1'H) - \cosh(2\omega\gamma_1''H)}. \tag{I.12d}$$

It is pointed out that if there is no passive sound absorber between the membrane and the rigid backing wall, $\gamma_1' = \gamma_0$, $\gamma_1'' = 0$, porosity $\pi_0 = 1$, and functions (I.12) are of the simpler form:

$$a_1(\omega) = 4\zeta\omega, \qquad a_2(\omega) = 0,$$

$$a_3(\omega) = \omega\left[\varrho\omega R^2 - \zeta\cot(\omega\gamma_0 H)\right], \qquad a_4(\omega) = -\omega\zeta.$$

Since the coefficient $a_2(\omega) = 0$ in the absence of the sound absorbing material, the absorption coefficient is then nonzero if and only if the viscosity (mechanical damping) of the membrane is nonzero.

The effect of the radius of the membrane curvature on the frequency dependence of the absorption coefficient is shown in Fig. I.3. The numerical results have been obtained using formula (I.11). The following values have been considered: thickness $h = 50\,\mu$m, radius of the membrane curvature $R = 16$ cm, distance $H = 20$ mm, mass density $\varrho = 1770\,\mathrm{kg\,m^{-3}}$, Young's modulus $Y_0 = 3.7$ GPa, and mechanical quality factor $Q_\mathrm{m} = 10$ where $Q_\mathrm{m} = Y_0'/Y_0'' = 10$. The porosity of the porous sound absorber has been assumed $\pi_0 = 0.99$ and its dynamic specific frictional resistance $\sigma_1 = 10^5\,\mathrm{Pa\,s\,m^{-2}}$. Physical properties of air have been taken at the normal conditions. The maximal values of the absorption coefficient take place in the frequency range around the resonant frequency of the uniform vibration mode $\omega_0 = (1/R)\sqrt{Y_0'/\varrho}$.

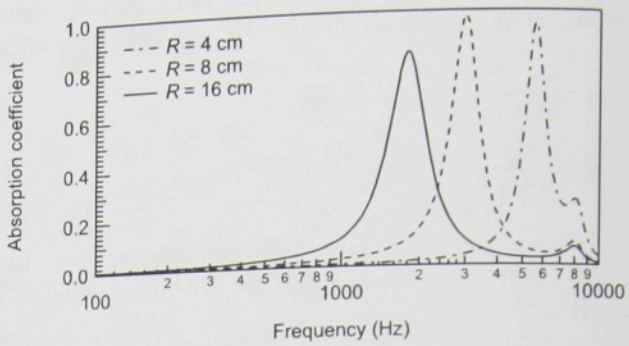

FIGURE I.3: Effect of the radius of the curvature R to the frequency dependence of the absorption coefficient: $R = 4$ cm (solid line), $R = 8$ cm (dashed line), and $R = 16$ cm (dot-and-dashed line).

I.4. EFFECT OF THE ELASTICITY CONTROL

Formula (I.11) poses the question, is it possible to make the value of the absorption coefficient at some fixed frequency ω_0 equal to some arbitrary value η, which is from 0 to1, only by an appropriate choice of the effective value $Y_\eta = Y_\eta' + iY_\eta''$ of the Young's modulus of the membrane? To answer the question, we simply write the equation

$$\alpha_0(\omega_0; Y_\eta', Y_\eta'') = \eta. \tag{I.13}$$

Using Eq. (I.11) we can derive the condition for the real (Y_η') and the imaginary (Y_η'') part of the Young's modulus in a form:

$$\left[Y_\eta' - y_1(\omega_0, \eta)\right]^2 + \left[Y_\eta'' - y_2(\omega_0, \eta)\right]^2 = y_R^2(\omega_0, \eta), \tag{I.14}$$

where

$$y_1(\omega, \eta) = a_3(\omega), \tag{I.15a}$$
$$y_2(\omega, \eta) = a_4(\omega) + a_1(\omega)/(2\eta), \tag{I.15b}$$
$$y_R(\omega, \eta) = (2\omega\zeta/\eta)\sqrt{1-\eta}. \tag{I.15c}$$

The condition (I.14) represents a circle of all complex values $Y_\eta' + iY_\eta''$ of the Young's modulus of the membrane that lead to the required value η of the absorption coefficient. The origin of the circle is given by functions y_1 and y_2 and its radius is equal to y_R. Values Y_η' and Y_η'' given by Eq. (I.14) can be expressed in the following parametric form:

$$Y_\eta'(\omega, \tau) = y_1(\omega, \eta) + y_R(\omega, \eta)\sin\tau, \tag{I.16a}$$
$$Y_\eta''(\omega, \tau) = y_2(\omega, \eta) + y_R(\omega, \eta)\cos\tau, \tag{I.16b}$$

where τ is a parameter running from 0 to 2π. After the substitution of Eqs. (I.16) into Eq. (I.11) we can directly show that the effective values of the Young's modulus that are constructed according to Eqs. (I.16) lead to the requested value η of the absorption coefficient at a given frequency. Examples of such circles are shown in Fig. I.4. Examples of the frequency dependencies of the absorption coefficient α_0 for four constant values of the Young's modulus that lead to $\alpha_0 = 0.5$ at the frequency $f = 1$ kHz (see circular markers in Fig. I.4) are shown in Fig. I.5. This figure also

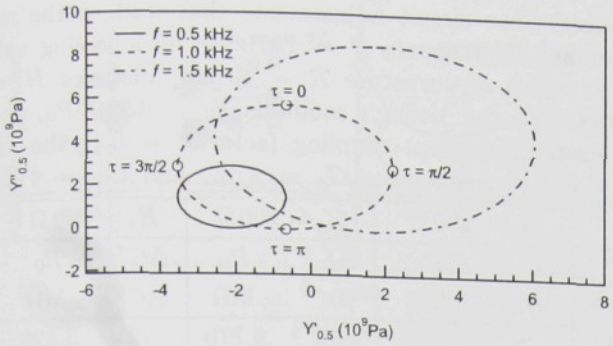

FIGURE I.4: Complex values $Y_{0.5}$ of the Young's modulus, which lead to the $\alpha_0 = 0.5$ value of the absorption coefficient at the frequency $f = 0.5\,\mathrm{kHz}$ (solid line), $f = 1.0\,\mathrm{kHz}$ (dashed line) and $f = 1.5\,\mathrm{kHz}$ (dot-and-dashed line).

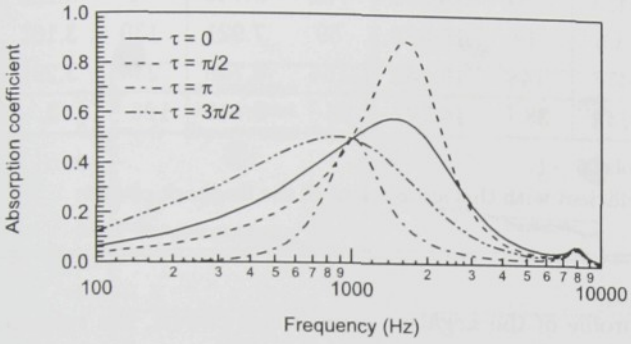

FIGURE I.5: Effect of the elasticity control to the frequency dependencies of the absorption coefficient α_0. Four constant values of the Young's modulus have been considered: $Y_{0.5}(1\,\mathrm{kHz}, \tau = 0)$ (solid line), $Y_{0.5}(1\,\mathrm{kHz}, \tau = \pi/2)$ (dashed line), $Y_{0.5}(1\,\mathrm{kHz}, \tau = \pi)$ (dot-and-dashed line), and $Y_{0.5}(1\,\mathrm{kHz}, \tau = 3\pi/2)$ (double-dot-and-dashed line).

indicates the possibility of the control of the frequency spectrum of the absorption coefficient by choosing the certain value of the parameter τ and, consequently, the effective value of the dynamic Young's modulus given by Eqs. (I.16)

Our task now is to determine the best adjustment of the feedback circuit, which makes the required effect. The basic idea of elasticity control is formulated by Eq. (I.1), which defines the effective value of the Young's modulus in form of the complex analytic function of a complex parameter $\alpha = \alpha' + i\alpha''$. The parameter α plays a crucial role and it can be expressed as an inverse function of the effective Young's modulus.

$$\alpha(Y_0/Y) = -1 + \frac{k_{31}^2}{1 - Y_0/Y}. \tag{I.17}$$

If we denote $\lambda = Y_0/Y = \lambda' + i\lambda''$, then it is equal to

$$\alpha(\lambda' + i\lambda'') = -1 - k_{31}^2 \frac{\lambda' - 1 - i\lambda''}{(\lambda' - 1)^2 + (\lambda'')^2}. \tag{I.18}$$

The pair of inverse complex functions defined by formulae (I.1) and (I.17) expresses the direct single-value correspondence between any complex value of the Young's modulus and its corresponding value of the complex ratio $\alpha = C/C_s$. The detail analysis of the realization of negative complex capacitances by circuits with operational amplifiers is given in [I4]. In case of the example presented in this article, it is convenient to use the negative capacitor shown in Fig. I.2. As it is discussed in [I7] for the transmission loss, the frequency range of the optimal performance of the SA system depends on matching the frequency dependencies of the *sample* ($C_s^\star$) and the *reference capacitor* ($C_0^\star$) capacitances.

In our experiments it is difficult to find the optimal working conditions of the feedback circuit in a broad frequency range. For that reason, and taking the stability conditions of the feedback circuit [I4] into account, the resistor R_s is connected to the sample capacitor C_s in series. This shrinks the frequency range of the optimal working conditions of the circuit and makes the circuit adjustment easier. The equivalent complex capacitance of this combined element is

$$C_s^\star(\omega) = \frac{C_s}{1 + i\omega C_s R_s}. \tag{I.19}$$

TABLE I.1: Examples of the negative capacitance circuit adjustments that lead to the required value α_0 of the absorption coefficient at the frequency $f = 1\,\mathrm{kHz}$. The following values have been used: thickness $h = 50\,\mu\mathrm{m}$, radius of curvature $R = 40\,\mathrm{mm}$, distance $H = 20\,\mathrm{mm}$, membrane mass density $\varrho = 1770\,\mathrm{kg\,m^{-3}}$, the Young's modulus $Y_0 = 3.710^9\,\mathrm{Pa}$, the mechanical quality factor $Q_m = 10$, the electromechanical coupling factor $k = 0.1$, the dielectric loss tangent of capacitors $\tan\delta_s = 0.01$, capacitances $C_s = 4\,\mathrm{nF}$, and $C_0 = 4\,\mathrm{nF}$.

						$R_s = 100\,\Omega$		$R_s = 200\,\Omega$		$R_s = 500\,\Omega$	
α_0	τ	Y'_η $10^7\,\mathrm{Pa}$	Y''_η $10^7\,\mathrm{Pa}$	$\alpha'+1$ 10^{-6}	α'' 10^{-6}	$\Delta\xi$ † 10^{-6}	R_0 MΩ	$\Delta\xi$ † 10^{-6}	R_0 MΩ	$\Delta\xi$ † 10^{-6}	R_0 MΩ
0.5	0	-4.153	35.690	108	-954	38	25.521	55	9.770	12	3.426
0.5	$\pi/2$	13.830	17.706	414	-475	-90	19.514	-73	8.740	-4	3.290
0.5	π	-4.153	0.277	111	-3.6	42	15.853	59	7.921	130	3.167
0.5	$3\pi/2$	-22.137	17.706	541	-478	148	19.552	164	8.748	235	3.291
1		-4.153	4.990	99	-142	38 ‡	16.777	56 ‡	8.145	126 ‡	3.

†Symbol $\Delta\xi$ stands for the numerical value of $0.5 - \xi$.
‡Frequency dependence of the absorption coefficient with this adjustment of the feedback circuit is shown in Fig. I.6.

Similarly, in order to tune the frequency profile of the negative capacitance circuit, the *reference capacitor* is made of a capacitor C_0 and a resistor R_0 connected in parallel. The equivalent complex capacitance of this element is equal to

$$C_0^\star(\omega) = C_0 + \frac{1}{i\omega R_0}. \tag{I.20}$$

Hence, the frequency dependence of the complex parameter α in the system, which consists of the capacitances $C_0^\star$ and $C_s^\star$, is according to Eqs. (I.3) equal to

$$\alpha(\omega; R_0, \xi) = -\beta(\omega; R_0)\,\frac{\xi}{1-\xi}, \tag{I.21}$$

where the complex function $\beta(\omega; R_0, \xi)$ is of the form

$$\beta(\omega; R_0) = \frac{C_0 + 1/(i\omega R_0)}{C_s/(1 + i\omega C_s R_s)}. \tag{I.22}$$

The given frequency profile of the parameter α can be adjusted using the resistance R_0 and the ratio ξ.

If we compare the real parts (denoted by a symbol α') and the imaginary parts (α'') of equations (I.18) and (I.21), the resistances R_0, R_1, and R_2 can be adjusted at any arbitrary *critical frequency* ω_0. Since both capacitors C_s and C_0 in the system are made of the PVDF film, the dielectric relaxation is introduced by means of the dielectric loss tangent: $C_s = C'_s(1 - i\tan\delta_s)$, $C_0 = C'_0(1 - i\tan\delta_s)$. Then, assuming $1 \pm \tan^2\delta_s \approx 1$ we finally obtain the values for the resistance R_0 and the ratio ξ:

$$R_0 = \frac{X}{\omega_0 C'_0\left[\omega_0 C'_s R_s\,(\alpha' - \alpha''\tan\delta_s) - \alpha''\right]}, \tag{I.23a}$$

$$\xi = \left\{1 - \frac{C'_0}{X}\left[\frac{1}{C'_s} + \omega_0 R_s\,(2\tan\delta_s + \omega_0 C'_s R_s)\right]\right\}^{-1}, \tag{I.23b}$$

where

$$X = \alpha' + \alpha''\,(\tan\delta_s + \omega_0 C'_s R_s). \tag{I.23c}$$

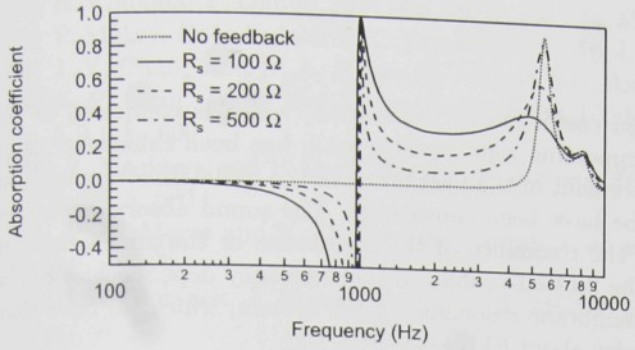

FIGURE I.6: Effect of the feedback circuit to the frequency dependency of the absorption coefficient α_0: no feedback action (dotted line), $R_s = 100\,\Omega$ (solid line), $R_s = 200\,\Omega$ (dashed line), and $R_s = 500\,\Omega$ (dot-and-dashed line).

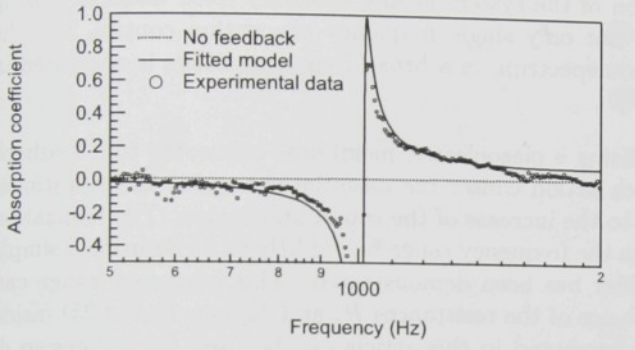

FIGURE I.7: Comparison of the experimental data and the theoretical prediction of the theoretical model.

The process of the circuit adjustment can be summarized as following: First, the required frequency profile of the absorption coefficient is decided. Second, knowing the given value of η at some fixed frequency ω_0, the appropriate value of the Young's modulus is calculated using Eq. (I.14) or (I.16). The choice of the value of the parameter τ must be done carefully in order to make a good agreement of the required frequency profile of the absorption coefficient and which can be realized using available feedback circuit components. Next, the value of the complex parameter $\alpha = \alpha' + i\alpha''$ is calculated using Eq. (I.17). Finally, the resistances R_0, R_1, and R_2 can be adjusted using values obtained from substitution of the values α' and α'' into Eqs. (I.23). The value of the resistance R_s determines the width of the frequency range, in which the action of the feedback circuit is optimal.

In our experiments, we have prepared a system with the radius of the membrane curvature $R = 4\,\mathrm{cm}$. Capacitances of the membrane C_s and the reference capacitor C_0 are equal to 4 nF and the dielectric loss tangent have been estimated to be $\tan\delta_s = 0.05$. Examples of the results of the feedback circuit adjustments of this system are shown in Tab. I.1. The theoretical predictions of the effects for this kind of the feedback circuit are shown in Fig. I.6. The numerical results shows the possibility of the absorption control in the frequency range from 1 kHz to 10 kHz. In the frequency range below the *critical frequency* 1 kHz, the piezoelectric membrane is over excited due to the mismatch of the frequency dependencies of complex capacitances $C_s(\omega)$ and $C_0(\omega)$. In this condition the membrane works as a sound speaker and the amplitude of the reflected sound pressure wave P_r is larger than the amplitude of the incident one. Then, the negative values of the absorption coefficient can be obtained and measured. This undesirable behaviour of the active sound absorbing system is caused by the very simple set-up of the feedback circuit and can be eliminated using more advanced electronics. The optimization of the frequency dependence of the reference capacitor capacitance $C_0(\omega)$ can reduce this unwanted attribute. Experimental data determining the effect of the feedback circuit was measured and fitted to our theoretical model. The results of the fitting are presented in Fig. I.7. The resulting values for the parameters $\xi = 0.4998$, $R_0 = 2.989\,\mathrm{M}\Omega$ and $R_s = 496\,\Omega$ are in a very good agreement with the actual values, which have been used in the experiment.

I.5. DISCUSSION

The normal incidence sound absorption coefficient of the system, which is composed of the cylindrically curved membrane and the supporting rigid backing wall, has been calculated using the vibration analysis. The uniform displacement of the membrane in the radial direction and the plane sound waves inside the acoustic tube have been considered. The sound absorption of the system reaches the maximal values when the resonance of the membrane or the air particles in the porous sound absorber takes place. The plotted profiles of the frequency dependencies of the absorption coefficient indicates that the membrane resonance of the system, which we have used in our experiments, takes place at frequencies about 6 kHz (see Fig. I.3).

The theoretical analysis of the formula for the absorption coefficient suggests the possibility of the total control of the sound absorption of the system at any arbitrary fixed frequency using the elasticity control method. Moreover, not only single frequency absorption control, but the possibility to influence the sound absorption spectrum in a broad frequency range is suggested in our theory (see Figs. I.5 and I.6).

Elasticity control has been realized utilizing a piezoelectric membrane connected to a feedback circuit inside the SA system. The feedback action causes the essential change of the vibrational response of the whole system, which leads to the increase of the sound absorption. The realization of the control of the absorption coefficient in the frequency range from 1 kHz to 2 kHz using a simple feedback circuit and an operational amplifier has been demonstrated. This frequency range can be arbitrarily shifted by the appropriate choice of the resistances R_s and R_0 (see Eqs. I.23) inside the external feedback circuit. The theory presented in this article can be used for the design of improved feedback circuits offering better performance of the whole SA system in the low frequency range, which is of practical importance.

This article is not only a description of the sound absorption control system, but also presents the general approach of noise and vibration control using piezoelectric materials and negative capacitance circuits. The method starts from the vibrational analysis concentrating on the effects of the elastic properties of the system. Making the essential system parts of piezoelectric materials and connecting them to the feedback circuits, the noise and vibration control can be realized in a narrow or broad frequency range. An example to find the optimal feedback has been presented. The advantages of this method stem from its generality and simplicity offering a noise and vibration suppression device that is of small weight and cost, and can be profitably used for sound absorption in the low frequency range where the passive sound absorbers are ineffective.

Acknowledgements

The authors would like to express their sincere gratitude to Dr. Hidekazu Kodama of Kobayasi Institute of Physical Research and Yuhei Oikawa of Gakushuin University for providing many experimental data and for many useful discussions. One of the authors (P.M.) acknowledges a Scholarship of the Japanese Government. The help of Professor Takeo Furukawa of Tokyo University of Science is greatly appreciated. This work would not be possible without the help and cooperation of Emeritus Professor Jinzo Kobayashi of Waseda University in Japan and Professor Jan Fousek of Technical University in Liberec, the Czech Republic.

References

[I1] M. C. Ray, J. Oh and A. Bar, J. Sound Vib. **240**(5), 921-934 (2001)
[I2] O. R. Lin, Z.-X. Liu and Z.-L. Wang, J Sound Vib. **246**(3), 525-541 (2001)
[I3] Ch. Davis and G. Lesieutre, J. Sound Vib. **232**(3), 601-617 (2000)
[I4] M. Date, M. Kutani and S. Sakai, J. Appl. Phys. **87**(2), 863-868 (2000)
[I5] T. Okubo, H. Kodama, K. Kimura, K. Yamamoto, E. Fukada and M. Date, in Proceedings of the 17th International Congress on Acoustics, Rome (2001).

[I6] H. Kodama, T. Okubo, M. Date and E. Fukada, Mat. Res. Soc. Symp. Proc. **698**, 43-52 (2002)
[I7] P. Mokrý, E. Fukada and K. Yamamoto, J. Appl. Phys. **94**, 789 (2003).
[I8] J. Y. Chung and D. A. Blaser, J. Acoust. Soc. Am. **63**(3), 907-913 (1980)
[I9] K. F. Graff, *Wave Motion in Elastic Solids*, (Oxford University Press, New York, 1975), Sec. A.9.1, p. 600.
[I10] Z. Maekawa and P. Lord, *Environmental and Architectural Acoustics*, (E&FN SPON, 1994), Sec. Sec. 1.5, p. 11.
[I11] P. M. Morse and K. U. Ingard, *Theoretical acoustics*, (McGraw-Hill, New York, 1968), Sec. 6.2, p. 243.
[I12] L. L. Beranek, J. Acous. Soc. Am. **13**, 248-260 (1942)

Paper J

Sound isolation by piezoelectric polymer films connected to negative capacitance circuits

Published in *IEEE Transactions on Dielectrics and Electrical Insulation*: Volume 11, No. 2, Pgs: 328-333 2004

List of citations

1. H. Kodama, T. Okubo, K. Kimura, K. Yamamoto, M. Date, and E. Fukada, Sound Shielding of Piezoelectric PVDF Panel, *Proc. the 33rd International Congress and Exposition on Noise Control Engineering (Internoise-2004)*, Prague, Czech Republic (2004): Art. No. 243

2. E. Fukada, M. Date, H. Kodama, Y. Oikawa, Elasticity control of curved piezoelectric polymer films, *Ferroelectrics* (accepted for publication, 2005) Ms. No. O-04

SOUND ISOLATION BY PIEZOELECTRIC POLYMER FILMS CONNECTED TO NEGATIVE CAPACITANCE CIRCUITS

E. FUKADA[16], M. DATE, K. KIMURA, T. OKUBO, H. KODAMA, P. MOKRÝ, and K. YAMAMOTO

Kobayasi Institute of Physical Research, Kokubunji, Tokyo 185-0022 Japan

Abstract

Sound isolation has been achieved using a piezoelectric polymer film connected to a negative capacitance feedback circuit. A curved PVDF film was located in the middle of an acoustic tube and the transmission loss of sound through the film was determined in the audio frequency range. At any chosen frequency, the complete isolation of sound was achieved by adjusting the feedback, i.e. the complex capacitance of the circuit was matched precisely to that of the film.

Keywords: Sound Isolation, Transmission Loss, Piezoelectric Polymer Film, Negative Capacitance Circuit

J.1. INTRODUCTION

Applications of piezoelectric polymers have been developed in various fields [J1]. This paper presents a novel method of sound shielding using such films. PVDF and its copolymers are available in large area flexible film form. Tanaka et al. [J2] reported that PVDF sensors bonded to a solid structure can act as a feed-forward control system to suppress vibration and sound. Nishigaki et al. [J3] succeeded in suppressing vibration in a cantilever beam by bonding the beam to two piezoelectric PVDF films. The films formed two arms of a bridge working as a self–sensing actuator.

Date et al. [J4] have recently invented a novel technique to control the elastic properties of piezoelectric materials by connecting an electric circuit that behaves as a negative capacitance. The combination of PVDF film and negative capacitance acts simultaneously as a detector and generator of vibration and sound. Some early applications of this system have been reported [J5,6]. This paper reports further experimental observations of electrical control of the Young's modulus of poled PVDF films, and attenuation of sound transmission through curved PVDF membranes coupled to negative capacitance circuits.

J.2. PRINCIPLE OF ELECTRIC CONTROL OF ELASTICITY

The basic idea for controlling the elasticity of piezoelectric materials is to superpose the direct and inverse piezoelectric effects. Application of mechanical stress to a piezoelectric material generates elastic strain. Simultaneously, electric polarization proportional to the strain is generated by the direct piezoelectric effect. The electric charge induced on the electrodes by the polarization is amplified and the resulting voltage is fed back to the electrode. The electric field due to this voltage generates strain by the inverse piezoelectric effect. The total strain is the sum of the stress-induced strain and the field- induced strain.

If the field-induced strain opposes the stress-induced strain, the total strain decreases and the elastic coefficient increases. On the contrary, if the field–induced strain reinforces the stress-induced strain, the total strain increases and the elastic coefficient decreases. In the case of sinusoidal stimulation, the magnitude and phase of the dynamic elastic coefficient are controlled by the magnitude and phase of the feedback voltage.

[16]e-mail: fukada@kobayasi-riken.or.jp

J.3. NEGATIVE CAPACITANCE

Figure J.1 shows the circuit that increases the elastic coefficient, designated circuit H. On the left of the figure a piezoelectric sample disconnected from the circuit is shown. A static stress is applied to this sample. The strain (the polarization proportional to it) is represented by an arrow. The magnitude of strain/polarization is shown by the length of the arrow. The polarization induces negative charge on the upper electrode, and positive charge on the lower electrode.

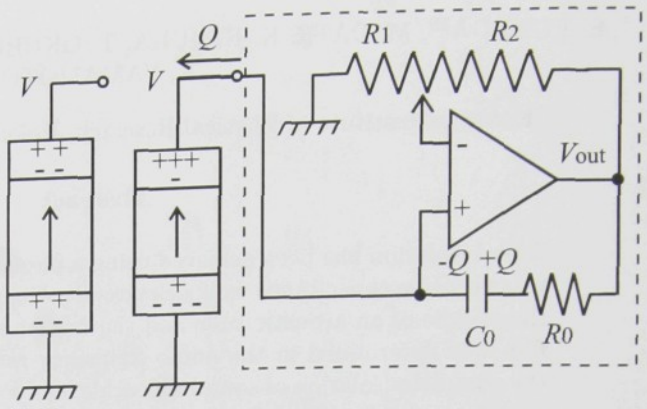

FIGURE J.1: Principle of operation of the negative capacitance circuit H

When the piezoelectric sample is connected to the circuit H, the non-inverting (+) and inverting (−) voltages of the operational amplifier (OA) are V_{in}^{+} and V_{in}^{-} respectively. To simplify the analysis of this circuit, we will temporarily ignore the resistor R_0 and consider C_0 as a perfect capacitor with zero dielectric loss. Straightforward circuit analysis gives

$$V_{\text{in}}^{-} = \frac{R_1}{R_1 + R_2} V_{\text{out}}, \qquad \text{(J.1)}$$

$$V_{\text{in}}^{+} = \frac{C_0}{C_0 + C_s} V_{\text{out}}, \qquad \text{(J.2)}$$

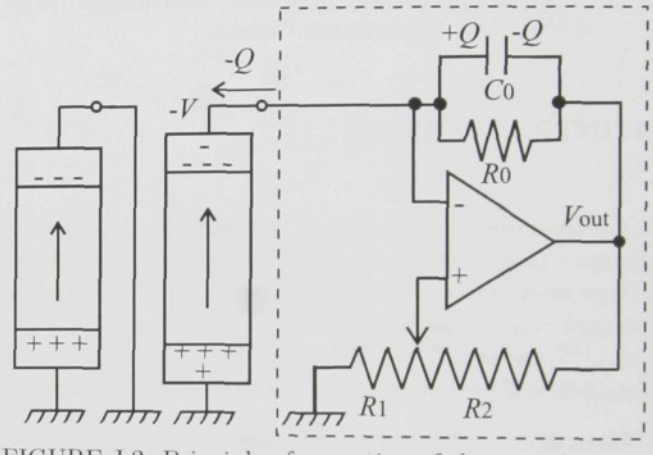

FIGURE J.2: Principle of operation of the negative capacitance circuit S.

where C_s is the capacitance of the sample. The charge Q on the capacitor C_0 is given by

$$Q = C_0 \left| V_{\text{in}}^{+} - V_{\text{out}} \right|. \qquad \text{(J.3)}$$

With the OA in negative feedback mode we may assume that $V_{\text{in}}^{+} = V_{\text{in}}^{-} = V$. From Eqs. (J.1-J.3) we recover

$$Q = C_0 \frac{R_2}{R_1} V. \qquad \text{(J.4)}$$

The input impedance of the OA at the non-inverting input is readily shown to be $Z_{\text{in}} = -R_1/(R_2 i\omega C_0)$, and so the OA circuit presents an effective capacitance of

$$C = -C_0 \frac{R_2}{R_1}. \qquad \text{(J.5)}$$

Thus circuit H may be considered as a negative capacitance circuit with a capacitance C given by Eq.(J.5).

Stable operation of the circuit (negative feedback) requires the condition $d(V_{\text{in}}^{+} - V_{\text{in}}^{-})/dV_{\text{out}} < 0$. Then from Eqs. (J.1) and (J.2) we have $(C_s/C_0) > (R_2/R_1)$. Combining with Eq. (J.5) the stability condition is $|C| < |C_s|$ (see [J4]).

If the absolute value of the capacitance C of the circuit approaches the value of C_s, the feedback increases and the apparent elastic coefficient also increases. It has been shown [J4] that the relation between the elastic coefficient and C/C_s is given by

$$\frac{Y}{Y_0} = \frac{1}{\{1 - k^2/(1 + C/C_s)\}} \tag{J.6}$$

where Y is Young's modulus of the film with the negative capacitance circuit attached, Y_0 is its value in short circuit, and k the electromechanical coupling factor. Since k=0.1 approximately for PVDF, we expect Y=1.11Y_0 at C/C_0=-0.9 but $Y = \infty$ at $C/C_s = -0.99$.

Figure J.2 shows another type of negative capacitance circuit designated circuit S, which decreases the elastic coefficient. The sample electrode is connected to the inverting (-) input of the OA. Equation (J.5) holds for this circuit also, and the stability condition requires $|C| > |C_s|$ [J4]. In this case we expect Y=0.91Y_0, 0.5Y_0 and 0.09Y_0 at C/C_s=-1.1, -1.01 and –1.001 respectively.

J.4. RESULTS AND DISCUSSION

J.4.1. Young's modulus of PVDF films

The complex Young's modulus $Y = Y' + iY''$ of a PVDF film connected to the negative capacitance circuits was measured as a function of C/C_s and frequency using a Rheolograph-Solid (Toyo Seiki). The dimensions of the rectangular film were approximately 25 x 5 x 0.05 mm. Figure J.3 shows the dependence of Y' on C/C_s measured at 9.8 Hz. C_s = 628 pF, C_0 = 30 nF and $R_1 + R_2$ = 100 kΩ. The value of C was varied by changing the ratio R_2/R_1 according to Eq. (J.5).

Since C/C_s in Eq. (J.6) is in fact a complex quantity, we must consider dielectric loss in analyzing the frequency dependence of Y. The complex capacitance C_s of the sample may be written as $C_s = C_s' - iC_s'' = C_s'(1 - i\tan\delta_s)$, where the dissipation factor of the sample $\tan\delta_s = C_s''/C_s'$. The resistor R_0 (Figure J.1) must be taken into account when considering the dielectric loss in C_s. Regarding the series combination of C_0 and R_0 as an equivalent capacitance C_{eq} and equating impedances gives

$$C_{eq} = \frac{C_0}{1 + i\omega C_0 R_0} = C_0 \frac{1 - i\tan\delta}{1 + \tan^2\delta} \tag{J.7}$$

where $\tan\delta = 2\pi f C_0 R_0$. By replacing C_0 in Eq. (J.5) by C_{eq}, we have the following expression

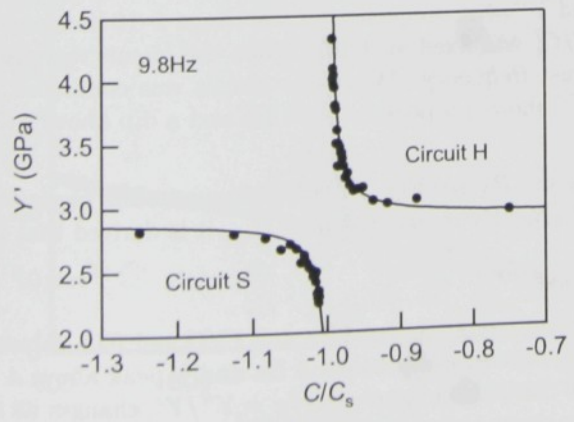

FIGURE J.3: Dependence on C/C_s of Young's modulus Y' of a PVDF film connected to circuits H and S.

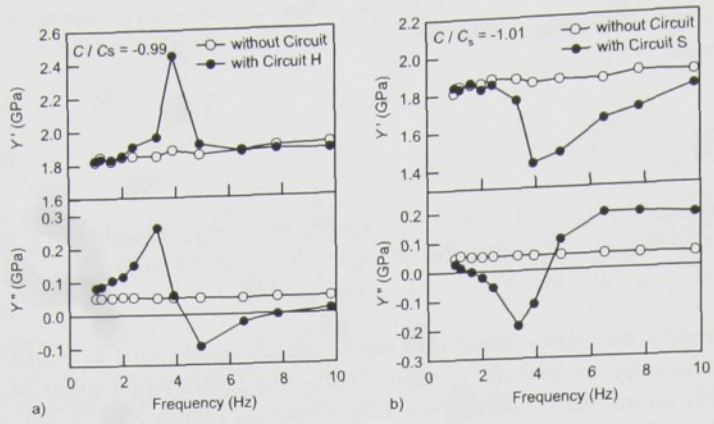

FIGURE J.4: Frequency dependence of Young's modulus $Y = Y' + iY''$ of a PVDF film connected to circuits H and S.

for C/C_s ignoring $\tan^2\delta_s$ ($\tan\delta_s = 0.02$ for PVDF).

$$\begin{aligned} \frac{C}{C_s} &= -\frac{C_0}{C_s'}\frac{R_2}{R_1}\{1 + i\,(\tan\delta_s - \tan\delta)\} \\ &= -\frac{C_0}{C_s'}\left\{1 + i\,\tan\delta_s\left(1 - \frac{f}{f_0}\right)\right\}, \end{aligned} \tag{J.8}$$

where f_0 is the frequency at which $\tan\delta$ is equal to $\tan\delta_s$. By substituting Eq. (J.2) into Eq. (J.6), Y' and Y'' are represented as a function of frequency f.

$$\begin{aligned} \frac{Y'}{Y_0} &= 1 + \frac{k^2\left(1 - k^2 - A\right)}{\left(1 - k^2 - A\right)^2 + A^2\tan^2\delta_s\left(1 - f/f_0\right)^2}, \\ \frac{Y''}{Y_0} &= \frac{k^2 A\tan\delta_s\left(1 - f/f_0\right)}{\left(1 - k^2 - A\right)^2 + A^2\tan^2\delta_s\left(1 - f/f_0\right)^2}, \end{aligned} \tag{J.9}$$

where $A = |C/C_s| = (C_0/C_s')\,(R_2/R_1)$. We expect Y' to increase steadily with increasing frequency up to a maximum at f_0 and then decrease steadily. We expect Y'' to be positive below f_0, zero at f_0 and negative above f_0.

Figure J.4a shows the variation of Y' and Y'' with frequency in the range 1–10 Hz measured using circuit H. f_0=4 Hz was selected and C/C_s was fixed at -0.96. When the circuit was disconnected, both Y' and Y'' were constant against frequency. When the circuit was connected, the maximum increase of Y' occurred at 4 Hz. Y'' showed a peak below 4 Hz and a dip above 4 Hz.

In circuit S, the parallel combination of C_0 and R_0 (see Fig. J.2) gives an equivalent capacitance $C_{eq} = C_0(1 - i\tan\delta)$ where $\tan\delta = (1/2)\pi f C_0 R_0$. By replacing C_0 by C_{eq}, it is derived that Eqs. (J.2) and (J.9) also hold for circuit S.

Figure J.4b shows the results obtained using circuit S. f_0=4 Hz and C/C_s=-1.03. Values Y' showed a maximum decrease at 4 Hz and Y'' showed a dip below 4 Hz and a peak above 4 Hz. Figures J.4a and J.4b indicate that the elastic dissipation factor, $\tan\delta_E = Y''/Y'$, changes its sign at f_0 . In other words, the phase between the stress and the strain changes by 180 degrees at f_0.

J.4.2. Acoustic tube experiments

The transmission loss of audible sound through PVDF films connected to negative capacitance circuits was measured using the acoustic tube shown schematically in Figure J.5. An oriented and poled PVDF film with dimensions of about 50 x 45 x 0.04 mm^3 was installed in the middle of a plastic tube with rectangular cross section of 40 x 40 mm and length of about 1 m. The radius of curvature of the PVDF film was about 100 mm. The plastic tube was rigidly fixed to the table and surrounded by thick urethane-foam blocks to prevent by-pass transmission of sound. Using a two-microphone method the transmission loss (TL) was determined in the frequency range 200 Hz – 4 kHz [J5,6,7].

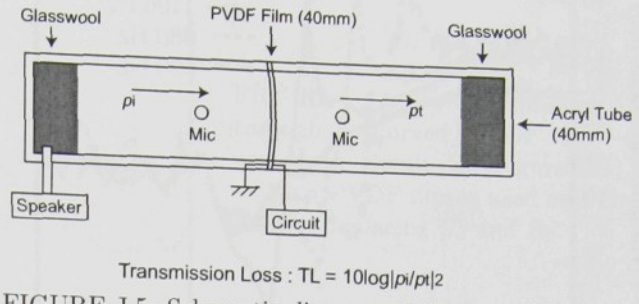

FIGURE J.5: Schematic diagram of the acoustic tube.

J.4.3. Transmission loss

Figure J.6 illustrates the frequency dependence of the transmission loss (TL) for a curved PVDF film connected to the negative capacitance circuit H. The circuit was tuned at f_0=1 kHz. When the circuit is attached, TL increases with increasing feedback voltage. The maximal increase in TL (relative to the TL without feed back) is 40 dB. Figure J.7 shows the results when the circuit was tuned at different frequencies. Tuning was achieved by adjusting R_2/R_1 so that C/C_s was close to -1, and then adjusting R_0 to make $\tan\delta$ ($= 2\pi f C_0 R_0$) of the circuit equal to $\tan\delta_s$ of the sample.

Figure J.8 shows that the TL as a function of frequency for a curved PVDF film connected to circuit S tuned to 1 kHz. It will be seen that the TL decreases by approximately 13 dB around 1 kHz. It is noteworthy that the transmission loss is increased or decreased depending on the attached circuit and that the magnitude of the change can be arbitrarily controlled by adjusting the feedback of the circuit.

Mokrý et al. [J8] have recently derived the following expression for the TL of a curved membrane:

$$\mathrm{TL} = 10\log_{10}\left[1 + \frac{2Y''}{\omega\zeta} + \frac{(Y'')^2 + (Y' - \rho\omega^2 R^2)^2}{(2\omega\zeta)^2}\right], \tag{J.10}$$

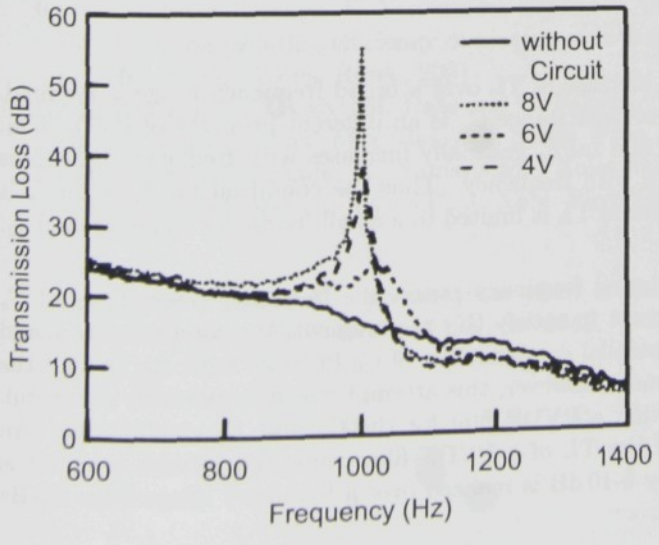

FIGURE J.6: Frequency dependence of the transmission loss through a curved PVDF film connected to circuit H tuned to 1 kHz, for three different feedback voltages.

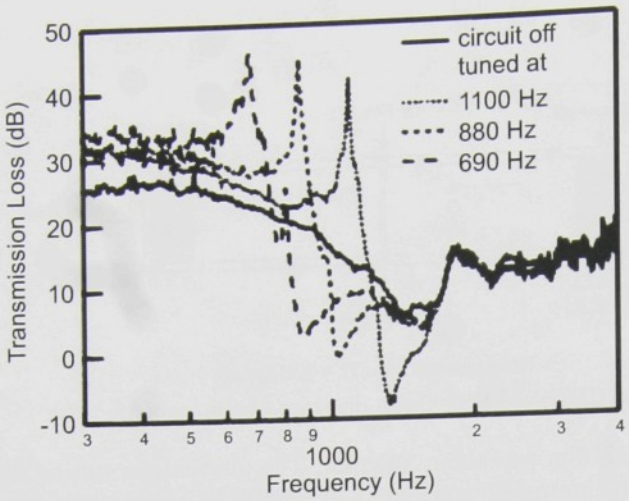

FIGURE J.7: Transmission loss through a curved PVDF film connected to circuit H tuned to various frequencies, 690, 880 and 1100 Hz respectively.

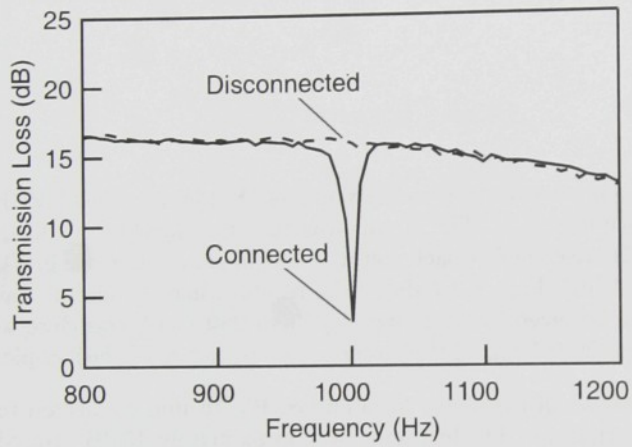

FIGURE J.8: Transmission loss through a curved PVDF film connected to circuit S tuned to 1 kHz.

where $\zeta = \rho_0 c_0 R^2/h$, R the radius of curvature, h the thickness of the film, $\rho_0$the density of the air, and c_0 the sound velocity of the air. It will be seen that TL increases with increasing Y and h, and with decreasing R and ω.

Equation 10 indicates that the frequency dependence of TL is governed by both Y' and Y''. As shown in Fig. J.7, TL shows a peak when Y' increases at f_0, where $\tan\delta$ of the circuit is adjusted equal to $\tan\delta_s$ of the sample. The dip of TL above f_0 corresponds to the sign reversal of Y'' illustrated in Fig. J.4 [J8].

For practical applications, a uniform increase of TL over a broad frequency range is required. The frequency dependence of the complex capacitance C_s is an inherent property of PVDF film. C_s' is nearly constant against frequency and $\tan\delta_s$ gradually increases with frequency [J1]. C_0 is constant, but $\tan\delta = 2\pi f R_0 C_0$ increases with frequency. Thus the condition $\tan\delta_s = \tan\delta_s$ is satisfied only at $f = f_0$, and so the increase in TL is limited to a small frequency range around f_0.

To obtain an increase of TL over a broad frequency range, the frequency dependence of C_s and C must be similar. In an initial attempt to satisfy this requirement, the components C_0 and R_0 in Fig. J.1 were replaced by several parallel combinations of C_0 in series with R_0, so that the circuit has a distribution of relaxation times. However, this attempt was only partially successful. Another attempt was made by substituting a PVDF film for the C_0 and R_0 combination. An example of the frequency dependence of the TL of a PVDF film connected to such a circuit is shown in Fig. J.9. The increase of TL by 5-10 dB is realized over a frequency range from 100 Hz to 2 kHz. Work is continuing in this area.

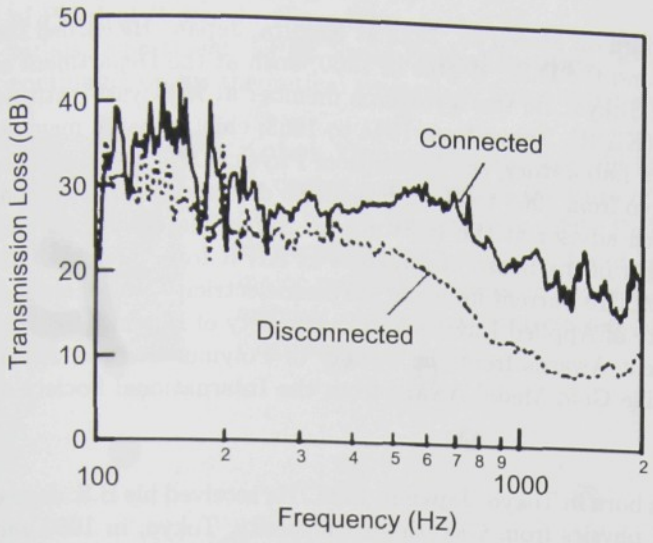

FIGURE J.9: Transmission loss through a curved PVDF film connected to circuit H (Figure J.1), in which a PVDF film is used as a circuit element replacing C_0 and R_0.

J.5. CONCLUSIONS

Attenuation of sound through a curved PVDF film connected to negative capacitance circuits has been determined. A 40 dB increase and a 13 dB decrease in TL at frequencies around 1 kHz have been observed. By using a PVDF film as a capacitance in the negative capacitance circuit, a uniform increase of TL by 5-10 dB in the range 100 Hz – 2 kHz has been obtained.

References

[J1] T. T. Wang, J. M. Herbert, and A. M. Glass, Eds. The Applications of Ferroelectric Polymers. Glasgow, Scotland: Blackie, 1988.

[J2] N. Tanaka and Y. Kikushima, "Active vibration control of distributed parameter structure using cluster control", Trans. Japan Soc. Mech. Eng. Vol.64, pp 788-796, 1998.

[J3] T. Nishigaki and M. Endo, "A self-sensing actuator using piezoelectric films with different thickness for vibration control of curved structures", 11th Int. Conf. Adap. Struc. Tech. Nagoya, 2000.

[J4] M. Date, M. Kutani and S. Sakai, "Electrically controlled elasticity utilizing piezoelectric coupling", J. Appl. Phys. Vol.87, pp.863-868, 2000.

[J5] J.Y.Chung and D.A.Blaser, "Transfer function method of measuring in-duct acoustic properties. T.Theory". J. Acoust. Soc. Am. 68, pp.907-913, 1980

[J6] T. Okubo, K. Kimura, K. Yamamoto, E. Fukada, H. Kodama and M. Date, "Sound-insulation and vibration-isolating efficiency of piezoelectric materials with negative capacitance circuits", 17th Int. Cong. Acous. Rome, 2001.

[J7] H. Kodama, T. Okubo, M. Date and E. Fukada, "Sound reflection and absorption by piezoelectric polymer films" Mat. Res. Soc. Symp. Proc. Vol.698, pp.43-52, 2002.

[J8] P. Mokry, E. Fukada, K. Yamamoto, "Noise shielding system utilizing thin piezoelectric membrane and elasticity control", J. Appl. Phys.Vol.94, pp.789- 796, 2003

This paper is based on a presentation given at the 11th IEEE International Symposium on Electrets, Melbourne, Australia, 1–3 October 2002.

Eiichi Fukada was born on March 28, 1922 at Kokura, Japan. He earned the B.Sc. degree in 1944 and the D.Sc. degree in 1960, both at the Department of Physics, University of Tokyo. He was a research member at Kobayasi Institute of Physical Research (KIPR), Tokyo from 1944 to 1963; chief research member at Biopolymer Physics Laboratory, the Institute of Physical and Chemical Research (RIKEN), Tokyo from 1963 to 1980; Executive director at RIKEN from 1980 to 1984; Research advisor at the Institute for Super Materials, ULVAC, Tsukuba from 1987 to 1998; and a member of the board of directors at KIPR from 1992 to 2002. He has been an advisor of KIPR since 2002. His current interests are piezoelectricity and sound isolation. He belongs to the Japanese Society of Applied Physics and the Society of Polymer Science, Japan. He received Scientific Achievement Awards from the Society of Polymer Science, Japan and the Society of Rheology and Poiseuille Gold Medal Award from the International Society of Biorheology.

Munehiro Date was born in Tokyo, Japan in 1937. He received his B.S. degree and Ph.D. degrees in physics from Gakushuin University, Tokyo, in 1960 and 1973, respectively. He worked at Kobayasi Institute of Physical Research from 1960 to 1963, and at the Institute of Physical and Chemical Research, Tokyo from 1963 to 1998. He studied the piezoelectric and ferroelectric properties of polymers. He earned 100 Japanese patents and 5 U.S. patents. Since 1998, he has been working at Kobayasi Institute of Physical Research. He is a member of the Society of Polymer Science, Japan, the Japan Society of Applied Physics, the Physical Society of Japan, and the Institute of Electrostatics Japan.

Kazunori Kimura was born in Tokyo, Japan, on September 27,1949. He received the B.S. degree in physics from Gakushuin University, Tokyo, Japan, in 1973 and the Dr. Eng. Degree from Mie University, Mie, Japan, in 2002. He joined Kobayasi institute of Physical Research in 1973. The area of his research covers the measuring technique and analysis of noise, the evaluation of environmental low frequency noise, and the measurement of oblique incidence absorption coefficient.

Tomonao Okubo was born in Chiba, Japan, in 1971. He received the Bachelor degree in 1994, the Master degree in 1996, and the D.E. degree in 1999, from Kyushu Institute of Design, Fukuoka, Japan. Since 1999, he has worked in the Kobayasi Institute of Physical Research. His major research interests are environmental noise from road traffic, sound-shielding efficiency of noise barriers, and numerical analysis of sound field.

Hidekazu Kodama was born in Chiba, Japan, on February 23, 1972. He received the B.S. degree in applied chemistry, the M.S. degree and the Ph.D. degree in chemistry from Tokyo University of Science, Japan, in 1994, 1996 and 1999, respectively. Since 1999, he has been with Rion Co., Ltd.. Since 2000, he has been working on the development of noise shielding system and vibration suppression system using piezoelectric polymers and ceramics at Kobayasi Institute of Physical Research.

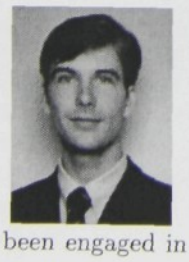

Pavel Mokrý, born in November 1975 in the Czech Republic, received his M.Sc.and Ph.D. degrees in applied physics from the Technical University of Liberec, in 1999 and 2001, respectively. His results on the theories of macroscopic properties of ferroic materials were awarded by the Siemens Prize in 2000 an 2001. In 2001 he won the Japanese Government Scholarship and for two years he was a research student at the Department of Chemistry of the Faculty of Science, Tokyo University of Science. During the years 2001-2003, he has been engaged in a research of noise and vibration suppression devices at the Kobayasi Institute

of Physical Research. Since 2003, he has been an assistant of the Ceramics Laboratory, the Materials Department, EPFL Swiss Federal Institute of Technology Lausanne, where he is currently continuing on his theoretical research of ferroelectric materials.

Kohei Yamamoto was born in Hyogo, Japan in 1950. He received the B. E. degree from Kyushu Institute of Design in 1974 and the Dr. Eng. degree from Kyoto University in 1995. He has been working for Kobayasi Institute of Physical Research since 1974 and currently the Director of this Institute. His major research subjects are prediction and control of road traffic noise. He is a member of the Acoustical Society of Japan and the Institute of Noise Control Engineering of Japan.

Summary

Resume

In the previous part, results of the both theoretical and experimental investigation of sound attenuation through the curved membrane made of a piezoelectric high polymer film has been presented in a form of a collection of papers, which were published on this topic. Brief comments on these papers are given in following Sections.

Comment on Paper H

This article is the first one in the series of publications concerning the sound suppression using cylindrically curved piezoelectric membrane connected to the negative capacitance feedback circuit.

Our investigation of the sound transmission through the curved membrane starts with the analysis of sound fields interacting with the curved membrane vibrations. Starting point in this analysis is a derivation of the equation of motion for the curved membrane [see Eq. (H.14)]. To obtain this equation, it is assumed that the displacement over the membrane surface is uniform. In this case, the membrane displacement in the radial direction w is proportional to the circumferential strain S_1 (i.e. elongation of the membrane along its curvature), which is shown in Fig. 26. In the original position, the membrane length in the circumferential direction is equal to

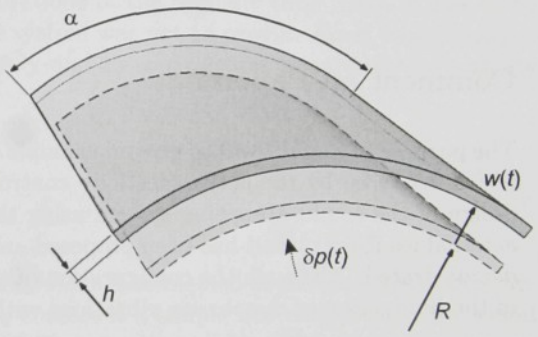

FIGURE 26: Assumption of the uniform displacement over the membrane surface.

$$l_0 = R\alpha,$$

where α is the angle with the origin on the symmetry axis of the cylindrical membrane. When the membrane is shifted by w in the radial direction due to the sound pressure difference δp at the opposite sides of the membrane, the total radius of the membrane curvature equals $R + w$ and the length of the shifted membrane is equal to

$$l = (R + w)\alpha.$$

Strain tensor component S_1 measures the relative elongation of the membrane in the circumferential direction:

$$S_1 = \frac{l - l_0}{l_0}$$

and with use of two above relations one finally gets the expression

$$S_1 = \frac{w}{R},$$

which is actually used in Eq. (H.8).

From the equation of motion [see Eq. (H.18)], the resonant frequency of the uniform mode can be expressed:

$$\omega_R = \frac{1}{R}\sqrt{\frac{Y}{\varrho}},$$

where R is the radius of the membrane curvature, Y is the Young's modulus and ϱ is the membrane density. From this equation it is seen that with an increase of the Young's modulus Y the resonant frequency ω_R of the uniform mode increases, and for all frequencies ω below the resonant frequency ω_R the amplitude of membrane vibrations is decreased. This results in an increase of the acoustic transmission loss for sound of frequencies below ω_R (see Fig. H.8).

Knowing the formula for the acoustic transmission loss as a function of the effective Young's modulus, the effect of the active elasticity control technique using the negative capacitance circuit on the value of the acoustic transmission loss can be analyzed. In Ref. [54] Date showed that the complex Young's modulus of a piezoelectric material connected to external capacitor is a function of the ratio of the external over piezoelectric capacitor capacitances. Thus, when the frequency dependencies of the considered capacitances are known [see Eqs. (H.24) and (H.25)], it is a straightforward task to predict the frequency dependence of the acoustic transmission loss. In Paper H two systems for sound shielding in narrow and wide frequency range have been proposed and analyzed. To verify this prediction, acoustic measurements were performed and their results were fitted to our model. A quite reasonable agreement of experimental results with predictions of the theory has been achieved.

Comment on Paper I

The purpose of Paper I was to give an example of a general approach for designing the NVC devices, which is offered by the active elasticity control technique. This approach was demonstrated on a design of the sound absorbing system using the piezoelectric curved membrane. In this work the external feedback circuit has been proposed and the front-end realization of such a device has been demonstrated. Although the configuration of measurement system has been changed, the principle of the interaction of membrane vibrations with surrounding sound fields remained the same.

Elastic properties of piezoelectric elements of the system controls the dynamic vibrational response of other parts of mechanical system mainly in the low frequency range. In addition, the elasticity control based on Date's idea gives a powerful tool to completely redistribute the vibration response over the mechanical system using piezoelectric elements. Detailed theoretical analysis of the system vibration is used for the determination of the critical conditions for elastic properties of piezoelectric elements, which results in a suppression of vibrations. Knowing these critical values, the optimal feedback circuits realizing such a control can be made.

Comment on Paper J

In Paper J, a quite wide range of possibilities in designing the systems for noise suppression devices utilizing curved piezoelectric polymer membrane and techniques for controlling the elastic properties of piezoelectric materials have been demonstrated.

Figure J.3 shows the direct measurements of complex Young's modulus of a PVDF film connected to the negative capacitance circuit, which was measured as a function of C/C_s ratio by means of Rheolograph-Solid (Toyo Seiki). It is seen that the large values of Young's modulus, which are of interest in noise shielding devices, are very sensitive to small deviations in the ratio of capacitances C/C_s from the ideal value $-1+k^2$. It is actually demonstrated that these phenomena represents the most limiting factor, which deteriorates the performance of the these devices. This is actually demonstrated in Fig. J.4 where the both real and imaginary parts of the effective value of Young's modulus are measured as functions of frequency and where the effect of the negative capacitance circuit is seen. An increase or decrease in the real part and the sign change of the

imaginary part of Young's modulus is caused by the mismatch in frequency dependencies of the both real and imaginary parts of capacitances of the piezoelectric polymer film and the negative capacitance circuit.

In Figures J.6 and J.7, the possibility of sound shielding at the single frequency is demonstrated. It is seen (Fig. J.7) that these systems are easily readjustable to any arbitrary frequency. Figure J.8 shows the possibility to decrease the transmission loss using the negative capacitance circuit for the effective softening of a piezoelectric material. The main drawback of the above systems for sound shielding is the narrow frequency range where the considerable increase of the transmission loss is achieved. Nevertheless, it is possible to eliminate this disadvantage by replacing the conventional reference capacitor C_0 in the feedback circuitry by the capacitor made of the same material as the piezoelectric membrane. By doing this, the very good matching of the both real and imaginary parts of capacitance of the membrane and of the feedback circuit can be achieved in a wide frequency range.

Figure 27 shows the experimental system for measurements of the acoustic transmission loss. It consists of an acrylic acoustic tube of rectangular cross-section with a sound generator and two moving microphones. In the center of the tube there is placed the sound shielding element, which is made of the cylindrically curved membrane made of piezoelectric PVDF polymer film of thickness 50 μm and provided by aluminium electrodes (see Fig. 28). The constant curvature of the film was kept by the steel wire mesh and polyurethane foam. Detail of the placement of sound shielding element in the acoustic tube is shown in Fig. 29. During the measurements, the acoustic tube was covered by pieces of glass-wool sound absorber to reduce the sound transmission through the surrounding environment and through the vibrations of the acoustic tube itself. It has to be pointed out that the purpose of this measurement system was not to provide exact measurements of the acoustic transmission loss but to qualitatively and to some extent quantitatively evaluate the performance of the sound shielding element.

Conclusions

It was shown that using a single piezoelectric element, which is connected to the feedback electronics involving an operational amplifier, it is possible to construct a simple but efficient tool for sound shielding. Using this system the possibility of 60 dB increase of acoustic transmission loss in narrow frequency range and about 10 dB in a wide (from 500 Hz to 2 kHz) frequency range was demonstrated (see Papers H and J). It has been also demonstrated that the technique of active elasticity control in piezoelectric materials offers a quite general tool, which can be used for a construction of other devices for noise and vibration suppression. In Paper I a general approach for design of such devices was demonstrated on a system for noise absorption. The method starts with analyzing the effect of elastic properties of piezoelectric elements in the system on the acoustic response of the system. Minimizing the values of acoustic properties with respect to the elastic ones, it is possible design a feedback electronics, which realizes the required acoustic response of the system.

The advantages of this method stem from the small weight, simplicity, low cost, and superb sound shielding performance of the whole system, offering a noise suppression device that can be profitably used in many places such as planes, high speed trains, and similarly noisy environments. However, as a limitation of its use in commercial applications should be recognized the low operational stability, which is sensitive to temperature changes. To eliminate this disadvantage, more advanced feedback electronics has to offer self-adjustable circuitry with distributed relaxation times and these are the devices, which are of interest in the ongoing research and design activity these days.

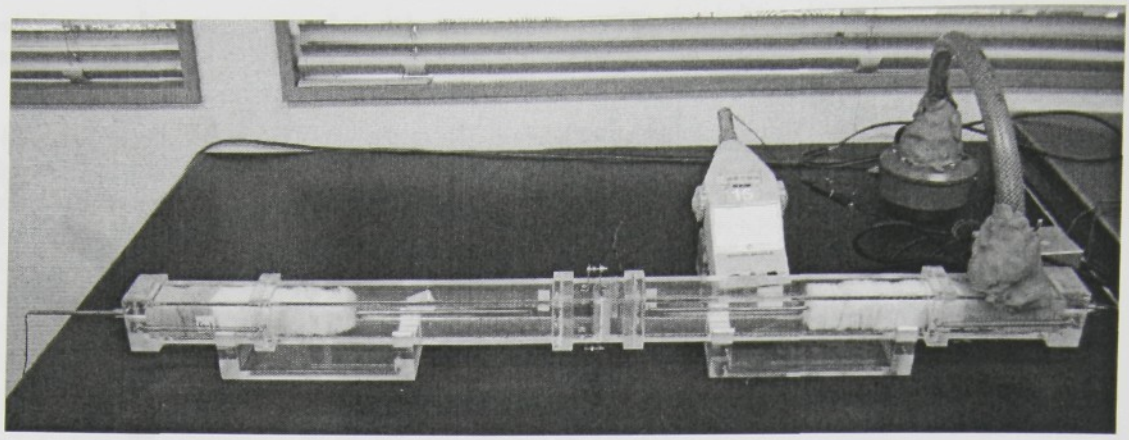

FIGURE 27: Experimental system for measurements of the acoustic transmission loss consists of acrylic acoustic tube of rectangular cross-section with a sound generator and two moving microphones at the both sides of the sound shielding element.

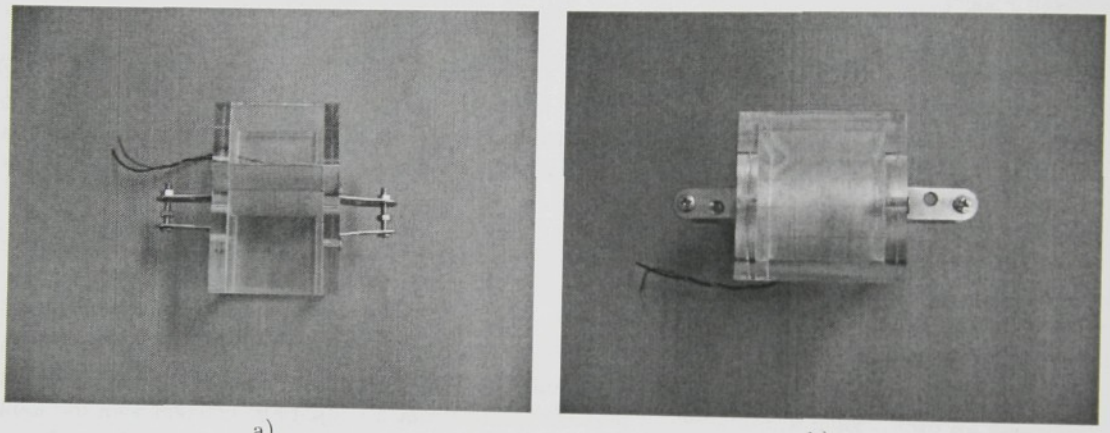

a) b)

FIGURE 28: Detail of the sound shielding element made of curved piezoelectric (ferroelectric) PVDF film that is clamped in the acrylic acoustic tube: side view a), top view b).

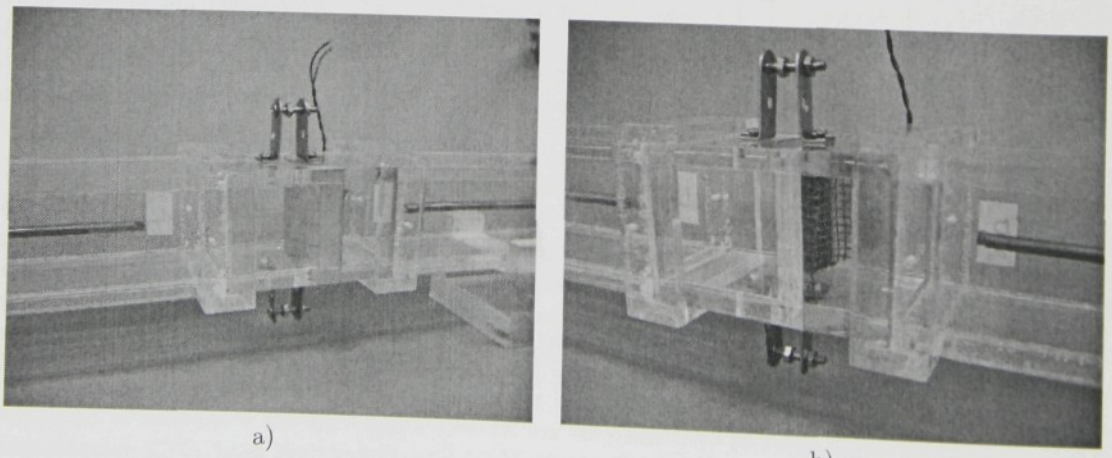

a) b)

FIGURE 29: Sound shielding element made of piezoelectric (ferroelectric) PVDF film of thickness 50 μm and provided by aluminium electrodes is placed in the acoustic tube; front view a), rear view where there is seen the steel wire mesh and polyurethane foam keeping the constant film curvature b).

Bibliography

[1] J. Valasek, *Phys. Rev.* **17**, 475 (1921)

[2] M. E. Lines, A. M. Glass, *Principles and Applications of Ferroelectrics and Related Materials* (Oxford University Press, 1977)

[3] B. A. Strukov, A. P. Levanyuk, *Ferroelectric Phenomena in Crystals* (Springer, 1998)

[4] T. T. Wang, J. M. Herbert, and A. M. Glass, *The application of ferroelectric polymers* (Blackie and Son Ltd., 1988)

[5] K. Uchino, *Ferroelectric Devices* (Marcel Dekker, Inc., 2000)

[6] Landolt - Börnstein, *Numerical Data and Functional Relationships in Science and Technology* **III/28b**, Ferroelectrics and related Substances (Springer-Verlag, Berlin, 1993)

[7] Y. Park and K. Kim, *Technical Digest,* 392394 (IEDM, 2001)

[8] P. C. McIntyre (privat communication).

[9] L. F.Scholl, P. C. McIntyre, B. C. Hendrix, S. M. Bilodeau, J. F. Roeder, S. R. Gilbert, *Appl. Phys. Lett.* **81**, 3218 (2002)

[10] R.-V. Wang and P. C. McIntyre, *J. Appl. Phys.* **97**, 023508 (2005)

[11] L. F.Scholl, P. C. McIntyre, B. C. Hendrix, S. M. Bilodeau, J. F. Roeder, S. R. Gilbert, *Appl. Phys. Lett.* **81**, 3218 (2002)

[12] A. I. Kingon, S. K. Streiffer, S. H. Kim, *DRAM and FRAM Based on Ferroelectric Films* (ISAF, 1998)

[13] S. B. Lang and D. K. Das-Gupta, *J. Appl. Phys.* **59**, 2151 (1986)

[14] Z. Chen and X. Yao, *Ferroelectrics* **109**, 155 (1990)

[15] A. K. Tagantsev, M. Landivar, E. Colla, and N. Setter, *J. Appl. Phys.* **78**, 2623 (1995)

[16] L. J. Sinnamon, R. M. Bowman, and J. M. Gregg, *Appl. Phys. Lett.* **78**, 1724 (2001)

[17] T. Hase, T. Sakuma, Y. Miyasaka, K. Hirata, N. Hosokawa, *Jpn. J. Appl. Phys.* **32**, 4061 (1993)

[18] S. Stemmer, S. K. Streiffer, N. D. Browning, C. Basceri, and A. I. Kingon, *Interface Science* **8**, 209 (2000)

[19] L. J. Sinnamon, M. M. Saad, R. M. Bowman, and J. M. Gregg, *Appl. Phys. Lett.* **81**, 703 (2002)

[20] K. Abe and Sh. Komatsu, *Jpn. J. Appl. Phys.* **32**, L1157 (1993)

[21] S. K. Dey, J. J. Lee, and P. Alluri, *Jpn. J. Appl. Phys.* **34**, 3142 (1995)

[22] C. Basceri, S. K. Streiffer, A. I. Kingon, and R. Waser, *J. Appl. Phys.* **82**, 2497 (1997)

[23] J. J. Lee, C. L. Thio, and S. B. Desu, *J. Appl. Phys.* **78**, 5073 (1995)

[24] O. G. Vendik, and S. P. Zubko, *J. Appl. Phys.* **88**, 5343 (2000)

[25] I. Stolichnov, A. K. Tagantsev, N. Setter, J. S. Cross, and M. Tsukada, *Appl. Phys. Lett.* **75**, 1790 (1999)

[26] V. Craciun and R. K. Singh, *Appl. Phys. Lett.* **76**, 1932 (2000)

[27] R. Kretchmer and K. Binder, *Phys. Rev. B* **20**(3), 1065 (1979)

[28] A. K. Tagantsev (privat communication).

[29] V. Janovec, *J. Chem. Phys.* **45**, 1874 (1966).

[30] S. K. Streiffer, J. A. Eastman, D. D. Fong, C. Thompson, A. Munkholm, M. V. R. Murty, O. Auciello, G. R. Bai, G. B. Stephenson, *Phys. Rev. Lett.* **89**(6), 067601 (2002)

[31] Y. Takahashi, A. Kitahama, and T. Furukawa, *IEEE Trans. Dielectr. Electr. Insul.* **11**, 227 (2004)

[32] T. Furukawa, *Phase Transitions* **18**, 143 (1989)

[33] Y. Cho, Sh. Atsumi and K. Nakamura, *Jpn. J. Appl. Phys.* **36**, 3152 (1997)

[34] X. Chen, H. Yamada, T. Horiuchi and K. Matsushige *Jpn. J. Appl. Phys.* **37**, 3834 (1998)

[35] M. C. Ray, J. Oh and A. Bar, *J. Sound Vib.* **240**(5), 921-934 (2001)

[36] O. R. Lin, Z.-X. Liu and Z.-L. Wang, *J. Sound Vib.* **246**(3), 525-541 (2001)

[37] J. K. Henry, R. L. Clark, *J. Sound Vib.* **249**(2), 325-349 (2002)

[38] M. S. Tsai and K. M. Wang, *J. Sound Vib.* **221**(1), 1-22 (1999)

[39] R. A. Morgan and K. W. Wang, *J. Sound Vib.* **255**(4), 685-700 (2002)

[40] R. L. Forward, *J. Appl. Optics* **18**(5), 690-697 (1979)

[41] R. L. Forward and C. J. Swigert, *J. Spacecrafts and Rockets* **18**, 5-10 (1981)

[42] R. H. Edwards and R. H. Miyakawa, *Hughes Aircraft Co. Report No.* 4132.22/1408 (1980)

[43] N. W. Hagood and A. von Flotow, *J. Sound Vib.* **146**(2), 143-268 (1991)

[44] Ch. Davis and G. Lesieutre, *J. Sound Vib.* **232**(3), 601-617 (2000)

[45] M. Ahmadian and K. M. Jeric, *J. Sound Vib.* **243**(2), 347-359 (2001)

[46] E. Fukada, M. Date and N. Hirai, *Nature* **211**, 1079 (1966)

[47] E. Fukada, M. Tamura and I. Yamamoto, *"Polypeptides Piezoelectric Transducers"*, presented at the 6^{th} *International Congress on Acoustics,* D-31, (Tokyo, 1968)

[48] H. Kawai, *Jpn. J. Appl. Phys.* **8**, 975 (1969)

[49] J. G. Bergman, J. H. MacFee, G. R. Crane, *Appl. Phys. Lett.* **18**, 203 (1971)

[50] T. Furukawa, M. Date, E. Fukada, *J. App. Phys.* **51**, 1135 (1980)

[51] M. Tamura, T. Yamaguchi, T. Oyaba and T. Yoshimi, *J. Audio. Eng. Soc.* **23**, 21 (1975)

[52] R. Lerch, *J. Acoust. Soc. Am.* **66**(4), 952-954 (1979)

[53] R. Lerch and G. M. Sessler, *J. Acoust. Soc. Am.* **67**(4), 1379-1381 (1980)

[54] M. Date, M. Kutani and S. Sakai, *J. Appl. Phys.* **87**(2) 2000, 863-868

[55] T. Okubo, H. Kodama, K. Kimura, K. Yamamoto, E. Fukada and M. Date, *Proceedings of the* 17^{th} *International Congress on Acoustics* (Rome, 2001)

[56] H. Kodama, T. Okubo, M. Date and E. Fukada, *Mat. Res. Soc. Symp. Proc.* **698**, 43-52 (2002)

[57] S. Edelman and A. S. DeReggi, *J. Audio Eng. Soc.* **24**(7), 549-552 (1976)

[58] A. S. Fiorillo, *IEEE Trans. Ultrason., Ferroelect. Frq. Contr.* **39**(6), 688-692 (1992)

[59] H. Naono, T. Gotoh, M. Matsumoto and S. Ibaraki, presented at 58^{th} *Convention Audio Eng. Soc.* (New York, NY, 1977)

[60] H. W. Wang and M. Toda, *IEEE Trans. Ultrason., Ferroelect. Frq. Contr.* **46**(6), 1375-1386 (1999)

[61] M. Toda and S. Tosima *IEEE Trans. Ultrason., Ferroelect. Frq. Contr.* **47**(6), 1421-1430 (2000)

[62] J. F. Nye, *Physical Properties of Crystals,* Ch. X, §4.1, p. 185 (Oxford University Press, 1957)

[63] L. D. Landau, *Phys. Z. Sovietunion* **11**, 26 (1937)

[64] A. F. Devonshire, *Phil. Mag.* **740**, 1040 (1949); **742**, 1065 (1951);

[65] V. L. Ginzburg, *Fyz. Tverd. Tela* **2**, 2031 (1960); [*Sov. Phys. - Solid State* **2**, 1824 (1960)];

[66] R. Landauer, *J. App. Phys.* **28**(2), 227 (1957)

Appendix K

Phenomenological theories of Landau and Ginzburg

Landau described in 1937 a general phenomenological theory of the second-order phase transitions based upon symmetry criteria. Although the detailed micromechanisms of phase transitions are different if particular substances, the Landau theory made it possible to examine the anomalies of physical properties of crystals in the second-order phase transitions and to get insight into their general physical causes without any reference to details of mechanisms on the microstructural level. The starting point of the theory is a general consideration that a certain temperature T_C, called *Curie temperature,* represents a transition point between two phases, which differ in symmetry. It is natural to consider that the symmetry of the phase above temperature T_C is higher than the symmetry of the phase below T_C. Hence these phases are called symmetric and non-symmetric. In Ref. [63] Landau formulated rigorous conditions[1] for the symmetries of the high and low temperature phases, which define a special type of the phase transition called *second order phase transition of the Landau type.* The practical meaning of these conditions on symmetry is that in the phase transitions of this type *the non-symmetric (ferroelectric) phase may be represented as a distortion of the symmetric (paraelectric) phase.*

The physical quantity, which actually "measures" the distortions of the symmetric phase, is called *order parameter.* By definition it has a zero and nonzero equilibrium values, which correspond to the symmetric and non-symmetric phase, respectively. Generally, it is not a simple task to find out a correct physical interpretation of the order parameter and its exact specification can require a comprehensive symmetry analysis of a crystal structure changes during the phase transition in a given material. However, in *ferroelectric materials* lowering of the crystal lattice symmetry is characterized by the *change of polarization.* On the other hand, in *ferroelastic materials* the phase transition results in the appearance of *strain* in the low symmetry phase. Therefore, two macroscopic properties can be used to "measure" distortions of the crystal lattice: the change of polarization $\Delta \boldsymbol{P}$ and mechanical strain e_{ij} (see Fig. K.1). The former is proportional to the relative displacement $\Delta \boldsymbol{x}_k$

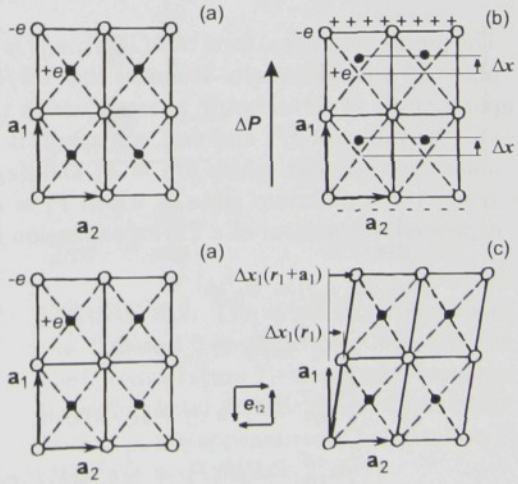

FIGURE K.1: Microscopic origins of ionic polarization and mechanical strain: (a) undistorted structure; (b) change of polarization; (c) appearance of shear strain.

[1] One of the conditions is a requirement that the point group of symmetry of the low temperature phase must be a subgroup of the point group of symmetry of the high temperature phase.

of a k-th set of ions in the crystal lattice from their symmetrical positions in the unit cell:

$$\Delta \boldsymbol{P} = \sum_k q_k \, \Delta \boldsymbol{x}_k / v_{\mathrm{uc}}, \tag{K.1}$$

where v_{uc} is the volume of the unit cell, q_k is the charge of k-th ion and k is running through all ions in the unit cell. The latter is equal to the strain due to deformations of the whole unit cell:

$$e_{ij} = \frac{1}{N} \sum_k \frac{1}{2} \left[\frac{\Delta x_{k,i}(\boldsymbol{r}_k + \boldsymbol{a}_j) - \Delta x_{k,i}(\boldsymbol{r}_k)}{a_j} + \frac{\Delta x_{k,j}(\boldsymbol{r}_k + \boldsymbol{a}_i) - \Delta x_{k,j}(\boldsymbol{r}_k)}{a_i} \right], \tag{K.2}$$

where N is a number of ions in the unit cell; $\Delta x_{k,i}(\boldsymbol{r}_k)$ and $\Delta x_{k,i}(\boldsymbol{r}_k + \boldsymbol{a}_j)$ are the relative displacements of k-th ion in the given and the next unit cell; and $\boldsymbol{a}_i$ are the orthogonal translational vectors of the crystal lattice. Since usually the polarization of the non-polar phase do not manifests itself in any way, however it already exists, it is simply ignored and we define the polarization of the crystal lattice by the bound charge on the sample surface, which is due to the relative displacements of ions in the crystal lattice. For the sake of simplicity, the symbol $\boldsymbol{P}$ is used instead of $\Delta \boldsymbol{P}$.

K.1 Second-order phase transition in ferroelectrics

Having defined the means that measures the distortions of the crystal lattice, it is possible to analyze the "dynamics" of the phase transition. In order to do this, the following thermodynamic considerations start with the definition of a thermodynamic function Φ per unit volume of the dielectrics called *Helmholtz free energy:*

$$\Phi(T, P_i, e_{ij}) = U(S, P_i, e_{ij}) - TS, \tag{K.3}$$

where U is the internal energy of the dielectrics, T and S are temperature and entropy of the dielectrics, respectively. At the constant temperature T, the change of the Helmholtz free energy is proportional to change in the distortions of the crystal lattice

$$\delta\Phi(T = T_{\mathrm{const}}, P_i, e_{ij}) = \frac{\partial \Phi}{\partial P_i} \delta P_i + \frac{\partial \Phi}{\partial e_{ij}} \delta e_{ij}. \tag{K.4}$$

The precise functional form of $\Phi(T, P_i, e_{ij})$ is now the question. In the equilibrium of the symmetric phase $\delta\Phi$ should be zero. It means that $\partial\Phi/\partial P_i = 0$ and $\partial\Phi/\partial e_{ij} = 0$ for all i and j. Since in the paraelectric or ferroelectric phases close to the Curie point, the distortions of the crystal lattice, i.e. the values of δP_i and δe_{ij}, are small, it is a common practice to define a linear or low-order nonlinear theory in which $\delta P_i = P_i$ and $\delta e_{ij} = e_{ij}$ are defined as small deviations from a high symmetry equilibrium state in which $P_i = e_{ij} = 0$ [2]. Then the Helmholtz free energy can be expressed in the form of a Taylor expansion in P_i and e_{ij} up to the terms of the fourth order:

$$\begin{aligned} \Phi(T, P_i, e_{ij}) = \Phi_0 + & \qquad (\text{K.5}) \\ & \frac{1}{2}\alpha_{ij}^{e,T} P_i P_j + \qquad (\text{second-order terms}) \\ & \frac{1}{3}\alpha_{ijk}^{e,T} P_i P_j P_k - h_{kij}^{T} P_k e_{ij} + \qquad (\text{third-order terms}) \\ & \frac{1}{4}\alpha_{ijkl}^{e,T} P_i P_j P_k P_l + \frac{1}{2} q_{ijkl}^{T} P_i P_j e_{kl} + \frac{1}{2} c_{ijkl}^{P,T} e_{ij} e_{kl} + \cdots . \qquad (\text{fourth-order terms}) \end{aligned}$$

For a given material, function Φ is a scalar quantity characterizing the physical property of the crystal and it must be invariant with respect to any transformation of the symmetric phase. Therefore, all the coefficients $\alpha_{ij}^{e,T}$, $\alpha_{ijk}^{e,T}$, h_{kij}^{T}, $\alpha_{ijkl}^{e,T}$, q_{ijkl}^{T} and $c_{ijkl}^{P,T}$ are tensor invariants under the operations of the appropriate symmetry group. It is generally quite difficult to investigate

[2] Note that now the polarization components P_i or strain components e_{ij} are defined in a way, which is in accord with the definition of the order parameter.

symmetry restrictions imposed on tensors of high rank, and simplification is often accomplished in non-linear theory by making use of a physical approximation. Considering that the symmetric phase is a centrosymmetric non-polar phase, all the odd rank tensor coefficients are zero. [3]

From the point of view of applications of ferroelectric materials, the dielectric properties, i.e. dielectric response of a system to an external electric field $\boldsymbol{E}$, is of practical importance. In this case, analysis of a system with a given constant applied field $\boldsymbol{E}$ requires a different thermodynamic function, which must determine the work performed over the system by external forces. In Appendix L there is given a detailed derivation of such a function, which is called *Gibbs electric energy:*

$$G(T,\, E_i,\, e_{ij}) = \Phi(T,\, P_i,\, e_{ij}) - E_i P_i. \tag{K.6}$$

Considering the constant electric field, variation of Gibbs electric energy is zero in equilibrium:

$$\delta G(T = T_{\text{const}},\, E_i = E_{\text{const},i},\, e_{ij}) = \left(\frac{\partial \Phi}{\partial P_i} - E_i\right) \delta P_i + \frac{\partial \Phi}{\partial e_{ij}} \delta e_{ij} = 0. \tag{K.7}$$

Since in general changes of polarization δP_i and strain δe_{ij} in ferroelectric are not zero during the phase transition, Eq. (K.7) is satisfied when

$$\frac{\partial \Phi}{\partial P_i} - E_i = 0, \qquad \frac{\partial \Phi}{\partial e_{ij}} = 0. \tag{K.8}$$

It should be noted that usually the system of Eqs. (K.8) has more than one solution for equilibrium values of $P_{0,i}$ and $e_{0,ij}$ and Eqs. (K.8) have to be accompanied by a system of complementary conditions which specify which values of $P_{0,i}$ and $e_{0,ij}$ correspond to minima of the Gibbs electric energy. In order to do this, Hessian matrix $H(G)_{mn}(P_i,\, e_{ij})$ of Gibbs electric energy with respect to all variables P_i and e_{ij} has to be calculated. The equilibrium values of $P_{0,i}$ and $e_{0,ij}$ correspond to the minimum of function G, if and only if the Hessian matrix $H(G)_{mn}(P_{0,i},\, e_{0,ij})$ is positively definite.

Having now established a general method of finding the equilibrium values for polarization and strain during the phase transition, these thermodynamic tools are demonstrated on the example of an analysis of dielectric properties of so called *uniaxial ferroelectric,* which undergoes a second order phase transition into the ferroelectric state by changing the symmetry at $T = T_C$ from 2/m into 2.

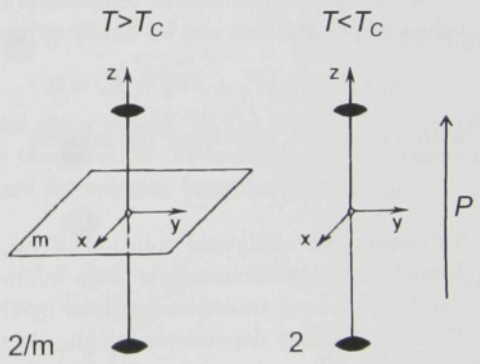

FIGURE K.2: The symmetry elements of the 2/m and 2 group, respectively. At the Curie temperature T_C the crystal loses the inversion center and the plane of symmetry leading to the appearance of polarization P along the two-fold axis 2.

In this particular case at the Curie temperature T_C, the instability of the crystal lattice leads to the appearance of polarization P along the two-fold axis 2 and the crystal loses the inversion center and the plane of symmetry (see Fig. K.2). Now the objective is to find the leading terms of the Helmholtz free energy Φ. Now it is considered that the driving force of a phase transition is an appearance of polarization and the fact that there could exist a coupling between the polarization and strain affecting the phase transition is neglected. It means that all terms containing strain e_{ij} can be ignored in the expansion of Helmholtz free energy. Although it is clear that during the thermal motion of ions in the symmetric case there exist fluctuations, which lead to the presence of polarization components perpendicular to the z-axis, these components do not take control over the phase transition due to

[3] Note that the group $\bar{4}2m$ is not centrosymmetric. This means that when studying the phase transition $\bar{4}2m \rightarrow mm2$, which takes place in potassium dihydrogen phosphate (KDP) family materials, the third-order rank tensors cannot be omitted.

symmetry reasons and they can be neglected from the expansion of function Φ. So the remaining terms contain only the z-component of polarization $\boldsymbol{P}$:

$$\Phi(T,\, P_z) = \Phi_0 + \frac{1}{2}\alpha P_z^2 + \frac{1}{4}\beta P_z^4. \tag{K.9}$$

Now the question is what can be said about coefficients α and β.

Here it should be emphasized again that in the second-order phase transitions of the Landau type, the non-symmetric phase is represented as a distortion of the symmetric phase. It should be also pointed out that $P_z = \delta P_z$ in Eq. (K.9) has a meaning of the change of polarization from the equilibrium of the symmetric phase. It means that function $\Phi(T,\, P_z)$ has a minimum for $P_z = 0$ in the symmetric phase and the variation of function Φ at temperatures above T_C is positive:

$$\delta\Phi(T) = \alpha(T)(\delta P_z)^2 > 0 \qquad \text{at } T > T_C. \tag{K.10}$$

Although the origin of polarization P_z in the symmetric phase is attributed to the thermal motion and only its average equilibrium value $P_z = 0$ is measured, it becomes a real measurable change of polarization in the nonsymmetric phase. As a result, in the distorted non-symmetric phase $P_z = 0$ is not the equilibrium value of polarization anymore and variation of function Φ below T_C is negative:

$$\delta\Phi(T) = \alpha(T)(\delta P_z)^2 < 0 \qquad \text{at } T < T_C. \tag{K.11}$$

Comparing the last two expressions, it is concluded that the coefficient α is strongly temperature dependent and changes its sign at the Curie temperature T_C. In the linear approximation, it is usually considered:

$$\alpha(T) = \alpha_0(T - T_C), \tag{K.12}$$

where $\alpha_0 > 0$. Since in the non-symmetric phase the crystal lattice has to be stable again, it is stabilized due to the higher order terms in the expansion of function Φ. Thus in the second-order phase transition, it is considered that coefficient β is temperature independent and positive.

Knowing the qualitative temperature dependencies of coefficients α and β, the equilibrium values of polarization can be finally expressed from Eqs. (K.8), (K.9) and (K.12):

$$\alpha_0\,(T - T_C)\,P_z + \beta P_z^3 - E_z = 0. \tag{K.13}$$

with a condition specifying the minima

$$\alpha_0\,(T - T_C) + 3\beta P_z^2 > 0. \tag{K.14}$$

To obtain the analytical solution of Eq. (K.13) in an explicit form, an approach called *hard ferroelectric approximation* is often followed, assuming that the polarization of the crystal lattice due to the phase transition is given by the constant contribution called *spontaneous polarization* P_0 and the linear dependence on the electric field

$$P_z \cong P_0 + \chi_{33}^{p,T} E_z \tag{K.15}$$

where

$$P_0 = \begin{cases} 0 & \text{for} \quad T > T_C \\ \sqrt{(T_C - T)/(\beta C)} & \text{for} \quad T < T_C, \end{cases} \tag{K.16}$$

$$\chi_{33}^{p,T} = \begin{cases} C/(T - T_C) & \text{for} \quad T > T_C \\ C/\left[2(T_C - T)\right] & \text{for} \quad T < T_C \end{cases} \tag{K.17}$$

and $C = 1/\alpha_0$ is called *Curie-Weiss constant*. Change of spontaneous polarization with temperature is measured by the *pyroelectric coefficient* at constant pressure γ^p:

$$\gamma^p = \left(\frac{\partial P}{\partial T}\right)_p = \begin{cases} 0 & \text{for} \quad T > T_C \\ 1/\sqrt{2\beta C\,(T_C - T)} & \text{for} \quad T < T_C. \end{cases} \tag{K.18}$$

K.2 Anomalous temperature dependencies of potassium dihydrogen phosphate

It is known due to Kobayashi that potassium dihydrogen phosphate (KDP) or rubidium dihydrogen phosphate (RbDP) crystals undergo the first order phase transition. Nevertheless, the discontinuous change of spontaneous polarization P_0 is relatively small. Moreover, all material constants ε_{33}, d_{36}, s_{66}^E fulfill the *Curie-Weiss law* in a wide temperature region over transition temperature. Therefore it can be said that the most of crystals from KDP and RbDP families undergo the first order phase transition, which is close to the second order phase transition, and following expansion of *Gibbs energy* can be adopted as an acceptable approximation:

$$G(T, E_3, \tau_6) = G_0 + \frac{1}{2}\alpha_0 (T - T_C) P^2 + \frac{1}{4}\beta P^4 + \frac{1}{2} c_{66}^P e_6^2 - h_{36} P_3 e_6 - P_3 E_3 - \tau_6 e_6, \quad \text{(K.19)}$$

where E_3 and P_3 are the electric field and polarization along the ferroelectric axis, respectively. Symbols e_{66} and τ_{66} represent the shear strain and stress in the plane perpendicular to the ferroelectric axis in the notation due to Voigt, respectively. It is known from experiments that the inverse dielectric constant β_{33}^e of this crystal along the ferroelectric axis at a constant shear strain e_6 vanishes at the transition temperature and at the same time the elastic compliance s_{66}^P of the crystal at a constant polarization P_3 is practically temperature independent. It is therefore natural to assume that the polarization in the expansion of the thermodynamic function is the primary order parameter; this assumption has been used as a basis for simple development of phenomenological theory of a phase transition in KDP and RdDP crystals.

The anomalous behavior of temperature dependence can be obtained for the ε_{33}^e component of permittivity tensor, d_{36} component of the piezoelectric coefficients matrix and s_{66}^E resp. c_{66}^E components of the elastic compliance resp. stiffness matrices at a constant electric field. Solution of two equations for equilibrium values of P_3 and e_6:

$$\frac{\partial G}{\partial P_3} = \alpha_0 (T - T_C) P_3 + \beta P_3^3 - h_{36} e_6 - E_3 = 0, \quad \text{(K.20a)}$$

$$\frac{\partial G}{\partial e_6} = c_{66}^p e_6 - h_{36} P_3 - \tau_6 = 0 \quad \text{(K.20b)}$$

yields the temperature dependencies of polarization and shear strain. In the absence of external electric field $E_3 = 0$ and mechanical stress $\tau_6 = 0$, the temperature dependencies of spontaneous polarization and shear strain can be obtained in the *hard ferroelectric approximation*

$$P_{0,3}(T) = \begin{cases} \sqrt{\alpha_0/\beta (T_0 - T)} & \text{for } T < T_0, \\ 0 & \text{for } T > T_0, \end{cases} \quad \text{(K.21)}$$

$$e_{0,6}(T) = \begin{cases} (h_{36}/c_{66}^P) \sqrt{\alpha_0/\beta (T_0 - T)} & \text{for } T < T_0, \\ 0 & \text{for } T > T_0, \end{cases} \quad \text{(K.22)}$$

where

$$T_0 = T_C + \frac{h_{36}^2}{c_{66}^P \alpha_0}$$

is the transition temperature.

From Eqs. (K.20), the electric field E_3 and shear stress τ_6 as functions of polarization P_3 and shear strain e_6 can be expressed:

$$E_3 = \alpha_0 (T - T_C) P_3 + \beta P_3^3 - h_{36} e_6, \quad \text{(K.23)}$$

$$\tau_6 = -h_{36} P_3 + c_{66}^P e_6. \quad \text{(K.24)}$$

From Eq. (K.24), it is can be shown that piezoelectric coefficient h_{36} and elastic stiffness at a constant polarization c_{66}^P are temperature independent during the phase transition. From Eq. (K.23), the derivative of electric filed E_3 with respect to polarization P_3 can be expressed considering the derivative of electric filed E_3 with respect to polarization P_3 can be expressed considering constant value of e_6, which is actually equal to the component of impermittivity tensor at constant strain β_{33}^e:

$$\beta_{33}^e = \left(\frac{\partial E_3}{\partial P_3}\right)_e = \alpha_0\,(T - T_C) + 3\beta\,P_{0,3}^2(T) = \begin{cases} h_{36}^2/\left(c_{66}^P \alpha_0\right) + 2\alpha_0\,(T_0 - T) & \text{for } T < T_0, \\ h_{36}^2/\left(c_{66}^P \alpha_0\right) + \alpha_0\,(T - T_0) & \text{for } T > T_0. \end{cases} \tag{K.25}$$

Differentiating Eqs. (K.20) with respect to E_3, the solution of the obtained system of linear algebraic equations

$$\begin{aligned} \left[\alpha_0\,(T - T_C) + \beta\,P_3^2\right]\,\tfrac{\partial P_3}{\partial E_3} - h_{36}\,\tfrac{\partial e_6}{\partial E_3} - 1 &= 0, \\ -\,h_{36}\,\tfrac{\partial P_3}{\partial E_3} + c_{66}^P\,\tfrac{\partial e_6}{\partial E_3} &= 0. \end{aligned} \tag{K.26}$$

for unknown partial derivatives $\partial P_3/\partial E_3$ and $\partial e_6/\partial E_3$ yields the expressions for relative permittivity ε_{33}^τ at constant stress

$$\varepsilon_0 \varepsilon_{33}^\tau \approx \left(\frac{\partial P_3}{\partial E_3}\right)_\tau = \frac{1}{\alpha_0\,(T - T_0) + 3\beta P_{0,3}^2(T)} = \begin{cases} 1/\left[2\alpha_0\,(T_0 - T)\right] & \text{for } T < T_0, \\ 1/\left[\alpha_0\,(T - T_0)\right] & \text{for } T > T_0 \end{cases} \tag{K.27}$$

and piezoelectric coefficient d_{36}

$$d_{36} = \frac{\partial e_6}{\partial E_3} = \frac{h_{36}}{c_{66}^P \alpha_0\,(T - T_0) + 3c_{66}^P \beta P_{0,3}^2(T)} = \begin{cases} h_{36}/\left[2c_{66}^P \alpha_0\,(T_0 - T)\right] & \text{for } T < T_0, \\ h_{36}/\left[c_{66}^P \alpha_0\,(T - T_0)\right] & \text{for } T > T_0. \end{cases} \tag{K.28}$$

Similarly, differentiating Eqs. (K.20) with respect to e_6 and considering the constant electric field E_3, the anomalous temperature dependencies of elastic stiffness at the constant electric field can be obtained:

$$c_{66}^E = \left(\frac{\partial \tau_6}{\partial e_6}\right)_E = c_{66}^P - \frac{h_{26}^2}{\alpha_0\,(T - T_C) + 3\beta P_{0,3}^2(T)} = c_{66}^P - \begin{cases} h_{36}^2/\left[2\alpha_0\,(T_0 - T)\right] & \text{for } T < T_0, \\ h_{36}^2/\left[\alpha_0\,(T - T_0)\right] & \text{for } T > T_0. \end{cases} \tag{K.29}$$

Finally, differentiating Eqs. (K.20) with respect to τ_6 and considering the constant electric field E_3, the anomalous temperature dependencies of elastic compliance at the constant electric field can be expressed:

$$s_{66}^E = \left(\frac{\partial e_6}{\partial \tau_6}\right)_E = s_{66}^P + \frac{h_{26}^2\,s_{66}^P}{\alpha_0\,(T - T_0) + 3\beta P_{0,3}^2(T)} = s_{66}^P + \begin{cases} h_{36}^2 s_{66}^P/\left[2\alpha_0\,(T_0 - T)\right] & \text{for } T < T_0, \\ h_{36}^2 s_{66}^P/\left[\alpha_0\,(T - T_0)\right] & \text{for } T > T_0. \end{cases} \tag{K.30}$$

K.3 Fluctuations of the order parameter

The above examples of ferroelectric phase transitions show that in the ferroelectric phase the crystal lattice can exist in two or more enantiomorphous states, which differ in a vector of spontaneous

polarization and a tensor of spontaneous strain. However, in the above examples it was considered that the non-symmetric phase is spatially homogeneous, i.e. that a phase transition occur into monodomain state. But this is actually not the case of many observation in real systems.

It has been already mentioned that the thermal motion plays a key role in the stabilization of the crystal lattice in the high temperature phase. In addition, it is known that the value of *specific heat* is sensitive to the number of degree of freedom in the system. Unfortunately, predictions of Landau theory for the temperature dependence of specific heat are in a disagreement with values of specific heat measured in the vicinity of a phase transition. The reason for this is that the components of the order parameter, which is considered to be uniformly distributed over the volume of the sample, represent the only degrees of freedom in the system in the classical Landau theory. When the temperature of the sample is decreasing towards the phase transition, the crystal lattice becomes very soft (see the temperature dependence of the parameter α Eq. K.12) and the *fluctuations of the order parameter* become to play an important role. It means that other degree of freedom in the system described within the Landau theory "are necessary" to reach the agreement with experimental results. In order to correct the Landau theory, the *spatial inhomogeneous distribution of the order parameter* is introduced into the considerations of the theory.

To refine the thermodynamic theory, the approach of Ginzburg [65] is followed considering the Taylor expansion of the Helmholtz free energy also in terms of derivatives of the order parameter with respect to the space coordinates. In order to follow the purely phenomenological considerations, following terms of the order parameter (i.e. polarization) and its derivatives are introduced into the expansion of function Φ:

$$\begin{aligned}\Phi(T,\, P_i,\, \partial P_i/\partial x_j) = \Phi_0 + & \qquad\qquad (\text{K.31})\\ \frac{1}{2}\alpha^T_{ij}P_iP_j \;+ \frac{1}{4}\alpha^T_{ijkl}P_iP_jP_kP_l + & \qquad (\text{second and fourth-order terms})\\ \mu^T_{ij}\frac{\partial P_i}{\partial x_j} + \lambda^T_{ijk}P_i\frac{\partial P_j}{\partial x_k} \;+\; \frac{1}{2}\delta^T_{ijkl}\frac{\partial P_i}{\partial x_j}\frac{\partial P_k}{\partial x_l} \;+ \cdots . & \qquad (\text{gradient terms})\end{aligned}$$

Again, function $\Phi(T,\, P_i,\, \partial P_i/\partial x_j)$ must be invariant with respect to any transformation of the symmetric phase and, therefore, restrictions imposed upon coefficients μ^T_{ij}, λ^T_{ijk} and δ^T_{ijkl} due to symmetry reasons have to be taken into account. In the symmetry 2/m the Helmholtz free energy expansion for one-component order parameter is written here as an example:

$$\Phi(T,\, P_z,\, \nabla P_z) = \Phi_0 + \frac{1}{2}\alpha P_z(\boldsymbol{x})^2 + \frac{1}{4}\beta P_z(\boldsymbol{x})^4 + \frac{1}{2}\delta\left[\nabla P_z(\boldsymbol{x})\right]^2 . \qquad (\text{K.32})$$

It can be pointed out that the coefficient δ is positive. This implies that spatially homogeneous distribution of polarization is energetically favorable. This *Ginzburg correction term* $(1/2)\delta\left[\nabla P_z(\boldsymbol{x})\right]^2$ in the expansion of function Φ brings fundamental consequences, which play an important role in the formation of equilibrium domain patterns.

Appendix L

Thermodynamics of ferroelectric domains

In this Appendix, the thermodynamic functions for a system of ferroelectric capacitor with domain patterns are defined. Without any proof the *Helmholtz free energy* per unit volume of the sample is defined by formula

$$\Phi(T,\, P_i,\, e_{ij}) = U(S,\, P_i,\, e_{ij}) - TS, \tag{L.1}$$

where U is the *internal energy of the dielectrics*, T and S are temperature and entropy of the dielectrics, respectively. Considering the first and second law of thermodynamics for the internal energy U, the zero variation of the Helmholtz free energy at the constant temperature T specifies the conditions for equilibrium of electrically and mechanically free sample

$$\delta\Phi(T = T_{\text{const}},\, P_i,\, e_{ij}) = \frac{\partial\Phi}{\partial P_i}\,\delta P_i + \frac{\partial\Phi}{\partial e_{ij}}\,\delta e_{ij} = 0. \tag{L.2}$$

Nevertheless, from the application point of view, the dielectric properties of a system with the constant electric field $\boldsymbol{E}$ is of practical importance.

L.1 Gibbs electric energy

Gibbs electric energy G is a thermodynamic function, which has a minimum with respect to the polarization $\boldsymbol{P}$ when the constant voltage is kept on the electrodes of the system. In that case, the definition of function G must determine the work performed over the system by external voltage sources:

$$G = \int_V \left[\Phi(\boldsymbol{P}) + \frac{1}{2}\varepsilon_0 E^2\right] dV - \sum_i^{\text{electrodes}} Q_i\varphi_i, \tag{L.3}$$

where $\Phi(P)$ is *Helmholtz free energy*, Q_i and φ_i are the charge and the potential on the i-th electrode, respectively. Considering the constant electric potential on electrodes, the second term on the right-hand side of Eq. (L.3) is equal to:

$$\sum_i^{\text{electrodes}} Q_i\varphi_i = -\oint_{S_E} (\varphi D_i) n_i\, dS_E, \tag{L.4}$$

where S_E is the surface of electrodes. By applying the Gauss theorem the following identity is immediately obtained:

$$\oint_{S_E} (\varphi D_i) n_i\, dS_E = -\int_V E_i D_i\, dV. \tag{L.5}$$

Thus the *Gibbs electric energy of the whole system* is equal to:

$$G = \int_V \left[\Phi(\boldsymbol{P}) - \frac{1}{2}\varepsilon_0 E^2 - E_i P_i \right] dV, \tag{L.6}$$

where the formula for the electric displacement

$$D_i = \varepsilon_0 E_i + P_i \tag{L.7}$$

has been used in the derivation. Having in mind that the electric field is constant in the sample, the *Gibbs electric energy per unit volume of dielectrics* is defined by the following formula:

$$G = G_0 + \Phi(\boldsymbol{P}) - E_i P_i. \tag{L.8}$$

It can be immediately obtained that zero variation of the Gibbs electric energy at constant electric field

$$\delta G = \left(\frac{\partial \Phi}{\partial P_i} - E_i \right) \delta P_i + \frac{\partial \Phi}{\partial e_{ij}} \delta e_{ij} = 0. \tag{L.9}$$

determines the *local equations of motion* in equilibrium of a system with fixed electric field at the electrodes.

L.2 Gibbs electric energy of a system with surface layers

Objective of this section is a derivation of a formula for the Gibbs electric energy of a system of ferroelectric capacitor with domain pattern and the electrode-adjacent (surface) layers considering that free (screening) charges σ_f are present at the interface of ferroelectric layer and surface layers.

The inhomogeneity of the system can be introduced in our theory by considering the different form of the Taylor expansion of Helmholtz free energy in the surface layer and in the ferroelectric layer:

$$\Phi(P) = \begin{cases} \Phi_f(\boldsymbol{P}) = (1/2)\,\alpha_a(P_x^2 + P_y^2) + (1/2)\,\alpha_c(T - T_C)P_z^2 + (1/4)\,\beta P_z^4 & \text{in ferroelectric film} \\ \Phi_g(\boldsymbol{P}) = (1/2)\,\alpha_g(P_x^2 + P_y^2 + P_z^2) & \text{in surface layer,} \end{cases} \tag{L.10}$$

Then, it is considered that screening charges σ_f are present only at the interface of ferroelectric and surface layers, which is denoted by symbol S_B:

$$(D_{g,i} - D_{f,i})\, n_i = \sigma_f, \tag{L.11}$$

where $D_{g,i}$ and $D_{f,i}$ are the components of the electric displacement in the surface and ferroelectric layers, respectively, and n_i are the components of the normal vector of the interface between the surface and ferroelectric layers.

Using the Gauss theorem and Eq. (L.11), the straightforward calculations yield the formula for the work of external voltage sources

$$\oint_{S_E} (\varphi D_i) n_i \, dS_E = \oint_{S_B} \varphi \sigma_f \, dS_B - \int_{V_f} E_i D_i \, dV_f - \int_{V_g} E_i D_i \, dV_g, \tag{L.12}$$

where V_f and V_g are the volume of the ferroelectric layer and the surface layer and S_B is the surface representing the interface of the ferroelectric and surface layers. Combining Eqs. (L.3), (L.4), (L.7), (L.11) and (L.12) it is immediately obtained:

$$G = \int_{V_f} \left[\Phi_f(\boldsymbol{P}) - \frac{1}{2}\varepsilon_0 E^2 - E_i P_i \right] dV_f + \int_{V_g} \left[\Phi_g(\boldsymbol{P}) - \frac{1}{2}\varepsilon_0 E^2 - E_i P_i \right] dV_g + \oint_{S_B} \varphi \sigma_f \, dS_B. \tag{L.13}$$

Considering the equations of motion $\partial\Phi/\partial P_i = E_i$ [see Eq. (L.9)], the integrals in Eq. (L.13) can be expressed in the hard ferroelectric approximation

$$G = \int_{V_f} \left[\Phi_f(\boldsymbol{P}_0) - \frac{1}{2}\varepsilon_0 \varepsilon_{ij}^{(f)} E_i E_j - E_i P_{0,i} \right] dV_f - \int_{V_g} \frac{1}{2}\varepsilon_0 \varepsilon_{ij}^{(g)} E_i E_j \, dV_g + \oint_{S_B} \varphi \sigma_f \, dS_B, \quad \text{(L.14)}$$

where $\varepsilon_{ij}^{(f)}$ and $\varepsilon_{ij}^{(g)}$ are components of the relative permittivity tensors of the ferroelectric and surface layers. Again with use of Eq. (L.11) and the Gauss theorem, the formula for Gibbs electric energy can be finally expressed in a form, which is profitably used for calculations in Papers A, B, C, D, E and F:

$$G = G_0 + \frac{1}{2} \oint_{S_B} \varphi (P_{0,i} n_i + \sigma_f) \, dS_B - \frac{1}{2} \oint_{S_E} \varphi \sigma_E \, dS_E, \quad \text{(L.15)}$$

where σ_E is the charge on electrodes.

L.3 Landauer formula

In Ref. [66] Landauer used another form of the Gibbs electric energy, which is convenient for use in theoretical considerations, however he provided no reasoning to confirm the correctness of his formula. In this section, the brief derivation of the Landauer formula under more general condition considering the presence of free charges in the ferroelectric is provided. Having in mind Eq. (L.3) it is considered that the electric potential φ is a superposition of two electrostatic potentials φ_d and φ_0, where the contribution φ_d is produced by free charges ϱ_f and by bound charges due to spontaneous polarization $-\partial P_{0,i}/\partial x_i$ according to the Poisson equation $\varepsilon_{ij}(\partial^2 \varphi_d/\partial x_i \partial x_j) = \partial P_{0,i}/\partial x_i - \varrho_f$ and where the value of φ_d is zero on electrodes ($\varphi_d = 0$ on S_E). In addition, it is considered that the contribution φ_0 satisfies the Laplace equation $\varepsilon_{ij}(\partial^2 \varphi_0/\partial x_i \partial x_j) = 0$ and the value of φ_0 is kept nonzero on electrodes by the external voltage sources.

Then with use of the identity

$$\int_V \varepsilon_0 \varepsilon_{ij} \left(\partial \varphi_d/\partial x_i\right) \left(\partial \varphi_0/\partial x_j\right) dV = 0 \quad \text{(L.16)}$$

the straightforward calculations involving several applications of Gauss theorem lead to the formula

$$G = G_0 + \int_V \left[\frac{1}{2}\varepsilon_0 \varepsilon E_d^2 - E_{0,i} P_{0,i} + \varphi_0 \varrho_f \right] dV, \quad \text{(L.17)}$$

where $E_{d,i} = -\partial \varphi_d/\partial x_i$ is the *depolarizing field in a situation when the electrodes are short-circuited* and $E_{0,i} = -\partial \varphi_0/\partial x_i$ is the *external electric field*.